Faculty of Science and Engineering

Department of Spatial Sciences

Development of a Property-Based Flood GIS

Maher Rashed Alsubhi

This thesis is presented for the Degree of

Doctor of Philosophy
of
Curtin University

July 2015

DECLARATION

To the best of my knowledge and belief this thesis contains no material previously published by any other person except where due acknowledgement has been made.

This thesis contains no material which has been accepted for the award of any other degree or diploma in any university.

Signature……..

Date……..

ABSTRACT

Coastal flooding is a common natural hazard threatening both natural habitats and urban areas. As global sea level is predicted to rise in the near-future, the likelihood of coastal flooding is expected to increase. Current studies on global warming and climate change confirm higher sea levels and an increase in the frequency and severity of extreme sea level events (e.g. storm surges). Given the current large concentration of people, businesses and infrastructure situated near to the coastline, potential consequences of coastal flooding on residential areas and coastal environment are of major concern to the community and the relevant decision makers. Thus, providing accurate and detailed information on the possible effects of coastal flooding is important to many stakeholders and the general public. Highly detailed information will help to manage and mitigate expected hazards, as well as increasing public awareness.

This project investigates the feasibility of developing a property-based flood GIS. Particular focus is given to residential areas, located close to the shoreline, to model and examine the effects of coastal flooding at very high spatial resolution, e.g. on a property-by-property level. This project also investigates the impact of coastal flooding on the coastal zone, coastal topography, man-made structures and geomorphology, including flood visualisation. This is accomplished by a four stage approach through: (1) modelling future sea level rise, (2) high-resolution flood modelling, (3) combination of flood information with property data, and (4) the development and implementation of a prototype for a property-based flood GIS. This is probably the first study in Australia looking at the development of a property-based flood GIS.

Geographic Information Systems (GIS) technology and remotely sensed LiDAR DEM data is, here, successfully implemented in the development of a prototype for a property-based flood GIS. The developed model is designed to quantify and visualise the risk of flooding at a very high spatial resolution (i.e. property-by-property based). This was accomplished through the use of the ArcGIS Model Builder.

To test and assess the developed model, two residential areas, Mandurah and Rockingham, situated along the South-West Australian coast, were chosen as study locations. For this, five flooding scenarios, based on the near-future sea level rise of 2.06 m; 5.98 m, 8.61 m, 10.12 m, and 18.73 m, were adopted. The test revealed the effectiveness of the developed model to provide detailed information on the vulnerability for each location with particular focus on a property-by-property level.

The results confirm the great benefit of using high-resolution topography data, especially in low-lying areas. Importantly, detailed information can only be acquired when high-resolution elevation data such as LiDAR data with 1 m spatial resolution is used. Comparison to lower spatial resolution elevation data (e.g. 30 m and 90 m) reveals that only the use of 1 m LiDAR DEM provides the level of detail and accuracy required for flood modelling on a property-by-property level.

Keywords:
GIS, Remote Sensing, Sea Level Rise, Flood, Visualisation, Flood Modelling, Urban Areas.

ACKNOWLEDGEMENTS

Thanks are due first and foremost to God for giving me the opportunity to complete my study. Without God‘s will and blessing, I would not have been able to finish this research. Similarly, I would not be where I am now without the guidance from my supervisors, and the support from my parents, my wife and my sons.

I wish to express my sincere appreciation to my main supervisor, Associated Professor, Dr Michael Kuhn, for providing invaluable advice, guidance and support. Dr Michael Kuhn initially encouraged me to conduct this research, and without his help, it would not have been completed.

I would also to extend thanks to my co-supervisor, Senior Lecturer, Dr Robert Corner. I am particularly pleased I had his help and support, and I truly believe his expertise and extensive knowledge of the subject contributed greatly to the high standard of work presented herein.

Thanks must also be extended to all students, and academic and administrative staff at the Department of Spatial Sciences, Curtin University of Technology, who have supported me, and facilitated my study, at every stage.

Special thanks and appreciation must go to my parents, whose love and prayers sustained me throughout my study. I would also like to acknowledge my brothers and friends for all their support.

Above all, I would like to thank my lovely wife, Hanaa Almehmady, for her prayers, support and encouragement, and my sons, Jassem and Hisham, who encouraged me daily with their smiles.

TABLE OF CONTENTS

LIST OF FIGURES

LIST OF TABLES

CHAPTER 1

INTRODUCTION

Climate change and associated near-future sea level rise remain a major concern for coastal areas. This is mostly due to sea level rise having four major implications to coastal areas (e.g. Verwey 2001 and Nicholls 1999), (1) inundation and displacement of lowlands and wetlands (Miller and Yates 2006), (2) coastal erosion (Leatherman, Zhang, and Douglas 2000), (3) exacerbation of the impact of storm surges (Dasgupta et al. 2011), and (4) an increase in the salinity of estuaries (Mitra 2013). Furthermore, a future sea level rise would have major socio-economic impacts on coastal areas by disturbing physical processes, economic activities, and social systems (Xingong 2009; Nicholls 1999).

The morphology of the topography plays a vital role in coastal flood modelling. Up until now, coastal flood modelling is mostly conducted at a regional level (Ward et al. 2010; Balica, Wright, and Meulen 2012; Aerts et al. 2009; Kuhn, Tuladhar, and Corner 2011; Eliot 2012; Thumerer, Jones, and Brown 2000; Colby, Mulcahy, and Wang 2000; Marfai and King 2008; Poulter and Halpin 2008; Purvis, Bates, and Hayes 2008), providing generalised information on the impact of flooding. However, on a local scale, the modelling effects of coastal flooding and its associated risks, require a more detailed and accurate representation of the coastal terrain.

Using up-to-date high-resolution data is crucial in the precise determination of the areas at risk, for example, at a property-by-property level. High-resolution maps of the expected flooded areas are an important tool for decision makers, such as local planners and managers, concerned with the effects of coastal flooding on developed areas (Gesch 2009). While there are some studies that have looked at high-resolution flood modelling, to the best of the author’s knowledge, no comprehensive study has yet been undertaken that combines high-resolution flood modelling with cadastral information (such as the shape and size of properties). This research tries to fill this gap by studying coastal flooding at high-resolution, on a property-by-property level, using a Geographic Information System (GIS).

1.1 Background

1.1.1 Sea level rise and coastal flooding

Sea level rise is currently a major issue that continues to attract widespread attention amongst scientists, policy makers and the general public. This is due to an increase in population, and economic activities in coastal areas, where a rise in sea level would have major socio-economic consequences (e.g. Nicholls 1999; Sarwar and Khan 2007; Dawson and Spannagle 2009). According to the 4th Intergovernmental Panel on Climate Change (IPCC) assessment report (Solomon et al. 2007), global sea level is expected to increase between 0.09 m and 0.88 m by the year 2100, and this is considered to be a major threat to coastal areas (Poulter 2008).

Due to potential flooding, global sea level rise will have major impacts on coastal areas around the world. Increased sea level in coastal areas, creates long term risks for people who live near to the shoreline (Smith and Petley 2004). Dawson and Spannagle (2009) estimate that currently more than 200 million people live in the coastal zone within a 1 m elevation from mean sea level. Therefore, major socio-economic impacts can be expected if no mitigation is done. According to the estimation by US Department of Defence Standards, already by 1990, on average about 10 million people per year experienced coastal flooding (Church et al. 2007). This is likely to increase considerably with rising sea level.

Several studies have been conducted to estimate potential flood risk for coastal areas (Yang 1997; Hennecke 2004a; Bas van de, Joost, and Claartje 2012; Imaduddina and Subagyo 2014; Kellens et al. 2012; Darsan, Asmath, and Jehu 2013; Kellens et al. 2011; Jongman, Ward, and Aerts 2012). Ward et al. (2010) estimated the inundation and potential damage due to future sea level rise in Jakarta, Indonesia. Also, an important global study, presented by (Rowley et al. 2007), calculated and visualised the global risk of sea level to population and coastal areas. Furthermore, a recent study by Anderson et al. (2010) warned about the currently underestimated impacts of rapid sea level rise.

Sea level rise can cause coastal erosion, which considerably increases shoreline retreat for various reasons. Firstly, higher sea levels enable waves to break closer to the shoreline. Secondly, deeper water reduces wave refraction and thus raises the capacity for shoreline transportation. Finally, with higher water levels, wave, and current erosion act at a higher elevation on the beach, resulting in the modification of the beach profile (Douglas 2001). Moreover, sea level rise, together with coastal erosion, can remove natural protections such as barrier islands, sand dunes along the coast, and bluffs, further increasing the impact of sea level rise to permanent structures (such as houses and other facilities along the shoreline (Smith 1992). There are many tools and methods that can be used to model and study coastal erosion. Bruun's Rule (1962) (BR) was probably the first attempt to study erosion on sandy beaches due to sea level rise (Zhang, Douglas, and Leatherman 2004).

Growing attention to the consequences of sea level rise is currently the result of different visualisation techniques that anticipate the potential impacts on coastal areas (Kellens et al. 2009a). Visualising flooding is important and helpful for a full understanding of associated implications and risks (Kellens et al. 2009b). It is also a simple tool that can be easily understood and used by the "lay-person". Flood maps can be classified into two main categories: (1) flood hazard maps and (2) flood risk maps. Flood hazard maps provide information about the magnitude of a flood event, while flood risk maps contain extra information on the impacts, such as the potential socio-economic damage and the vulnerability of population and infrastructure. There are several different types of flood hazard maps, including flood extent maps, flood depth maps, flood danger maps, and maps displaying other flood parameters, such as exposure and coping capacity (De Moel, Alphen, and Aerts 2009).

According to Merwade (2008), flood mapping involves determining on a map the area covered by water due to a flood event. Moreover, digital mapping of a flood event involves matching the new (raised) water surface to digital elevation data and then flagging the areas covered by water. GIS can be considered a suitable tool for modelling, analysing, and the visualization of flooding. Gambolati et al. (2002) used GIS in flood simulations, combining DEM data with sea level rise scenarios and corresponding shoreline recession, indicating permanently flooded areas.

Jude et al.(2006) utilised a GIS to visualise the inundation areas along the Norfolk Coast in England. They adopted a new system called virtual reality GIS. This new system employs two techniques: (1) interactive visualisation, produced by ArcView 3D analyst extension, and (2) static visualisation, exporting the result obtained from GIS into World Construction Set, a photorealistic rendering package from 3D Nature (see http://3dnature.com).

1.1.2 High-Resolution Flood Modelling

In order to mitigate the impact of coastal flooding, accurate flood modelling is required. Both GIS and Light Detection and Ranging (LiDAR) technologies have been recently used in detailed and localised flood modelling. Webster et al (2004) utilised flood modelling with topographic LiDAR data, within a GIS, to examine the effects of sea level rise on Prince Edward Island in Canada. The authors confirmed that a high-resolution (0.9 m by 0.9 m) DEM, derived from LiDAR, was a very efficient and useful tool in flood modelling. Coastal morphology and man-made structures can have a great influence on coastal flooding. These, however, can only be modelled when high-resolution data is available. This has also been confirmed by Sole et al. (2008), who stated that the importance of high-resolution data, showing details such as small changes in the surface, and man-made structures, can have great influence on the identification of flood water distribution. Therefore, it can be concluded that high-resolution modelling is crucial when information on property-level is required.

Several other authors have also acknowledged the importance of high-resolution terrain information, in detailed flood modelling. Yang (1997) used the integration of remote sensing and GIS to analyse coastal changes and their environmental impacts in Lingding Bay, Pearl River Estuary, South China. Also, Thumerer, Jones, and Brown (2000) used a GIS based model to simulate the potential impacts of sea level rise on shoreline recession. All the aforementioned authors confirmed that using high-resolution data in flood modelling provided them with an effective tool for allocating and mapping flood boundary zones.

1.1.3 Combination of flood information with property data in GIS

GIS is already recognised as a powerful tool in the management and analysis of geo-referenced data over land. Similarly, GIS can become a powerful tool for modelling flood scenarios through the integration of various spatial data with other flood information (Wyatt 2003). GIS is also useful when combining data management, as well as when analysing and visualising the vulnerability of coastal areas due to sea level rise. Flood modelling in urban areas, however, can be challenging due to the complexity of flood flow patterns and paths (Syme 2008). Flood modelling in urban areas depends on the complexity of urban elements, such as buildings, roads, fences, houses, etc. Several approaches, using a GIS, have been proposed to model urban elements, using either a two-dimensional (2D) or three-dimensional (3D) approach.

The advantages of using a 2D model are: it can be applied relatively simply; it is cost effective, and it consumes less computational resources than a 3D model, which requires powerful computers and/or sophisticated software (Charteris, Syme, and Walden 2001). The benefits of using a 3D model in flood modelling are: the accurate representation of the coastal terrain, including buildings and infrastructure, and the enhancement of analysis tools through the use of 3D visualisation. Furthermore, 3D visualisation can be used to generate interactive maps to realistically simulate the effects of sea level rise on coastal areas. While 3D data can be easily be converted to 2D data, this is not the case for the contrary (Stanchev, Palazov, and Stancheva 2009).

Syme (2008) utilised the 2D model approach, with simulated buildings and fences, to study flooding in urban areas. Yu and Lane (2006) used a 2D raster-based diffusion-wave model, to define the pattern of river flood inundation in residential areas, by utilising high-resolution topographic data and examining the influence of spatial resolution upon estimated flood extent and flow routing processes. Lai et al. (2011) used a 3D numerical flow model to simulate water and the flow velocity field. The authors utilised the outcomes of the simulation process to build up a 3D virtual environment.

The authors stated that 3D modelling can be used in a virtual environment and can provide sophisticated information, presenting both hydraulic and geometric data.

1.1.4 Vulnerability Indices

Quantification of flood risk is often performed through a Vulnerability Index (VI), which can be beneficial in terms of increasing knowledge and improving (public) awareness regarding flooding (Ebert, Kerle, and Stein 2009). The advantage of a VI is its ability to map complex physical phenomenon into one simple numerical index or classification (e.g. high/low risk). A variety of methods can be utilised when assessing the vulnerability of coastal areas, due to sea level rise, on a global, regional and local scale, such as the Bruun Rule (Bruun 1962), Coastal Vulnerability Indices (CVI) (Gornitz et al. 1994) and Dynamic Interactive Vulnerability Assessment (DIVA) (Hoozemans, Pennekamp, and Rijkswaters 1993). While many studies provide a more regional VI, a literature review revealed that not many studies have been conducted to assess vulnerability based on a property-by-property level.

Papathoma (2003) developed and applied the new methodologies, building vulnerability (BV) and human vulnerability (HV), to assess vulnerability caused by tsunamis in coastal villages in the Gulf of Corinth in Greece. Dominey-Howes and Papathoma (2007) used the Papathoma Tsunami Vulnerability Assessment Model, ‘‘PTVAM’’, to validate the vulnerability caused by tsunamis. The “PTVAM” approach is very sensitive and can test the vulnerability at high-resolution (i.e. ‘detail bottom-up model’ at building-to-building scale).

1.2 Research Objectives, Significance and Outcomes

1.2.1 Objectives of this study

The main objective of this study is to assess the feasibility of utilising GIS technology, together with high-resolution LiDAR-derived DEMs, to develop and deploy a property-based flood-model.

To achieve the main objective, the following specific objectives are examined:

1. The effects of coastal flooding, due to near-future sea level rise, on residential areas located close to the shoreline, including:
   a) The impact of sea level rise on the coastal zone, man-made structures, coastal topography, and geomorphology.
   b) The contribution of different sea level rise scenarios, based on information such as tide gauge observations, climate changes scenarios, melting ice masses from Greenland and Antarctica, and storm surges.
   c) The role of other factors, which may lead to increased flood vulnerability, like beach erosion.
2. The impact of Digital Elevation Model (DEM) resolution on flood modelling, obtained via a comparison of low- and high-resolution models.
3. The core of this thesis will focus on the feasibility of developing a property-based flood GIS, including:
   a) Examination of the possibility of flood modelling, on a property-by-property level, using high-resolution data.
   b) Use of 2D cadastre data (e.g. boundary lines) augmented by height information.
   c) The development of a vulnerability index based on information on a property-by-property scale.

1.2.2 Significance of this study

This research is significant because understanding and modelling coastal flooding is an important topic in today's society. This is mostly due to a large amount of the world's population currently living in coastal areas (e.g. ~200 million within 1 m elevation of mean sea level (Dawson and Spannagle 2009), and thus, coastal flooding will have a direct socio-economic impact. Improved knowledge will help to find mitigation strategies to reduce the impact of coastal flooding. This is of particular significance to Australia, where more than 85% of the total population live within 50 km from the sea, and 20% of the total population live in small coastal towns and regional cites located near to the sea (Green 2010).

This amount is expected to increase in the future, further increasing the probability of a coastal population exposed to coastal flooding. From this perspective, the significance of this project can be summarised as:

1. A large number of Australia's population, as well as the world's population, will benefit from high-resolution flood modelling. This will help to mitigate the effects of coastal flooding on urban areas, infrastructure, and natural habitats.
2. Through the selection of two study areas, this study will help to provide exemplary quantification of coastal vulnerability in Western Australia.
3. The results of this research project will be beneficial to many public and private sector entities, such as governmental authorities, real-estate agents, insurance companies, and researchers.

To the best of the author's knowledge, this will be the first comprehensive study in Australia (and probably world-wide) to model coastal flooding, due to future sea level rise, on a property-by-property level, combining high-resolution LiDAR-derived elevation data with cadastral information.

1.2.3 Outcomes of this study

The main outcome of this study is a prototype for a property based flood GIS using different coastal flooding scenarios. Scenarios are calculated based on future sea level rise predictions for two study areas in Western Australia. The past sea level trend, obtained from tide gauges, will be analysed and used for future sea level predications. The effects of coastal flooding on a property-by-property scale will also be shown and reported. Moreover, vulnerability indices will be developed based on selected criteria. This will identify and rate all areas at risk of coastal flooding within the selected study locations. The outcomes identified by this project can then potentially be used at different levels, by both national and local authorities (i.e. the Department of Transport and/or the Department of Water in Western Australia). The study can also potentially be used as an indicator tool, to identify flood risks, which can be assigned to a certain location, along with the associated statistics and flood maps.

1.3 Study design and methodology overview

In order to achieve the research objectives, this research has been divided into four main stages (cf. Figure 1.1): (1) the modelling of future sea level rise, (2) high-resolution flood modelling, (3) the combining of flood information with property data, and (4) the development and implementation of a property-based flood GIS. As illustrated in the *research stages flowchart* (cf. Figure 1.1), the first three stages will cover important preliminary work that will be consolidated in the final stage (i.e. stage 4).

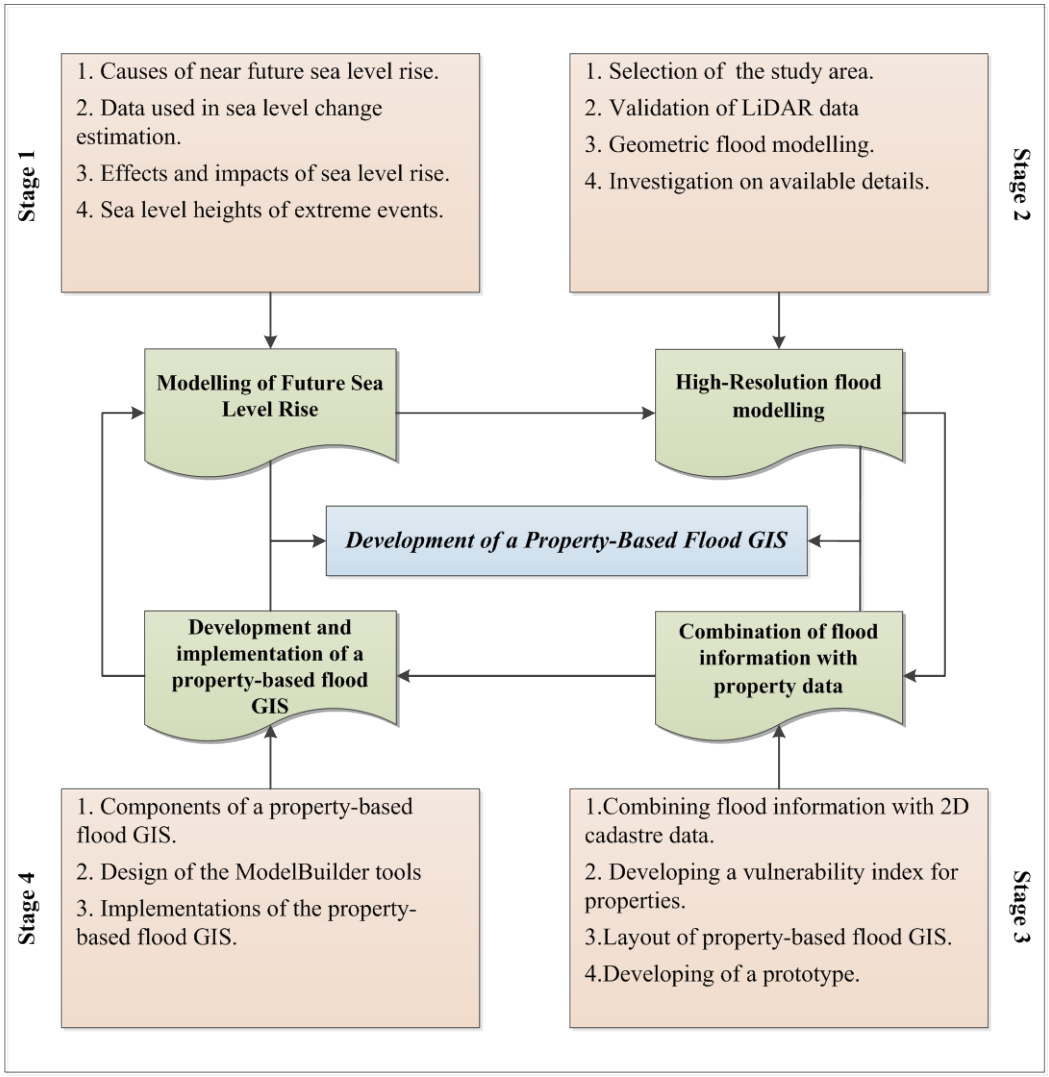

Figure 1.1 Research stages flowchart.

1.3.1 Stage 1: Modelling future sea level change

The first stage (cf. chapter 3) is mostly a review of existing studies and the methods and data used for modelling future sea level change, so to ensure that assessments and practical studies within this research are based on realistic sea level change estimates. The following aspects of sea level change are covered:

- Steric change (e.g. thermal expansion).
- Mass change (e.g. melting ice).

This is achieved through an investigation of the factors contributing to sea level rise.

The data types used, for sea level rise estimation, are identified and discussed regarding their suitability for this study. Attention is given to the relationship between sea level rise, coastal erosion, and salt-water intrusion. Additionally, the relationship between extreme sea level events (e.g. storm surge), corresponding sea level heights (and the impact on coastal areas) is also studied.

1.3.2 Stage 2: High-resolution flood modelling

The second stage (cf. chapter 4) assesses data and methods for high-resolution flood modelling in urban areas. For practicality, two suitable test sites, along the south west coast of Western Australia (between Perth and Busselton), have been selected. These study sites are located at Mandurah and Rockingham. Coastal flooding is modelled and assessed using Digital Elevation Models (DEMs) of varying resolution. This includes a comparison between low- and high-resolution DEM data, in order to assess suitability for high-resolution flood modelling. Furthermore, this study assesses the level of detail that can be obtained using DEMs of varying resolution. At this stage of the project, a variety of spatial data sets will be used, such as high-resolution DEMs for the study area, low-resolution DEM data 30 m ASTER, 90 m STRM DEMs, topographic data and infrastructure information, road network and geodetic surveys data, geology data and maps, and erosion information.

1.3.3 Stage 3: Combining flood information with property data

The third stage (cf. chapter 5) assesses the combination of flood information (obtained from the previous stages (cf. chapter 4)) with 2D cadastre data. There will be a particular focus on information gathered on a property-by-property level (e.g. boundary information). Here, any flood information, which is 3D in nature, will be matched with the 2D cadastre data, or alternatively, the 2D cadastre data will be augmented with height information (e.g. from the DEMs). At the end of the third stage, developing a property-based vulnerability index will be achieved using criteria based on the outputs obtained throughout the previous stages.

1.3.4 Stage 4: Development and implementation of a property-based flood GIS

The final stage (cf. chapter 5) of this project focuses on the possible layout of the property-based flood GIS. Firstly, this final stage defines the main components of the property-based flood GIS and assesses how various information (obtained from stages 1 to 3) can be included and presented to an end user. The implementation aspect focuses on how such a model can be conveniently used by the end user, including information, such as the input data, output data, and the interface of the tools developed.

1.4 Organisation of the Thesis

This thesis consists of six chapters, as follows:
The first chapter (this chapter) outlines the statement of the problem, the study objective, the significance of the study, the national and community benefits, and the study design.

The review of relevant work within this field of study is very useful when gaining a better understanding of the topic; therefore, the review of previous studies is essential and important. Based on this, the second chapter reviews past works in the field, highlighting what other researchers have found. The contents are divided into sub-headings, reflecting the chosen main categories.

The third chapter focuses on the modelling of future sea level rise (cf. stage 1 in Figure 1.1), and the causes of near-future sea level rise. Also, the data used in sea level estimation studies is highlighted, while different flood scenarios are defined, based on future sea level projections and other metrological factors.

The representativeness of various tide gauge stations, to model sea level change in the region, has been documented through correlation analyses between the tide gauge records. At the end of this chapter, the representativeness of Satellite Altimetry data, along the coast line of the South West coast of WA, is studied.

The fourth chapter is dedicated to high-resolution flood modelling (cf. stage 2 in Figure 1.1). This chapter begins by selecting suitable study area locations, which satisfy the research aim and objectives. Subsequently, the LiDAR data used in this study is checked for accuracy and reliability. Geometric flood modelling, and the comparison between low- and high-resolution DEM data (in terms of the level of detail which can be obtained from each), is reported here.

Chapter five deals with the combination of flood data with property data (cf. stage 3 in Figure 1.1). The methodology used in matching flood information with the cadastral data is clearly explained, along with the method used to obtain the vulnerability index for the study areas. The results obtained from the data processing, using the methods mentioned in this chapter, are also discussed. In addition, an interpretation of the results, and their reporting in the form of maps, is provided.

Also in chapter five, the main components of the property-based flood GIS, the development of the ModelBuilder tools, and the implementation of the property-based flood GIS are discussed. Detailed information about the flood-modelling tool developed in this study, including how it operates and how it can be used by the end user, is also provided.

Conclusions of the study are provided in the final chapter. This includes a summary of the whole thesis and the highlights of the overall results. A statement of the contribution of this study to the area of flood modelling is also included in this chapter. Finally, recommendations for future studies are suggested in the light of obtained results.

1.5 Chapter summary

In this chapter, objectives for the development of a property-based flood GIS were established. The research stages were highlighted, along with the necessary steps to be followed in order to achieve the thesis objectives. The next chapter will provide an overview of the thesis topic and will review related literature concerning sea level rise and flood modelling.

CHAPTER 2

LITERATURE REVIEW

2.1 Introduction

In the previous chapter, the main objectives of the thesis were stated. The methodology adopted in this research, along with the research stages, was briefly presented. This chapter provides background information on topics related to this thesis. Particular focus is given to natural hazards, sea level rise and coastal flooding. This chapter also reviews some of the literature related to the use of GIS in flood modelling, the application of high-resolution LiDAR data in flood modelling studies, the effects of grid resolution on topography representation, as well as flood modelling and development of a Flood Vulnerability Index. Selected references are summarised, and important findings are highlighted.

2.2 Natural hazard and disaster

The term natural disaster has been defined by many authors. The American Geological Institute (1984) describes a natural disaster as a geological condition or phenomenon which can happen naturally, or is man-made, which poses danger to both humans and the built environment. White (1974) defined a natural hazard as an interaction between human and nature governed by the current “state of adjustment of the human use system and the state of nature in the natural system”. Furthermore, the Office of the United Nations Disaster Relief Coordinator UNDRO (1982) specified a natural hazard as the probability of occurrence, within a limited time period and for a specified zone, of a likely damaging phenomenon. While Alexander (1993) defined a natural disaster as some quick, sudden or deep effect of the natural environment upon people and properties. The widely approved definition of a natural disaster, however, was provided by Burton and Kates (1964). They defined a natural disaster as “those elements in the physical environment, harmful to man and caused by forces extraneous to him”.

Here, the term natural disaster includes environmental, natural, geological, atmospheric, wildfire and hydrologic phenomena that, due to their location, severity, and frequency, are likely to adversely impact people, their property, or their daily life. The word natural eliminates all the other phenomena resulting from man-made activities, such as pollution and contamination (Organization of American States 1990), although man-made activities may certainly exacerbate natural disasters.

Life on Earth can be very dangerous; most parts of the Earth are under real threat of natural hazards and disasters (Tobin and Montz 1997). According to Alesch, Atkisson, and Petak (1984), there are more than 516 active volcanoes around the world, with eruptions happening approximately once every two weeks. Currently, earthquake monitoring systems record more than 2000 tremors every day, and at least two of these earthquakes occur with enough magnitude to damage houses and infrastructures. Similarly, 1800 thunderstorms occur at any one time around the globe. In one summer season, more than 50 hurricanes are recorded around the world, as well as approximately 600 to 1000 tornadoes in the US. This is, on average, about 4 tornadoes per day, and this is only in the United States (Alesch, Atkisson, and Petak 1984).

Due to a recent increase in natural hazards, human and economic loss has also increased dramatically. Many people in different parts of the globe are harmed by natural hazards such as floods, volcanoes, earthquakes, and others. Alexander (1993) stated that the average death toll in the world is around 250,000 per year, around 140,000 of which are killed by natural disasters. He went on to state that more than 95% of these deaths occur in third world countries.

According to Keller and Blodgett (2008), natural disasters, in the past few decades, are the main cause of death for millions around the world. The mean loss of human life, due to natural disasters, is approximately 150,000 yearly, confirming the findings provided by Alexander (1993). Every year, floods are responsible for killing an average of 9000 people around the world, while 115 million people are affected by flood incidences (CRED 2010).

In 1970, floods and hurricanes killed more than 300,000 citizens in Bangladesh, and in China, more than 300,000 people were killed in an earthquake in 1976. Likewise, the 2004 Indian Ocean tsunami killed around 230,000 people, and in the United States, more than 1600 were people killed by Hurricane Katrina in 2005, the damage costs of which exceeded US$100 billion. The cost of natural hazards to the world economy exceeds US$50 billion per year (United Nations Centre for Regional Development 1996). This figure includes the amount spent on predicting, preventing, and mitigating natural hazards, as well as the cost of any direct loss. The amount does not include loss of jobs, physiological effects and reduced productivity (Keller and Blodgett 2008).

2.3 Flood

Flood is treated as one of the most common types of natural hazard to have a considerable effect on human and natural habitat (Gallopín 2006). Floods come in second place behind windstorms as the most costly natural disaster (Balica and Wright 2010). The demand for reliable and highly accurate data concerning flood behaviour is growing as floods have increased in frequency and severity in many parts of the globe (Haile and Rientjes 2005). The constant fluctuation of both the world's climate and the Earth's temperature have increased the likelihood of coastal flooding, maximising danger to natural ecosystems and the residential areas near to shoreline. Increased sea levels in coastal areas create long term risk to people who live near to shorelines (Smith and Petley 2004).

Records from the Centre for Research on the Epidemiology of Disaster (CRED) show that there have been more than 3000 flood disasters since 1900. This makes flooding one of the most frequent and dangerous natural disaster events to both humans and the built-up environment (Smith and Petley 2004). Usually, land-based flooding is accompanied by severe rain in a very short period of time. Furthermore, such natural phenomena can cause huge damage and great loss to the economy, especially in urban areas. Flood damage can extend to natural habitat and wildlife.

Low-lying areas, such as coasts and deltas, are often at high-risk of both freshwater and marine floods. Usually these areas are highly populated (Smith and Petley 2004). Floods can occur on very large regional scales, such as over a large drainage system. These are usually high-magnitude and low frequency events. Regional flooding is the type of natural disaster which causes the largest death toll. The number of floods around the world seems to have increased due to various reasons, like global climate change and urbanisation. The Organization of American States (1990) classified floods into two main types:

1. Land-based floods or river floods are floods resulting from extreme run-off caused by severe storms and heavy rain. River floods are natural events and are difficult to predict. River floods are expected to happen randomly on all rivers and streams. Consequently, urban areas located within the flood zone areas are in major threat of flood damage.
2. Sea-based floods or coastal floods are regarded as major threats to coastal areas around the world. Coastal flooding is caused by storms and surges, usually exacerbated by storm run-off from the land. Tsunamis are considered a special form of coastal flooding. Storms and surges often cause a rise in sea level and are accompanied by heavy rain at sea. The surges occur due to strong winds, very low pressure cells and ocean storms. The water level is influenced by different factors, such as wind, tide, atmospheric pressure, waves and swell, local shoreline topography and bathymetry, and also the storm's proximity to shore.

The increase of urbanisation near to flood plains makes those human settlements more vulnerable to flood damage (Haile and Rientjes 2005). It is estimated that more than 200 million people are currently living in the coastal zone within 1 m from the mean sea level (Menoni and Margottini 2011). Major socio-economic impact can be expected if mitigation is not embraced. It is projected that an average of 10 million people per year will experience coastal flooding (Church et al. 2007). Highly accurate data is strongly recommended, in order to mitigate the impact of coastal flooding. A major objective for this study is to evaluate the effects of sea level rise on coastal areas.

2.4 Selected studies on the effect of sea level rise

As global warming continues, global sea level rise is expected to increase due to melting of the ice sheets in Greenland and Antarctica. This issue has been studied by several others (e.g. Gornitz, Couch, and Hartig 2001; Snoussi et al. 2009; Marfai and King 2008; Urbanski 2001).

Gornitz, Couch, and Hartig (2001) studied the impact of sea level rise in the city of New York metropolitan area. The authors stress the importance of this study due to the continuing change in global climate and the greenhouse effect. The study projected that, based on climate change, sea levels will rise above late 20th century levels by 18–60 cm by 2050, and 24–108 cm by 2080. This has been confirmed by Urbanski (2001), who studied the impact of rising sea levels on the natural environment along the Polish Baltic coast. Based on their analysis, a rise of sea level by 40 cm could cause the dune ridge vegetation to deteriorate.

Pethick (2001) demonstrated the effect of sea level rise on two beach type assemblages in the United Kingdom: estuaries and open beach. The author showed that a rise in sea level at a rate of 6 mm/year will shift the estuaries toward the mainland at the rate of 10 m per year, and the open beach landforms will have an along-shore shift at a rate of 50 m per year. Leatherman, Zhang, and Douglas (2000) suggested that rising sea levels is one of the most important factors in long-term coast erosion. The authors stated that a rise of 10 cm could result in 15 m of coastline erosion.

Coastal erosion is one of the common issues in coastal areas, and affects around 70% of the beach habitats around the world (Dionne, Richard, and Vincent 1987). Coastal erosion can be caused by local factors (e.g. the drop in sediment supply), and can also be due to global factors (e.g. global sea level changes) (Feagin 2005). If there is no protection or natural barriers, coastal erosion will cause a landward displacement of the beach environment, especially in sediment-rich locations (Martínez 2008).

The acceleration of coastal erosion will decrease the amount of land available for coastal plants and animals (Feagin, Sherman, and Grant 2005). Feagin (2005) studied coastal erosion due to sea level rise and found that coastal plants will be restricted to very limited areas, leading to a failure of the successional process. Jones (2005) conducted a study about the possible shoreline erosion of the Swan coastal plain resulting from sea level rise. The author showed that the section from Mandurah to Bunbury seems to be most vulnerable to coastal erosion during the coming century, due to particular issues of geology and morphology.

Rising sea levels will also have huge consequences for coastal urbanisation. Snoussi et al. (2009) explored the effects of sea level rise on the Moroccan coastal zone. In this study, Tangier Bay was chosen because it is considered the most important socio-economic hub in Northern Morocco. According to the authors, it is expected that the impact of floods will become more severe with a rise in sea level. Based on their study, the authors indicated that the impact of sea level rise will affect different sectors, including the industrial area, tourist coastal infrastructure, railway network defences and the port. According to their research, around 20% of beach areas will be affected by shoreline erosion based on a predicted rise in sea level of 7-39 cm by 2050. By 2100, this will increase to 45% if sea levels rise by 20-86 cm as predicted.

Nicholls (2002) estimated that 16-388 million people globally will experience flooding if sea level rises by 55 cm in 2100, and around 510 million will be affected if sea level rises by 96 cm. The author argued the decision makers should adopt policies which could help to mitigate the effects of climate change, and that they should improve shoreline planning and management. Rowley et al. (2007) investigated the global impact of sea level rise on people, and land, in eight regions around the world: South Asia and North Australia, South United States, the Mediterranean, North-western Europe, Alaska, the Amazon Delta Region, East Asia, and South Asia. Their calculations showed the regions of South and East Asia and northern Australia will be the most highly affected, as the number of people and the total land affected are both high compared to the other regions included in the study.

Marfai and King (2008) studied the socio-economic effects of rising sea levels, and their analysis showed that a 120 cm to 180 cm sea level rise could shrink the coastal region of Semarang, Indonesia, due to inundation, and will affect around 150,000 people living on 5398.8 hectares of affected area. It is estimated that the total economic loss would be about 1.8 billion Euros if there is a 120 cm sea level rise, and there will be a total loss of 2.3 billion Euros if there is a 180 cm sea level rise. Yohe et al. (1996) calculated the cost of sea level rise on the developed shoreline in the United States, and they estimated that a rise in sea levels of 100 cm by 2100 will cost the United states around $6.3 billion.

Any residential areas located near to the coastline are subject to varying levels of coastal flooding due to sea levels rising. The world's population density continues to increase, especially in coastal areas, with potential losses resulting from flood incidence expected to be high for economy and communities (Hallegatte and Corfee-morlot 2011; Fukuzono, Ikeda, and Zhai 2003). The impact of flooding, to residents in flood zone areas, can have two major effects: damage to the resident's properties and a dramatic decrease of land values (Rambaldi et al. 2013).

Internationally, the consequences of flood to property values have been discussed in a few studies, such as in the United States (e.g. Bin, Kruse, and Landry 2008; Bartosova et al. 2000; Donnelly 1989; Bin and Kruse 2006) in Japan, (e.g. Fukuzono, Ikeda, and Zhai 2003) and in Europe (Daniel, Florax, and Rietveld 2009). All these studies show a 5 to 10% decrease of the value of properties located within the flood zones compared to properties located outside the flood zones. According to Bray (2011), following the flood incidence in Brisbane, Australia in January 2011, private properties were revalued; some of these property prices dropped by up to 20%, resulting in a decrease of the city council's land taxes. Rambaldi et al. (2013) reported, for the same flood, a decrease in house price of 5.5%. It can be concluded from the above-mentioned studies, that sea level rise is a serious issue, and it can have huge impacts on humans, the environment, and the economy. However, it can be said, there is growing interest in this topic, attracting the attention of many researchers, governments, and world agencies. These efforts will help to mitigate the consequences of a sea level rise.

2.5 The use of spatial sciences in environmental modelling and disaster management

Information is important to a large number of people because it has the potential to increase their knowledge of specific issues. Humanity is facing many challenges, and many questions need to be answered to assist us in facing current problems and making important decisions. Mitigating the effects of natural disasters is only possible when detailed information is provided about the potential characteristics of the hazard, such as frequency and magnitude. In this regard, most of the information required in environmental modelling and disaster management is of the sort that has an essential spatial component such as thematic maps, satellite imagery, GPS survey, aerial photography, etc.

Much of this data comes from different sources within different spatial settings, projections and co-ordinate systems. This spatial data needs to be unified and brought into one base-map, in order to effectively manage it (Andrew 2002). Developments in the field of science and technology, in the last several decades, especially in the period after 1950, have enhanced human ability to understand the physical processes of many natural phenomena.

GIS and remote sensing have the ability to provide users with maps, allocating the hazard zones. Delineating hazard zones is an essential part of any disaster management project, and it should provide decision makers and urban planners with adequate, accurate and understandable information (Singh 2009). For example, the combination of GIS and GPS data plays a vital role in search and rescue operations. Remote sensing can help in the damage assessment stage by providing a quantitative base for the relief stage.

Furthermore, GIS can assist during the disaster rehabilitation stage by providing the post-disaster census data, supplying information on damage and suggesting suitable locations for reconstruction (Andrew 2002).

2.6 Photogrammetry

Mikhail, McGlone, and Bethel (2001) defined photogrammetry as the method of obtaining metric data, belonging to a physical object, collated by measuring an image of that object. Linder (2009) defined photogrammetry as the art and science of measuring. According to Linder (2009), photogrammetry is the process of providing quantitative data to the user and is historically considered as part of geodesy and the field of remote sensing. McGlone et al. (2004) stated that photogrammetry is the art, knowledge and skills to extract accurate and reliable data about an object and the environment, by measuring, recording and analysing an image.

The data can be obtained in different forms, e.g. physical, temporal, semantic, and geometric. Obtaining quantitative data for an object, from a photographic image through visual analysis, is called photo interpretation. According to Atkinson (2001), photogrammetry should meet the following essential requirements:

- The ability to self-diagnose (quality control).
- The ability to provide a high level of accuracy and reliability.
- The functionality to reconstruct 3D objects.

The term photogrammetry comes from the Greek language and can be divided into three parts. The first part is phot or phos meaning light. The second part - gramma - means letters, and the final part - metrein - means measure. Based on the type of use and other variables, like the type of platform and sensors used, different types of photogrammetry are in use, such as close range photogrammetry, terrestrial, and aerial photogrammetry, architectural photogrammetry, biostereometrics, and others.
The first forms of photogrammetry were close range photogrammetry and terrestrial photogrammetry, although today the term photogrammetry usually refers to aerial photogrammetry (Awange and Kiema. 2013). The main application of photogrammetry is to produce topographic maps, either in the form of orthophoto maps or line maps. Photogrammetry provides geodata to GIS, and this geodata can be acquired by methods of photogrammetry and laser scanning (Kraus 2007).

A Digital Elevation Model (DEM) is considered one of the most important outputs of photogrammetric processing. It is defined as a digital representation of the terrain surface and the man-made structures on the Earth's surface. During the past few decades, the use of DEMs in many areas (such as geology, urban planning, resource management, environmental monitoring, remote sensing and GIS) has rapidly increased (Vaze, Teng, and Spencer 2010).

The term DEM is usually used as a shared term for a digital surface model (DSM) and a digital terrain model (DTM). The DTM refers to data, without recording the lifeform data (such as trees and plants), and artificial data (such as man-made structures, including buildings, roads, and others). The term DSM, however, refers to all the objects on the Earth's surface (Schwarz 2012).

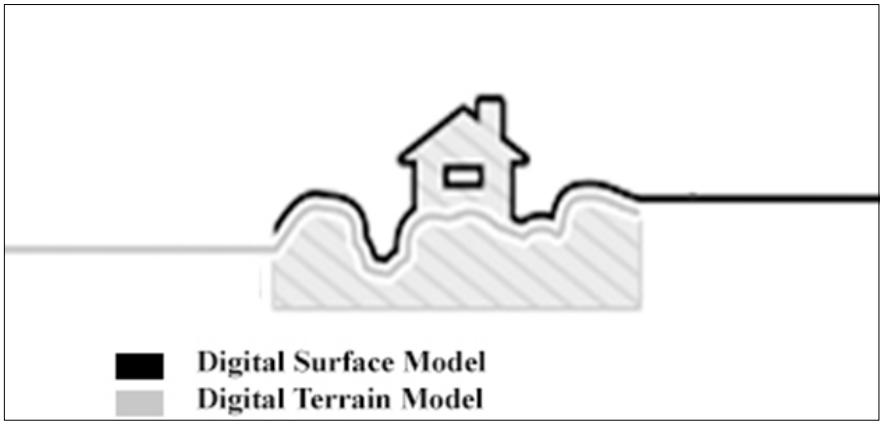

Figure 2.1 The difference between digital surface model (DSM) and digital terrain model (DTM) (source: Schwarz 2012).

DEMs can also be regarded as important features of land-surface analysis and spatial modelling studies. As previously argued, highly accurate representations of land surface is strongly recommended, in order to mitigate the impact of flooding (Haile and Rientjes 2005). Studies by Haile and Rientjes (2005); Sole et al. (2008); Turner et al. (2013); Bas van de, Joost, and Claartje (2012); Gesch (2009); Knight et al. (2009); Schumann et al. (2008) demonstrated the need for high-resolution data in flood modelling, especially for low-lying areas. When low-resolution data is used, it is not possible to obtain highly accurate results for flood boundaries.

The efficiency of low-resolution DEM has been widely used when modelling simple areas, where the topography doesn't have much variation. However, there is a growing demand for the use of high-resolution DEM in urban and rural areas, where representation of the terrain is more complex. This is due to the presence of relatively small scale elements, such as roads, houses, and dykes, which can affect the flood pattern. This issue has convinced many researchers and modellers to apply highly accurate and detailed DEM for flood modelling studies in urban area floodplains with residential settlements. The recent development of LiDAR data has further encouraged researchers to benefit from the use of high-resolution representations of the Earth's surface in flood modelling (Vaze, Teng, and Spencer 2010).

One of the major drawbacks, of using low-resolution DEM as input data, is the danger of omitting some of the important small scale elements that affect flood simulation, especially in low-lying built-up areas. Through the resampling process, or the transformation from high-resolution to low-resolution, many of the important details are generalised due to the averaging (as part of the transformation process). There is a need to quantify and report the impact of such processes on the performance and reliability of low-resolution data in flood modelling. Several studies have been conducted, comparing spatial indices obtained from different low-resolution DEMs (e.g. 100 m vs.1000 m grid resolution), and many researchers have studied the impact of using lower DEM resolution on the outputs from hydrological and hydraulic modelling.

It can be noted that most of these studies focus on the low DEM resolution (e.g. 100 m spatial scales or larger). However, with the introduction of high-resolution data such as LiDAR data and the availability of high computational resources, which can manage and handle large datasets, there is a need to report and quantify the differences of using different DEM resolutions (e.g. 1 m, 30 m and 90 m) on the modelling outputs, and also the change in accuracy and reliability when transforming from high to low resolution. In order to demonstrate the benefits/needs of high-resolution flood modelling studies in this study, the flood has been modelled at two test sites by using various DEMs resolutions (cf. chapters 4.8 and 4.9).

2.7 Light detection and ranging (LiDAR)

LiDAR technology has been used for many years in environmental applications and studies. Although the cost of LiDAR is relatively high, the use of LiDAR technology has increased in many fields (Bartlett and Smith 2005). LiDAR – an acronym for "light detection and ranging"- is now a common remote sensing technology. It is based on distance measurements, from the sensor to the object, to provide users with very accurate topographic data (Cracknell and Hayes 2007).

The basic LiDAR concept is very simple. A beam of light is sent by a laser mounted on a platform (e.g. aeroplane, cf. Figure 1.3) at distance *D* above the surface of the Earth and is reflected back. An electronic measurement is made of the travel time of the light pulse, covering the tow-way distance. Using the speed of light *c*, the distance can be calculated from the following (cf. Equation 2.1):

$$D = \frac{ct}{2}$$

Equation 2.1 The basis of LiDAR measurement

With the known height *h* of the sensor (e.g. ellipsoidal height obtained by GPS), the height of the surface h_s can be obtained by:

$$h_s = h - D$$

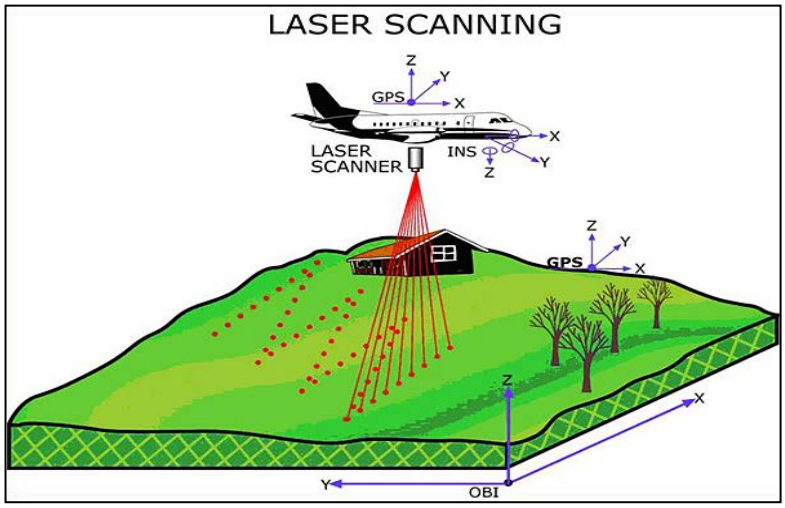

Figure 2.2 Shows the common LiDAR system components. The system consists of an aircraft, laser scanner, Global Position System (GPS), and inertial navigation system (INS) (source: Schuckman 2009).

LiDAR technology is classified into two main types:

1. Terrestrial: this is land based data collection. The laser scanner unit is mounted on top of a vehicle or on a tripod. In this instance, the data collection process can be static when using a tripod, or mobile when using a vehicle (Fiorani 2008).
2. Airborne LiDAR is classified into two types; topographic LiDAR and bathymetric LiDAR. Topographic LiDAR is used for dry land surfaces. This type of data collection can be utilised to create DEM for base maps, flood modelling, urban planning, natural resource management, and others. The second type of airborne LiDAR is the bathymetric LiDAR which is water-penetrating, e.g. providing information on water depth. The data gathered from bathymetric LiDAR is extremely important, in particular to places located near the water surface, such as coast lines and river banks.

The high-resolution and accurate data obtained from LiDAR systems make them suitable for many applications. This is reflected by the increased use of LiDAR data. Furthermore, LiDAR data can be used in applications such as creating digital elevation model (DEM), as well as the digital terrain model (DTM), which usually has a rather high spatial resolution (e.g. metre) and vertical precision (e.g. sub-metre).

These applications make LiDAR a very powerful tool for topographic mapping and surveying. LiDAR data is also used in hydrological applications such as flood plain mapping and coastal engineering, as well as many more applications.

2.8 Using LiDAR DEM and GIS in flood studies

The advanced technology of GIS and the high-resolution LiDAR DEM has attracted many to use them in flood modelling studies such as (Betts 2002; Tsubaki and Fujita 2010; Huang et al. 2011; Sanders 2007; Turner et al. 2013; Xiaojun 1997; Hennecke 2004b; Hennecke 2004a; Thumerer, Jones, and Brown 2000; Gambolati, Teatini, and Gonella 2002; Viehhauser, Larsson, and Stålnacke 2006; Brivio 2002; Ashleigh et al. 2013; Shatnawi and Goodall 2010).

French (2003) confirmed that the topography representation obtained from LiDAR data is very close to the real representation of the topography. Also, he added that high-resolution LiDAR data helps to identify important and small terrain variations. As a result, allocating inundation areas becomes very accurate. The analysis by Haile and Rientjes (2005) revealed that the quality of the results is highly affected by the DEM resolution.

Haile and Rientjes (2005) agreed with French (2003) regarding the need for high-resolution data when modelling a flood in urban areas. Chen, Hill, and Urbano (2009) have also used a GIS based model for flood modelling in urban areas at the main campus of University of Memphis, United States. According to all the authors, it is very difficult to model floods in urban areas, due to limited availability of high-resolution topographic and hydrologic data, and the complexity of the built-up environment. Sole et al. (2008) used a digital surface model DTM (5 m resolution), obtained from high-resolution LiDAR data and global position systems (GPS data) when modelling river floods in Italy. Sole et al. (2008) concluded from their study that the high accuracy of the terrain representation helps to provide highly accurate representation of the flood zones with 5 m resolution.

Similarly, Mandlburger et al. (2009) used Digital Terrain Models (DTMs) from LiDAR for river flood modelling and they emphasised that the estimated flood flow and velocity can vary depending on the quality and accuracy of the data used.

Webster et al. (2004) used LiDAR data to model coastal flooding, due to sea level rise, on Prince Edward Island in Canada. They agreed with Sole et al. (2008) and Mandlburger et al. (2009) that DEMs, derived from LiDAR data, provide efficient and accurate information for flood modelling. Dowling, Alexanderson, and Möller (2013) acknowledged the high-resolution of DEM data derived from LiDAR, and confirmed that LiDAR data has the ability to provide an unprecedented level of information for the landscape. Schumann et al. (2008) indicated that DEMs play an important role in most of the environment modelling and disaster management studies. In this context, they compared DEMs from LiDAR with DEMs from the Shuttle Radar Topography Mission (STRM) and reported that DEMs from LiDAR provide more reliable and accurate results compared to the DEMs from STRM.

It can be seen from the above articles that GIS tools and LiDAR data have been widely used in environmental modelling, with particular focus on flood modelling. However, GIS and LiDAR, to the best of the author's knowledge, have never been applied to flood modelling on a property-by-property scale.

2.9 Using raster based analysis in flood modelling

The raster based modelling approach has recently become more important in flood studies due to the requirement for high accuracy, but also because of the simplicity of processing and representation. Horritt and Bates (2001) investigated the scaling properties of a raster based flood flow model. In their analysis, the model was tested using different resolutions varying between 10 m and 1000 m. The model was compared with satellite images for flooded areas and survey observations for flood wave travel time. Based on their analysis, the authors expected that the water level can be enhanced using high-resolution raster data, as given by DEMs.

Poulter and Halpin (2008) also conducted a study on raster modelling of coastal flooding due to sea-level rise. The authors used a DEM obtained from LiDAR information for coastal North Carolina, USA, to examine the consequences of horizontal resolution and its relationship to the extent and timing of flooding caused by sea level rise. They discovered that the rate and extent of flooding depends directly on two factors: horizontal resolution and assumptions made on hydrological connectivity.

Coveney et al. (2010) indicated that medium-resolution (30 to 100 m) DEMs, when modelling the risk of coastal flooding, are in common use. In their study, the authors used both post-processed and static Real Time Kinematic (RTK) dual-frequency GPS observations, as well as high-resolution Terrestrial Laser Scanning, and Digital Surface Model (DSM) information, to measure the magnitude. The spatial distribution of the elevation error, on a 10km coastal section, was estimated on a medium resolution photogrammetric DEM.

With the tendency to notice larger errors at the modelling stage, the results demonstrated that the DEM resolutions tested in this study are unsuitable for spatial modelling - especially for coastal inundation - and highlights the problems that may occur when such DEM datasets are used in coastal applications in different places.

2.10 Flood vulnerability index

In response to the growing threat of flood incidences, there is a high demand to develop enhanced methods to help decision makers in the field of flood management (Balica and Wright 2009). One type of methodology is an indicator based approach: Flood Vulnerability Index (FVI). Connor and Hiroki (2005) indicated an increase in scientific studies dealing with both the reasons leading to climate change and also the expectations of the world’s climate in the future. According to them, recent studies in the field have shown and examined the possible effects of climate change on human societies.

Based on the current climate change figures, Connor and Hiroki (2005) expect that the likelihood of flood will increase in the future. The authors worked on developing a method to help reduce the impact of flooding and mitigate the effect on human societies. In their study, the authors used multivariate analysis to develop a Flood Vulnerability Index (FVI). The input parameters used were:

(1) Total population in the flood area.
(2) TV penetration rate.
(3) Investment amount.
(4) Advancement rate.
(5) Population completing high school.
(6) Elderly population.
(7) Specific discharge.

Through this tool, a comparative analysis of flood vulnerability can be made between different basins. It also helps the potential user to determine the main reasons leading to the basin's vulnerability.

Since the potential effects of flooding are a combination of metrological, hydrological and socio-economic measures and countermeasure, key conceptual models of FVI are formed from these four components. Connor and Hiroki (2005) use multiple linear regression analysis to assess the possible damage when floods occur, and they categorise the damage into both human damage and economic damage. The results obtained from FVI are compared with available historical records, showing that FVI is affected by the characteristics of the flood basin - such as the meteorological, hydrological and social-economic characteristics - and potential damages are linked with sudden and unpredictable phenomena.

Balica and Wright (2010) noticed that current FVI uses 71 indicators (calculated and developed by the authors) in order to provide a clear and easy tool for the user, to use in flood assessment studies. They worked on reducing the complexity of the FVI to identify the most significant indicators and to make the FVI more accessible for many users.

To do this, the author used mathematical tools (a derivative and a correlation method) and a survey questionnaire. The methods were combined in order to reduce the number of indicators and select the most important. The methodology adopted in this research can be applied to different spatial scales, such as river basin, sub-catchment and urban areas. Also, it covers different flood vulnerability components, such as socio-economic, environmental, and physical.

The authors went on to expand the study (Balica, Wright, and Meulen 2012) and developed a FVI to be used and applied to coastal cities. One of the main objectives of the study was to make the Flood Vulnerability Index more understandable in the decision making process. The authors focused on developing a Coastal Cities Flood Vulnerability Index (CCFVI), taking into account three factors: exposure, susceptibility, and resilience to coastal flooding. In order to test the tool's performance in different environments, this study has been applied in nine different cities around the world.

The cities were chosen based on their size and physiographic setting. The tool developed works by assessing the FVI in the selected study area using three components: social-economic, hydro-geological, and politico-administrative. The tool classified the cities by giving them a number between 0 and 1, which reflected the flood vulnerability level (low to high). This then showed which city needed more investigation by decision makers. The authors used the above classification to compare the cities under current conditions and also to study the effects of climate change on the vulnerability of selected cities over a longer period (e.g. more than 10 years). The results showed that the tool gives general information about flood vulnerability and the possible impact of an adaptation solution. While many studies provide more regional VIs, a literature review revealed that few studies have assessed vulnerability on a property-by-property level.

Prakasa Rao, Murty, and Amminedu (2005) utilised GIS and remote sensing (RS) to estimate the vulnerability index of flooding in delta areas. This study was conducted in Andhra Pradesh, which is situated on the east coast of India. The cyclonic impact is assessed in delta regions using GIS and RS technology, and the methodology adopted in this study involved several steps; first, the area boundaries and the coastline were extracted from satellite imagery. Then a supervised classification technique was used for land use cover preparation. Several cyclone tracks, between 1990 and 1996, were also digitised and included in this study.

The population density map for each study area was made by using population data from the 2001 census. 10 km buffer zone maps were created from the cyclone track direction, and the terrain slope was derived from the topographic maps. Finally, the vulnerability index map was created using all the above mentioned parameters in a GIS environment. The outcome of this study showed that GIS and RS are suitable to be used in flood vulnerability assessment studies. Furthermore, the developed technique can be used in other areas with a high frequency of land falling cyclones. The study also indicated the feasibility of using similar indices for other natural disaster assessments.

2.11 Chapter summary

This chapter reviews some of the literature relevant to the development of a property-based flood GIS. The studies chosen were examined in terms of aims, objectives, the methods used and the study outcomes.

A number of papers concerning the impacts of sea level rise, and the possible consequences for people and built-up environments were also reviewed. This chapter also discussed the applications of LiDAR data and (GIS), as well as the advantages and disadvantages of using both technologies in flood modelling. It has been found that different case studies used a combination of GIS and LiDAR data in flood modelling. The results showed efficient performance and an accurate result, especially when generating DEMs from LiDAR data and when creating flood inundation.

The use of raster based analysis, and the possible impacts of the raster resolution on flood modelling, has also been reviewed. It has been shown that many studies have examined the relationship between the resolution of the raster data and the accuracy achieved using different resolutions. The results varied depending on different factors such as the topography of the study area, the purpose of the study and the level of details required. Many studies, however, concluded that high-resolution raster data is required for high-resolution flood modelling in low-lying areas, while the lower raster resolution can be used to give a general idea about the flood risk over regional areas. The use of vulnerability indices in flood modelling studies have also been covered, including the methodology adopted and the results obtained.

The next chapter will cover the first stage of the research. The theoretical part of the next chapter will discuss the causes of sea level rise and the methods used for the sea level estimations. The practical part will estimate sea levels from tide gauge measurements, the relationship between each tide gauge station within the study area, and the relationship between Fremantle tide gauge measurements and satellite altimetry measurements.

CHAPTER 3

MODELING FUTURE SEA LEVEL RISE

3.1 Introduction

The previous chapter covered general information in relation to the thesis topic and a review of the relevant literature to sea level rise and flood modelling. This chapter will discuss the causes of sea level rise and the methods used in sea level rise estimation. Sea level rise measurements from both tide gauge stations and satellite altimetry are gathered and analysed. Correlation analyses are undertaken between tide gauge measurements. Similarly, correlation analysis is performed between Fremantle tide gauge measurements and satellite altimetry measurements.

Sea level change is considered a major threat to human society. The worst case scenario would involve the melting of all land-based ice masses, most notably the Greenland and Antarctic ice sheets, due to climate change and associated global warming. In this instance, sea levels could potentially rise by up to 70 m. Such a scenario would cause many of the coastal regions in the world to be flooded, having a major impact on human society. Both the measuring of currents and the modelling of future global sea level change can provide significant and important information to study and mitigate this problem. This study is mostly concerned with relative sea level rise, the change of sea level with respect to a vertically changing land surface.

3.2 Causes of near-future sea level rise

Global sea level rise, defined as an increase in the volume of water in the global oceans, has many causes, relating to both natural changes and human activities (Bird 1993; Janin and Mandia 2012; Pugh 2004; Cazenave and Nerem 2004; Milliman and Haq 1996; McGuire 2013). Sea level varies over a large range of temporal and spatial scales, from very short term variations (e.g. in seconds, such as waves) to geological time scales (e.g. over thousands of years, such as glaciation cycles), and spatially, from localised to global changes (Pugh 2004).

Historical sea level records show that sea level began to rise at current rates from the middle of the 19th century (Jevrejeva et al. 2008; 1998). According to several studies, sea level rose by about 1.7 mm/year during the last century (Dawson and Spannagle 2009). According to the recent IPCC estimation, sea level will rise between 29 and 82 cm by the end of this century (IPCC 2013).

Douglas (1991) reported an average rise of global sea level of between 1.0 to 3.0 mm/yr over the 20th century based on long-term tide gauge records. Nakada and Inoue (2005) studied and analysed the causes and rates of sea level rise over the last two decades using the tide gauge records from seven different locations collected throughout the past 140 to 200 years. Their results showed an average rate of ~ 1.50 mm/yr for all study locations. Emery (1980) also used 247 tide gauge stations to analyse the global annual mean sea level. Based on his research, he discovered an approximate 3 mm rise per year over the past 40 years. In the following studies, some of the main causes of sea level rise are discussed:

- General overviews are given by, for example, Church et al. (2010), Cazenave and Nerem (2004), Janin and Mandia (2012), Solomon et al. (2007).
- Other studies identified and explained sea level variations as due to various causes (e.g. Nerem 1995; Milliman and Haq 1996; Solomon et al. 2007; Church et al. 2007; Pilkey 2009).
- The Intergovernmental Committee on Climate Change (IPCC) identified seven factors that lead to long-term sea level changes IPCC (2001).

    1. Changes in ocean processes.
    2. Melting of glaciers and ice caps.
    3. Melting of Greenland and Antarctic ice sheets.
    4. Interaction of ice sheets, sea level and the solid Earth.
    5. Changes in surface and ground water storage, and permafrost.
    6. Tectonic land movements.
    7. Changes in atmospheric pressure.

There are two main causes for sea level change: (1) steric change (thermal expansion; e.g. water expands as it warms) and (2) mass change (e.g. the addition or subtraction of water masses due to changes in the cryosphere or land hydrology) (Wigley 1987). Thermal expansion is considered one of the major contributors to 20th and 21st century sea level change (IPCC 2001). In the event of ocean warming, the density of ocean water decreases while keeping the same mass, thus resulting in an expansion of the ocean water volume. Based on ocean temperature data over the last few centuries, many studies have quantified recent steric contribution to sea level rise (Lombard et al. 2007; García et al. 2007; Ishii et al. 2006; Antonov, Levitus, and Boyer 2002).

The fourth IPCC assessment report (IPCC 2007) predicts that thermal expansion is a major cause of near-future sea level rise, contributing to sea level rise by approximately 55% to 70% over the 21st century. For the period between 1961 to 2003, thermal expansion has contributed about one quarter of the observed global sea level rise, while fresh water influx from melting ice is estimated to have contributed just under half of the observed global sea level rise (Solomon et al. 2007). More recent records (1996-2003) show that the combined contribution of thermal expansion and fresh water influx from ice melting is more than half of the observed global sea level rise (Solomon et al. 2007). Thermal expansion, in fact, plays a relatively minor role in recent sea level rise (see for example references in Baur et al. 2013). The exact contribution is rather disputed in the literature.

Apart from thermal expansion, another major cause of recent and future sea level rise is due to ocean water mass changes from melting land ice and also changes in land hydrology. With more than 160.000 glaciers, and approximately 70 ice caps around the world, melting ice has been reported as one of the main causes of recent and near-future sea level rise (Chuvieco 2008; Greve and Blatter 2009). This is because glaciers and ice caps are particularly sensitive to small temperature changes. Only a small change in global average temperature can cause a partial or total melt of these ice masses over short time periods (e.g. decades to centuries). The fresh water currently contained in the global glaciers and ice caps is equivalent to a global sea level rise of about 0.5 m.

The contribution of the world's glaciers to sea level rise for the period between 1961 to 1990 is estimated at approximately 0.25±0.10 mm/yr, or about 10% of global sea level rise (IPCC 2001). Looking further ahead (e.g. centuries to millennia), fresh water influx from melting ice sheets over Greenland and Antarctica will be another major cause of future sea level rise. For example, the combined fresh water currently contained in ice sheets over Greenland and Antarctica has the potential to raise global sea level by 70 m (Rignot and Thomas 2002; Alley et al. 2005). As a result, even a small change in ice volume can have a serious effect on global sea level.

Due to considerable differences in the climate conditions over the Greenland and Antarctic ice sheets, the ice mass balance is very different for each ice sheet (Warrick, Barrow, and Wigley 1993). For instance, over Antarctica, air temperatures are usually well below zero, so there is minimal runoff due to ice melt. The ice sheet mostly loses ice by discharge along ice shelves, e.g. ice calving. Over Greenland, on the other hand, summer temperatures are above zero, allowing for widespread melting and associated fresh water influx into the oceans. This is in addition to ice calving.

Mörner (1976) stated, sea level changes can also be the effect of mass changes in the Earth gravity field, displacing the mean ocean surface (e.g. geoid). Today, it is commonly modelled by the so called sea level equation.

$$S = N - U$$

Where S refers to the sea level variation, N refers to the change in the sea surface relative to the Earth's centre and U refers to the vertical crustal movement (e.g. Milne and Mitrovica 1996).

There are many potential causes of sea level variation, including the impact of human-induced climate change, which can directly affect both current and future sea level rise.

There are three major processes linked to climate change, which can directly impact on sea level:

(1) Ocean temperatures increase due to global warming (e.g. thermal expansion).
(2) An increase in world temperature, leading to melting of glaciers and ice caps.
(3) An increase in world temperature, resulting in the melting of the Greenland and Antarctic ice sheets (Church et al. 2007).

Today much attention is given to the human influence in global warming due to increased greenhouse gasses in the Earth's atmosphere. Rising sea level is often taken as a proxy for global change or alternatively greenhouse gas scenarios are used for the prediction of future global sea level rise (Pugh and Woodworth 2014). Sea level rise along a coast can be caused by vertical ground motion, such as subsidence due to ground water withdrawal (Orcutt 2012). In this case, extracted ground water causes the sediments of the aquifers to be combined and compressed by the mass of the overlying rock formations and artificial structures, such as buildings, leading to subsidence of the land surface.

Changes in the volume of water stored in the ground, and water in lakes and reservoirs on the Earth's surface, are considered important factors in present day sea level rise. These type of processes would change the surface properties and affect the runoff and evaporation rates (Bird 1993). Vertical tectonic movement is another source of apparent sea level change. The vertical movement of tectonic plates cause relative sea level changes along many coasts around the world (Bowen et al. 2014). The tectonic movement is defined as vertical and horizontal movement of the crust that is of non-glacio-isostatic origin. Horizontal land movement can occur due to glacio-isostatic adjustment, which is the slow visco-elastic response of the Earth's crust to loading and unloading by changing ice masses. Both vertical tectonic movements and glacio-isostatic adjustments are spatially very large scale movements and, as a result, sea level variations are not expected to be spatially uniform. However, this study is interested only in the vertical crustal motion. Tectonic movement also includes sporadic movements related to earthquakes.

Large proportions of the Earth are subject to tectonic movement, which lead to changes in the level between sea surface and land surface, often causing coastline recession (IPCC 2001).

3.3 Sea level observations

Today two main techniques are used to observe recent sea level changes: (1) tide gauge and (2) satellite altimetry. Tide gauges measure sea level relative to the Earth's surface (e.g. relative sea level change). Tide gauge observations have been used over the last two centuries to estimate mean sea level by long-term averaging of sea level changes. Satellite altimetry measures (absolute) sea level with respect to a geo-centric reference system (e.g. w.r.t. to the Earth's geo-centre). Tide gauge observations have a high temporal resolution but spatially have a rather sparse distribution along the world's coast lines. Satellite altimeter observations, on the other hand, have a low temporal resolution but good spatial resolution and coverage. Some tide gauge records cover several centuries (e.g. Amsterdam), while satellite altimetry extends only over the last few decades.

3.3.1 Tide gauge observations

A tide gauge observes sea level changes relative to the Earth's surface, which is subject to horizontal and vertical motion (cf. Figure 3.1). Tide gauge observations usually refer to a local land benchmark, from which vertical stability is monitored (e.g. through repeated GNSS observations) (Douglas, Kearney, and Leatherman 2001). General information about tide gauges are given by: (Pugh 2004; Committee on the National Requirements for Precision Geodetic Infrastructure, Committee on Seismology and Geodynamics, and National Research Council 2010; Tregoning and Rizos 2008; Valiron 2001). Historically, global, regional and local sea level variations are estimated from tide gauge records, some extending back over several centuries. Tide gauge records cover a large temporal variation, from short-term periodic and a-periodic variations (e.g. tides, storm surge, tsunami, etc.) to longer variations (e.g. seasonal and decadal) to very long-term variations (e.g. secular).

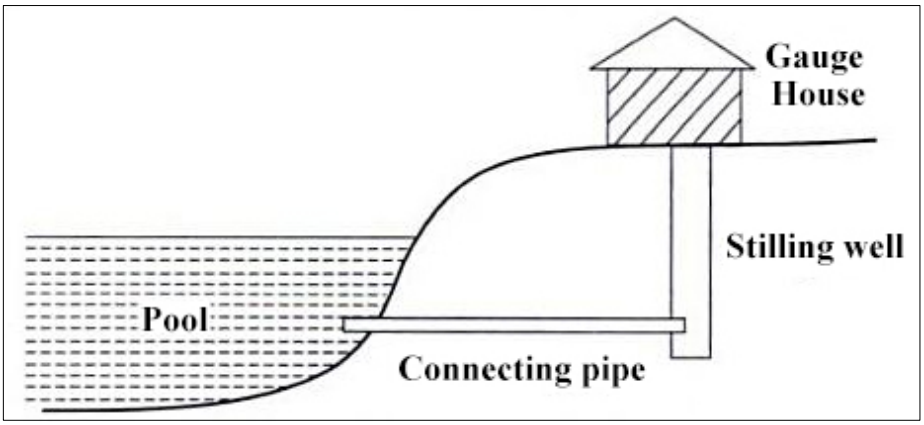

Figure 3.1 A typical stilling well tide gauge station (source: Duggal 2004).

Although tide gauge stations have a rather poor spatial distribution around the globe, they currently provide the only source for reliable, accurate, long-term (century-scale) sea level variation. Currently (in 2014), there are several thousand tide gauge stations installed around the world (The Permanent Service for Mean Sea Level (PSMSL) 1999). There are 291 tide gauge stations in the data holding of the Permanent Service for Mean Sea Level (PSMSL) with record lengths longer than 50 years, and there are 77 tide gauge stations with a life span of more than 100 years (Tamisiea et al. 2014). More than 80% of the global tide gauge networks are less than 60 years old. Long-term tide gauge measurements are provided mostly from locations in northern Europe and the United States. This means that global oceans are not uniformly sampled along all coastlines (Douglas, Kearney, and Leatherman 2001).

Importantly, tide gauge records with more than 50-60 years of data can provide very useful information about long-term sea level change. Tide gauge records covering more than 50 years are required in sea level estimation, so that spurious trends due to low-frequency variability can be eliminated (Douglas 1997; Scales et al. 1998). As Douglas (1991) stated, long-term sea level records are extremely important to identify potential acceleration in sea level rise.

In this regard, short-term tide gauge records are usually not suitable for the determination of long-term trends or accelerations. This is due to long-periodic fluctuations in sea level on local, regional, and global scales.

The longest tide gauge records are provided by stations based at Amsterdam, Brest, Sheerness, and Stockholm (for more than two centuries). These records can be used to provide some estimates on long-term sea level rise and acceleration (Allen and Pye 1992; Barnes 1993; Jevrejeva et al. 2008; Nationalkomitee der Bundesrepublik Deutschland für das Internationale Hydrologische Programm der UNESCO und das Operationelle Hydrologische Programm der WMO 1993; *Encyclopedia of Coastal Science* 2006). As an example, Figure 3.2 shows annual sea level variations at Amsterdam between 1700 and 1925.

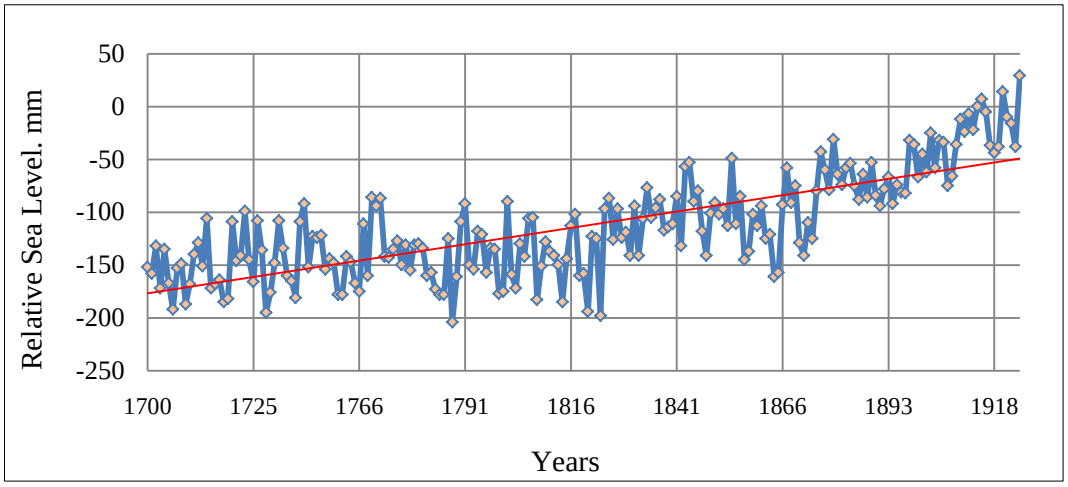

Figure 3.2 Amsterdam mean annual relative sea level (1700-1925) (source: PSMSL, www.psmsl.org).

The largest collection of sea level data and information is currently provided by the Permanent Service for Mean Sea Level (PSMSL), located in the Proudman Oceanographic Laboratory in the United Kingdom (see: www.psmsl.org). The PSMSL database maintains more than 4500 station-years of monthly and yearly averaged sea level records from almost 2000 tide gauge stations around the world.
The tide gauge observations are received from 200 national authorities (The Permanent Service for Mean Sea Level (PSMSL) 1999, 2013).

PSMSL provides monthly and annual averages of relative mean sea level data and are routinely analysed using time series analysis software such as CATS. The PSMSL data holding has been used by many to estimate long-term global and regional sea level rise. As an example, Table (3.1), published by IPCC (2001), provides references to several studies and their respective findings in terms of long-term sea level change rates.

Table 3.1 Recent estimation for sea level rise from tide gauges records. (source: (IPCC 2001)).

Reference	Region	Rate mm/yr
Gornitz and Lebedeff (1987)	Global	1.2
Peltier and Tushingham (1989, 1991)	Global	2.4
Trupin and Wahr (1990)	Global	1.7
Nakiboglu and Lambeck (1991)	Global	1.2
Douglas (1991)	Global	1.8
Shennan and Woodworth (1992)	NW Europe	1.0
Gornitz (1995)	N America E Coast	1.5
Mitrovica and Davis (1995), Davis and Mitrovica (1996)	Global far field (far from former ice sheets)	1.4
Davis and Mitrovica (1996)	N America E Coast	1.5
Peltier (1996)	N America E Coast	1.9
Peltier and Jiang (1997)	N America E Coast	2.0
Peltier and Jiang (1997)	Global	1.8
Douglas (1997)	Global	1.8
Lambeck et al. (1998)	Fennoscandia	1.1
Woodworth et al. (1999)	British Isles	1.0

Tide gauge observations have been used in sea level variation analysis for quite some time. However, there are two main problems associated with tide gauge records. The first problem is the poor spatial distribution of tide gauge stations along the world's coastlines. Being located along the coastline, tide gauge stations do not sample the open oceans (except at some island locations). The second issue is that tide gauge stations only observe sea level variations relative to a benchmark on land, which is subject to vertical movements at similar rates to the actual sea level signals (Douglas 1995). Both these disadvantages are in part eliminated by satellite altimeter observations (see next section).

3.3.2 Satellite altimetry observations

Another method of measuring sea level change is by satellite altimetry. The altimetry radar scans the sea surface and provides near-global sea level observations, which can also be taken as an approximate observation of the marine geoid. Because of this, satellite altimetry is a very efficient method for remotely mapping the ocean surface and marine geoid. Satellite altimetry has the ability to scan very large areas of the ocean in a very short period of time, and can supply highly detailed representations of the ocean's surface, in both time and space. Thus, satellite altimetry provides data of the sea surface with near-global coverage, high accuracy, reliability, temporal continuity, and homogeneity.

Satellite altimetry measurements are regarded as an independent alternative to in-situ techniques such as tide gauge observations (AVISO 2012). In addition, satellite altimetry measurements allow for spatially varying characteristics of the sea surface. General overviews about satellite altimetry are provided by: e.g. (Fu and Cazenave 2000; Seeber 2003; Douglas, Kearney, and Leatherman 2001; Vignudelli et al. 2011). Satellite altimetry measures the sea surface height by sending an electromagnetic pulse to the sea surface and measuring the two-way travel time of the reflected pulse. Satellite altimetry measures the sea level with respect to the Earth's geo-centre, e.g. given as heights above a reference ellipsoid. This is in contrast to tide gauge stations, which measure the sea level relative to the Earth's surface and is subject to vertical movements (Heliani et al. 2013).

The first satellite altimetry mission started in 1978 with the Seasat mission. It was quickly recognized as a great tool for global and regional sea level variation analyses. Today, the longest continuous satellite altimeter record (since 1992) is provided by the TOPEX/POSEIDON (T/P) mission and its follow-on mission Jason 1 and 2. In general, satellite altimetry measures the height and the characteristics of the ocean surface. Along with highly accurate satellite locations (cf. Figure 3.3) obtained from GPS positioning, the sea surface height is estimated through subtraction of the distance, between the satellite and sea surface (cf. Figure 3.3).

A satellite altimetry measurement does not provide direct measurement of the sea floor but it can be indirectly derived through the variation of gravity (Douglas, Kearney, and Leatherman 2001).

The T/P and follow-on Jason 1 and 2 missions are cooperative projects between the USA and France. The T/P satellite mission provided near-global observations of sea level between 1992 and 2005. Jason-1 and 2, launched in late 2001 as the successor to T/P, continued these records by providing an estimate of near-global mean sea level approximately every 10 days with an uncertainty of 3-4 mm (Boon et al. 2010). Researchers now have the opportunity to access this highly accurate data, which is useful for many different studies (Douglas, Kearney, and Leatherman 2001). Satellite altimetry measurements can be used for many applications in marine geodesy, oceanography, the Earth's crustal structure and global change studies. They can be used to measure sea level changes and develop and/or enhance accurate global geopotential models, the marine geoid, and gravity models (Shum, Ries, and Tapley 1995; Cheney et al. 1984).

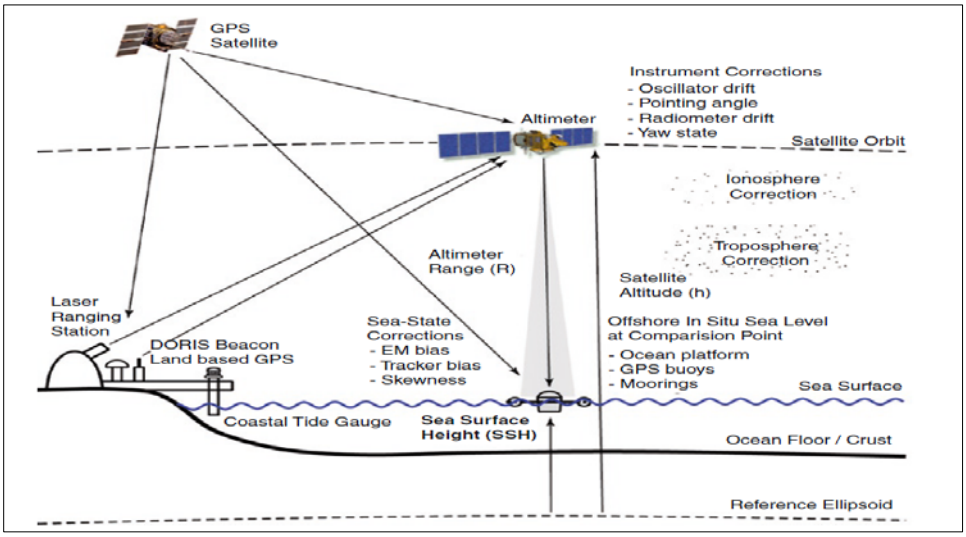

Figure 3.3 Satellite Altimetry (source: Vignudelli et al. 2011).

Since the launch of Seasat in 1978, satellite altimetry data has been used in many studies related to sea level change. For instance, Nerem (1995) estimated sea level change by using satellite altimetry data. According to his study, sea level change was +3.9 ±0.8 mm/yr during 1993 and 1994. Furthermore, Nerem (1995) stated that satellite altimetry shows enough precision to detect sea level changes caused by climate change. Vigo et al. (2011) also analysed a 16 year period of satellite altimetry data (1992-2008) to investigate sea level change in the Mediterranean Sea. They found satellite altimetry data was a great source of information from which to study and understand sea level variations.

Fenoglio and Tel (2010) studied the coastal and global mean sea level change over the period January 1993 to December 2008. A set of 267 stations were selected from the PSMSL, co-located under satellite altimetry tracks. Thus, a precise representation of coastal and global mean sea level rise was shown in this study. Furthermore, they showed that sea level rise can be significantly higher than the global average over short periods, while being slower over longer periods. The global trend for the period between 1993 and 2008 was estimated to be 2.9 ±0.5 mm/year. According to the authors, the variation in the trend is referred to as the inter-annual variation of coastal sea level, which partly averages out when calculating the global average.

3.4 Sea level rise impacts

Impacts of near-future sea level rise vary based on location and geomorphological properties of the coastal area affected. They also depend on a wide range of bio-physical features, socio-economic aspects, and human response. Probably the most important impact of sea level rise is related to physical changes in the coastal environments. These changes affect whether the coastal area, is used for industry, shipping, agriculture tourism, recreation or wild life conservation. The most serious physical changes due to sea level rise in low-lying coastal areas are: (1) inundation and land displacement in low-land and wetland areas; (2) coastal erosion; (3) increased vulnerability for flooding and storm surge damage; and (4) increased salinity of surface and ground water (Claussen et al. 2001).

With continued global warming expected in the future, sea level rise has become a serious threat to coastal areas around the globe. This will have a major socio-economic impact on today's society, as a large portion of the world's population lives in close proximity to the coastline (Dawson and Spannagle 2009).

Living near to the shoreline, however, has many advantages. It provides easy access to transportation, trade and recreation. Nevertheless, people living in these critical areas are very vulnerable to coastal flooding. Therefore, the major impact of sea level rise will be in countries where large parts of their land surfaces are a few metres from current mean sea level. This includes many of the mega-cities around the world.

Several low-lying tropical islands such as Kiribati, the Maldives, Tuvalu and the Marshall Islands are all very vulnerable to sea level rise. Furthermore, many of the highly populated countries, such as the Netherlands and Bangladesh, are also very vulnerable to sea level rise. It is anticipated that with a 1 m sea level rise, Bangladesh will lose about 20% of its land surface, and 70% of the population of the Netherlands will be affected by a similar rise in sea level (Dawson and Spannagle 2009).
These impacts will be even more exacerbated in the future with an expected population increase in low-lying coastal areas exposed to flooding.

Hoozemans, Pennekamp, and Rijkswaters (1993) estimated that more than 200 million people are living in coastal areas are vulnerable to flooding due to sea level rise. This population is projected to increase to 800 million by 2080. Furthermore, around half of the world's population lives in vulnerable areas between land and water, and 13 out of 20 of the world's largest cities, with a population of more than 5 million, are located within 10 m of current sea level (Church et al. 2007). It's reported that 30 of the major cities in the world are very vulnerable to a sea level rise of only 1 m, including the biggest financial cities in the world such as London, New York and Tokyo. Other vulnerable cities include Shanghai, Calcutta, Mumbai, Lagos, Bangkok and Amsterdam. For instance, in China, 11% of the total population (144 million people) are living within this critical zone (Dawson and Spannagle 2009).

The implications of sea level rise also extend to the properties located near to the shoreline. By 2100, it is estimated that the cumulative loss on coastal properties, based on a half metre sea level rise, ranges from around 20 billion to around 150 billion. This estimate doesn't include other consequences, such as the effects on wetland areas and recreation amenities (Claussen et al. 2001). The effects of sea level change range from household income and livelihoods, to social solidity, and to political stability. The amount of coastal infrastructure at risk, even with a small rise in sea level and storm surges, is substantial. (Dawson and Spannagle 2009).

It is well known that coastal areas generally have a large concentration of industry (such as oil refineries and factories) and port infrastructure, which is very important for national and international trade. For instance, London has properties in the value of about $220 billion located on its low-lying floodplain. The coastal infrastructure in Miami, United States, is worth around $900 billion, and it is also very vulnerable to sea level rise (Dawson and Spannagle 2009).

3.5 Extreme sea level events

Combined with sea level rise, extreme sea level events such as storm surges can significantly raise sea level, especially in low-lying coastal areas. Extreme sea level events are often caused by extreme weather conditions forcing sea level to be substantially higher than under normal/average conditions.

These extreme events have many causes such as heat wave, cyclones, storm surges, extreme cold snap, and others. Although these natural phenomena form part of the world climate, many experts expect that global warming will cause an increase in their intensity and occurrence in the near-future (Dawson and Spannagle 2009). Therefore, the increase in magnitude and frequency of storm surges, along with related extreme sea level rise, will result in increased risk for future populations, especially in coastal populations (cf. Table 3.2).

Extreme sea level events, due to weather and tsunami, can have significant socio-economic impacts. In particular; these events can have a huge impact on developing countries of the world and the poorest communities within these countries. This is because:

- The main sources of income in developing countries are from economic activities that are strongly sensitive to climate change, such as fisheries, agriculture, and tourism (Dawson and Spannagle 2009; Mertz et al. 2009).
- The number of low income households in developing countries are generally more affected and more likely to feel the negative impacts of climate change (Yohe and Tol 2002).
- Most of the developing countries are very limited in terms of technology and their economic capacity to adapt to the changes in the climate (Mertz et al. 2009).
- The majority of the population in developing countries is concentrated in the low- and mid-latitude areas, and they will experience more substantial negative socio-economic impacts of warming (at low to moderate levels) compared to those populations in higher latitudes (Dawson and Spannagle 2009).
- The cost of insurance cover, fund adaptation measures, and the availability of hospitals and relief services, are less likely to be secured by developing countries (Dawson and Spannagle 2009).

This section concentrates on extreme events that lead to extreme sea levels such as storm surges and tsunamis. The term storm surge refers to additional sea level rise caused by a severe storm and means unexpected and rather fast movement of water (NOAA 2014). During a storm surge, sea level can rise considerably due to water pile-up caused by strong onshore winds combined with low atmospheric pressure and heavy rain.

In Bangladesh, a quarter of a million people were killed due to a severe storm and surge event in 1970. Bangladesh has been very vulnerable to storm surges over the last 300 years, with severe storms hitting Bangladesh 23 times.

The extreme weather event in November 1970 claimed the lives of more than 250,000 people (cf. Table 3.2). Also, in New Orleans, United States, waves generated by Hurricane Katrina killed around 1000 people and created a loss of more than $US 100 billion. Table (3.2) provides some historical records for the estimated impact of storm surges in different parts of the world. As can be seen from Table (3.2), the highest sea level observed due to a storm surge was in Bangladesh in 1970 when sea level rose by 9 m. The second highest sea level rise was recorded in India in 1999 when sea level rose about 7-8 m, killing around 10,000 people.

Common examples of these natural phenomena are freak tides, storm tides, and tidal waves. Moreover, there are both positive and negative surges. When weather factors raise the sea level, it is a positive surge; and when the sea level decreases, it is a negative surge. Positive surges can be further intensified during high tide and through increased wave activity. This often results in severe coastal flooding and damage.

Negative surges can further be intensified during low tide and pose a potential risk for safe navigation (Pugh 2004). Usually, storm surges are linked with extreme coastal erosion, potentially causing considerable geomorphologic changes over a short period of time.

Table 3.2 Estimated impact of some historical surge events (source Pugh 2004).

Date	Region	Maximum surge level above MSL (m)	Lives lost
September 1900	Galveston, Texas	4.5	6,000
September 1928	Lake Okeechobee, Florida	2.5	1,800
September 1938	New England	3.5	600
February 1953	Southern North Sea	3.0	2,000
March 1962	Atlantic Coast, USA	2.0	32
August 1969	Mississippi, USA	7.0	256
November 1970	Bangladesh	9.0	250,000
November 1978	Sir Lanka/ Tamilnadu	4.0	373
November 1988	Bangladesh	4.4	5,708
April 1992	Chittagong, Bangladesh	4-8	150,000
August 1992	Miami, Florida	5.1	50
October 1999	Orissa, India	7-8	10,000

Changes in weather can affect sea level in two different ways. The first impact is caused when the variation in atmospheric pressure causes a vertical movement of the sea surface. This is usually termed as the inverse barometric effect (e.g. 1 cm per 1 mbar pressure change) (Ikeda 1995; Farmer and Cook 2013). The second impact is caused by forces resulting from wind drag at the water surface (Pugh 2004). Apart from storm surges, sea level rise can be influenced by other natural processes such as tsunamis. Tsunamis are waves caused by seismic events. The word tsunami comes from the Japanese language and means “harbour wave”, and often occur near to Japanese coastlines.

Tsunamis are also known as tidal waves or seismic waves (Pugh 2004). This natural phenomenon causes a fluctuation in sea level, which is observed along the coast of the affected area. There is no relation between tsunamis and tidal waves because tsunamis are not of astronomical origin and lack the regularity related to tides (Pugh 2004). However, tsunamis are not always linked to seismic activities and can also be caused by landslides into the sea, as well as seismic and sub-marine slumping. Tsunamis can have significant consequences for coastal areas and marine ecosystems. The waves generated by tsunamis can cause severe coastal flooding, resulting in disastrous consequences for both built-up and natural environments. Post tsunami surveys, to evaluate the effects of tsunamis on offshore and inshore areas, revealed huge ecological damage (Joseph 2011).

3.6 Sea Level Variability in the Study Area

The main aim of this study is to examine the effects of coastal flooding on a property-by-property level. This section focuses on estimating future sea level rise, in order to provide reasonable values, and to project potential flooding scenarios, for the South-West coast of Western Australia.

3.6.1 General

Mean sea level (MSL) is defined as the mean height of the sea surface, usually compared to a local benchmark and averaged over a given time period (IPCC 2001). Mean sea level can be calculated from tide gauge or satellite altimetry measurements by averaging over a long period, such as a month, year or over 18.6-years (the lunar nodal cycle). Averaging the tide gauge records or satellite altimetry data over long periods removes all short-term variations, such as waves, storm surge effects, seasonal variations, and tides. Usually, mean sea level is determined based on data that covers at least one year, thus eliminating the often rather strong seasonal cycle. However, to eliminate other long-term changes, lasting longer than one year, such as air pressure, prevailing winds, and long-term tidal changes, longer records are required (Pugh 2004).

Various methods can be used to remove short-term variations in MSL change estimates. A common way to do so is to build daily, monthly, and yearly averages. Many national authorities around the world use this technique to provide monthly and yearly sea level data based on higher frequency tide gauge observations (e.g. minutes to hours). The same technique can be applied to satellite altimeter data, although the original observation intervals are weeks to months.

3.6.2 Sea level change in Western Australia

Projecting future sea level variation is a complex task. However, estimating these changes has, in recent times, been highly improved. It can now be done by reviewing the historical changes of sea level and projecting the future trend. In this regard, four tide gauge stations have been used, located at: Fremantle, Hillarys Boat Harbour, Bunbury, and Geraldton (cf. Figure 3.4). However, as can be seen in Table (3.3), apart from the Fremantle tide gauge station, all of the other tide gauge stations have rather short-term records (less than 50 years long).

Due to the importance of removing long-term variations in MSL, and MSL change estimates, the Fremantle tide gauge station has been used as key station for this study. This is because it has longer-term records with near-continuous data starting in 1897, and continuing to the present day with only a few gaps in data, primarily in the early years. The Fremantle tide gauge station provides the longest and most complete record in the southern hemisphere. Only Sydney has a longer record but it is not as complete (73% complete) as the record from Fremantle tide.

The remaining tide gauge stations are used to study the relationship between tide gauge records in the study area and the possibility of using them to bridge gaps in tide gauge records. The relationship between tide gauge records is mainly studied through correlation analysis, which also includes satellite altimetry data within the study area.

Table 3.3 Tide gauge stations used in the study.

Station Name	Operation since (year)	Time span (Year)	Minimum sea level (m)	Maximum sea level (m)	Mean sea level (m)	Standard deviation (m)
Geraldton	1963	47	-0.306	1.716	0.571	0.2373
Bunbury	1963	47	-0.277	2.43	0.591	0.2359
Fremantle	1897	113	-0.100	1.947	0.698	0.2227
Hillarys	1991	20	-0.143	1.916	0.678	0.233

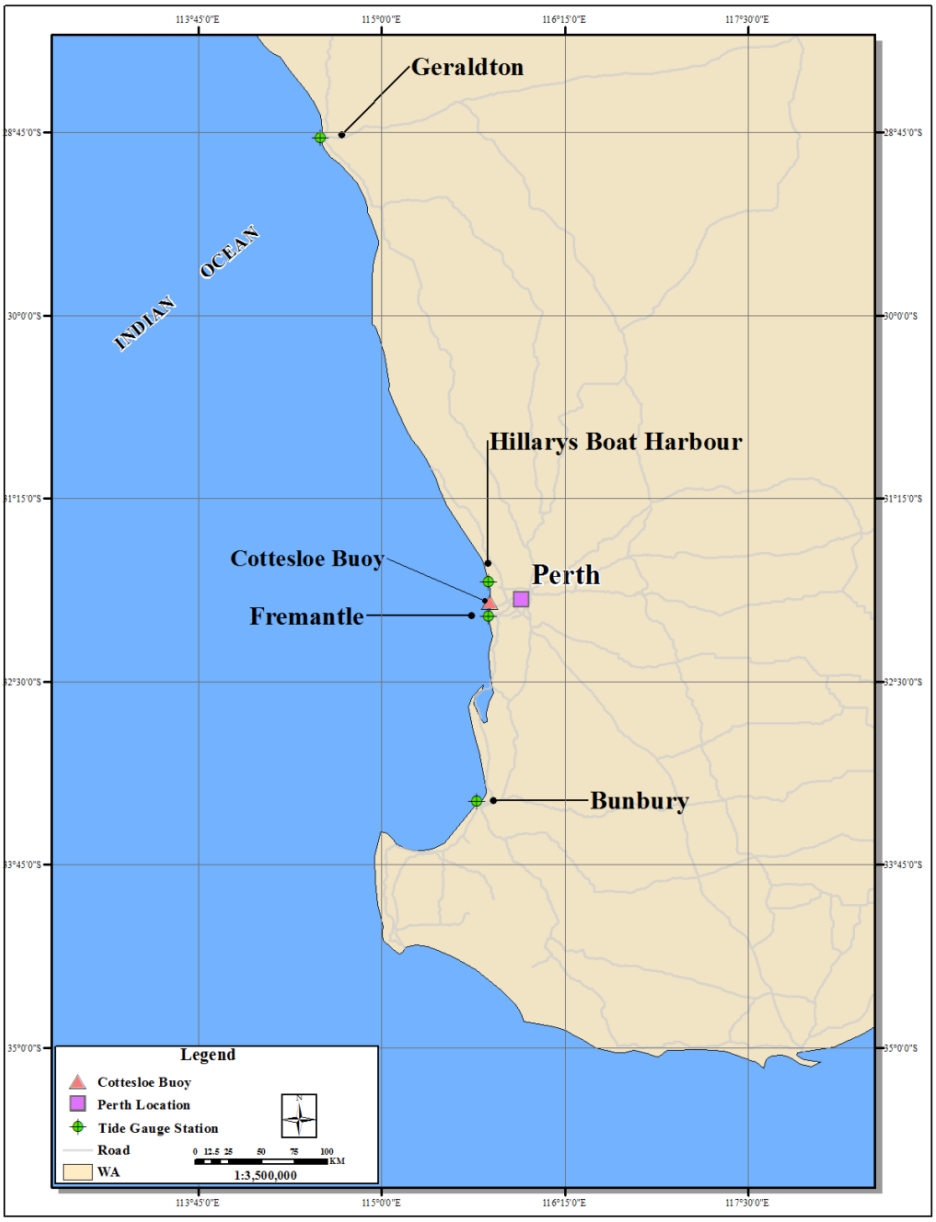

Figure 3.4 Locations of the tide gauge stations used in the study.

3.6.3 Quantifying sea level change in the study area

Tide gauge data is provided by the Australian Baseline Project through the Australian Bureau of Meteorology (http://www.bom.gov.au), and managed and run by the National Tide Centre (NTC). The main aim of this project is to provide information regarding sea level changes by monitoring the Australian coast (BOM 2012). The data has been obtained as monthly averages from the Bureau of Meteorology's website in the form of text files (*.txt). The data contains information on the month and year in which the observations have been recorded, as well as the minimum, maximum, mean, and the standard deviation for each month.

In order to eliminate seasonal effects, yearly averages have been built from the monthly averages. In order to get a better understanding of the behaviour of MSL in the study area, the monthly and yearly mean sea levels have been plotted for visual inspection (cf. Figures 3.5 to 3.16).

3.6.3.1 Sea level change at the Fremantle tide gauge station

In this study, the Fremantle tide gauge station is used to provide information on long-term sea level change for the study area. The tide gauge is located at 32° 04´ North 115° 44´ East (cf. Figure 3.4) and started monitoring the sea level in 1897. It has more than 115 years of observation from which yearly and monthly sea level records are available (cf. Figures 3.5 and 3.6). However, there are some data gaps during the period 1899 – 1942. Data gaps are present in the years 1899, 1902, 1907, 1910, 1913, 1926 and 1942 (as can be seen in Figure 3.5) for the monthly sea level average. Since 1942, the tide gauge has been in continuous operation with no data gaps, right up until the present day. Overall, the completeness of the records is 93%.

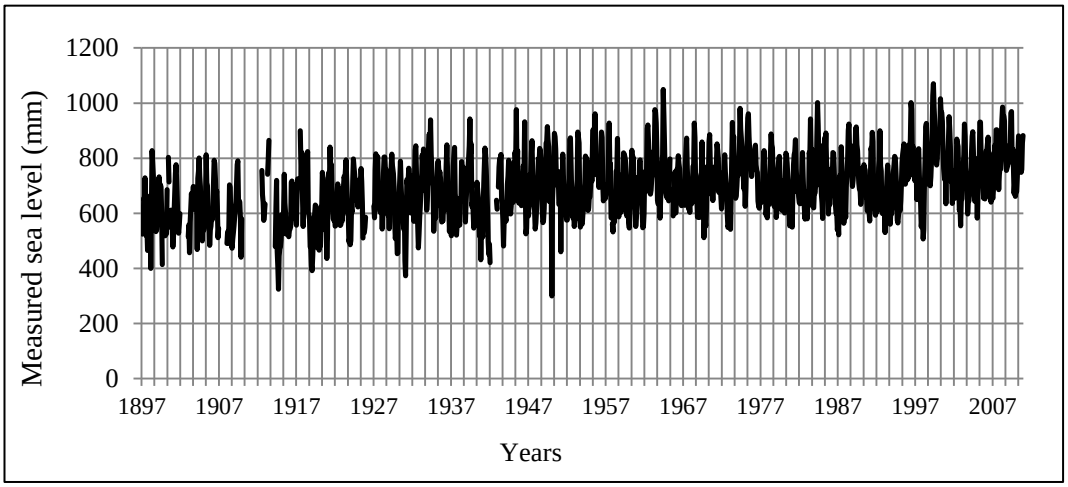

Figure 3.5 Monthly average sea level at Fremantle from 1897 to 2010.

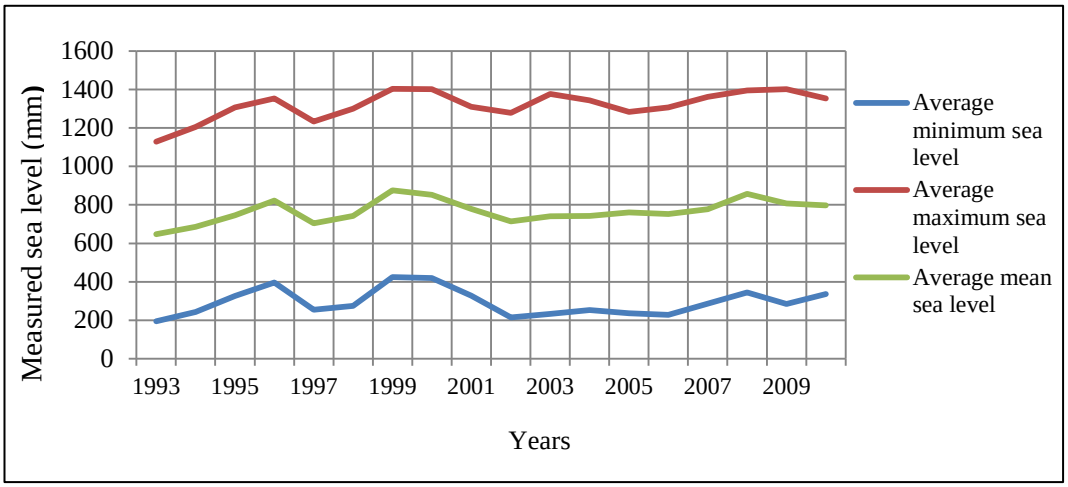

Figure 3.6 Yearly average sea level at Fremantle from 1993 to 2010.

In order to compare the results obtained from the Fremantle tide gauge with other tide gauge stations in the study area, only the 18 year record between 1993 and 2010 (cf. Figure 3.6) has been considered. This is a common data period to all stations and has no gaps (cf. Figure 3.6). The linear trend for the Fremantle tide gauge has been derived for the above period by using the Least Squares Method, which results in an estimate of 5 mm/yr with a coefficient of determination R^2 of 0.19. Based on this linear trend estimate, linear sea level changes over the next century (2010 to 2100) will be 0.45 m.

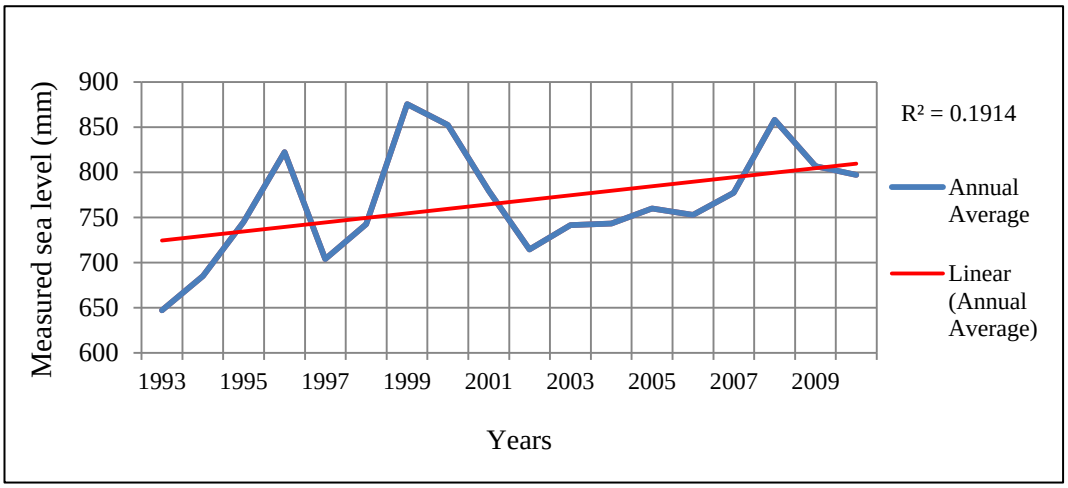

Figure 3.7 Linear sea level trend at Fremantle from 1993 to 2010.

3.6.3.2 Sea level change at the Geraldton tide gauge station

The Geraldton tide gauge station has been monitoring sea level in Western Australia from 1963 to the present. It covers the northern part of the study area and is located at 28° 47´ North 114° 35´ East, approximately 400 km north of Fremantle. The data obtained from the Geraldton tide gauge has a gap for the period between 1963 and 1965 (cf. Figure 3.9). However, since 1966, the record has no gaps until the present. For the purpose of comparing the record with other tide gauge stations, only the data between 1993 and 2010 is used (cf. Figures 3.8 and 3.9).

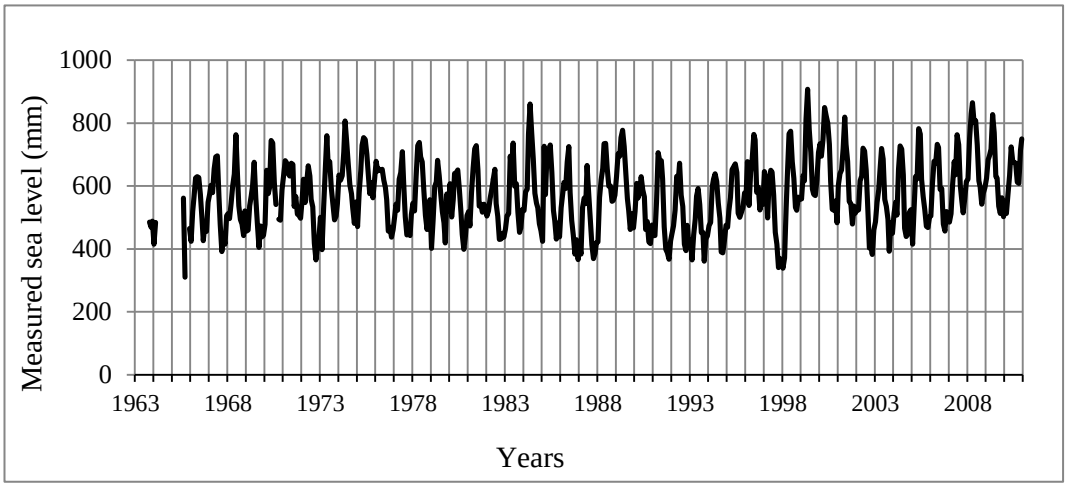

Figure 3.8 Monthly average sea level at Geraldton from 1963 to 2010.

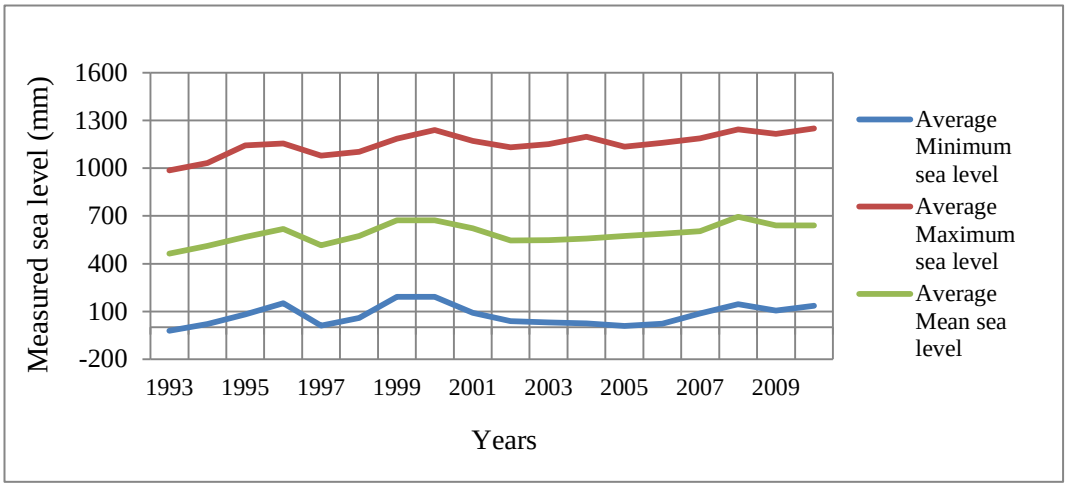

Figure 3.9 Yearly average sea level at Geraldton from 1993 to 2010.

The linear trend for the Geraldton tide gauge station has been estimated to 6.2 mm/yr with a coefficient of determination R^2 of 0.289. Based on this linear trend estimate, linear sea level change over the next century (2010 to 2100) will be 0.56 m (cf. Figure 3.10).

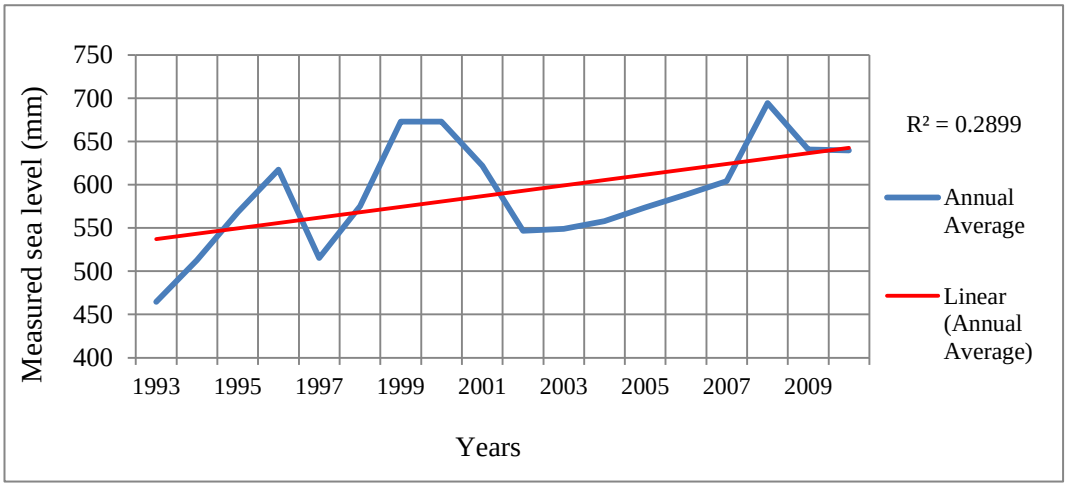

Figure 3.10 Linear sea level trend at Geraldton from 1993 to 2010.

3.6.3.3 Sea level change at the Bunbury tide gauge

The Bunbury tide gauge station is located at the southern end of the study area. The tide gauge is located 33º 19´ North 115º 38´ East, approximately 200 km south of Fremantle. It has been operating and monitoring sea level from 1963 until the present. The records from this tide gauge have a long gap between 1963 and 1965, one month gaps in the years 1970, 1976 and 1988, and a gap of one year in 1987. Since 1989, the tide gauge data has been continuous without any gaps until the present (cf. Figures 3.11 and 3.12).

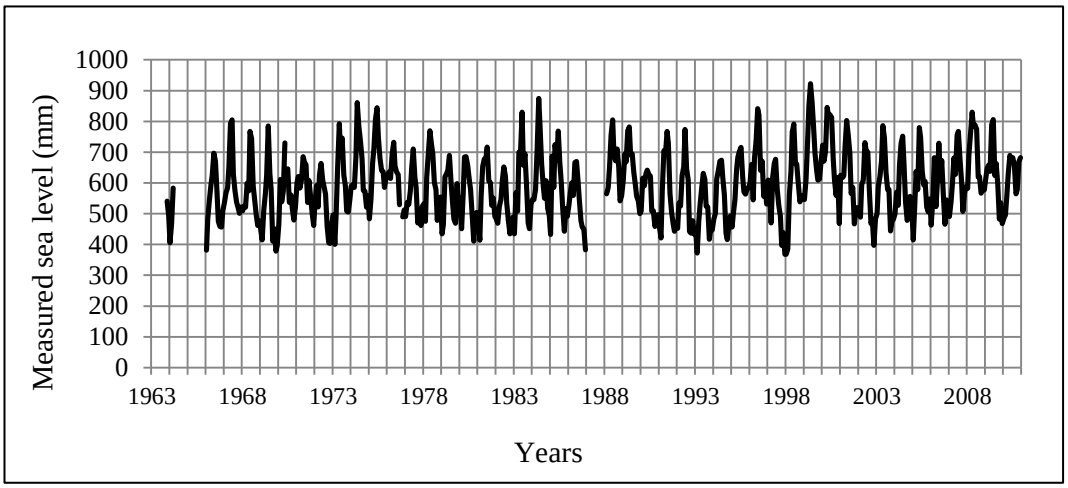

Figure 3.11 Monthly average sea level at Bunbury from 1963 to 2010.

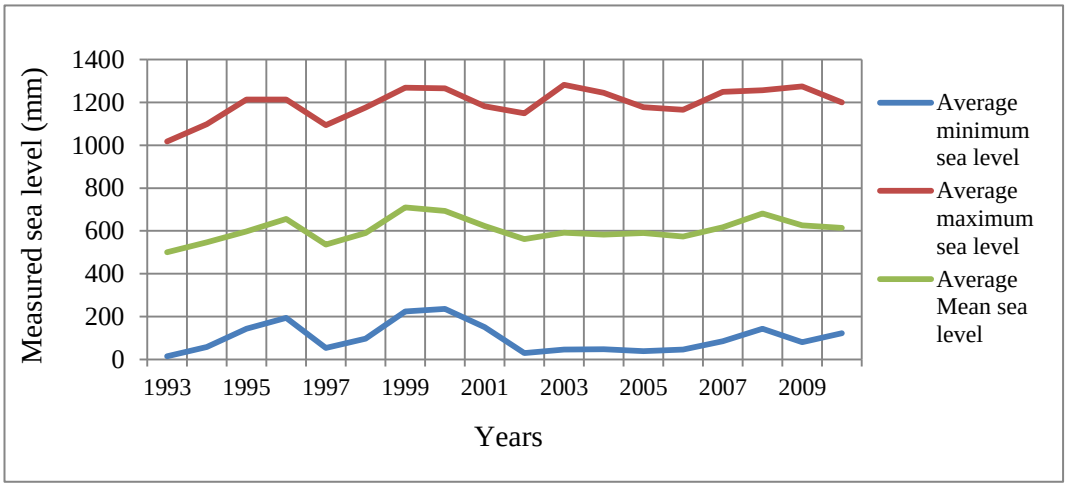

Figure 3.12 Yearly average sea level at Bunbury from 1993 to 2010.

The linear trend for the Bunbury tide gauge station has been estimated to 3.2 mm/yr with a coefficient of determination R^2 of 0.097. Based on this linear trend estimate, linear sea level change over the next century (2010 to 2100) will be 0.29 m (cf. Figure 3.13).

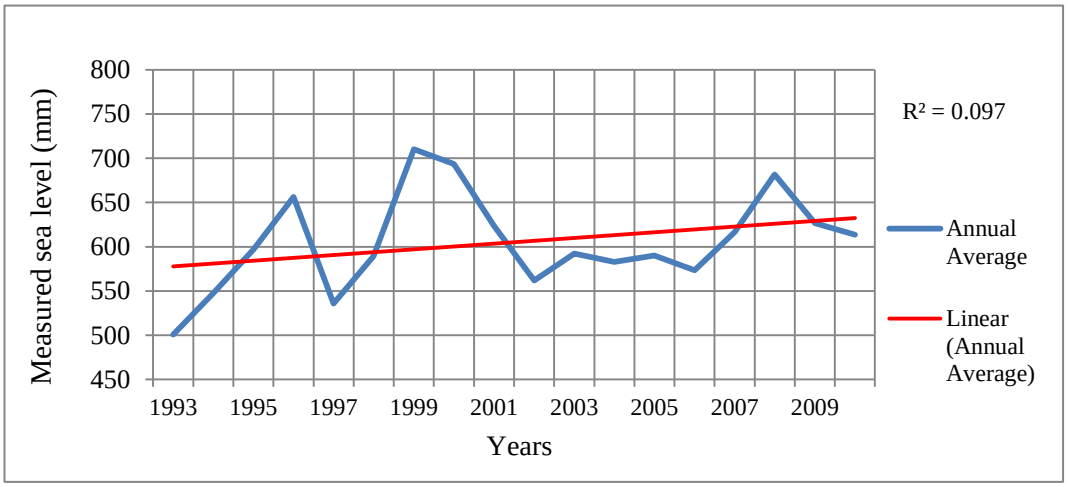

Figure 3.13 Linear sea level trend at Bunbury from 1993 to 2010.

3.6.3.4 Sea level change at the Hillarys Boat Harbour tide gauge

The Hillarys Boat Harbour tide gauge is located at -31° 49' North and 115° 44' East, approximately 20 km north of Fremantle. The Hillarys tide gauge is operated and managed by The National Tidal Centre and has been monitoring sea level since December 1991. It is the most recently activated tide gauge station used in the study and currently has only about 23 years of data, although without any data gaps. As the station started operating in late 1991, the records used in this study are from 1993 to 2010 (cf. Figures 3.14 and 3.15).

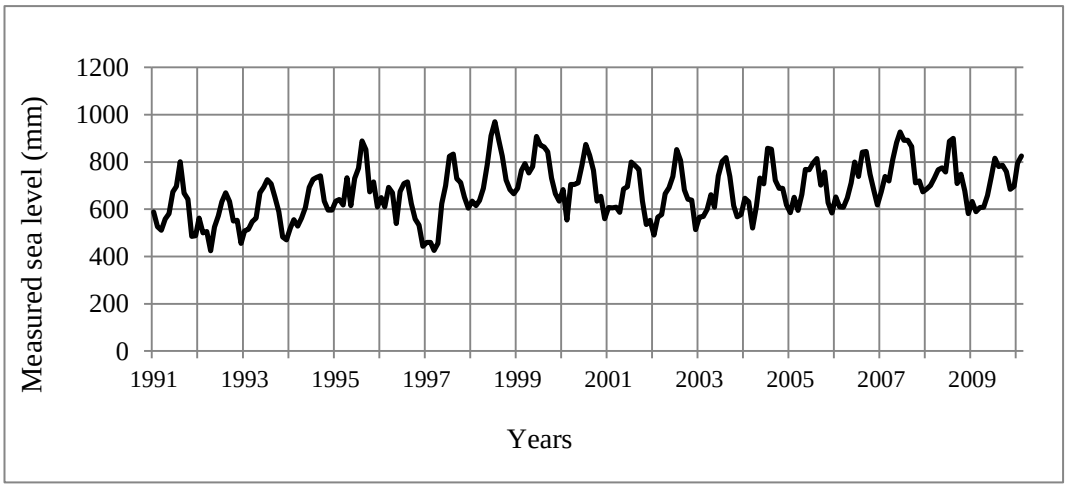

Figure 3.14 Monthly average sea level at Hillarys from 1991 to 2010.

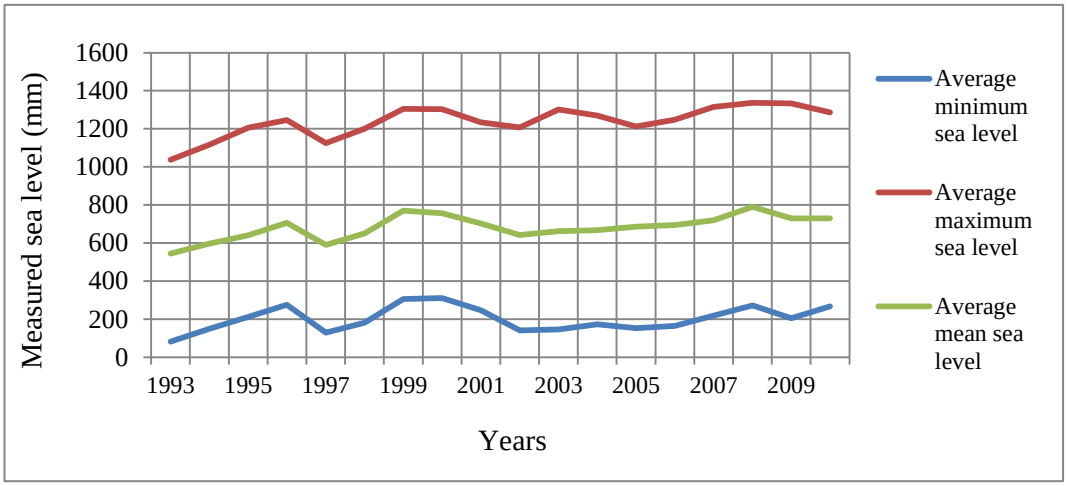

Figure 3.15 Yearly average sea level at Hillarys from 1993 to 2010.

The linear trend for the Hillarys Boat Harbour tide gauge station has been estimated to 7.78 mm/yr with a coefficient of determination R^2 of 0.41. Based on the linear trend estimate, sea level change over the next century (e.g. 2010 to 2100) will be 0.70 m (cf. Figure 3.16).

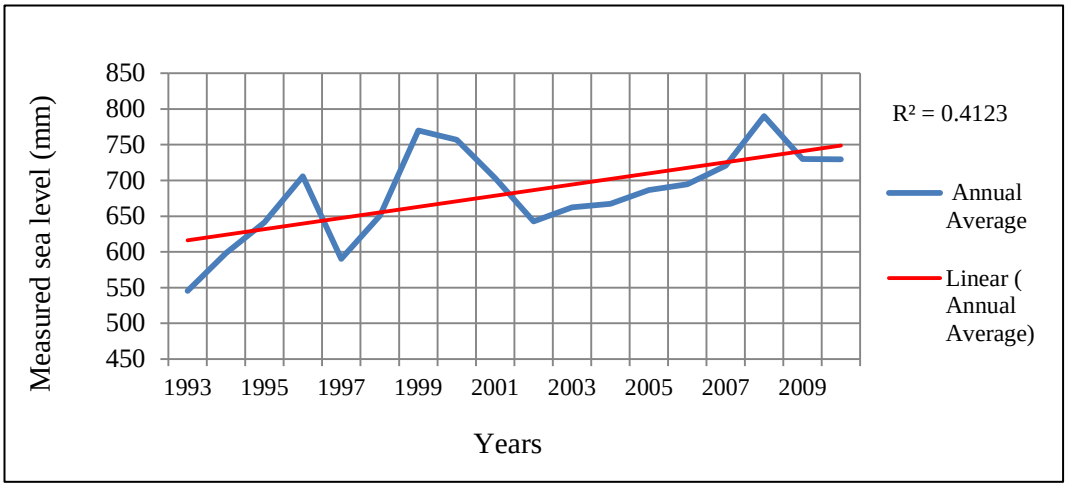

Figure 3.16 Linear sea level trend at Hillarys Boat Harbour from 1993 to 2010.

3.6.4 Quantifying short- and long-term sea level variability

Apart from long-term sea level changes (cf. chapter 3.6.3), many other factors influence sea level on short- to long-term time scales (e.g. seconds to decades). Common short-term variations are caused by surface waves, tide, storm and surges, and tsunamis (e.g. seconds to days) while long-term variations are caused by seasonal changes (e.g. Leeuwin Current in Western Australia), and inter annual and decadal changes (e.g. ENSO). Decadal or longer variations are of particular interest for the projection of future sea level scenarios based on linear trend estimates (cf. chapter 3.6.5).

Tides change sea level mostly on a sub-daily to daily basis. Based on the gravitational influence of moon, sun and, to a much lesser extent, other planets, tide signals change considerably depending on location (e.g. Pugh 2004). For instance, in the deep ocean, the tidal signal is usually only a few tens of centimetres. However, in some coastal regions, they can build up to several metres, and in extreme cases, 10 to 15 metres (e.g. Bristol Channel or Australian North-West Shelf). The highest astronomical tide at Fremantle is about 0.8 m above MSL, and the maximum wave height observed is 3.24 m (cf. Table 3.5).

Surface waves lead to very short-term changes in the range of seconds. Waves are usually much smaller over the deep oceans and can build up in shallow water. As waves get close to the shoreline, they usually break when encountering shallow water. This natural process results in a decrease of the wave height and energy. The further a wave breaks from the shoreline (e.g. well offshore), the smaller and less intensive are the waves that reach the shore. In contrast, in cases of deep water near to the shoreline, waves can travel very near to the shoreline before breaking. In this instance, waves can be larger and stronger closer to the coast. Moreover, the short term variability in sea level occurs when the lost energy from the breaking wave is converted into a shoreward momentum flux, which leads to a rise in sea level near the coastline (Thorpe 2007).

In order to gain a better understanding of wave behaviour within the study area, half hourly wave data has been analysed for the period between May 2007 and March 2012. This data has been observed at the Cottesloe buoy (cf. Figure 3.4) and the data includes information regarding wave height, wave period and the direction of the wave. Monthly and yearly averages are calculated from the daily records (cf. Figure 3.17). Some wave data is missing in 2007 and 2008 but after that, the data record is continuous without any gaps until March 2012. Any trends in the data have been estimated and used for projections to the year 2100. The maximum wave height recorded was on 12 July 2010 at 6:46 am. The wave height was 3.24 m and it lasted for 14.29 seconds. The average wave height has been estimated at 0.90 m (cf. Figure 3.17).

Table (3.4) shows the maximum sea level recorded at Fremantle of almost 2 m. The value represents the combination of a storm surge and high tide. Compared to MSL of about 0.6 m at Fremantle, the combined effect results in a sea level rise of 1.4 m, which coincides approximately with the maximum estimates in Table (3.5) (e.g. 0.8 m + 0.8m = 1.6 m ~ 1.4 m).

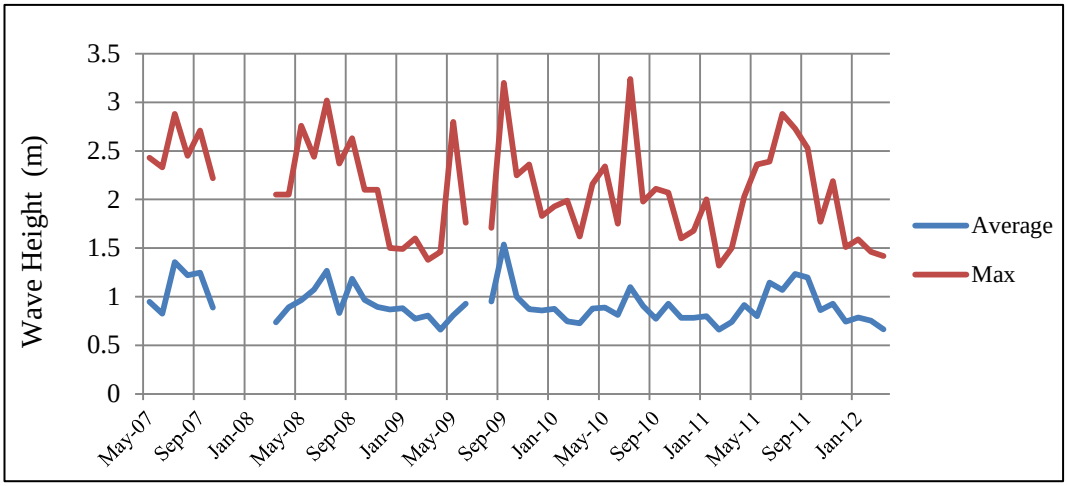

Figure 3.17 Monthly wave heights at Cottesloe buoy from 2007 to 2012.

Table 3.4 Highest water levels recorded at Fremantle 1897–2004 (source: Pattiaratchi & Eliot, 2005).

Date	Sea Level
16-May-2003	1.98 m
9-May-2004	1.90 m
18-May-2009	1.87 m
10-Jun-1956	1.86 m
20-Sep-1988	1.85 m

Table 3.5 Major processes influencing sea level variability along the southwest WA coastline (source: Pattiaratchi & Eliot, 2005).

Time scale	Short term Processes	Maximum amplitude
Seconds	Wave activity	3.24 m
12-24 hours	Astronomical tide	0.80 m
1-10 days	Storm surge	0.80 m
Seasonal	Leeuwin Current	0.30 m
Inter-annual	ENSO	0.30 m

Sea level can be affected by seasonal changes, such as the warming and cooling of ocean water or the change in ocean currents (e.g. Leeuwin Current in Western Australia). As an example for the study area, Figures 3.18 and 3.19 illustrate the seasonal variation at Geraldton and Fremantle tide gauge stations. The plots are obtained by averaging all monthly values for each tide gauge station. In the study area, the magnitude of seasonal variation is about 0.3 m (cf. Figures 3.18 and 2.19 and Table 3.5; see also Pattiaratchi & Eliot, 2005).

As shown in Figures (3.18 and 3.19), seasonal variations in Western Australia result in an increased sea level in winter, especially during the period between April and July. The sea level decreases during summer, especially during the period between September and December.

Long-term changes can be caused by long-term tide signals (e.g. 18.6 years based on the revolution of the lunar node) and climate variations such as the El Niño - Southern Oscillation (ENSO). Pattiaratchi & Eliot (2005) estimate these long-term changes at a magnitude of 0.3 m and for periods of years to several decades.

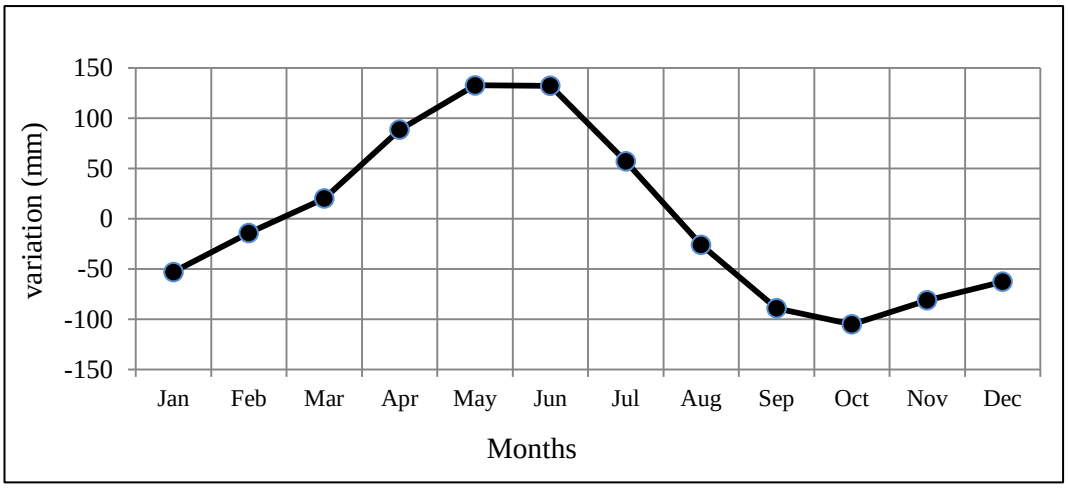

Figure 3.18 Geraldton monthly averaged water level variation (1966-2010).

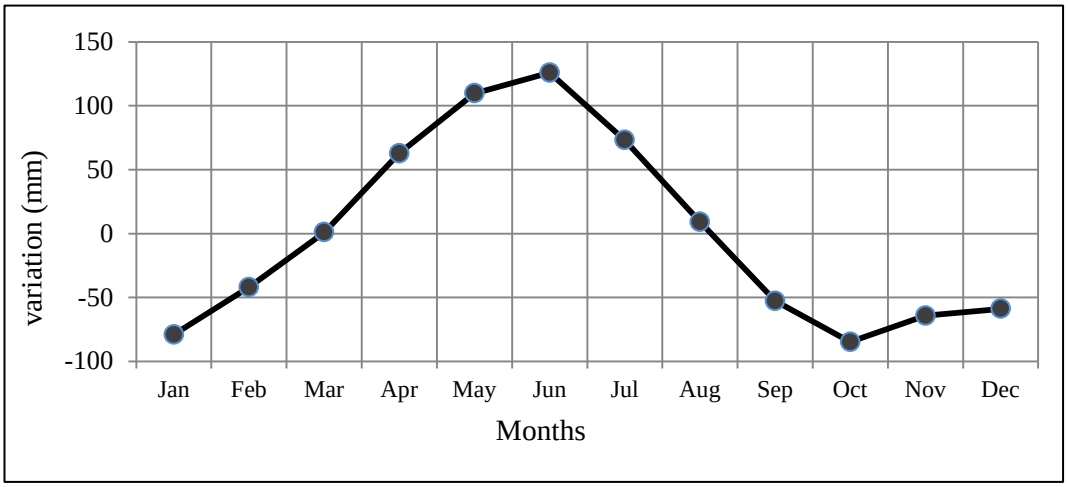

Figure 3.19 Fremantle monthly averaged water level variation (1915-2010).

Tsunami is another cause of short term sea level changes, with similar periods to storm surges. Tsunamis are defined as high water waves, generated from some form of geological activity, such as seismic activity, under water volcanoes, and submarine landslides (Shetye 2005). Most tsunamis form large earthquakes move in wave trains towards the coast. These waves consist of large waves in deep water, having amplitudes of less than 0.4 metres in deep oceans (Pugh 2004), although these can build up considerably in shallow water.

The wave periods for tsunami range between 100 to 2000 seconds (1.6-33 minutes); this is known as the tsunami window (Bryant 2014). Tsunami waves travel at an approximate speed of 600-900 km per hour in the deepest part of the ocean, slowing down in shallow waters (e.g. continental shelf) to speeds of 100 to 300 km per hour (Bryant 2008). In recent history, Australia has experienced many tsunami events. Since 1886, 43 tsunami events have been reported in Australia. The major source of tsunami events comes from the Alpine fault located on the west coast of the southern island of New Zealand, and also from the Sunda Arc, south of the Indonesian islands (Bryant 2014). The Alpine fault can cause an earthquake with a magnitude of up to 8.0 degrees on the Richter scale. The corresponding tsunami can arrive at Sydney within 2 hours (Bryant 2008).

On 10 May 1877, one of the largest tsunamis in history was recorded at the Sydney tide gauge, (after the Arica earthquake in Chile) with an amplitude of 1.07 metres. Additionally, a run-up of 4.5 metres above mean sea level was recorded on 22 May 1960, following the Chilean tsunami. However, the largest run-up ever recorded in Australia was in Cape Leveque, Western Australia on 19 August 1977 at a height of 6 metres (Bryant 2008).

The Australian Northwest coast is more vulnerable to tsunami events, due to the occurrence of many earthquakes along the Sunda Arc, south of the Indonesian islands (Burbidge et al. 2008). The tide gauges located at Port Hedland and Dampier have recorded waves of 1.5 metres and 2.5 metres in height. The same area was struck by a tsunami on 3 June 1994 with a run-up of 4 metres. Furthermore, Geraldton was hit by a Tsunami in 1883, due to the Krakatoa eruption, which resulted in a run-up of 2.5 metres (Bryant 2008).

The worst tsunami, however, was recorded on Boxing Day 2004 and was generated from an oceanic earthquake close to the Indonesian islands. The earthquake was recorded as a 9 on the Richter scale, impacting the whole coast of Western Australia with significant wave heights of 1.75 m (recorded at the Bunbury tide gauge). This event resulted in one of the worst tsunamis in recent history with more than 270,000 people killed and millions of coastline residents from 11 countries becoming homeless. However, it had relatively minimal effects on Western Australia (Cummins, Kong, and Satake 2009) (cf. Table 3.6).

Table 3.6 Records of tsunamis affecting Western Australia (adapted from (Bureau of Meteorology 2012) (http://www.bom.gov.au).

Date	Source	Comments
15/8/1868	North Chile	
27/8/1883	Indonesia	Result of Krakatoa eruption
6/1/1885	Unknown	
19/8/1977	Sunda Islands	Land inundation reported at Cape Leveque, Dampier and Port Sampson
3/6/ 1994	Java	Fish, rocks, and coral carried two to three hundred metres inland along parts of the coastline near the Northwest Cape.
26/12 2004	Sumatra	35 people rescued from rip currents, boats damaged in marinas (especially in WA, but also including as far as Tasmania), some limited and localised inundation of immediate foreshores in a small number of WA coastal towns.
17/7/ 2006	Java	Affected parts of the WA coast particularly Steep Point (WA). Widespread erosion, extensive vegetation damage, and several campsites destroyed. Evidence of inundation up to 200 metres inland.
15/7/ 2009	New Zealand	

3.6.5 Future sea level rise scenarios for 2100

In this study, the risk of coastal flooding is modelled within the study area using five different sea level rise scenarios (i.e. scenario 1 to 5). The sea level rise scenarios are determined for the year 2100 and are based on a combination of linear sea level rise estimates, based on tide gauge data, average and extreme wave and storm surge heights, maximum astronomical tide, as well as the melting ice of the Greenland and Antarctic ice shields. It is believed that sea level estimates are not better than 0.1 m, thus all estimates in this thesis are only given to the cm-level (e.g. one order of magnitude higher than the assumed precision).

Scenarios 1 and 2 model respectively, today's average and extreme sea level conditions together with a raised sea level according to the projected sea level rise based on the linear trend estimate (cf. Table 3.7). These scenarios are very likely to happen by 2100. Scenarios 3 to 5 look at more extreme sea level rise scenarios that include major ice melt. As the magnitude of the projected sea level rise is considerably larger than in scenarios 1 and 2 but less likely only average sea level conditions are considered here.

Scenario 1:

The first sea level rise scenario for 2100 uses a sea level change of 2.06 m with respect to present mean sea level. The sea level rise projected in this scenario is based on the contribution of linear trends from the Fremantle tide gauge (e.g. (108 years* 5 mm/yr – Australian Height datum) sea rise of 0.36 m). To this, the average wave height of 0.90 m, as well as the average sea level height of 0.80 m for storm surges, are added (cf. Table 3.7). Scenario 1 uses average sea level conditions together with the linear trend (cf. Table 3.7). This scenario largely models sea level variations that are part of today's flood zone, though with a slightly raised level corresponding to the projected sea level rise based on the linear trend estimate.

Scenario 2:

Coastal flooding is usually accompanied by extreme wave heights associated with a storm surge, in combination with high astronomical tides. Therefore, the second scenario considers extreme conditions, instead of average conditions as in the previous scenario. This scenario has adopted an extreme wave height (i.e. 3.24 m). The short term effects (seasonal effects) have also been considered, such as: the contribution of astronomical tide (0.80 m), maximum storm surge height (0.98 m), the Leeuwin Current (0.30 m), and ENSO (0.30 m). These results combine to a total sea level rise of 5.98 m by 2100 (cf. Table 3.7).

Scenario 2 uses extreme sea level conditions together with the linear trend (cf. Table 3.7). Again this scenario largely models extreme sea level variations that are part of today's flood zone though with a slightly raised level corresponding to the projected sea level rise based on the linear trend estimate.

Scenario 3:

Scenario 3 is based on the complete melt of the Greenland ice sheet together with average sea level conditions (e.g. scenario 1 plus the contribution of the Greenland ice sheet). The third scenario projects a sea level rise of 8.61 m. This scenario is based on scenario 1 but now includes the contribution of melting ice from the Greenland ice sheet. According to Kuhn et al. (2010), the melting of the Greenland ice sheet will result in an average sea level rise of 6.8 m. However, mostly due to gravitational feed-back effects, sea level rise will be spatially variable and result in a rise of 8.5 m within the study area (Kuhn, Tuladhar, and Corner 2011).

The United State Geological Survey (USGS) has provided a fact sheet about sea level rise and climate change, including a potential sea level rise due to melting of current glaciers and ice shields. According to their statistics, the contribution of the Greenland ice sheet to global sea level is 6.55 metres, which is the figure adopted in this study (Poore et al. 2011).

Scenario 4:

Scenario 4 is based on the complete melt of the West Antarctic ice shield (WAIS) together with average sea level conditions (e.g. scenario 1 plus the contribution of the WAIS). The fourth sea level rise scenario projects a rise in sea level of 10.12 metres (cf. Table 3.7). Instead of considering the complete melt of the Greenland ice sheet (as in scenario 3), this scenario considers the complete melt of the West Antarctic ice shield (WAIS). According to the IPPC, fourth assessment report collapsing of the WAIS will result in a global average sea level change of ~5 metres (IPCC 2007).

Mitrovica, Gomez, and Clark (2009) studied the contribution of the WAIS, and estimated a corresponding global sea level rise of 6.3 metres. Another study done by USGS suggested that melting of the WAIS will raise global sea level by 8.06 metres; this is the figure adopted in this study.

Scenario 5:

Scenario 5 is based on the complete melt of the Greenland ice sheet and WAIS together with average sea level conditions (e.g. scenario 1 plus the contribution of the Greenland ice sheet and WAIS). The fifth sea level change scenario is based on the combination of scenario 3 and 4, thus a complete melt of both the Greenland and West Antarctic ice shields. This will result in a global average sea level rise of 18.73 m (cf. Table 3.7).

Table 3.7 Sea level rise scenarios.

SLR Scenario	Description	Value in (m)	SLR(m)
1	Projected sea level by 2100 based on linear trend.	0.36	2.06
	Average wave height.	0.90	
	Average storm surge height.	0.80	
2	Projected sea level by 2100 based on linear trend.	0.36	5.98
	Maximum wave height.	3.24	
	Short term effects: Astronomical tide.	0.80	
	Short term effects: Maximum storm surge height.	0.98	
	Short term effects: Leeuwin Current.	0.30	
	Short term effects: ENSO.	0.30	
3	Projected sea level by 2100 based on linear trend.	0.36	8.61
	Average wave height.	0.90	
	Average storm surge height.	0.80	
	Melting Ice sheet in Greenland.	6.55	
4	projected sea level by 2100 based on linear trend.	0.36	10.12
	Melting Ice sheet in West Antarctic.	8.60	
	Average wave height.	0.90	
	Average storm surge height.	0.80	
5	Contribution of scenarios 3.	8.61	18.73
	Contribution of scenarios 4.	10.12	

3.7 Correlation analysis between tide gauge records

Tide gauge measurements have traditionally been used for sea level analysis. However, two main problems are encountered when using tide gauge data for future sea level projections. The first problem is that tide gauge stations measure sea level variations relative to a benchmark on land. As such, any vertical movements of the Earth's crust are observed as apparent sea level changes in the tide gauge records. Therefore, vertical crustal motion has to be identified and removed, so to obtain the absolute sea level change. Thus, monitoring and knowledge of the vertical motion of the Earth's crust, and how these movements effect the tide gauge measurements, are essential (Tregoning and Rizos 2008; Vignudelli et al. 2011). However, for the purpose of flood modelling the relative sea level is of interest.

Secondly, the poor spatial distribution of the tide gauge stations around the world does not allow for homogeneous observations of the global oceans. As tide gauge stations are only located along the shore, the open ocean is poorly sampled (Douglas, Kearney, and Leatherman 2001).

In this section, the relationship between the four tide gauge stations located in the study area (Fremantle, Geraldton, Bunbury, and Hillarys) will be investigated. For this, correlation analysis is used to study the relationship between tide gauge measurements depending on the distance between them. This provides vital information on the possibility of modelling sea level variations over a larger area by only one tide gauge record.

Here, the correlation analysis is performed using monthly sea level data from the four tide gauge stations for the time period 1993 to 2010. This time period coincides with the major period of satellite altimetry observation (cf. chapter 3.7). Distances between the tide gauge stations have been calculated based on their geographic location (cf. Table3.8). Distances in Table (3.8) are in reference to the most southern tide gauge station in Bunbury, and are ordered according their distance from Bunbury tide gauge station.

Table 3.8 Distance between tide gauge stations (unit: km).

	Bunbury	Fremantle	Hillarys	Geraldton
Bunbury		173	192	592
Fremantle	173		27.4	446
Hillarys	192	27.4		421
Geraldton	592	446	421	

Correlation coefficients have been derived and documented in Table (3.9). From these results, it can be seen that the tide gauge measurements are highly correlated to each other, even over long distances of about 600 km (i.e. Bunbury to Geraldton). This means that the data from any of the stations can be used to model sea level variations along the whole coastline within the study area. Furthermore, incomplete data sets can be “filled” by the information from other near-by tide gauge stations.

Since very high correlation coefficients (0.98 - 0.93) are obtained between tide gauge stations located within 600 km, the result shows that the variations in sea level measurement is only minimally affected by the distance between tide gauge stations. This has been confirmed by (AL-Habsi 2012), who studied the correlation between tide gauge stations in WA and confirmed a rather strong relationship between the distance and sea level variations when considering longer distances (e.g. it decreases considerably for distances beyond 900 km). For distances shorter than 900 km, Al-Habsi (2012) found correlation coefficients of similar magnitude (as provided in table 3.9).

Table 3.9 Correlation coefficient between tide gauge stations.

	Bunbury	Fremantle	Hillarys	Geraldton
Bunbury	1	0.980	0.959	0.935
Fremantle	0.980	1	0.983	0.965
Hillarys	0.959	0.983	1	0.9719
Geraldton	0.935	0.965	0.971	1

3.8 Correlation between tide gauge stations and satellite altimetry

Satellite altimetry measurements have provided highly accurate data monitoring global sea level variations over the last two decades. This section studies the relationship between satellite altimetry and tide gauge observations, within the study area, using correlation analysis. This provides information on how representative a sea level signal, measured at the coast, is for the open ocean, or vice versa. The information can be used to bridge gaps in tide gauge observations and/or provide sea level information for areas not covered by tide gauge observations.

Ultimately, both data sources can be used to combine coastal sea level variations (e.g. from tide gauge stations) with sea level variations measured in the open ocean. Satellite altimetry is designed to measure sea level accurately over the open ocean, but may be biased closer to the shoreline due to potential returns of the radar beam from land (Durand et al. 2008). In contrast, tide gauge measurements show the opposite behaviour, providing accurate observations along the coastline but may be less representative for locations further away. Therefore, using a combination of both data sets, more reliable and accurate estimates, on sea level variations over the whole study area, can be provided.

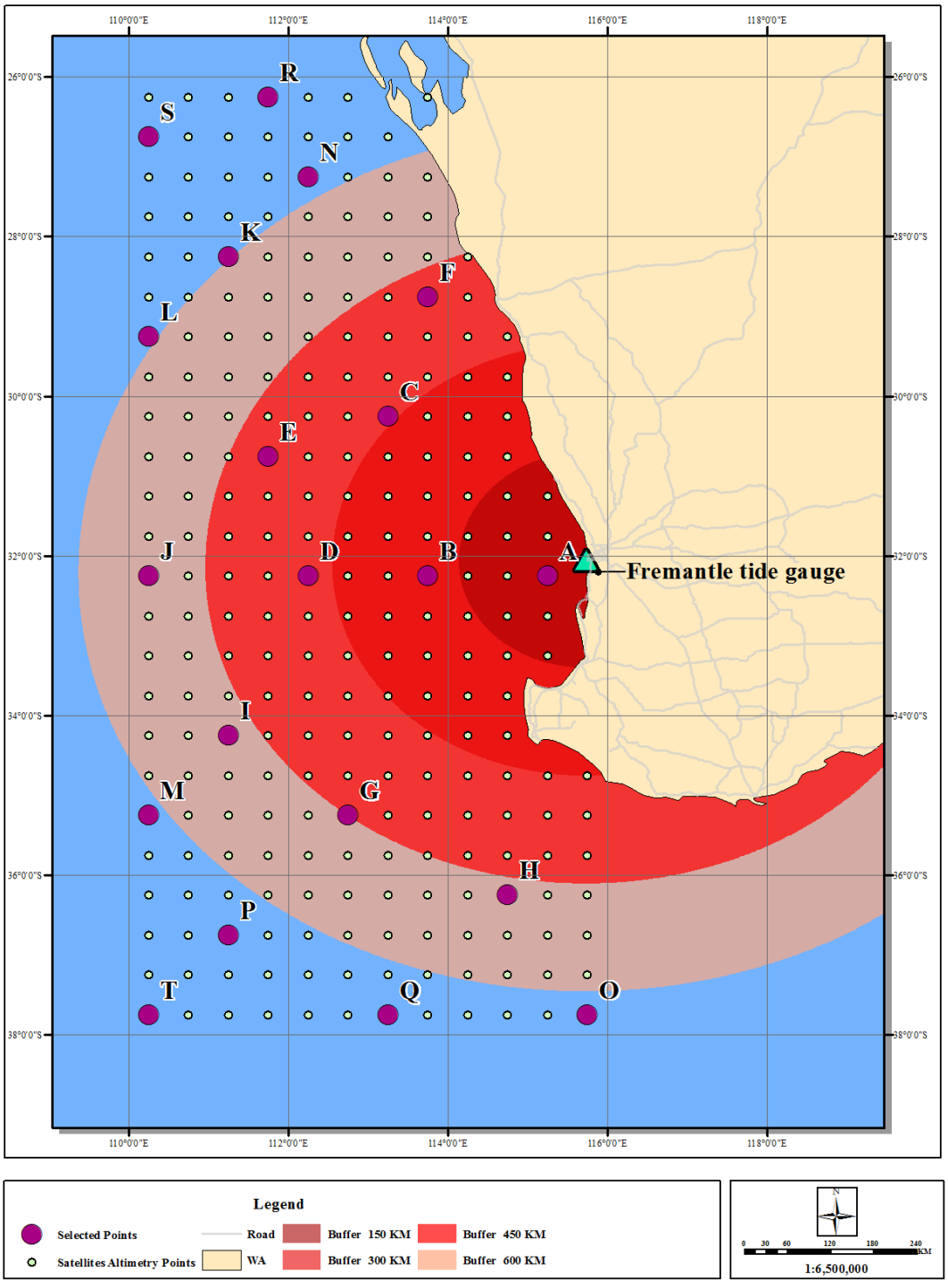

Figure 3.20 Satellite altimetry data coverage (circle; 30'x30' resolution) and location of the Fremantle tide gauge station. Selected altimeter points (purple circles) used for the correlation analysis between satellite altimetry and Fremantle tide gauge station.

In this study, mean sea level anomalies (e.g. difference to MSL) derived from satellite altimetry observations have been obtained from the Archiving, Validation, and Interpretation of Satellites Oceanographic (AVISO) Data website (http://www.aviso.altimetry.fr/en/home.html). Monthly sea level records, along the coastline of Western Australia, were obtained for the period between 1993 and 2009. The data is based on observations from both the Topex/Poseidon (T/P) and Jason satellite altimetry missions, and has been provided on a near-global grid with the resolution of 20-arc-minutes by 20-arc-minutes. For the purpose of this study, the monthly sea level data has been re-gridded on a 0.5 degree by 0.5 degree grid with 246 grid elements (cf. Figure 3.20). The complete data set provides a monthly time series of sea level variations at each 0.5 degree by 0.5 degree grid element within the study area.

For a complete understanding of the spatial behaviour of the satellite altimetry data, first their relationship has been studied using various statistical functions within ArcGIS. For this, the data was imported into ArcGIS as text files and converted into shape files. Initially, the statistical properties of the monthly mean sea level values were examined. For this, one particular month and year has been selected (June 2005), and the respective 246 mean sea level values analysed in terms of a histogram. The number of bars of the histogram has been chosen based on the following relationship:

$$Number\ of\ bars = Log_2 (N) + 1$$

Where N is the number of data values considered. Based on N = 246 data points within the study area and 10 bars with the constant width of 0.21 mm (cf. Figure 3.21).

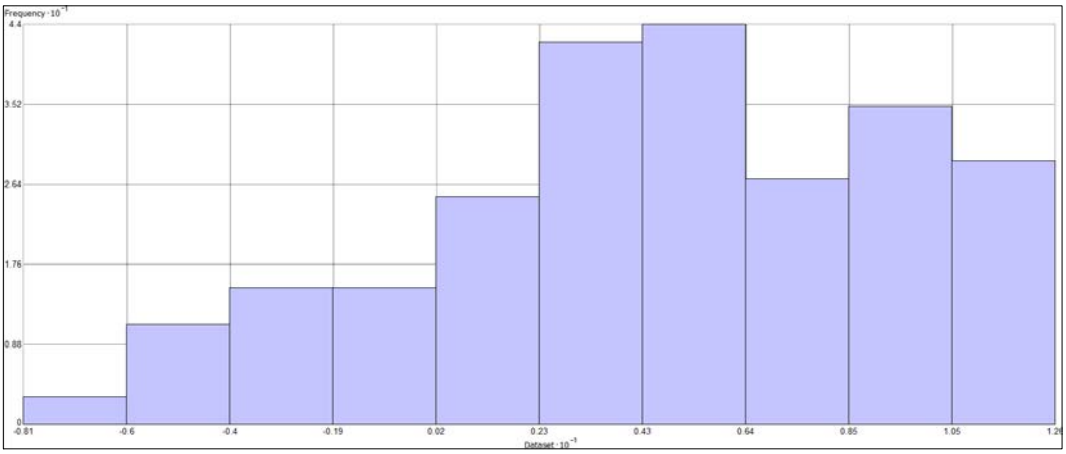

Figure 3.21 Histogram for mean sea level anomaly values during June 2005. Unit in millimetre.

The histogram displays the 246 points and shows that -8.1 mm is the minimum value recorded within the data set, while the maximum value is equal to 12.6 mm. The mean for the sea level anomaly values is 4.7 mm and the median is 5.0 mm. The standard divation is 4.77 mm and the skewness is -0.43. Figure (3.21) shows some characteristics of normal distribution for the data, also showing some similarity to the clasical bell-shape. Furthermore, the skewness value is rather close to zero, thus the histogram is almost symmetrical, as well as the mean and median value being very similar.

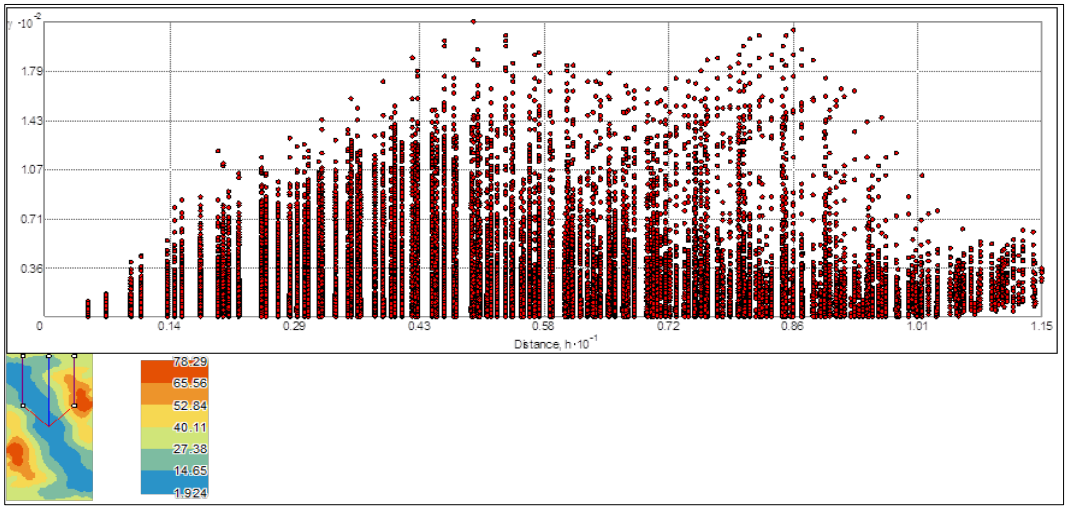

Figure 3.22 Semivariogram for mean sea level values during June 2005. Unit in meters.

In order to study the spatial relationship between monthly sea levels, observations from satellite altimetry semivariogram and Voronoi maps are analysed. Figure (3.22) shows a semivariogram, based on the satellite altimetry mean sea level values, for June 2005. It provides an insight into the spatial relationship with respect to the distance between the data points (ESRI 2012). As can be seen in Figure (3.22), the variance between the points increases as the distance is increased, confirming that points located close to each other have a high relationship.

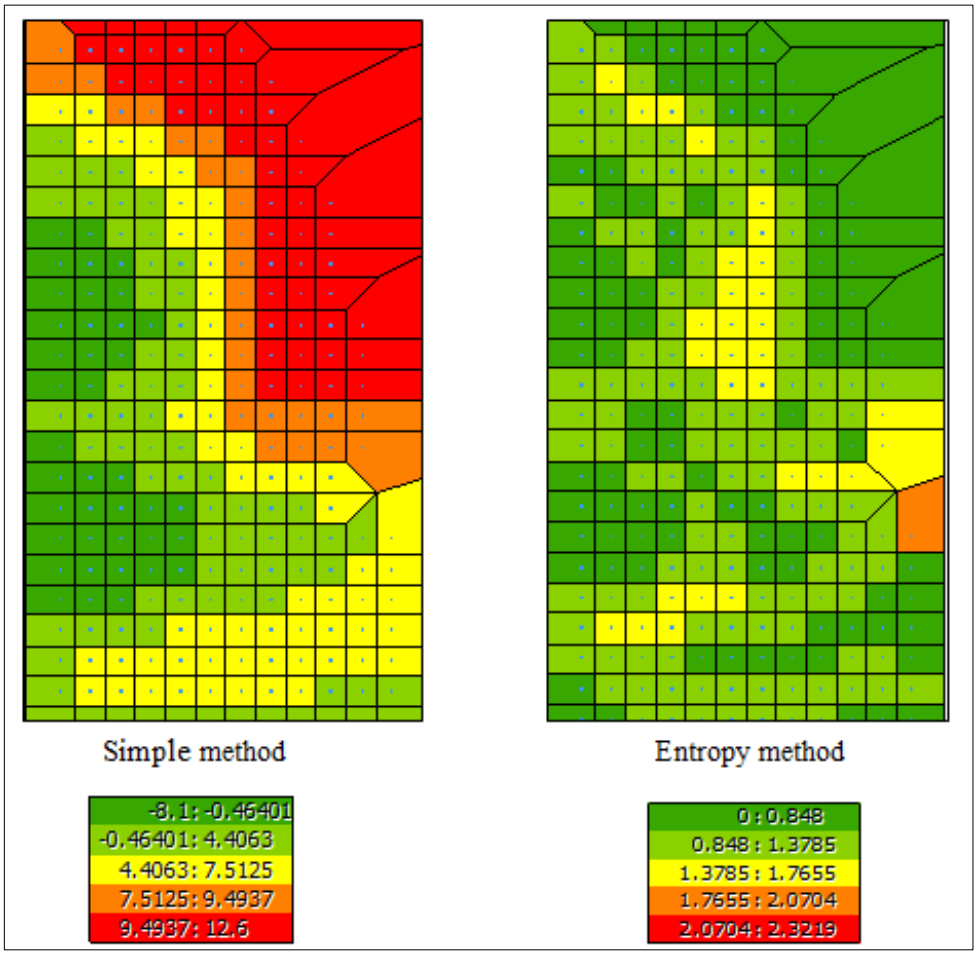

Figure 3.23 Voronoi maps for the satellite altimetry points.

Figure (3.23) shows a Voronoi map, which is used to allocate the local variation across a set of values (i.e. points). It is defined as a set of polygons surrounded by a group of points. All sites within a polygon are nearer to the object it surrounds than to any other object in the group. Moreover, in each individual polygon, the value is obtained based on the values for the nearby polygons. Figure (3.23) shows the results for the simple and Entropy method used to compute the value in each polygon.

The value associated with each polygon, using the simple method, represents the value of the sample point inside that polygon, and is used to measure the local influence within the desired set of data. The left map in Figure (3.23) shows that the variations between the data increase as the sample points of the satellite altimetry observations get closer to the coastline, and showing less variation further away from the coastline.

The second technique used is the Entropy method where the polygons are classified into five catogaries based on the natural classification of the data values. The values assigined to each polygon are computed based on the value in each polygon and the surrounding values. This techinque is used to identify the local variation amongst a set of records. The map on the right, in Figure (3.23), shows the results for the Entropy method. It shows a variation of the values along the coast line. In addition, the values of the polygons offshore show the same results, obtained by using the simple method on the left map (Figure 3.23).

The last analysis provides a study on the correlation between tide gauge station measurements and satellite altimetry. For this, sea level measurements for 20 random points were selected from satellite altimetry and compared with the Fremantle tide gauge station. For each point, the sea level time series, between 1993 and 2009, has been correlated to the tide gauge observations at Fremantle. The result of the correlation, for the monthly and the yearly data, shows that there is strong positive correlation between tide gauge measurements and satellite altimetry measurement for the points A, I, K, E, M, P, O, Q, B, and S. The points D, F, H, C, J, G, and T show a moderate correlation, while the points R, N, and L show a weak positive correlation with the Fremantle tide gauge (cf. Table 3.10).

Table 3.10 Correlation between Fremantle tide gauge and the selected Satellite Altimetry points.

No	Altimeter points	Distance (km)	Correlation Coefficient (R)	correlation
1	A	50.6	+ 0.70	Strong
2	I	328.6		
3	K	404.7		
4	E	413.3		
5	M	483.7		
6	P	516.6		
7	O	603.5		
8	Q	609.8		
9	B	633.8		
10	S	807.0		
11	D	188.0	+0.50	Moderate
12	F	309.0		
13	K	404.0		
14	C	457.7		
15	J	630.9		
16	G	673.0		
17	T	793.1		
18	R	619.7	+0.30	Weak
19	N	664.9		
20	L	751.9		

However, there is considerable correlation between the satellite altimetry records (for the yearly average values up to a distance of approximately 450 km), which can be seen from the Figures (3.24) showing clusters of high correlations between neighboring records. The outcome of these analyses confirms that satellite altimetry measurements are less reliable near to the coast due to generally lower correlations as compared to correlations between tide gauge records (cf. chapter 3.7). The limitation and low quality of satellite altimetry, near to the coastline, results in contaminated radar pulses. This is due to reflection from land areas. Because of this, satellite altimetry data is not accurate, and is unreliable within 40 km of the shoreline (Lionello 2012). Despite this, satellite altimetry data does provide an accurate representation of the ocean surface over open oceans and is a great source of information for marine studies.

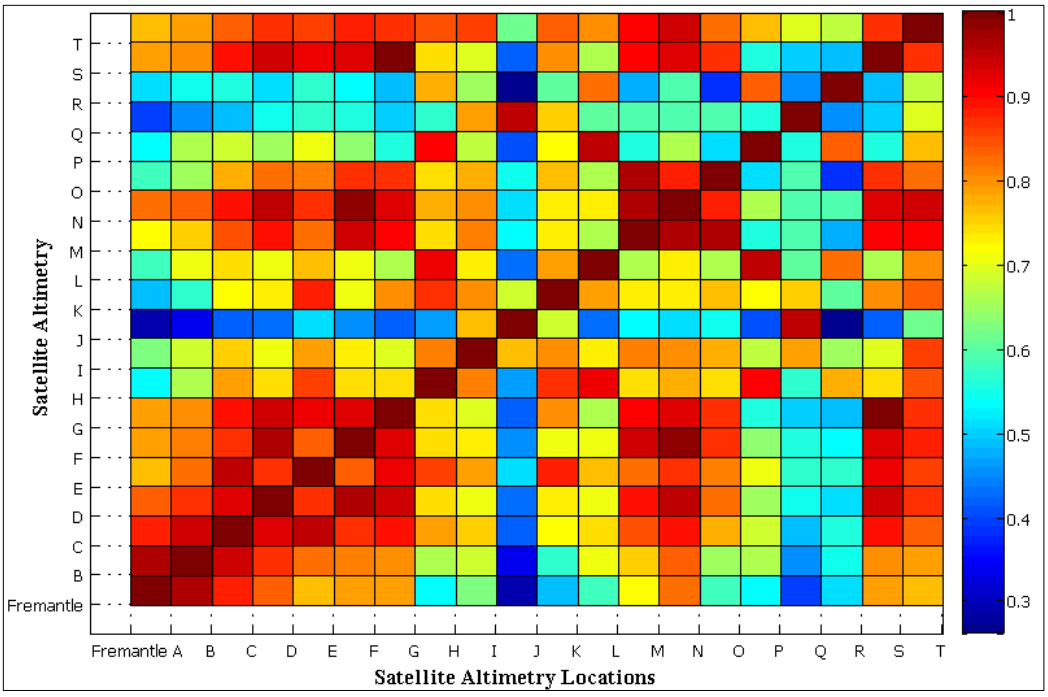

Figure 3.24 Correlation analysis between tide gauge record at the Fremantle tide gauge and satellite altimetry for the yearly averaged measurements.

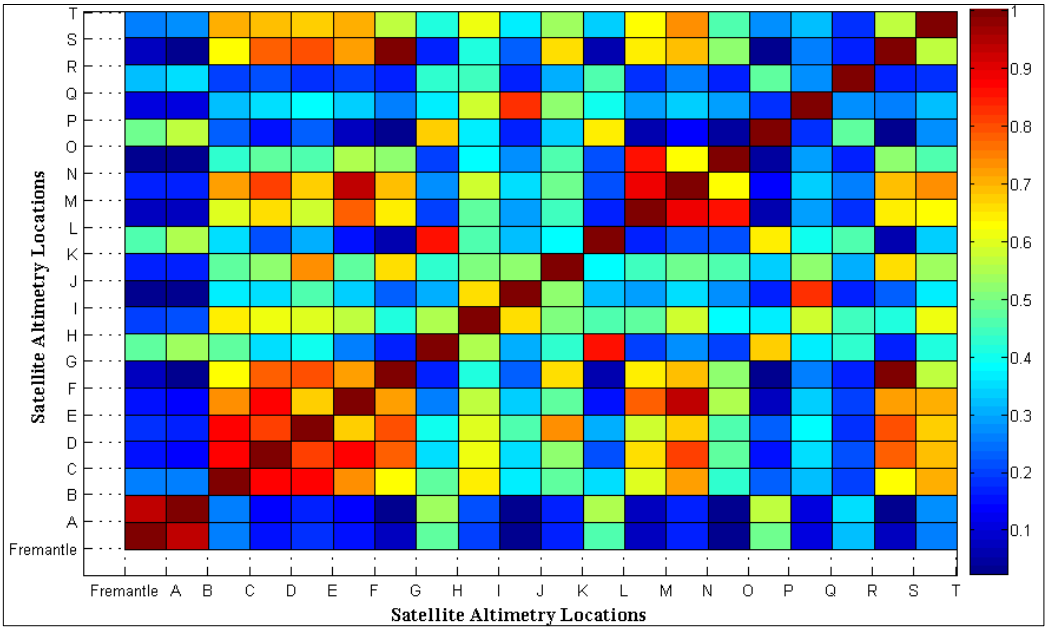

Figure 3.25 Correlation analysis between tide gauge record at the Fremantle tide gauge and satellite altimetry for the monthly averaged measurements.

3.9 Chapter summary

This chapter deals with the modelling of future sea level rise and can be considered as the first stage of this research. The study in this chapter is divided into several steps, covering many aspects concerning the modelling of future sea level rise, such as the different types of data used in sea level rise modelling and the short- and long-term sea level rise analysis. The chapter is divided into two main parts: theoretical and practical.

The theoretical section focuses on the causes of sea level rise and the data used in sea level analysis. In this regard, some of the important terms related to sea level rise are reviewed and briefly discussed. The data used in sea level prediction is also presented and described. Two main data sources are reviewed; (1) satellite altimetry and (2) tide gauge station data. Furthermore, the impact of extreme sea level events on sea level rise is covered in more detail.

The practical section deals with the estimation of sea level rise using satellite altimetry and tide gauge data. Monthly and yearly averaged tide gauge data is used from four tide gauge stations in Fremantle, Hillarys Boat Harbour, Geraldton, and Bunbury. Based on past sea level trends, future sea level rise is projected. The short - and long-term - effects on sea level rise have been considered within the sea level analysis, such as the effects of storm and surges, waves, and also the melting of the ice shields of Greenland and West Antarctica. Five scenarios with different projections for sea level rise (2.06 m, 5.98 m, 8.61 m, 10.12 m, and 18.73 m respectively) have also been defined.

The relationship between tide gauge records, within the study area, has been discussed. The correlation analysis is performed with respect to distance between tide gauge stations. The results obtained show high correlation between the tide gauge records at distances up to 592 km. Correlation analysis between the Fremantle tide gauge records and satellite altimetry has also been undertaken.

Sea level measurements from 20 random satellite altimetry points were selected and compared with the Fremantle tide gauge record. The analysis revealed that there is lower correlation between satellite altimetry records than there is between tide gauge stations along the coast line.

The next chapter will deal with the second stage of this research and present the method used in high-resolution flood modelling. Flood information will be gathered from two study locations. The differences between high-and low-resolution elevation data, in terms of flood modelling, will be studied as well.

CHAPTER 4

HIGH-RESOLUTION FLOOD MODELLING

4.1 Introduction

In the previous chapter, theoretical information about the causes of the near-future sea level rise and the methods used in sea level rise estimation were presented. The sea level rise in the study area was estimated using tide gauge measurements and five flooding scenarios were adopted. The relationship between tide gauge measurements and the relationship between tide gauge measurements and satellite altimetry measurements were discussed. This chapter provides a study on high-resolution flood modelling. Particular focus is given to the spatial resolution of the topography data used. The chapter provides an overview of the methods used for flood modelling using high-resolution topography data. In order to demonstrate the principles, two study locations along the south west coast of Western Australia have been selected. Results are provided, on the level of detail that can be modelled using high-resolution data compared to low-resolution data, and then discussed.

4.2 An overview on flood modelling

Coastal flooding can be regarded as a major threat to coastal areas around the world. Changes in the world climate have increased the likelihood of coastal flooding and the danger to both natural ecosystems and residential areas near to the shoreline. Sea level rise creates a long term risk for people who live near to the shoreline (Smith and Petley 2004). It is estimated that more than 200 million people are currently living in the coastal zone within 1 m from the mean sea level. Major socio-economic impacts can, therefore, be expected if no mitigation is done. Digital Elevation Models (DEMs) play an important role in flood modelling. A DEM is a digital representation of both the natural terrain surface and man-made structures on the Earth’s surface.

During the past few decades, the use of DEMs in many areas, such as geology, urban planning, resource management, environmental monitoring, remote sensing, and geographic information systems, has rapidly increased (Vaze, Teng, and Spencer 2010). In order to mitigate the impact of flooding, a highly accurate representation of the land surface is important in flood modelling studies (Haile and Rientjes 2005). Studies by Haile and Rientjes (2005); Sole et al. (2008); Turner et al. (2013); Bas van de, Joost, and Claartje (2012); Gesch (2009); Knight et al. (2009); Schumann et al. (2008) demonstrate the need for high-resolution data in flood modelling, especially in low-lying areas. When using low-resolution data, it is not possible to obtain highly accurate and detailed results for flood boundaries.

It has been widely reported that low-resolution DEM data can be efficient for modelling areas with small topography changes. However, there is a growing demand for the use of high-resolution DEM data in urban areas and in areas with more complex terrain. This is due to the presence of relatively small scale topographic features and elements, such as roads, houses, and dykes, which can affect the flood pattern. This issue has prompted researchers and modellers to apply highly accurate and detailed DEMs to flood modelling studies in urban areas and floodplains with residential settlements. Recent development and availability of LiDAR data has further encouraged the use of high-resolution representations of the Earth's surface in flood modelling (Vaze, Teng, and Spencer 2010).

One of the major drawbacks of using low-resolution DEMs, as input data, is its inability to show some of the important small scale topographic features and elements that affect flood simulation, especially in low-lying areas. Through a re-sampling process, or the transformation from high-resolution to low-resolution data, many of the important details are generalised or are missing. Thus, there is a demand to quantify and report the impact of such a process on the performance and reliability of flood modelling. Several studies have been conducted, which compare spatial indices obtained from different low-resolution DEMs (e.g. 100 m versus 1000 m grid cell resolution), such as Wolock and McCabe (2000); Jenson (1991); Hutchinson and Dowling (1991).

Furthermore, several studies have investigated the impact of using lower resolution DEMs on the outputs of hydrological and hydraulic modelling (e.g. Horritt and Bates 2001; Haile and Rientjes 2005; Horritt and Bates 2002). It should be noted that most of these studies focus on low-resolution DEMs with a resolution of 100 m or lower. However, with the introduction of high-resolution data, such as from LiDAR as well as the increased availability of high performance computers that can manage and handle large datasets, there is a need to quantify and report the differences on flood modelling across a range of DEM resolutions (e.g. 1 m, 30 m, and 90 m). In order to demonstrate the benefits of using high-resolution data, flood modelling has been performed, in this study, at two test sites using various DEM resolutions.

4.3 Study area

The south west coast of Western Australia (WA), which extends from Perth in the North to Busselton in the South, has been chosen as the study area (cf. Figure 4.2). It is located between 115° 34’ and 115° 58’ in eastern longitude and between 31° 27’ and 33° 48’ in southern latitude. The coast selected has an approximate length of 300 km (Brachmanis 2002). The study area is home to a large variety of wild animals and native plant species, as well as a lot of built-up areas close to the coast line (Smith 2010). Highly populated residential areas, constructed within metres of the coast line and elevated only a few metres above sea level, are located predominantly between Perth and Mandurah.

4.3.1 Geological setting of the South West Coast of WA

The majority of Western Australia consists of geologically old, igneous, metamorphic, and sedimentary rocks, which have been weathered and eroded for many millions of years (Western Australian Planning Commission 2003). However, some parts of WA consist of younger sedimentary rocks, mainly sandstone and limestone. The rock type and structure broadly determines the nature and shape of the coastline. Landforms, at any particular place, are a result of interactions between local geology, coastal dynamic processes and vegetation (Crostella, Backhouse, and Geological Survey of Western Australia 2000).

Broadly, there are two types of coastal landforms: (1) composed of rock and (2) composed of unconsolidated sediments (mainly sand and silt). For example, the cliffs of the Nullarbor, Zuytdorp, and Kimberley contrast with the long sandy beaches of the Roe Plain and the coast between Cape Naturaliste and Geraldton, which also includes the study area. Usually, the coast is a mix of solid rock and unconsolidated sediments, with sand and mud abutting or overlying basement rocks. The nature of the coast between rock outcrops (e.g. between Cape Naturaliste and Geraldton) is based on geology, sediment supply and the intensity of coastal processes (Crostella and Backhouse 2000). The south west coast is located in, what is known geologically as, the Perth Basin, a thick sedimentary basin situated west of the Darling Scarp. The Perth Basin stretches north-south between Geraldton and Augusta for almost 1000 km, covering an area of about 100 000 km^2.

More than half of the basin lies offshore in water depths of up to 1000 m (Cadman, Pain, and Vuckovic 1994). The area between Guilderton and Cape Naturaliste (part of the study area) is geologically part of the Perth Basin, and contains quaternary coastal sand dune sequences, including lithified Pleistocene calcarenites and unconsolidated Holocene calcareous sands (Western Australian Planning Commission 2003). Generally, the topography of the study area consists of temperate reefs and islands, foredune plains, coastal lagoons, parabolic dunes, sheltered sandy beaches, cuspate forelands, and tombolos. The major coastal processes include low discharge from rivers (during the wet season), mid-latitude cyclones, strong sea breezes, micro-tidal range, and a low to moderate wave environment (Western Australian Planning Commission 2003).

4.3.2 Climate setting

The climate along the south west coast of WA is described as a Mediterranean climate, typically hot and dry in summer, and temperate and wet in winter. Based on the records obtained from the Australian Bureau of Meteorology, for the Perth metro station between 1994 and 2014, the average minimum temperature in summer (i.e. December, January, and February) is around 17.6º Celsius.

The average maximum temperature is 30.6ºC. In winter, the average minimum and maximum temperatures range between 7ºC and 18ºC. Annual rainfall averages at around 738.1 mm with higher values for areas south of Perth (Australian Bureau of Meteorology 2014).

4.3.3 Demographic setting

Based on the data from the Australian Bureau of Statistics (ABS), the study area is the home of approximately 2.52 million people as of June 2013. The population, within the study area, is concentrated between Perth and Rockingham. There are also high concentrations of people in other towns, such as Mandurah, Bunbury, Margaret River, Busselton, and Albany (Australian Bureau of Statistics 2011a).As of June 2013, the population density for Western Australia was 1.0 people per square kilometre. It is the second lowest population density in Australia after the Northern Territory (0.2 people per square kilometre), and low in comparison to the average population density for the whole of Australia (3.0 people per square kilometre (Australian Bureau of Statistics 2011a). It is also low when compared to the much higher population density of the Greater Perth region, including the coastal areas that reach values beyond 2,000 people per square kilometre (cf. Figure 4.1).

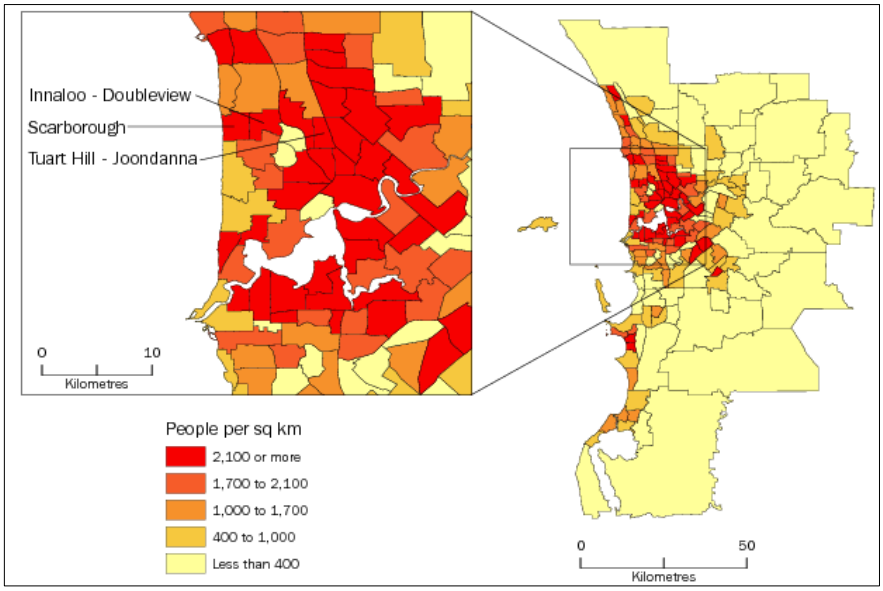

Figure 4.1 Population density for greater Perth as of June 2013 (source: Australian Bureau of Statistics 2011).

4.4 Study Locations

Within the study area (cf. chapter 4.3), two locations have been selected for detailed study on high-resolution flood modelling. Initially, the following eight sites were considered: (i) Coogee (new marina), (ii) Rockingham (Safety Bay), (iii) Mandurah, (iv) Wannanup (marina), (v) Bunbury, (vi) Peppermint Grove Beach, (vii) Port Geographe Marina, and (viii) Busselton (cf. Figure 4.2). In order to select the most suitable sites for this study, the following criteria were used:

1. The study locations should contain low-lying residential areas located close to the shoreline.
2. The study locations should contain mix land-use patterns, such as vegetated and built-up areas.
3. The study locations should have varied geomorphology, geology, and topography.
4. The study locations should be covered by both high-resolution DEM data (i.e. LiDAR) and low-resolution DEM data (e.g. ASTER and SRTM).

Based on the above criteria, Mandurah and Rockingham were selected as the most suitable study locations.

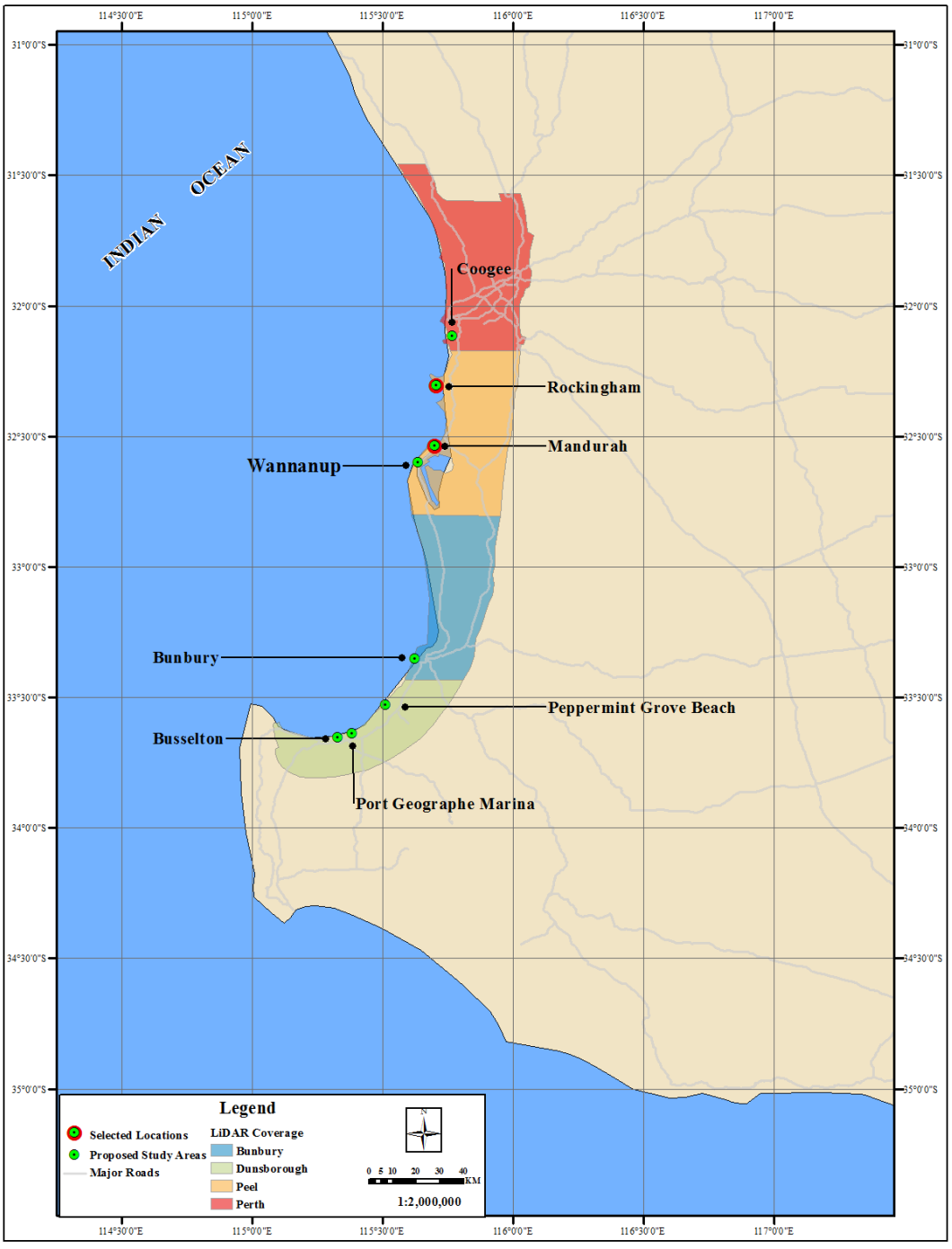

Figure 4.2 Proposed and selected study locations.

4.4.1 Mandurah

The city of Mandurah is situated on the south west coastline, approximately 70 km south of Perth, and covers a total area of 173.5km^2 (cf. Figure 4.3). The length of Mandurah's coastline is about 50 km, stretching from Madora Bay in the north to Yalgorup National Park in the south. According to the ABS 2011 census, the total population of the city of Mandurah is 69,903 as of 30th June 2011. Mandurah has a population density of 439.3 persons per square kilometre and 153 households per square kilometre (Australian Bureau of Statistics 2011a).

Like most of the south west area, Mandurah has a Mediterranean climate with an average maximum temperature of 23.3°C, for the period between 2001 and 2014, and an average minimum temperature of 14.8 °C for the same data period. It has an annual average rainfall of approximately 700 mm (Australian Bureau of Meteorology 2014). The selected site is surrounded by the Indian Ocean on three sides; it is bordered to the north by Doddi's Beach, the east by Mandurah Bay, and the west by Blue Bay Beach. Therefore, it is very vulnerable to coastal flooding (cf. Figure 4.3). The total area of the selected location is 2.41 km^2. The mean height of the Mandurah study site (obtained from DEM from LiDAR data) is 5.7 m above mean sea level (e.g. Australian Height Datum). The maximum height is 30.2 m, and the minimum height is -0.45 m (cf. Figure 4.4).

Figure 4.3 Satellite image for the study area of Mandurah, Western Australia. (source: Google 2010a).

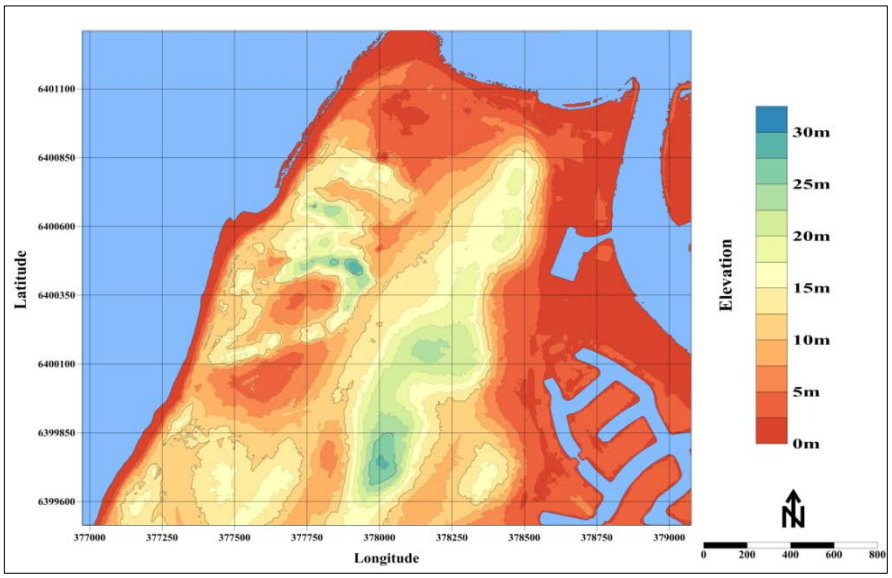

Figure 4.4 Contour map for the study area of Mandurah. Elevations are referenced to the Australian Height Datum (AHD). Gridlines are referred to the Map Grid of Australia.

4.4.2 Rockingham

Rockingham is a main centre in Western Australia, located approximately 40 km south of Perth and 30 km north of Mandurah. The city of Rockingham is surrounded by the Indian Ocean to the north and west, and it covers a total area of about 290 km^2, including residential areas, park land and coastal areas (cf. Figure 4.5). According to the ABS 2011 census, the city of Rockingham has a population of 104,105 as of 30th June 2011. The population density is 424.7 people per square kilometre (Australian Bureau of Statistics 2011b).

The chosen study area extends from Liverpool Street in the north to Safety Bay Road in the south. Shoalwater Bay borders the study area to the west, and to the east, Safety Bay Road. The total area of the selected location is 1.61 km^2. Based on the data obtained from the LiDAR DEM, the average height within the study area is 2.8 m above mean sea level. The maximum height is 12.8 m and the minimum height is -0.1 m (cf. Figure 4.6). Therefore again, the area is very vulnerable to coastal flooding (cf. Figure 4.5).

Like Mandurah, Rockingham has a Mediterranean climate. The average temperature, recorded between 2001 and 2014, is 18.5 °C. For the same data period, the average maximum temperature in Rockingham is 22.7°C, and the average minimum temperature is 15.0 °C. The average annual rainfall is approximately 614.3 mm (Australian Bureau of Meteorology 2014).

Figure 4.5 Satellite image for the study area of Rockingham, Western Australia (source: Google 2010b).

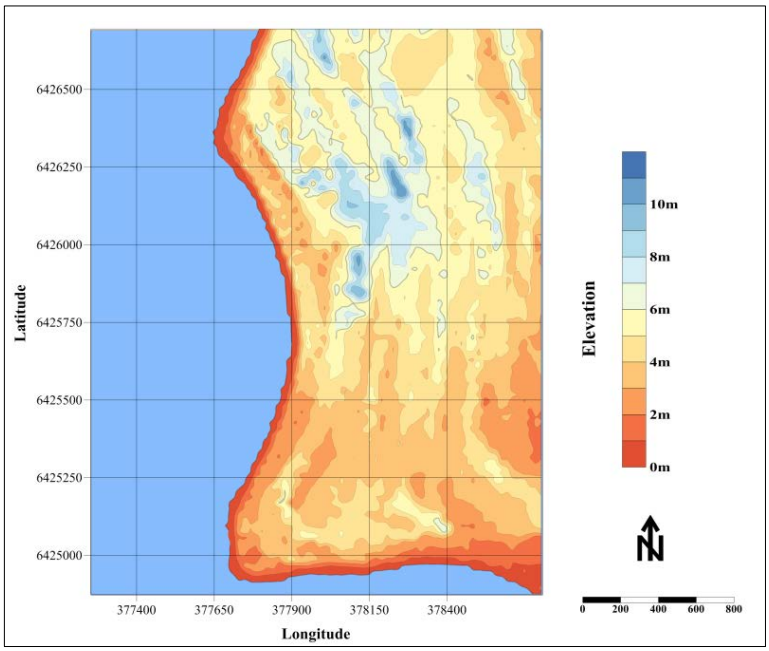

Figure 4.6 Contour map for the study area of Rockingham. Elevations are referenced to the Australian Height Datum (AHD). Gridlines are referred to the Map Grid of Australia.

4.5 DEM Data

Three types of DEM data have been used in this study: LiDAR, ASTER, and SRTM. The spatial resolution of the DEMs used ranges from less than one meter to 90 metres. LiDAR provides the highest-resolution DEM data, while ASTER and SRTM provide the lower-resolution DEM data.

4.5.1 LiDAR DEM data

LiDAR DEM data was obtained from the Western Australian Department of Water, as custodian of the LiDAR DEM database for the Swan Coastal Plain (AAMHatch 2010). This data has a horizontal resolution of approximately 1 m and a vertical accuracy of 0.15 m. LiDAR-derived elevation data provides an optimal basis for high-resolution flood modelling down to a property-by-property level. Table (4.1) below shows the availability of LiDAR DEM data from the Department of Water's database. The Swan Coastal Plain project was undertaken in November 2006, by the AAM group, and captured Airborne Laser Scan (ALS) data from above the Serpentine River (between Forrestdale and Mandurah) for both water modelling and associated engineering tasks. An additional survey was carried out over adjacent areas, between Mandurah and Jandakot, on May 7th, 2007 (cf. Table 4.1). Data from these two surveys were combined to form one seamless dataset (AAMHatch 2010). The data was projected to MGA Zone 50 and elevations referenced to the AHD. The current coverage is illustrated in Figure (4.2).

Table 4.1 LiDAR projects for Western Australia (source: AAMHatch 2010).

Name	Project	Area (km^2)
Perth	Swan Coastal Plain	2,123.6
Williams	FPM	20.2
Boddington	FPM	95.6
Lake Grace	FPM	44.6
Moora	Moora FS	80.7
Dunsborough	Swan Coastal Plain	1,268.4
Bunbury	Swan Coastal Plain	1,607.3
Peel	Swan Coastal Plain	1,948.5

The LiDAR DEM data for the Swan Coastal Plain project covers a total area of 6947.8 km^2 and is separated into four areas: Perth, Peel, Dunsborough, and Bunbury (cf. Figure 4.1 and Table 4.1). The data was captured over a six month period between November 2006 and May 2007. The complete dataset contains a total of 348,404,000 data points, each classified as ground, non-ground or water. The vertical accuracy is 0.15 m and the horizontal accuracy is < 0.60 m.

4.5.2 SRTM and ASTER DEM data

As well as high-resolution LiDAR DEM data (cf. chapter 4.5.1), this study also uses lower resolution DEM data (30 metre resolution ASTER and 90 metre resolution SRTM). This meant it was possible to analyse both low- and high-resolution flood models. The ASTER GEDEM data was obtained from the Japan Space Systems web-portal (http://gdem.ersdac.jspacesystems.or.jp) and covers the global land area. The data is the result of a collaboration between the Ministry of Economy, Trade and Industry of Japan (METI), and the National Aeronautics and Space Administration (NASA) (Japan Space Systems 2012). The SRTM DEM data was obtained from the Consortium for Spatial Information (CGIAR-CSI) website (http://www.cgiar-csi.org) providing a DEM for the global land areas. The digital elevation data provided by CGIAR was processed to fill data voids (Jarvis et al. 2008).

4.6 LiDAR DEM data validation

Despite the best endeavours by the data vendors to supply clients with quality data, there is still the chance of data anomalies or inconsistencies. These might include holes in the data coverage or irregular minimum bounding shapes. The LiDAR data, for the selected study areas, was therefore checked for accuracy and reliability. More specifically, the LiDAR data was validated at different stages using the ArcGIS software. The validation process included checking the LAS point count, the point spacing z values and the LiDAR coverage for the selected sites (cf. Figures 4.8 and 4.9). See Figure (4.7) for the detailed data validation procedure.

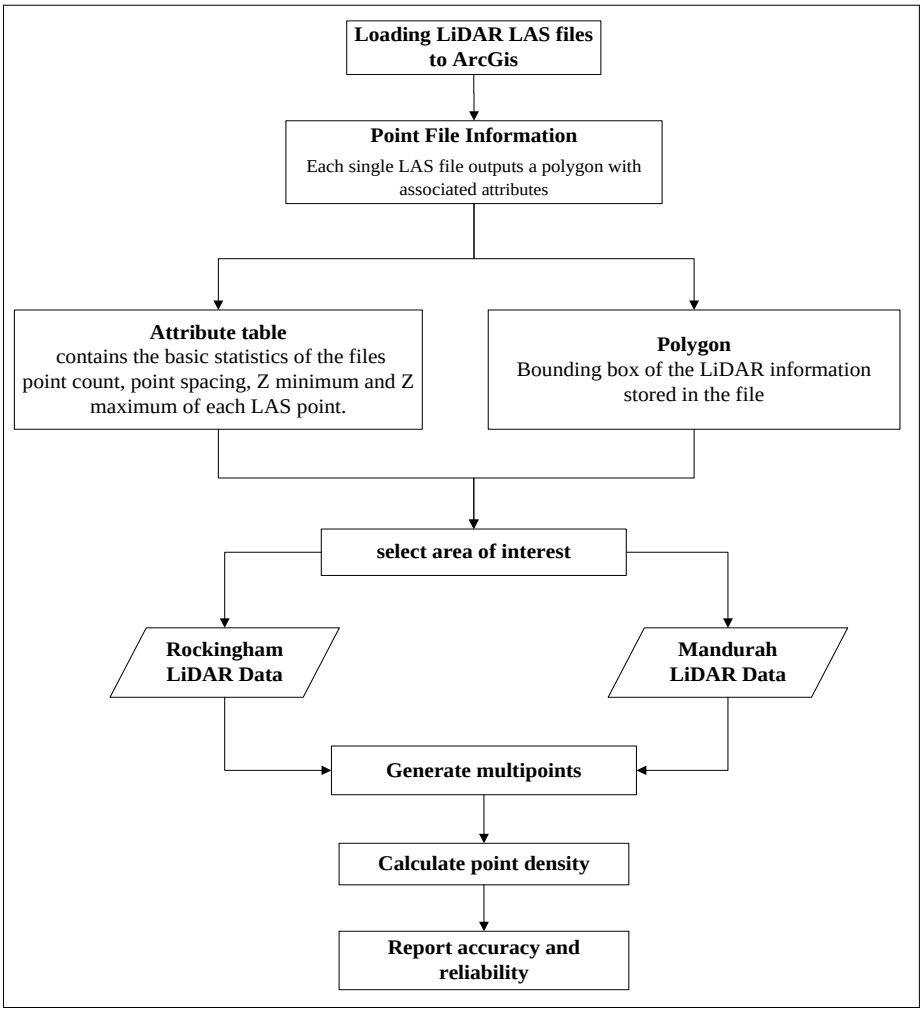

Figure 4.7 LiDAR DEM data validation procedure.

4.6.1 Validation of data coverage

The accuracy and reliability of the LiDAR DEM data was validated. The parameters used in the documentation were: point spacing between the LAS points, point count, point density, and the data coverage within the selected study area. The raw LiDAR data was provided in either Log ASCII Standard (LAS) binary format or in standard ASCII format. The complete dataset was provided as a series of files that covered the whole study area, and consisted of 7,655 files, occupying 286 GB of hard disk storage.

An advantage of LAS format, over the standard ASCII files, is the increased storage capability (i.e. the files occupy less storage space). LAS files also contain more detailed header information and can be read more quickly. Moreover, LAS files provide the user with the opportunity to easily reclassify the data into different forms, such as digital elevation models (DEMs) and digital surface models (DSMs). Here, LAS files obtained from the WA Department of Water were checked for accuracy and reliability via the five-step procedure summarised below:

4.6.1.1 Calculating the basic statistics for the whole dataset

The data in LAS files needs to be organised by first calculating the basic statistics, and then organising the data based on spatial proximity for the whole dataset. This process was performed using the *Point File Information* tool available in the 3D Analyst Conversion toolbox of ArcGIS. The results are captured in attribute tables, which contain basic statistical information, for each LAS point file used in the study, and include:

i. Point count: refers to the number of laser points in each LiDAR tile.
ii. Point spacing: refers to the distance between the laser points analogous to the pixel size of an aerial image (also known as posting density or nominal point spacing) and determines the grid resolution.
iii. Z minimum: refers to the minimum elevation recorded for the LiDAR points
Z maximum: refers to the maximum elevation recorded for the LiDAR points.

In the tables, a separate header row was created for each input file used, ensuring that the files can be read properly. The point spacing is an estimate that assumes all points, contained in the input file, are evenly spaced over the maximum spatial extent. In ArcGIS, point spacing is calculated by applying a binning method that incrementally assesses small areas of the file to allocate the final value. The scan angle and flying height determine the average point spacing in the cross-flight direction, while the flying height and airspeed determine the average point spacing in the in-flight direction. Z_{min} and Z_{max}, respectively, indicate the minimum and maximum elevation values.

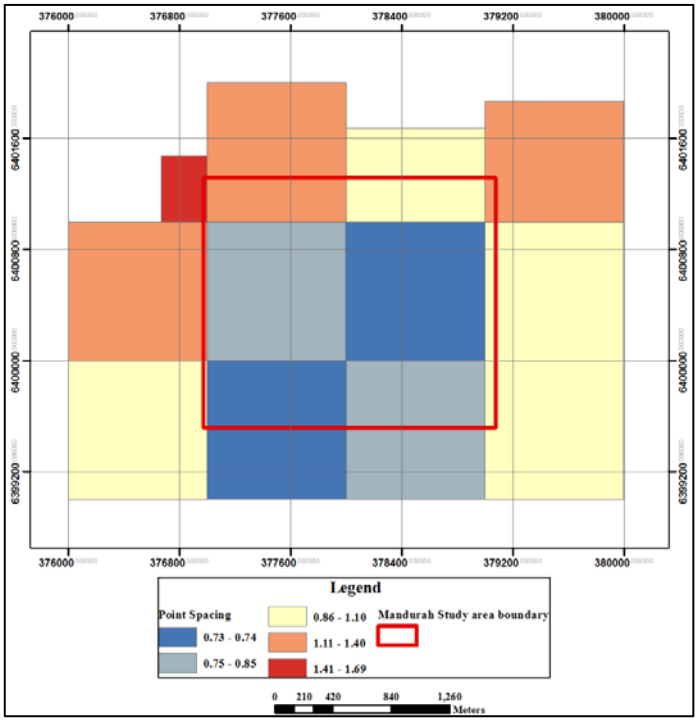

Figure 4.8 Average point spacing within the Mandurah study location. Rectangles indicate the coverage of LAS data files used (units in metres).

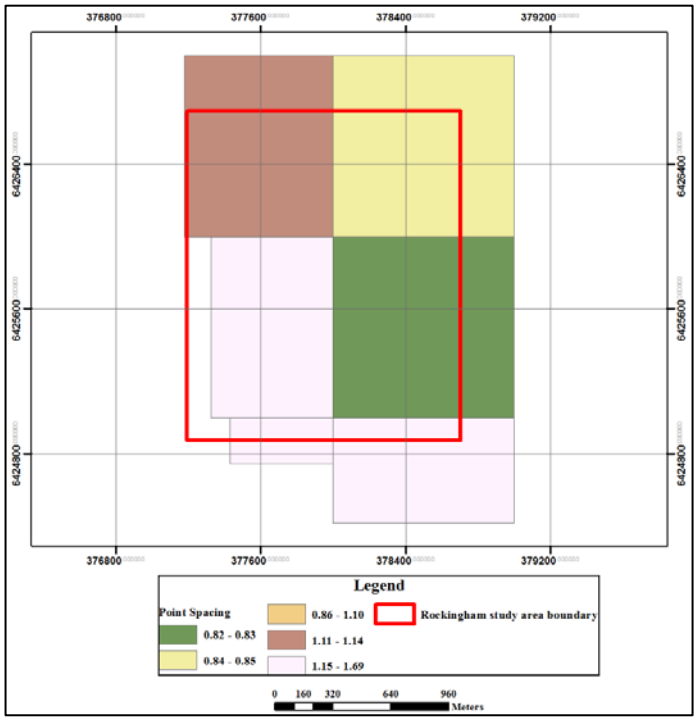

Figure 4.9 Average point spacing within the Rockingham study location. Rectangles indicate the coverage of LAS data files used (units in metres).

It can be noticed, both from the basic statistics tables and from the visual inspection of both study locations, that there is a trade-off relationship between the point count and the point spacing. The point spacing is not uniform but spatially variable, and the vertical accuracy increases when the measured points are very close to the true value. Both the point spacing and point count have an effect on the quality of the representation of the terrain for the desired locations.

4.6.1.2 Selecting the area of interest

The second step involves extracting the data from within each study location. This process considerably reduces the data amount and, in turn, allows faster processing and analysis. This has been achieved by defining a polygon shape file around each study location (i.e. Mandurah and Rockingham). The total area of the study location in Mandurah is 10.69 km^2. The study area in Rockingham is 4.22 km^2 (cf. Figure 4.2), which is smaller than the study area in Mandurah by 6.47 km^2.

Table 4.2 Statistics for the LiDAR data for both study areas

Study Location	Points count	Average point spacing (m)	Z minimum (m)	Z maximum (m)	Area (km^2)
Mandurah	12,223,658	1.06	-0.45	30.2	10.69
Rockingham	4,366,737	1.18	-0.1	12.8	4.22

The average point spacing within the Mandurah study location is 1.06 m, while the average point spacing within the Rockingham study location is 1.18 m (cf. Table 4.2). Both study areas have an approximate average point spacing of one metre. Figures (4.8 and 4.9) indicate that the average point spacing is below one metre in the built-up areas of both study areas (e.g. 0.78 m in Mandurah and 0.83 m in Rockingham). The LiDAR point spacing is larger along the coastline in both study locations.

This means that the laser scanning data is less detailed when closer to the water surface. Average point spacing around the coastal area is, however, still within a one metre range (cf. 4.8 and 4.9). It is also very similar (i.e. approximately 1 metre) in both study locations (see also Figures 4.8 and 4.9). According to (Sanborn 2010), the average point spacing within both study locations can be considered a highly detailed and accurate representation of the terrain, thus suitable for high-resolution flood modelling.

4.6.1.3 Generating multi-points from the LiDAR dataset

In this study, the size of a typical LAS file is between 60 MB and 100 MB and contains several million points. If this large amount of data was loaded directly into a geodatabase, it would create millions of records, take up considerable storage space and result in huge data files, which are difficult to manage and process. LAS files were therefore converted to a multi-points feature using the ArcGIS 3D analyst extension.

The *LAS to multi-point* conversion tool can be considered part of LiDAR data management solutions in ArcGIS, allowing the user to extract and load only the data required into a geodatabase as a feature type known as multi-points. Using the *LAS to multi-point* conversion tool enables the user to store several thousand points in a single database row and is an efficient way to store a large number of points in a database. As a result of this process, file sizes are reduced and are easier to manage and process. In addition, using LAS files, the LiDAR data can be classified based on the class code provided by the vendor. The classified data has been used here to calculate the point density (cf. step 4). The class codes, for the LiDAR data used in this study, are shown in Table 4.3.

Table 4.3 Class code for LiDAR data.

Class	Code
Non-ground	1
Ground (or Bare earth)	2
Water	9

Converting the raw LiDAR data into multi-point enables the user to build a terrain geodatabase and also means it can be used directly by ArcGIS tools. Subsequently, the terrain geodatabase can be used to generate DEM raster using the multi-point feature class. Similarly, the *point to raster* tool in ArcGIS is used to convert the multi-point feature class into a raster DEM. The MOST_FREQUENT method is applied to assign a value to the raster cell when more than one feature is located in the cell. This method assigns the feature with the most common attribute (in the particular field specified by the user) to the cell.

Apart from creating DEMs, the multi-point feature class can also be used to create DSM, slope, aspect, terrain datasets that define surfaces based on vector measurements, Triangulated Irregular Networks (TINs), contours, viewsheds, curvatures, shaded relief and intensity imagery.

4.6.1.4 Point density

Point density is different from point spacing, as it refers to the number of points in a given area, while point spacing is a one-dimensional measure referring to the distance between points (ESRI 2010). Calculating point density is one of the standard methods of assessing LiDAR data and counts the number of points within a raster cell taken as the cell value, e.g. points per raster cell. The cell value is evaluated based on the raster resolution of the dataset used. The cell size needs to be set at several times greater than the point spacing, in order to avoid an unnecessarily large raster size. The cell size, however, should be small enough to enable the identification of gaps within the dataset.

For example, for data with a point spacing of one metre, the cell size needs to be set to at least 4 m, i.e. each cell, on average, should contain at least 16 points. In order to calculate the point density for a given dataset, the multi-point feature is converted to a raster image using the ArcGIS conversion tool (*point to raster*). As a result, both a raster image and an attribute table, with the number of points assigned to each cell, are obtained. The output of the previous steps is an attribute table and a raster image (cf. Figures 4.10 and 4.11).

Figure (4.11) shows the point density distribution in both study locations (i.e. Mandurah and Rockingham). The ‘stripe’ features indicate areas of overlap between flight lines and show areas with the highest point density. The red areas indicate cells with less than 16 points per cell, mostly located around the marina area or along the coastline (in both study locations) where the LiDAR data has less detail of the terrain. The raster images show that most of the cells within the datasets have a sufficient number of points per cell (i.e. more than 15 points). It can be concluded that, overall, the data has a dense coverage, suited to high-resolution flood modelling at a 1 metre spatial resolution, at a horizontal accuracy well below 1 metre and at a vertical accuracy of 0.15 m.

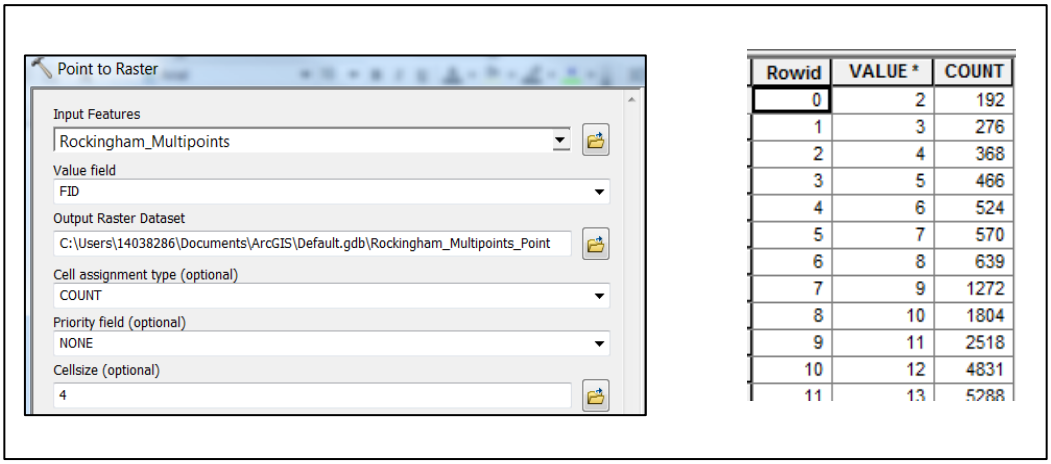

Rowid	VALUE *	COUNT
0	2	192
1	3	276
2	4	368
3	5	466
4	6	524
5	7	570
6	8	639
7	9	1272
8	10	1804
9	11	2518
10	12	4831
11	13	5288

Figure 4.10 Example for the point to raster tool (left) and LiDAR Point density table (right).

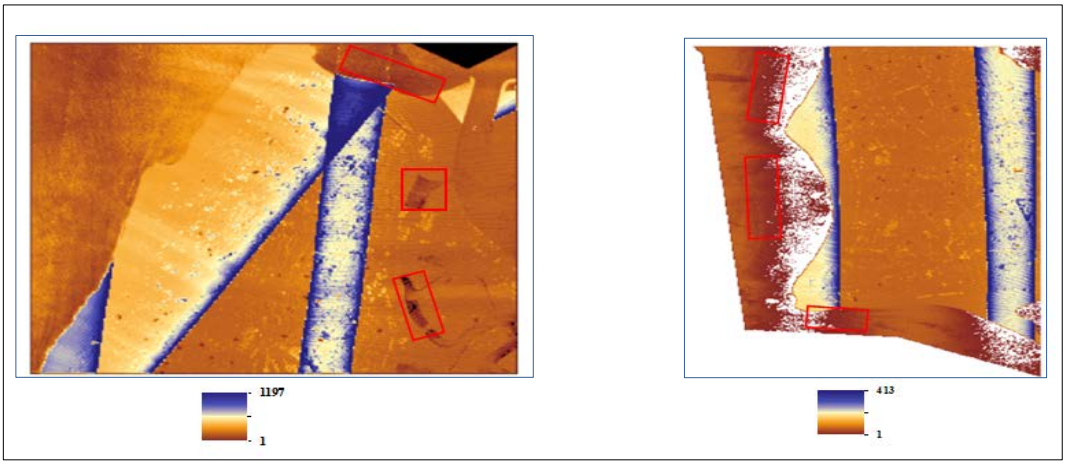

Figure 4.11 LiDAR point density in Mandurah (left) and Rockingham (right) study locations. Areas highlighted in red indicate low point density (the point density is provided in points per raster cell, e.g. 4 m by 4 m).

4.6.1.5 Intensity images

The intensity image is one of the outputs of LiDAR data and provides, in the form of a raster image, information on the strength of the return signal from the LiDAR beam. The strength of the return signal directly depends on the reflectivity of the object illuminated. Intensity images have many applications and benefits. They can be used, for example, as initial images to document coverage over the study area. Through simple visual inspection, intensity images provide a good tool for checking LiDAR data coverage within the desired study location (Cantzler 2012).

Moreover, intensity images can help in the extraction, detection, and classification of features within LiDAR points. In this study, intensity images have been used to check the LiDAR data coverage for the desired study locations. Intensity images were created using the LAS files and analysed using the ArcGIS toolbox. Figure (4.12) shows the respective intensity images for the Mandurah and Rockingham study locations. The white colour shows the terrain of the study area, while the black colour shows the road network and sea surface.

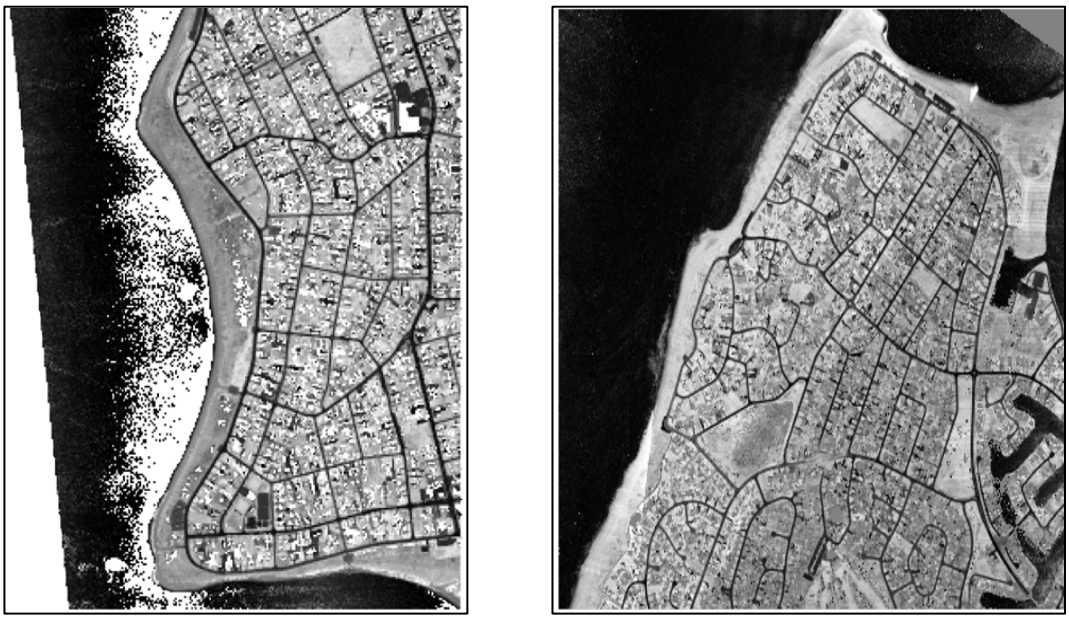

Figure 4.12 Intensity image for the Rockingham (left) and Mandurah (right) study locations. White colour shows the terrain, and black colour shows the road network and sea surface.

The intensity images for both study locations show a satisfactory LiDAR coverage. The features, such as houses and roads, can be easily identified, reflecting the strength of the return signals in both study areas. The *no-data* has been coloured white, and it can be clearly noted, by using visual inspection, that there are no large gaps in either study area. There are a few small areas in Rockingham showing no data in white along the beach area. This does not have much impact, however, as the mainland is clearly shown. Based on the above mentioned factors, it can be seen that the return signals of the LiDAR survey cover the whole study area at an acceptable level of strength (cf. Figure 4.13).

Overall, it can be seen from the results of the assessment process that the given LiDAR data is suitable for this research in terms of the resolution, point spacing, and coverage. Furthermore, it can be concluded that the data has a dense coverage suitable for high-resolution flood modelling at a 1 metre spatial resolution. It can also be concluded that the LiDAR dataset can be used to achieve the project objectives.

4.7 Flood Modelling

In this section, high-resolution LiDAR DEM data is employed to model coastal flooding based on the five different sea level rise scenarios presented in chapter 3. A detailed description of the methodology and results, in terms of the spatial extent of flooding for each study location, will be given. ArcGIS has been chosen for this study as it is the most commonly used GIS software, capable of dealing with and managing large data sets.

ArcGIS, together with ArcGIS 3D Analyst and geospatial analyst toolboxes, have been used to process the LiDAR DEM data and to derive and analyse flood information. While this section and the following section deal with the original resolution (< 1 m) of the LiDAR DEM data, section 4.9 uses re-sampled lower-resolution (30 m and 90 m) DEM data. The general processing methodology for extracting DEM data, as well as the derivation, modelling, and analysing of flooded areas, is summarised in the flow chart in Figure (4.21).

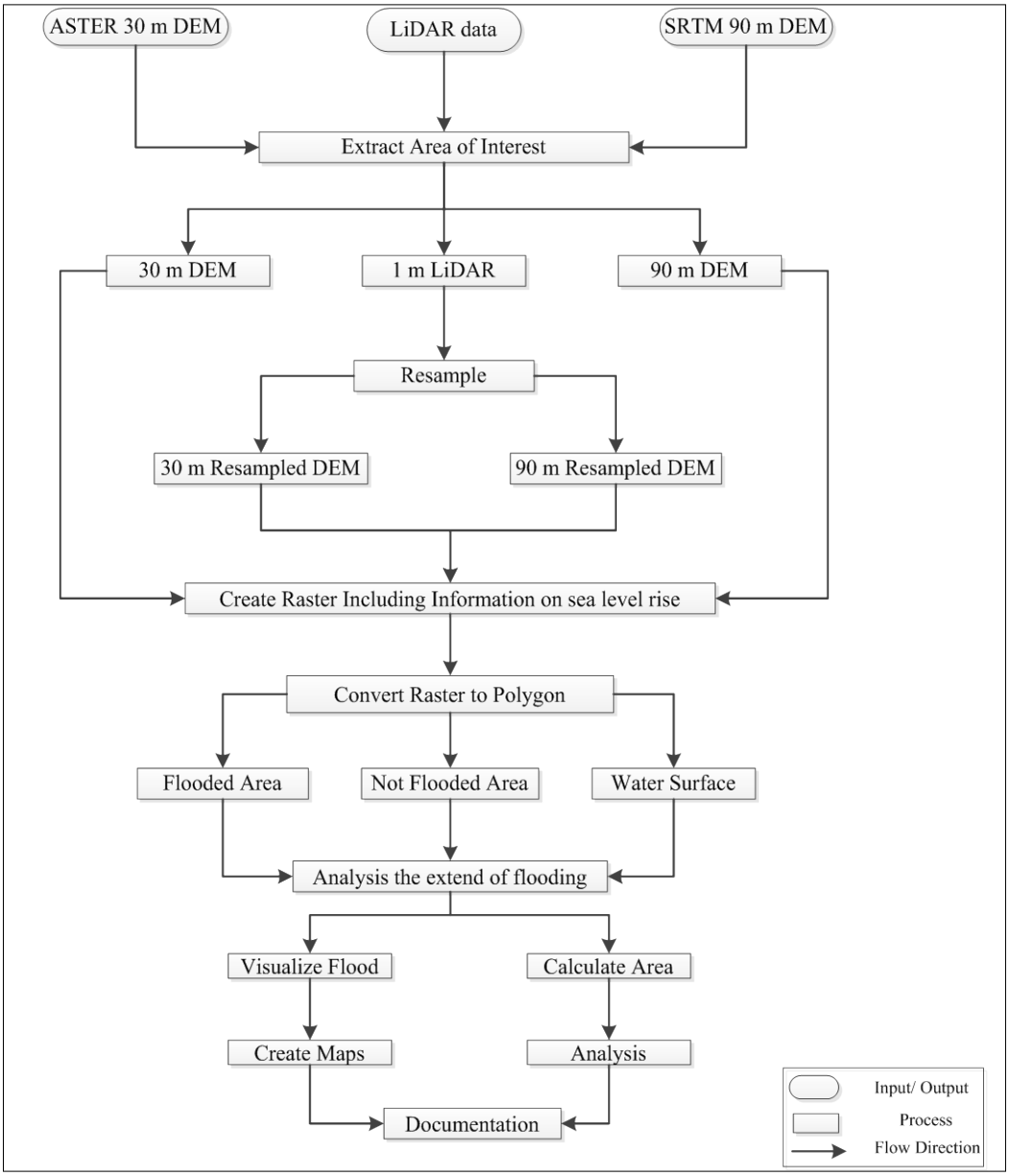

Figure 4.13 Methodology used for flood modelling.

4.7.1 Data processing

Coastal flooding, in both selected study locations, is examined using five different sea level rise scenarios representing likely global climate change effects. The sea level rise scenarios have been presented in chapter 3 and correspond to a 2.06 m, 5.98 m, 8.61 m, 10.12 m or 18.73 m rise. The flooded areas are identified using various DEM resolutions. In order to do this, the following steps are followed (cf. Figure 4.13):

4.7.1.1 DEM data acquisition

Three types of DEM have been used in this study. The spatial resolution of the DEMs used ranges from less than one metre to 90 metres. LiDAR data provides high-resolution DEM data. Apart from the high-resolution LiDAR DEM data (cf. chapter 4.5.1), lower resolution DEM data has also been used. This means it was possible to analyse both low- and high-resolution flood models. Here, both the 30 metre resolution ASTER and the 90 metre resolution SRTM were used (cf. Figure 4.13).

4.7.1.2 Extracting the area of interest

The new DEMs for the study locations are extracted from the ASTER 30 m DEM and the SRTM 90 m DEM data. For this, the clip toll in ArcGIS is used to subset the desire study areas. Polygon features, representing the study area boundaries, are used as the output extent. The output raster datasets, for both study locations, are stored in a personal geodatabase as TIFF images (cf. Figure 4.13).

4.7.1.3 Re-sampling LiDAR data

One of the objectives of this study is to assess the difference between high-resolution and low-resolution DEM data for flood modelling purpose. The high-resolution LiDAR data is, therefore, re-sampled to the lower resolutions of 30 m and 90 m. The re-sampling was performed using the *resample* tool in the data management toolbox in ArcGIS, which re-samples the raster imagery by resizing the cell size to the desired resolution (i.e. 30 m and 90 m) using bilinear interpolation. Re-sampling raster datasets can be performed by altering the cell size, depending on the re-sampling method used. Although the cell size can be altered, the spatial extent of the raster will not be changed. Re-sampling raster, using bilinear interpolation, defines the new value for the raster cell as a weighted average of the centres of the surrounding four input cells (i.e. 30 m and 90 m resolution obtained by calculating the average of all 1 m cells located within a 30 m or 90 m cell). The value is then altered to account for the distance from the centre of the re-sampling cell (cf. Figure 4.13).

4.7.1.4 Deriving flooded areas from the raster datasets

Based on the raster DEM data, the spatial extent of flooding, for a sea level rise scenario, is modelled using the raster calculator in ArcGIS (cf. Figure 4.14). The raster calculator can be used to identify grid elements that satisfy an algebraic condition defined by the user. In this study, the following simple geometric condition is used:

*[*DEM elevation of grid element*]* < *Sea level rise scenario*

(4.1) Geometric condition used to identify flooded DEM grid elements.

The above condition is used to identify the spatial extent of flooding based on all grid elements identified as flooded. This approach assumes that the DEM elevation of zero corresponds to current mean sea level, which is true for the AHD. The raster calculator is used to identify all raster pixels that have an elevation smaller (i.e. the flooded grid elements) than the given sea level rise (cf. equation 4.1).

The resulting raster image is classified by the two values 0 and 1. The value 0 is assigned to all pixels which satisfy the given condition (i.e. elevation is smaller than the sea level rise; e.g. flooding) and value 1 is assigned to all pixels which did not satisfy the given condition (i.e. elevation is greater than the sea level rise; e.g. no flooding). The final output is a new raster image showing the inundation areas, within each study location, based on the given sea level rise scenario (cf. Figure 4.13).

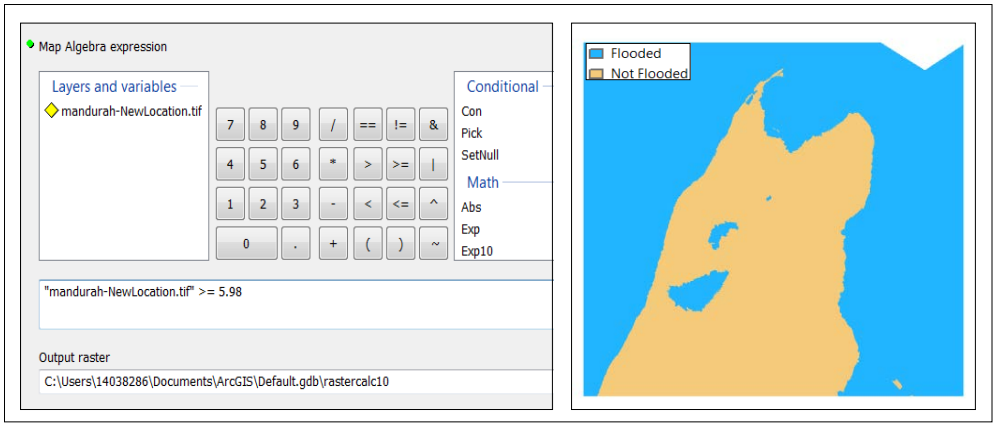

Figure 4.14 Example for the raster calculator tool (left) and the output flooding raster (right).

4.7.1.5 Converting the raster dataset to vector feature

The raster dataset is converted to vector data using the conversion tool in ArcGIS 3D Analyst. The polygon shape file obtained represents both the flooded and not flooded areas. The vector shape file, therefore, needs to be classified in terms of flooding (i.e. flooded or not flooded) (cf. Figure 4.13).

Because the raster image deals with two numbers only (0 for a flooded area and 1 for non-flooded area), the classification can be achieved by creating a new field in the attribute table (in which to store the flood condition value), then by selecting the values representing flooded areas, and then finally, by assigning the appropriate flood condition (cf. Figure 4.13 and 4.15).

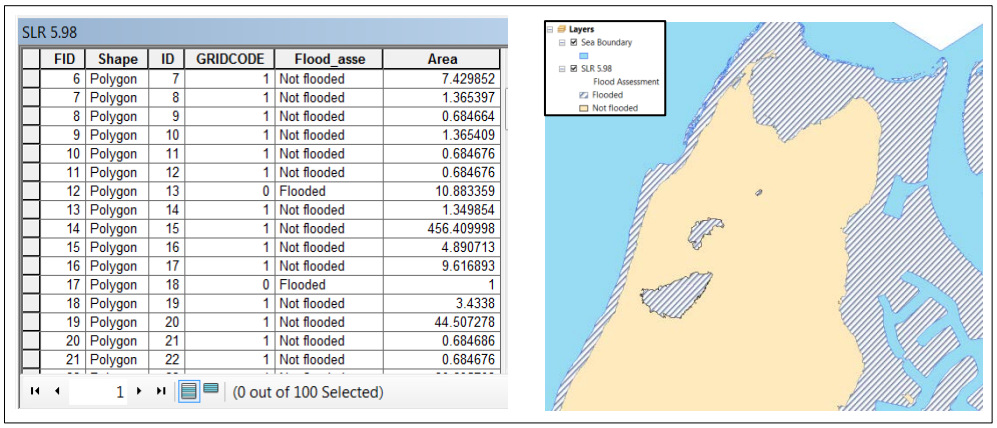

Figure 4.15 Example for the calculation of the flooded areas (left) and the classified polygons (right).

4.7.1.6 Calculating the flooded and not-flooded areas

The polygon shape files can be used to calculate the inundated areas for the purpose of analysing the extent of each flood scenario. This calculation can be performed using the *Calculate Area* tool in ArcGIS. The resulting table is shown in Figure (4.15) (cf. Figure 4.13).

4.7.1.7 Visualising the extent of flooding on thematic maps

Thematic mapping is a useful way of showing the extent of flooding for each of the different sea level rise scenarios. Thematic mapping is used in this study for many reasons including its ability to both provide information about the flooded areas and its ability to show the spatial pattern of both the flooded and not-flooded areas. As a result, it becomes easy to compare the pattern in two thematic maps, each presenting information pertaining to a particular sea level rise scenario (cf. Figure 4.13).

4.7.1.8 Documentation

This step encompasses the actual report writing that documents all results. It includes the description of the flooded areas, for each scenario, and the presentation and discussion of statistical values (cf. Figure 4.13).

4.8 Flood modelling based on LiDAR DEM data

Applying the flood modelling tool (described in chapter 4.7.1), to the five sea level rise scenarios, this section reports on all results within each study location (i.e. Mandurah and Rockingham). Coastal flooding is simulated based on high-resolution LiDAR DEM and the five sea level rise scenarios of 2.06m, 5.98 m, 8.61 m, 10.12 m, and 18.73 m (cf. chapter 3.6.5). Maps are produced, showing the spatial extent of flooding and the statistics of the flooded and non-flooded areas. The results obtained will form the basis for advanced flood modelling on a property-by-property level (cf. chapter 5.3.2).

4.8.1 Sea level rise of 2.06 m

The first flooding scenario represents the projected sea level rise, under average conditions, by the year 2100, and includes average wave and storm surge heights (cf. chapter 3.6.5). The projected sea level rise in this scenario is 2.06 m. High-resolution DEM obtained from LiDAR was used for the modelling process. The above sea level rise scenario has been applied to both Mandurah and Rockingham. The maps in Figure (4.18) show the spatial extent of flooding in both study locations. For the Mandurah study location, it can be clearly seen that most flooding takes place along a fringe of the coast line, although there is some considerable flooding along the Mandurah channel. The study area in Rockingham is only minimally affected in this flooding scenario, as the flood is limited only to small areas along the coastline (cf. Figure 4.18).

Figure (4.18) shows the extent of the flooded and non-flooded areas. For Mandurah, the flooded area is 364,191 m^2, which corresponds to 15% of the total study area. The non-flooded area is 2,049,665 m^2, representing 85% of the total study area. In Rockingham, the flooded area is 128,143 m^2, which corresponds to 8% of the total study area, while the non-flooded area is 1,482,460 m^2, representing 92% of the total study area. Based on this, rather modest, sea level rise scenario, Figure (4.18) shows that projected flooded areas are slightly higher for the Mandurah area than for the Rockingham study location. This shows that Mandurah has a larger coastal area with an elevation of less than 2.06 m (cf. Figures 4.17 and 4.18).

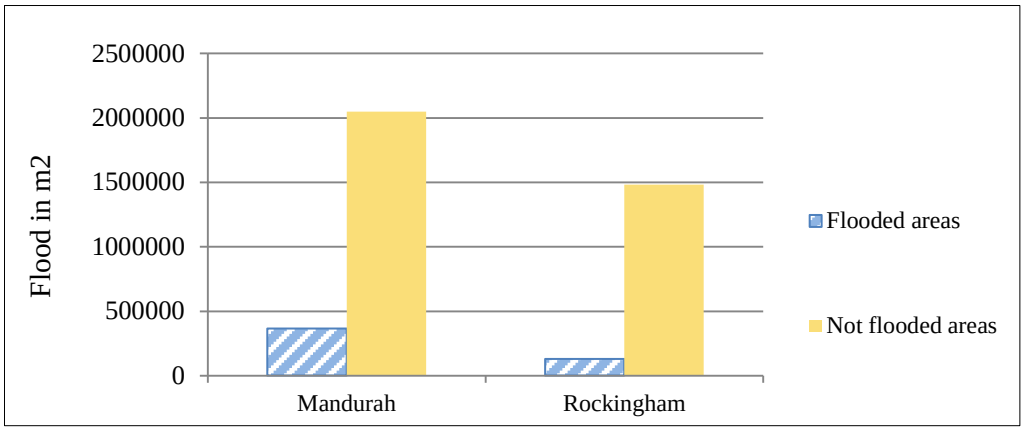

Figure 4.16 Flooded and non-flooded areas in Mandurah and Rockingham at a sea level rise of 2.06 m.

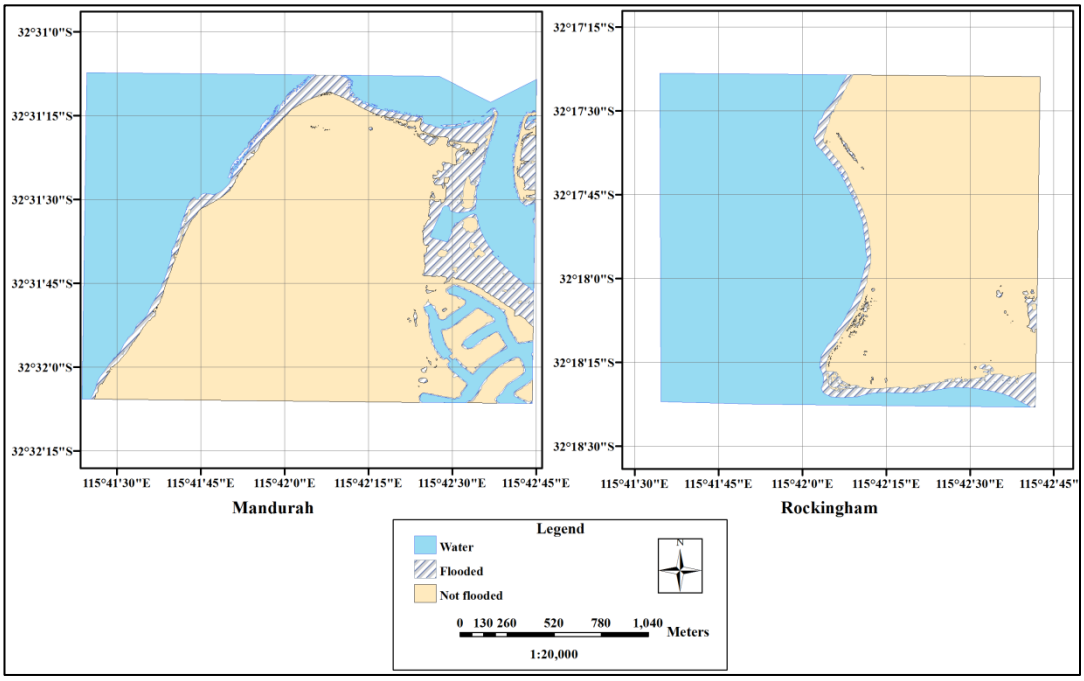

Figure 4.17 Spatial extent of the flooded areas in Mandurah and Rockingham at a sea level rise of 2.06 m.

4.8.2 Sea level rise of 5.98 m

The extent of coastal flooding in both study locations has also been examined based on a projected sea level rise of 5.98 m. This flooding scenario represents the projected sea level by the year 2100 and includes short term effects, such as maximum tide, wave, and storm surge heights (cf. chapter 3.6.5). The figures obtained at the modelling stage show that more than 40% of the total land area in Mandurah will be flooded if the sea level rises to 5.98 m. The water will cover a main land area of 975,155 m^2, which means that Mandurah will be classified as high risk, with more than 40% of the main land flooded. Non-flooded areas equate to less than 60% (1,438,702 m^2) of the study location.

Figure (4.19) shows that the flood extent in Mandurah, for this scenario, is larger than for the previous scenario (cf. chapter 4.8.1). The area mostly affected is located on the eastern side, around the marina; this is due to the low-lying main land. The figure shows that the water has now totally covered the marina area on the eastern side compared to the partial flooding shown in the previous flooding scenario. Also, a large area in the north of the study area is flooded in this scenario. Smaller flooded areas can be noted in the centre of the study location, indicating a trough of lower elevations surrounded by higher elevations that are not flooded. The results indicate that, compared to the previous flooding scenario, the flooded areas have increased by more than 20%.

The flooding model of Rockingham shows a higher flooding extent compared to the flooding extent in Mandurah, which highlights the difference in topography between the two sites. More than 1,346,642 m^2 of the study location at Rockingham is flooded, which represents about 83.6% of the total land area. Approximately 16.4% (263,963 m^2) of the land will not be flooded. Large areas of the study location in Rockingham are, therefore, flooded, showing that elevations are mostly below 6 m (cf. Figures 4.19 and 4.20). Compared to the previous scenario, the affected area has increased by 76% (cf. chapter 4.8.1). Furthermore, apart from some higher elevation areas, in the north of the study site, most of the area is flooded. In the previous flooding scenario, the flood is limited to small areas along the coast line.

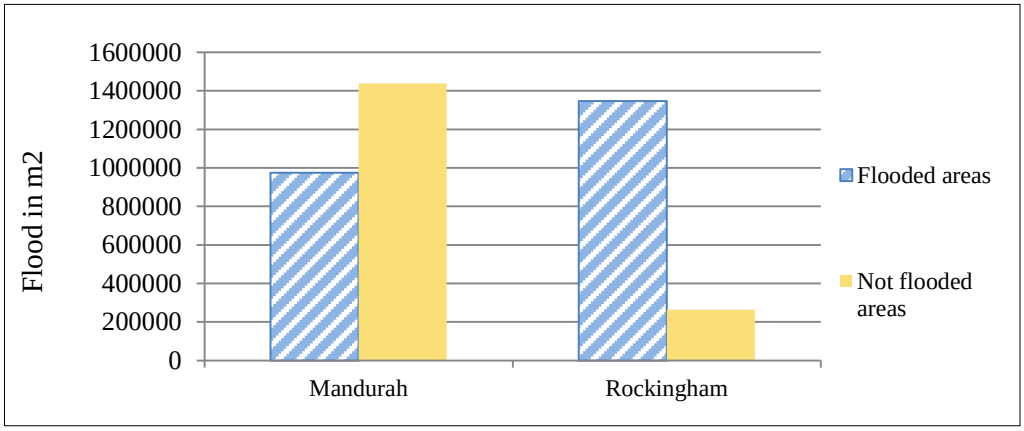

Figure 4.18 Flooded and non-flooded areas in Mandurah and Rockingham at a sea level rise of 5.98 m.

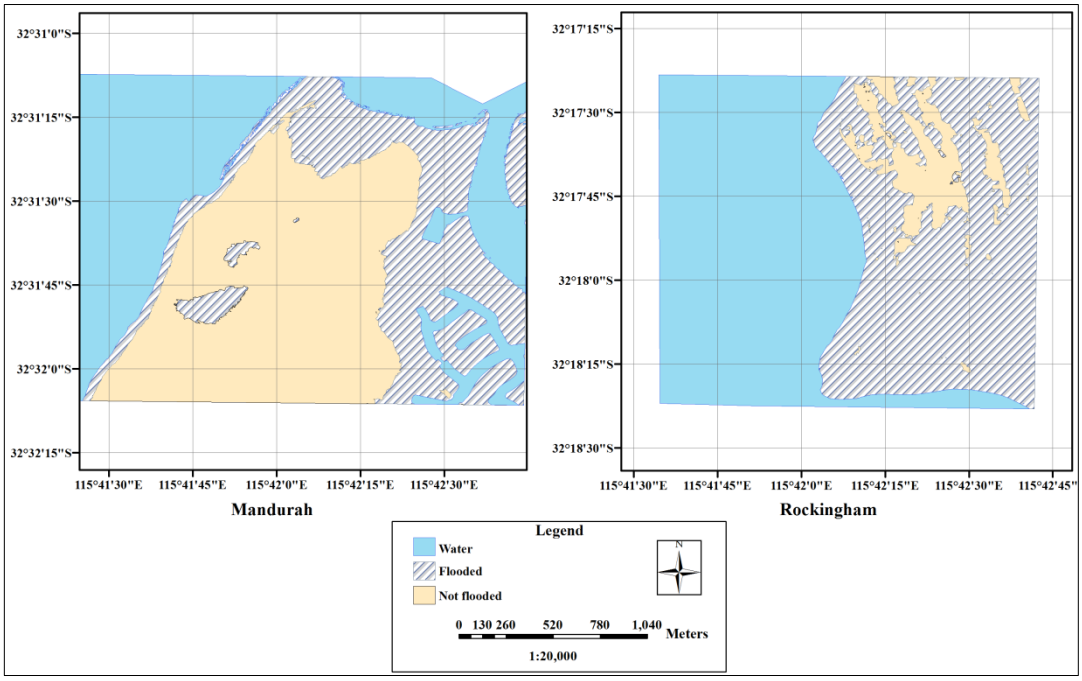

Figure 4.19 Spatial extent of the flooded areas in Mandurah and Rockingham at a sea level rise of 5.98 m.

4.8.3 Sea level rise of 8.61 m

The melting of Greenland's ice sheet, due to global warming and climate change, is considered one of the main sources of sea level rise. The rise in sea level resulting from this phenomenon can cause a real threat to residential areas located near to the shoreline. In this sea level rise scenario, the contribution of Greenland's melting ice sheet has been added to the sea level rise projected by the year 2100, including the short term effects (cf. chapter 3.6.5).

Modelling the flood at 8.61 m shows that, in Mandurah, an area of 1,175,846 m^2 will be flooded, and the flood will cover around 48.7% of the mainland. An area of 1,238,010 $m^{2,}$ in this flooding scenario, will not be flooded (51.3% of the land). The flooding extent in this scenario is larger than in the last flooding scenario by almost 9% (cf. chapter 4.8.2). It also increases considerably on the northern side and around the marina. There is also an increase of the flooded area in the centre of the study area. However, the flood extent is still minimal on the west coast of the study area.

The flood situation in Rockingham is more extreme than in Mandurah, since the flood extent covers almost all of the land, being 98.6% of the study area (1,588,840 m^2). Only less than 1.4% of the study area (21,764 m^2) will not be flooded at an 8.61 m sea level rise (cf. Figures 4.21 and 4.22). The map shows that Rockingham is almost fully flooded when the sea level rises to 8.61 m, with the flooded area increasing by 15% compared to the previous flooding scenario (cf. chapter 4.8.2).

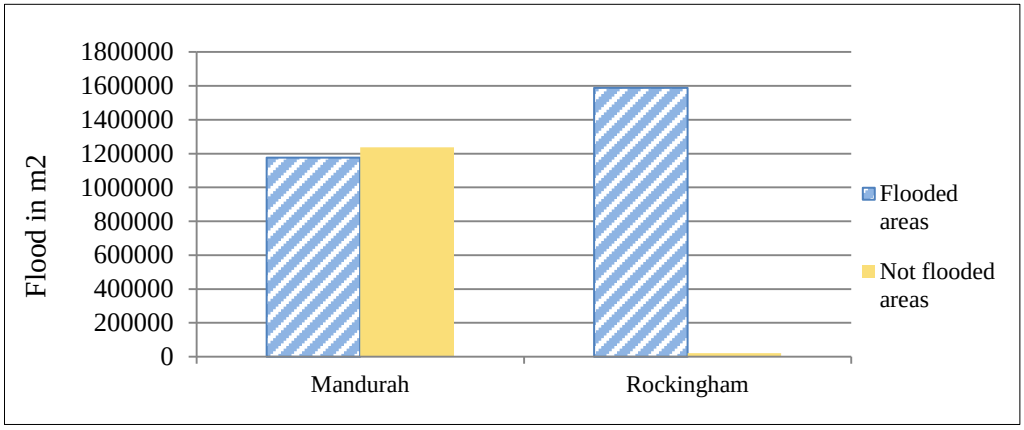

Figure 4.20 Flooded and non-flooded areas in Mandurah and Rockingham at a sea level rise of 8.61 m.

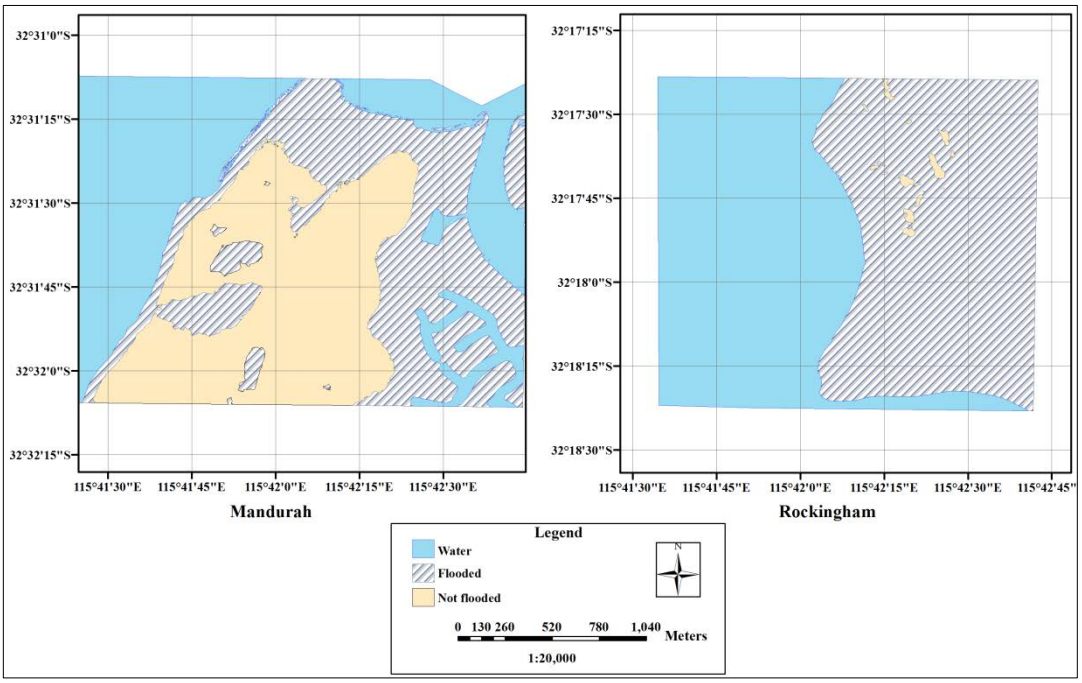

Figure 4.21 Spatial extent of the flooded areas in Mandurah and Rockingham at a sea level rise of 8.61 m.

4.8.4 Sea level rise of 10.12 m

The fourth flooding scenario (cf. chapter 3.6.5) modelled in this research is when the sea level rises to 10.12 m. This would be due to the melting of the West Antarctic Ice Shelf (WAIS). It is estimated that the melting of the WAIS will raise global sea level by around 8 m. In this flooding scenario, the projected sea level rise by 2100 is added to the contribution of the melting WAIS.

The result of the modelling stage for Mandurah shows that 1,345,051 m^2 (55.7% of the total land area) is at risk of coastal flooding. An area of 1,068,805 m^2 will not be flooded, representing around 44.3% of the total land area. The above can be seen in Figure (4.23). With only a 7% increase in the total flooded area, the flood extent in Mandurah is quite similar to the previous scenario (cf. chapter 4.8.3).

In Rockingham, however, almost the total land area, e.g. 1,606,866 m^2 (99.7%) is flooded in this scenario. The non-flooded area will occupy only 3,738 m^2. It can be seen in Figure (4.23) that Rockingham is fully flooded in this flooding scenario. The extent of flooding, however, is quite similar to the previous scenario (cf. chapter 4.8.3), the total flooded area increasing by only 1%. Nevertheless, the figures reveal that the extent of the coastal flooding in Rockingham at 10.12 m will be much higher than in Mandurah, since the entire study location is fully flooded (cf. Figures 4.23 and 4.24).

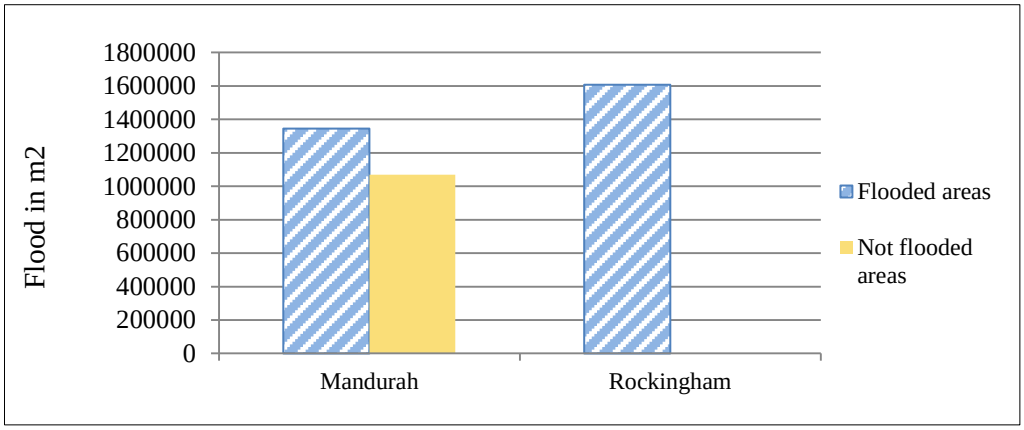

Figure 4.22 Flooded and non-flooded areas in Mandurah and Rockingham at a sea level rise of 10.12 m.

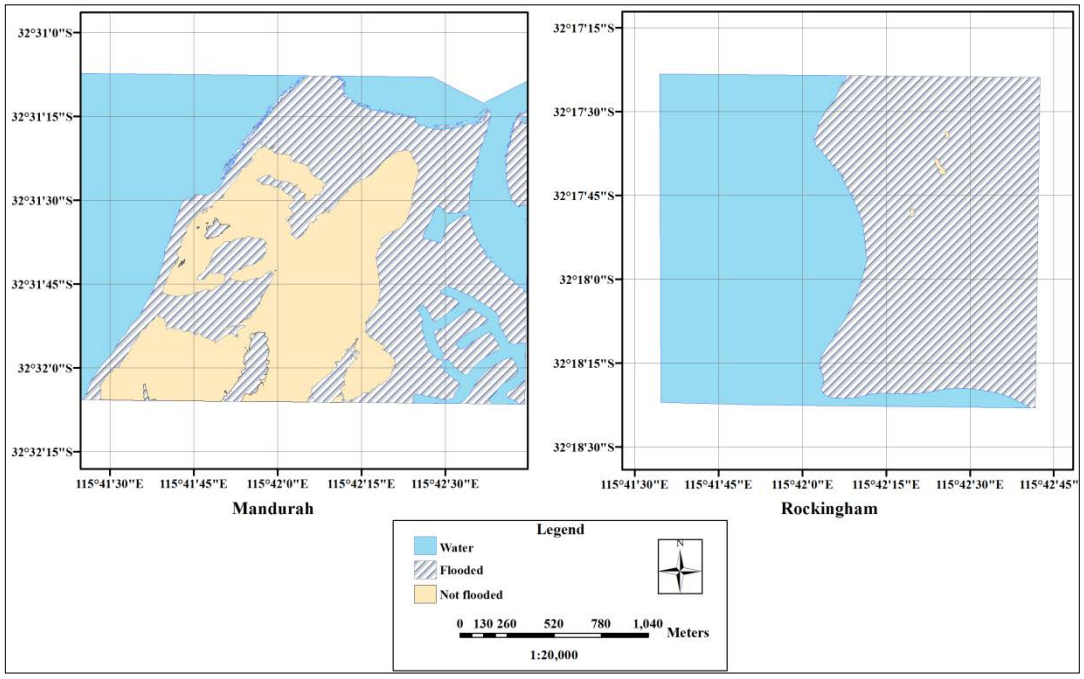

Figure 4.23 Spatial extent of the flooded areas in Mandurah and Rockingham at a sea level rise of 10.12 m.

4.8.5 Sea level rise of 18.73 m

The final sea level rise scenario applied in this flood modelling study is a projected sea level rise of 18.73 m (cf. chapter 3.6.5). This value has been estimated by adding the contribution of both the melting ice sheet in Greenland and the melting West Antarctic Ice Shelf (WAIS) with the projected sea level by the year 2100. The contribution of Greenland's ice sheet, in this scenario, is 6.5 m, while the contribution of the West Antarctic Ice Shelf (WAIS) is 8.06 m. The contribution of short term effects on sea level rise, such as tide and storm surges effects, have also been considered in this flooding scenario.

As shown in chapter 4.4.2, the highest elevation in the Rockingham study area is 12.8 m above the current mean sea level, whereas the highest elevation in Mandurah is 30.2 m above sea level. The study area in Rockingham, therefore, will be fully flooded in this flooding scenario, and flood modelling will be conducted only for the study area in Mandurah.

The extent of coastal flooding has significantly increased in the Mandurah flooding scenario. Most of the land area is now flooded, since flood water now covers around 93% of the total land area, which is an area of 2,246,761 m^2. The areas not at risk of coastal flooding have shrunk to less than 7% of the total area. This is equal to an area of 167,095 m^2. The study area in Mandurah is now highly affected compared to the previous scenario (cf. chapter 4.8.4), as the flood extent increases by 37% (cf. Figures 4.25 and 4.26).

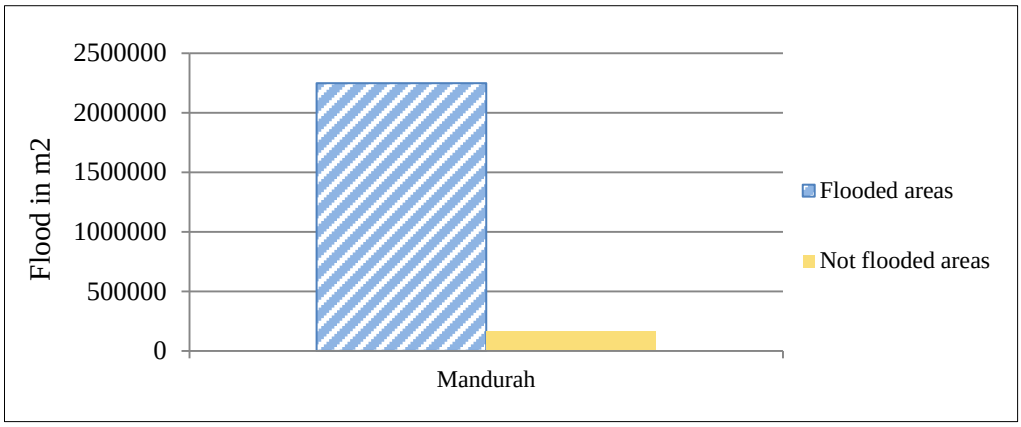

Figure 4.24 Flooded and non-flooded areas in Mandurah at a sea level rise of 18.73m.

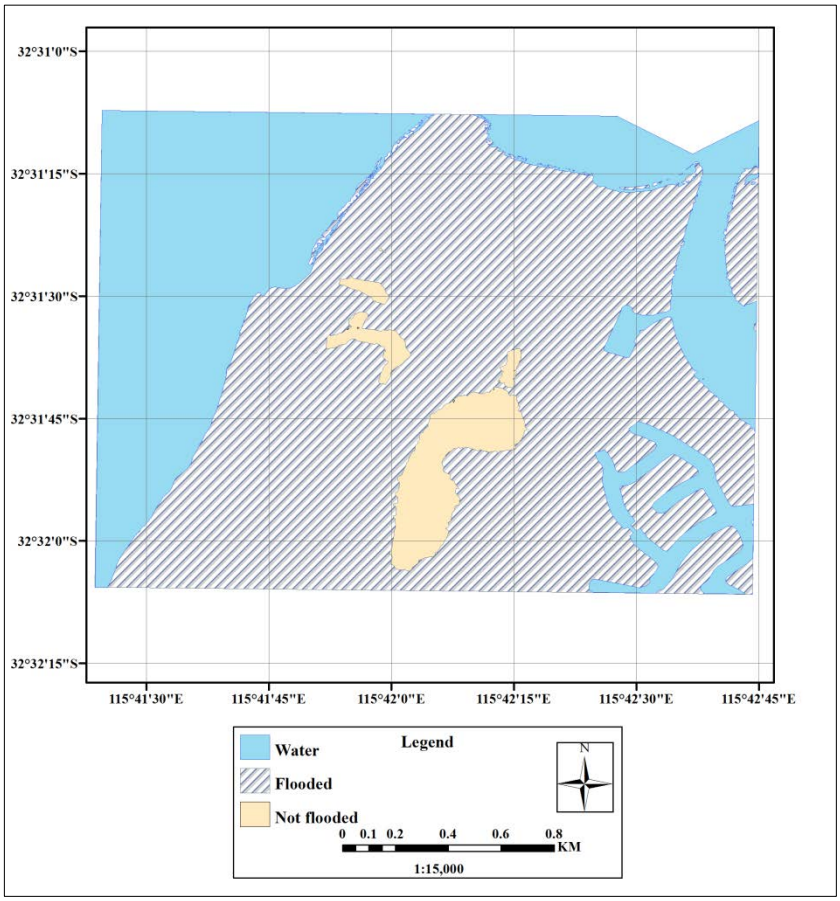

Figure 4.25 Spatial extent of the flooded areas in Mandurah at a sea level rise of 18.73 m.

4.9 Comparison between low- and high-resolution flood modelling

The comparison between the use of low- and high-resolution DEM data for flood modelling is one of the objectives of this study. In this section, the attention will be focused on the level of detail that can be modelled when using either high- or low-resolution DEM data. This comparison will be conducted using high-resolution LiDAR DEM data (< 1 m spatial resolution) and lower resolution DEM data, such as 30 metre resolution ASTER and 90 metre resolution SRTM data. In addition, LiDAR DEM data, re-sampled to 30, and 90 metre resolutions, is used. Using the DEM data, coastal flooding is examined in two different terrain geomorphologies, i.e. the two study locations. The effect on flood modelling, when using different DEM resolutions, is reported in terms of the spatial extent of flooding and the areas flooded.

For the flood models using lower resolution DEM data, the original ASTER and SRTM data (cf. chapter 4.7.1) was clipped in order to extract the DEM data over the selected study locations. Furthermore, the original LiDAR DEM has been re-sampled to 30 m and 90 m resolution DEMs. The re-sampling has been conducted using the data management toolbox in ArcGIS, and flood modelling has been carried out with the flood modelling tool presented in chapter 4.7.2. For brevity, only one sea level rise scenario (5.98 m rise) has been selected here as an example. For completeness, the results for all other scenarios are given in appendix A.

4.9.1 Sea level rise of 5.98 metres in Mandurah

Based on the sea level rise scenario of 5.98 metres, flooding has been modelled for all DEMs and resolutions within the Mandurah study location. Figure 4.29 shows the spatial extent of flooding based on the different DEMs and resolutions. The analysis of the flood extents for the 1 m, re-sampled 30 m, and re-sampled 90 m DEMs resolutions, used in this study, show similar flood boundaries. However, flood extents obtained by ASTER 30 m and SRTM 90 m show a different pattern compared to the 1 m, re-sampled 30 m, and re-sampled 90 m data.

The results for the re-sampled LiDAR DEMs generally show smoother and less fragmented flood boundaries. The general similarity is also demonstrated by the almost identical areas recorded for the three DEM resolutions. This trend is further supported by the near identical mean elevation in the study area for all the DEM resolutions (cf. Figure 4.27). While the re-sampled LiDAR DEM data has practically identical mean elevation values, there is a small bias between the LiDAR DEM data, the ASTER, and SRTM DEM data.

It can be clearly noticed that the DEM resolution has a considerable impact on the shape of the flood extent. Using high-resolution DEM data results in highly detailed flood boundaries, whereas ASTER 30 m and SRTM 90 m data shows coarse flood boundaries. The results show that re-sampled LiDAR DEMs provide similar spatial extents, as does the 90 m SRTM DEM. However, the results for the ASTER DEM seem odd, bearing little resemblance to the other results. Re-sampled LiDAR DEMs (i.e. 30 m and 90 m) provide smoother results when compared to the ASTER DEM and SRTM DEM.

This gives an indication of both the performance and quality of the low-resolution raster (re-sampled from LiDAR data), when re-sampled from high- to low-resolution. It proves high-resolution data can perform better and provide much more detailed results compared to the low-resolution data (cf. Table 4.4 and Figures 4.27 and 4.28).

Figure (4.28) documents the flooded and non-flooded areas for the three DEM resolutions used. Modelling the flood, using a 1 m resolution derived from LiDAR data, shows that less than half of the study area is flooded. The total area flooded is 975,155 m^2 (40.4%). For the lower resolution DEM data, the results show that the inundation area (when ASTER 30 m DEM is used) is 544,379 m^2 and occupies around 18.2% of the total area. The result obtained, using SRTM 90 m DEM, shows that 975,608 m^2 of the total land area is flooded when sea level rises to 5.98 m. In this instance, the flooded areas occupy approximately 37.6% of the total land area (cf. Table 4.4).

The re-sampled 30 m and 90 m DEM data, derived from LiDAR data, is also used when modelling the flood (using the same sea level rise scenario). The result for the re-sampled 30 m DEM shows that an area of 982,702 m^2 is flooded, which is equivalent to approximately 40.9% of the study area. In addition, modelling the flood using 90 m DEM (re-sampled from LiDAR) shows a similar result to the re-sampled 30 m DEM. A total of 938,193 m^2 is located within the inundation area, which is equivalent to 40.2% of the total land area (cf. Table 4.4 and Figures 4.28 and 4.29).

Table 4.4 Flooded and not flooded areas using different DEMs resolutions for the study area in Mandurah. Uint in square meters.

	Flooded	Not Flooded	Total
1 m LiDAR	975,155 40.4%	1,438,702 59.6%	2,413,857 100%
Re-sampled 30 m	982,702 40.9%	1,420,819 59.1%	2,403,521 100%
ASTER 30 m	544,379 18.2%	2,445,397 81.8%	2,989,776 100%
Re-sampled 90 m	938,193 40.2%	1,393,121 59.8%	2,331,313 100%
SRTM 90 m	975,608 37.6%	1,619,830 62.4%	2,595,438 100%

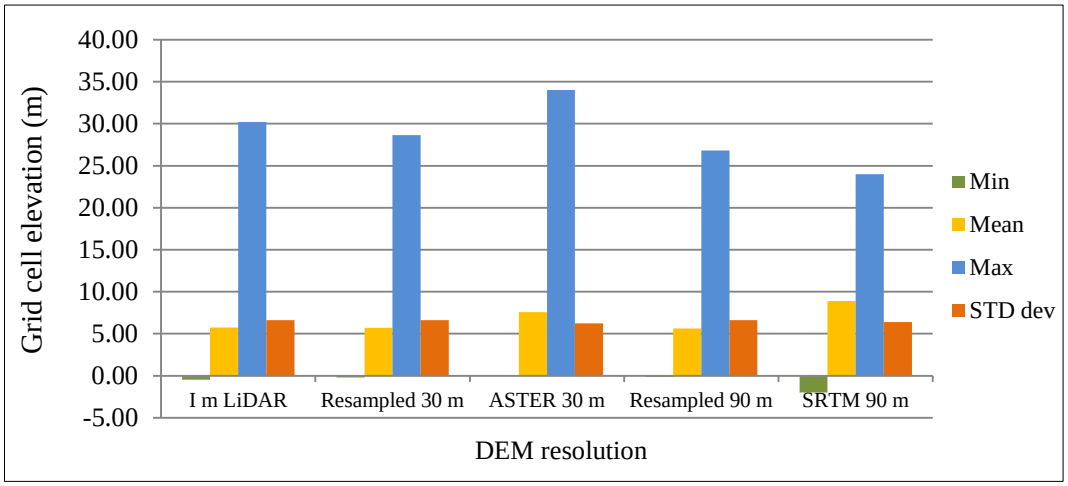

Figure 4.26 DEM resolution and grid cell Elevation Mandurah study area. Re-sampled 30 m and 90 m stands for the re-sampled LiDAR DEM data.

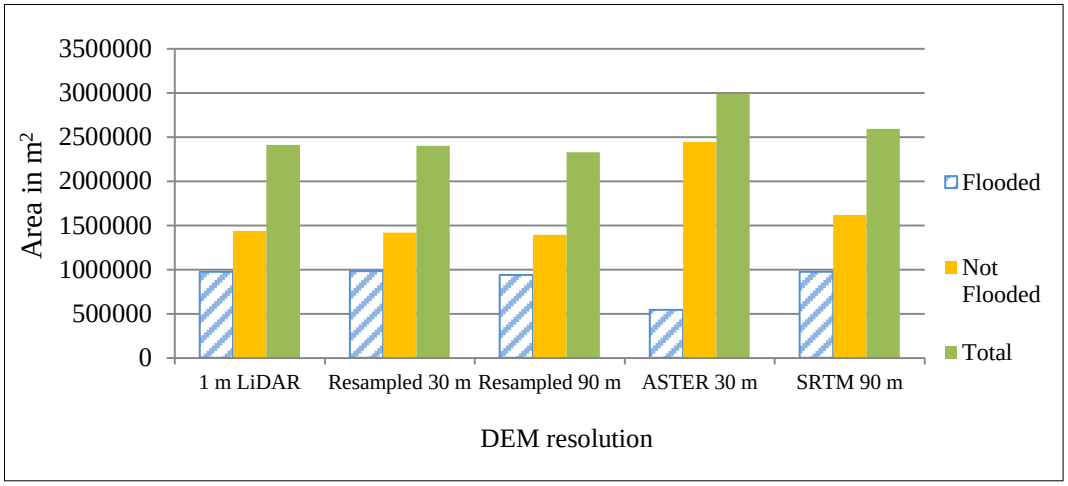

Figure 4.27 Flooded and non-flooded areas in Mandurah at a sea level rise of 5.98 m for different DEMs and resolutions.

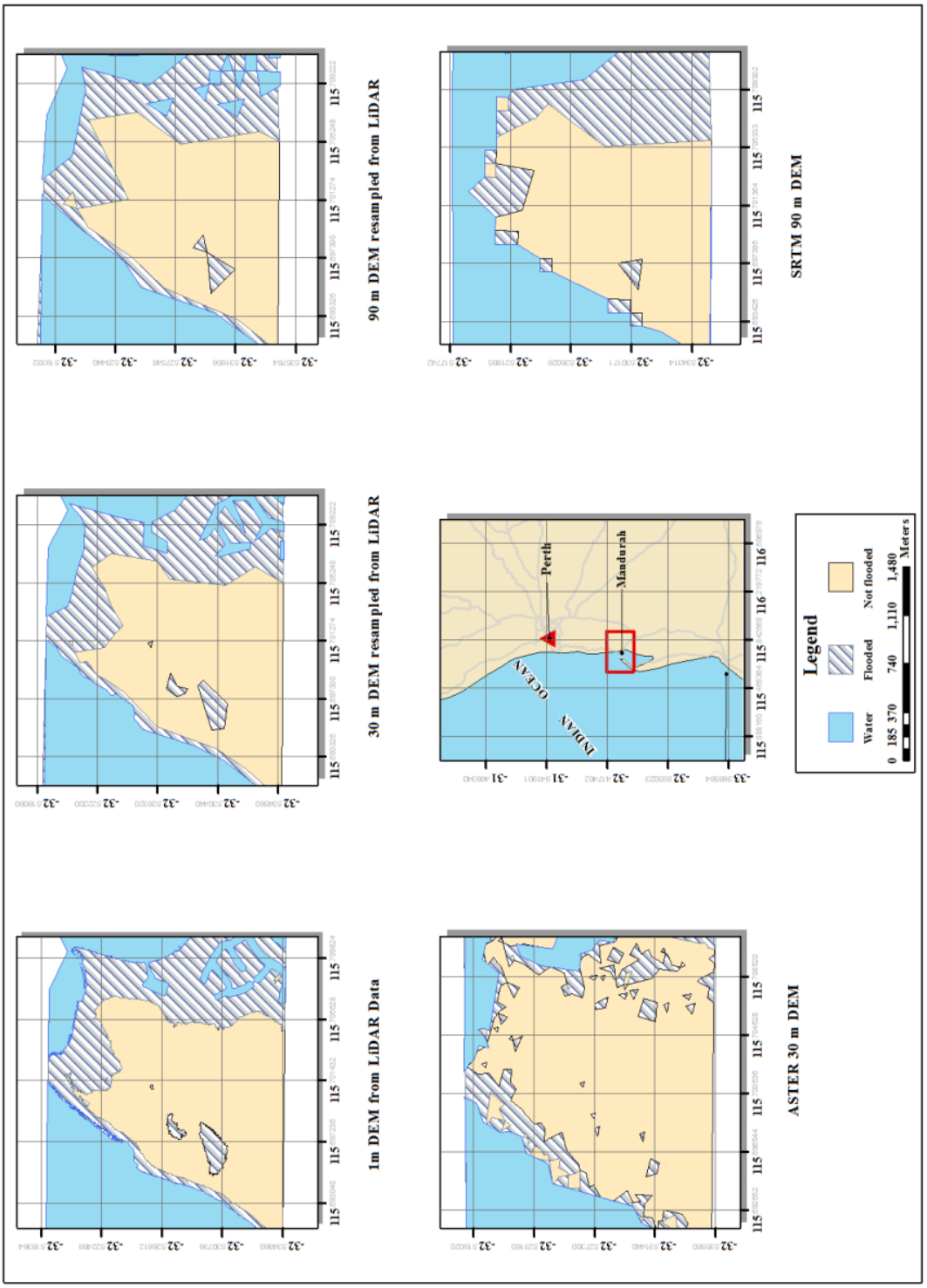

Figure 4.28 Comparison of flooded areas between different DEMs and resolutions at a sea level rise of 5.98 m within the Mandurah study location.

4.9.2 Sea level rise to 5.98 metres in Rockingham

Modelling coastal flooding in different topography settings provides information on the need to use high-resolution data in certain cases. Thus, the impact of coastal flooding, due to sea level rise, has also been modelled in Rockingham, using the same DEM resolutions and sea level scenario as for Mandurah (cf. chapter 4.9.1). Figure (4.32) shows the spatial extent of flooding using the three DEM resolutions.

As for the Mandurah study area, the analysis shows similar flood extents when using 1 m LiDAR DEM, 30 m, and 90 m re-sampled LiDAR DEMs. As expected, the 30 m and 90 m re-sampled DEMs provide considerably less detail compared to the 1 m LiDAR DEM. Although the previous DEMs (i.e. 1 m, re-sampled 30 m, and re-sampled 90 m) have a different raster cell size, they show a similar flood extent (cf. Figure 4.30). The maps show that the flood extents are completely different when using low-resolution DEMs compared to the high-resolution DEMs. The SRTM 90 m DEM shows a different behaviour to the results obtained in Mandurah. Using the same DEM resolution for the Rockingham study area, the results for both low-resolution DEMs (i.e. ASTER 30 m and SRTM 90 m) again seem to be odd. The variation in flood extent, amongst the low-resolution DEMs, demonstrates the need for high-resolution DEMs, especially in low-lying areas like Rockingham. When using the 30 m and 90 m DEMs, many of the details are omitted having a huge effect on predicted flood boundaries in low-lying areas (cf. Figure 4.3.2).

The result, when using the 1 m LiDAR DEM, shows that an area of 1,346,642 m^2 is flooded when sea level rises to 5.98 m, and an area of 263,963 m^2 is not flooded. This means that around 84% of the study area is located in the flood zone. When lower DEM resolutions are used, the results show a very different value from that obtained when using the 1 m DEM resolution. When using the ASTER 30 m DEM, the results show that an area of 131,706 m^2 is flooded. This is approximately 7% of the total area. Using SRTM 90 m DEM, the results show that 743,517 m^2 is inundated, representing approximately 46% of the total area (cf. Table 4.5 and Figures 4.31 and 4.32).

The 30 m and 90 m DEMs, re-sampled from the 1 m LiDAR DEM, have also been used in the modelling process. The figures obtained, using the re-sampled 30 m DEM, show that a total area of 1,214,349 m^2 is inundated when sea level rises to 5.98 m. In this scenario, almost 76% of the total area is located within the flood zone and approximately 23% of the study area is not flooded. The figures for the re-sampled 90 m DEM show a similar result to the re-sampled 30 m DEM. In this scenario, the total inundation area is 1,317,720 m^2 (80%), and 323,457 m^2 (19%) is not flooded (cf. Table 4.5 and Figures 4.31 and 4.32).

Table 4.5 Flooded and not flooded areas using different DEMs resolutions for the study area in Rockingham. Uint in square meters.

	Flooded	Not Flooded	Total
1 m LiDAR	1,346,642 83.6%	263,963 16.4%	1,610,605 100%
Re-sampled 30 m	1,214,349 76.4%	374,333 23.6%	1,588,681 100%
ASTER 30 m	131,706 7.3%	1,665,905 92.7%	1,797,611 100%
Re-sampled 90 m	1,317,720 80.3%	323,457 19.7%	1,641,176 100%
SRTM 90 m	743,517 46.3%	861,466 53.7%	1,604,983 100%

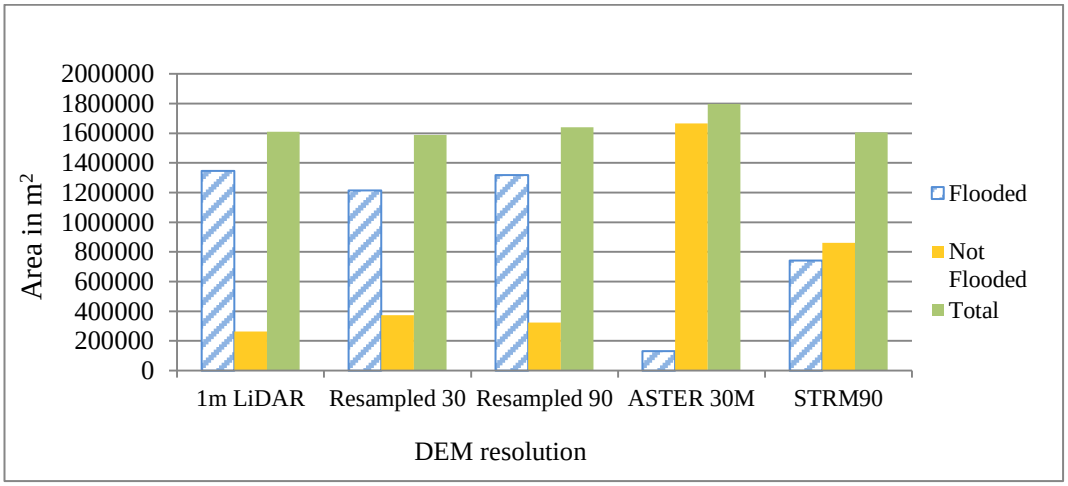

Figure 4.29 DEM resolution and grid cell elevation for Rockingham study area.

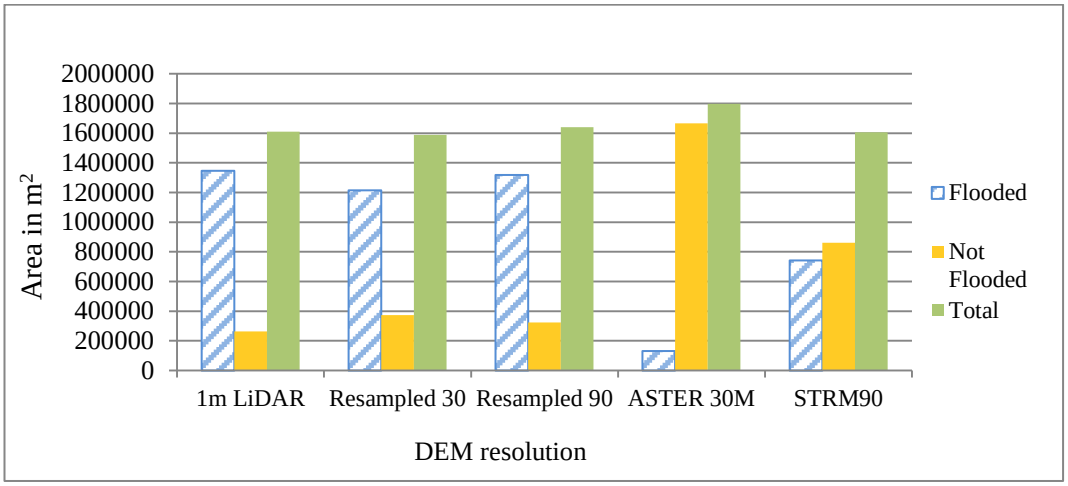

Figure 4.30 Flooded and non-flooded areas in Rockingham for a sea level rise of 5.98 m for different DEMs and resolutions.

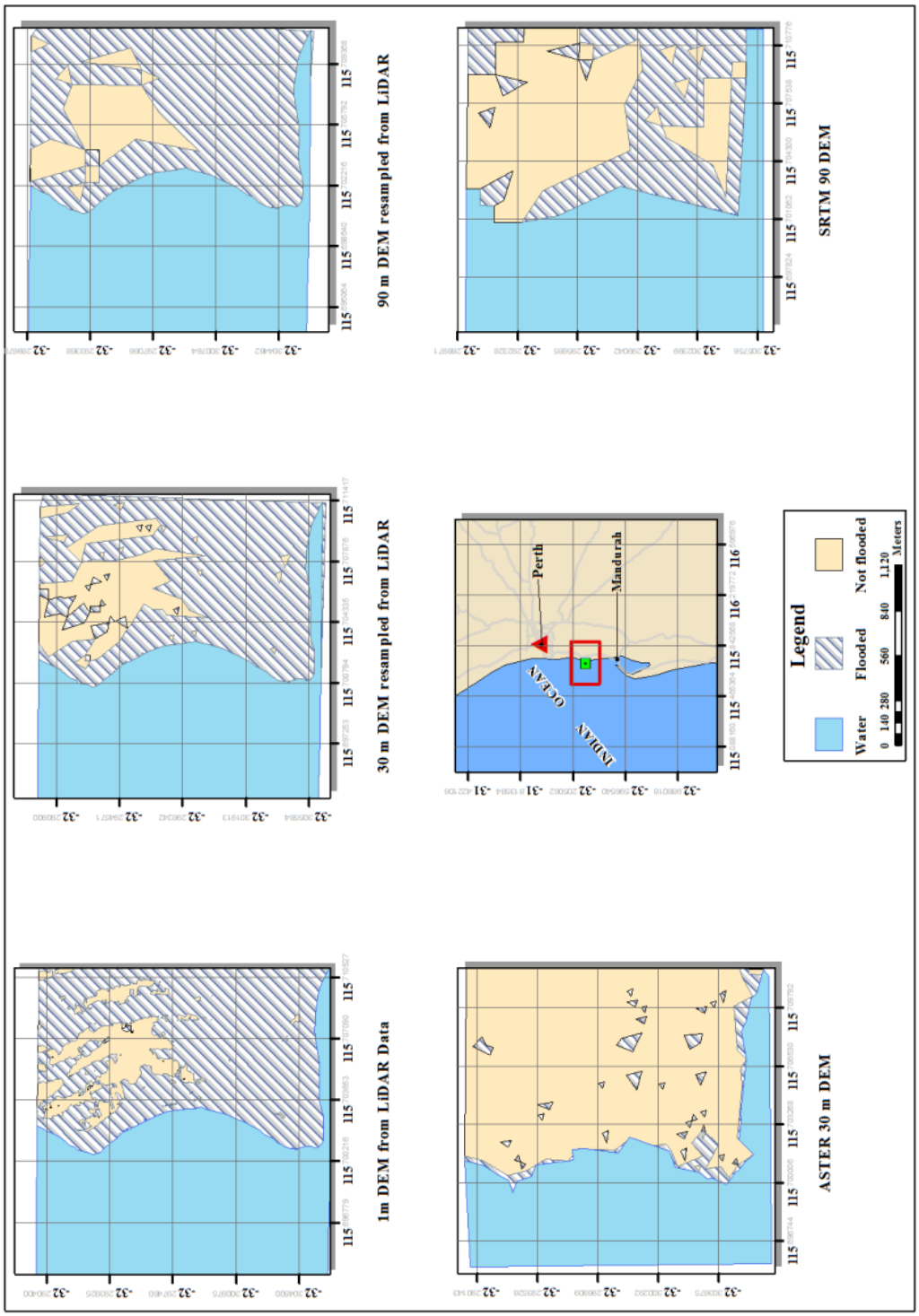

Figure 4.31 Comparison of flooded areas between different DEMs and resolutions for a sea level rise of 5.98 m within the Rockingham study location.

Various flooding scenarios have been modelled, in this study, to analyse the extent of coastal flooding, due to sea level rise, in Mandurah and Rockingham. The analysis has been based on different DEM resolutions (i.e. 1 m, re-sampled 30 m, re-sampled 90 m, ASTER 30 m, and 90 m SRTM), and it can be seen from the flood modelling analysis, the representation of the terrain is highly affected by the spatial resolution of the DEM used. Significant differences can be found between flood extent results when using different DEM resolutions. In addition, the overall results for both study sites have clearly confirmed the high sensitivity of the flood extent results to the DEM resolution used in the analysis. Moreover, it has been found that the higher the DEM resolution used, the better and more detailed flood boundaries can be obtained. The analysis also shows that when low-resolution ground elevation data is used, the flood boundaries can vary considerably.

As a consequence of the above findings, it can be concluded that incorporating low-resolution flood extent information in detailed urban planning is not recommended. In small scale applications, especially in low-lying areas, high-resolution ground elevation data is much more useful. In order to model the flood in low-lying areas, such as Rockingham, where the average height is around 2.8 m, using high-resolution elevation data is strongly recommended. Using high-resolution data may not be necessary in areas where the elevation heights are much larger. However, when the delineation of the flood extent needs to be precise, the use of high-resolution elevation data is required, regardless of the elevation.

A comparison of the different flood extents, determined by the various resolutions of the ground elevation data, highlighted a considerable loss of the topographic features when using low-resolution data. This is due to the generalization of small scale topographic features over larger elements and the interpolation of ground elevation data. This has a great influence on the reliability of flood extent results obtained. All the flood extents, obtained by different DEMs, show the same flood patterns, apart from the extent obtained by using ASTER DEM.

The re-sampled 30 m and 90 m DEMs, from LiDAR, show more detailed results in comparison to the 30 m ASTER and 90 m SRTM. Although the flood extents (using the re-sampled DEMs) have sharp edges, and a lot of details missing, they still provide a better representation of the terrain and a more accurate flood extent compared to ASTER DEM and SRTM DEM. It can be clearly noted that, in both study areas (Mandurah and Rockingham), ASTER appears to contain a bias (e.g. a higher mean value for the elevations). This can also be seen in Figure (4.30) where the results show that the ASTER DEM elevations are generally higher than 5.98 m.

The results obtained by using SRTM DEM data, in low-lying areas, are more detailed when compared to the result of the flood extents using ASTER DEM data. This has also been confirmed by (Du et al. 2015). The ASTER DEM data provides bad coverage of the coast where the study was conducted, due to the high degree of error. This proves the limitation of the freely available DEM data (such as ASTER and SRTM), as well as the use of this type of data in coastal applications.

Guth (2010) reported that ASTER Global Digital Elevation Model (GDEM) data provides less accurate results compared to SRTM data. Based on their research, they noted a negative elevation bias and confirmed that 20% of the ASTER tiles sample (10/52) showed substantial artefact (compared to SRTM). In addition, Hirt, Filmer, and Featherstone (2010) compared ASTER GDEM and SRTM coverage in Australia, and they noted a significant number of artefacts in the ASTER GDEM. They also showed that the vertical accuracy of the SRTM DEM is around 6 m, compared to 15 m for the ASTER GDEM.

4.10 Chapter summary

At the beginning of this chapter, brief information regarding the chosen study area (i.e. the south west coast of Western Australia) was provided. This particular study area was chosen due to the availability of high-resolution LiDAR data and also the diversity of geological and geomorphologic structures. Eight locations, within the study area, were proposed for further study. However, Rockingham and Mandurah were chosen as the most suitable study locations. Each of the chosen sites has very different geomorphologic and topographic structures.

A detailed description of the different types of DEM data used in this study was then provided. As the aim of this study is flood modelling using various DEMs and resolutions both high-resolution LiDAR data and low-resolution SRTM and ASTER elevation data was used. The LiDAR data was validated for suitability to this study. Data processing sections (cf. chapter 4.7.1), which deal with technical aspects, were applied to obtain the desired results, using different software such as ArcGIS. The spatial extent of flooding, based on the high-resolution LiDAR DEM data, has been shown and discussed for five sea level rise scenarios. These scenarios cover all likely near-future sea level rise scenarios. The flooded and not flooded areas are documented for each scenario and study location, with the support of figures showing spatial extent of the flooding. The chapter concludes by comparing different flood models, each based on different DEMs and resolutions. Particular focus was given to the comparison between low- and high-resolution DEM data, and the results demonstrate that there is a similar flood extent for all of the DEMs resolutions, except for ASTER DEM, and therefore, prove the need for high-resolution data when flood modelling low-lying areas.

The next chapter will cover the third and the fourth stages of this research. It will discuss the methodology used to model the flood on a property-by-property level. Also, the development of a property-based flood vulnerability index will be explained as well. Finally the development and implementation of a property-based flood GIS will be presented.

CHAPTER 5

DEVELOPMENT AND APPLICATION OF A PROPERTY-BASED FLOOD GIS

5.1 Introduction

In the previous chapter, two case study locations were selected to model flooding using various sea level rise scenarios and DEMs resolutions. The spatial extents of the flood scenarios, obtained by both low- and high-resolution elevation data, were compared and analysed. This chapter now describes the methodology used for the development of a property-based flood GIS, which is the fundamental aim of this thesis.

The chapter first describes the combination of flood information (obtained in chapter 4) with cadastral data, which allows flood related information to be provided on a property-by-property basis. For practical application, the five flooding scenarios (as described in chapter 4) have been applied to the study locations of Mandurah and Rockingham. As a central aim, inundation risks are derived and assigned to each individual property located near to the shoreline. This is based on the property's location within the flooded areas.

In addition, this chapter describes and discusses the methodology used for developing a property-based flood vulnerability index. Maps, displaying the vulnerability associated with each flooding scenario, are provided, analysed and discussed.

Finally, combining the above information, the implementation of a prototype for a property-based flood GIS is presented. In this study, the implementation is based on the ArcGIS ModelBuilder. Detailed information is provided on the development of ModelBuilder tools as part of the flood GIS. This includes information on the design of the tools, together with flow charts, user interfaces and the description of input and output data.

5.2 Combination of flood and cadastral information

This section will assess the feasibility of using high-resolution data for flood modelling at a property-by-property level, which is a main objective of this research. This requires the combination of flood information (cf. chapter 4) with 2D cadastre data with particular focus given to information on a property-by-property level (e.g. related to boundary information). Flood information, which is 3D in nature, will be matched with 2D cadastre data, or alternatively, the 2D cadastre data will be augmented with height information (e.g. from the high-resolution DEMs used). Single properties will be assessed as being fully, partly or not flooded. In the case of partly flooded properties, the degree of flooding will be assessed (e.g. percentage, area affected, etc.).

It is worth mentioning that, until now, most flood modelling is conducted over regional areas with limited resolution. This does not allow for information to be provided at a property-by-property level. For property-based flood modelling, high-resolution DEM data (e.g. 1 m resolution from LiDAR) is essential. This is exemplified in Figures (5.2 and 5.3) (in chapter 5.3), which show the spatial distribution of both 1 m resolution DEM heights (cf. Figure 5.2) and 30 m resolution DEM heights (cf. Figure 5.3). For the 1 m resolution, each property is covered by many DEM height elements, while for a 30 m resolution there are often only 1 or 2 DEM height elements that cover a single property. This situation worsens even further for a 90 m resolution, proving that a 1 m resolution is much better suited to the modelling of topography changes within a parcel of land, while lower resolutions are not.

5.3 Methodology for combining flood information with 2D cadastre data

In the previous chapter, flood information was derived for the selected study locations (i.e. Rockingham and Mandurah) for five different sea level rise scenarios. In this section, high-resolution flood information is now used to evaluate the effects on a property-by-property level. This means that relevant flooding conditions are modelled differently for each property within the study location. This allows for individual modelling of properties in the area of interest, rather than more generalised modelling information derived from the whole study area. Importantly, with this approach, neighbouring properties can be assigned distinctively different flood risk and vulnerability levels. In this study, the ArcGIS spatial analysis tool package is used for data acquisition, analysis, and visualisation.

The overall methodology of extracting data, and modelling and analysing flooded areas, is summarised in the flow chart in Figure 5.1. Details regarding each processing step are provided in the following sub-sections.

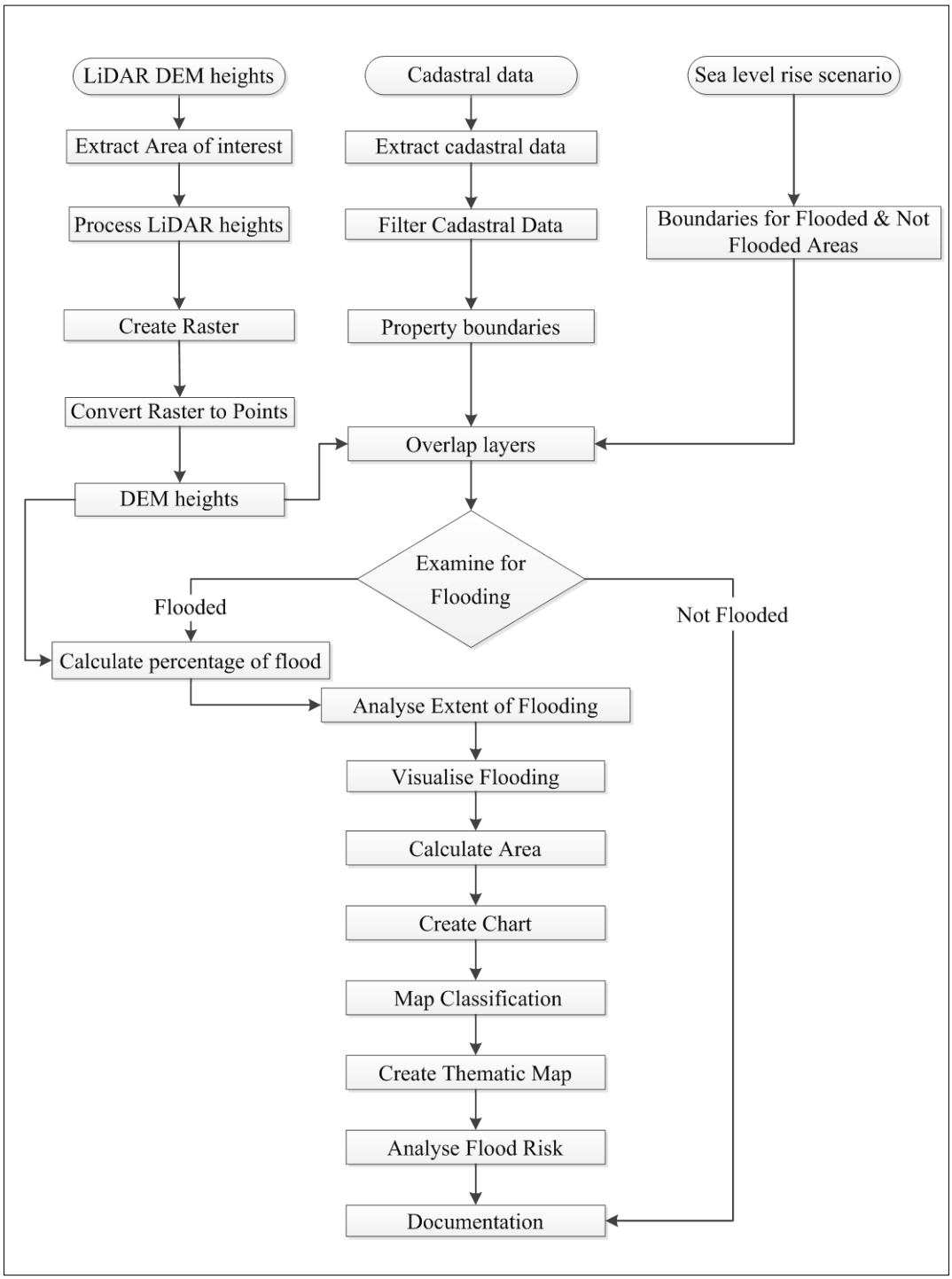

Figure 5.1 Methodology used for flood modelling on a property-by-property level.

5.3.1 Data acquisition

Cadastral data is essential when analysing coastal flooding on a property-by-property level. The cadastral data defines property boundaries and also the land use pattern for the area of interest. For this study cadastral data for both study locations were obtained from the Landgate SLIP web-portal (www2.landgate.wa.gov.au).

Landgate owns, manages and operates the Spatial Cadastral Database (SCDB) for the whole of Western Australia. The database contains the following approved information:

- Cadastral boundaries as polygon feature class.
- Lodged cadastral boundaries.
- Control marks.
- Easements.
- Surveyed mining tenement boundaries.
- Administrative boundaries.

The cadastral data available to users is provided in the following formats: ESRI shape file, DWG, DXF, DGN, SDE, and CSD. Due to a download size limit, the data for the Mandurah and Rockingham study areas were downloaded in several patches. ArcGIS was used to merge the cadastral datasets into a single dataset. Also, ArcGIS was used to filter out unwanted information, such as control marks, administrative boundaries, easements, and some duplicated layers, as the result of converting between different data formats (cf. Figure 5.1).

5.3.2 Concept of property-based flood modelling

Several methods have been used to assign the flood risk for a single property (e.g. the parcel of land enclosed by cadastral boundaries). The methods employed depend on the area inundated (cf. chapter 5.3.2.1) and the terrain height (e.g. DEM height; cf. chapter 5.3.2.2). The methods are also dependent on the DEM resolution and parcel location.

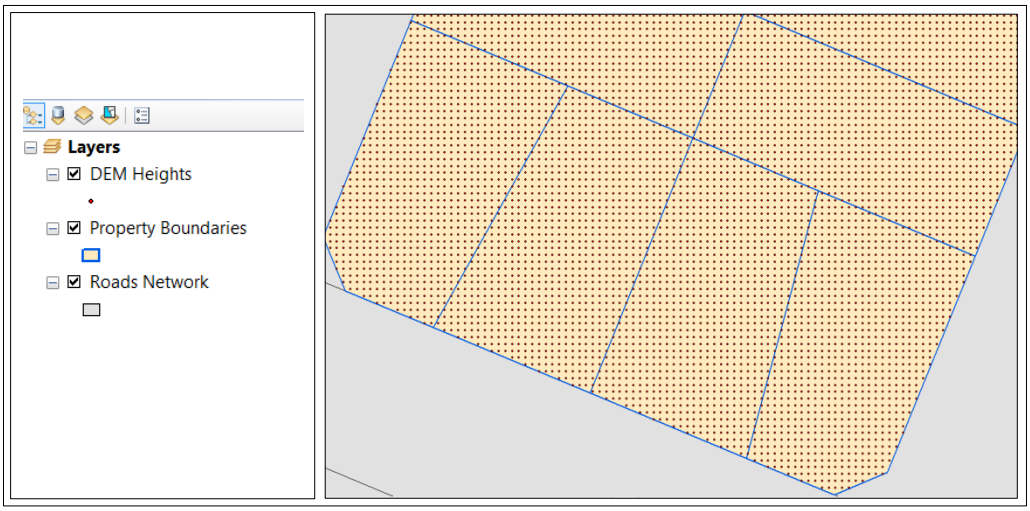

Figure 5.2 An example of spatial distribution using 1 m resolution DEM heights (red dots) covering the land parcels bound by property boundaries (blue lines).

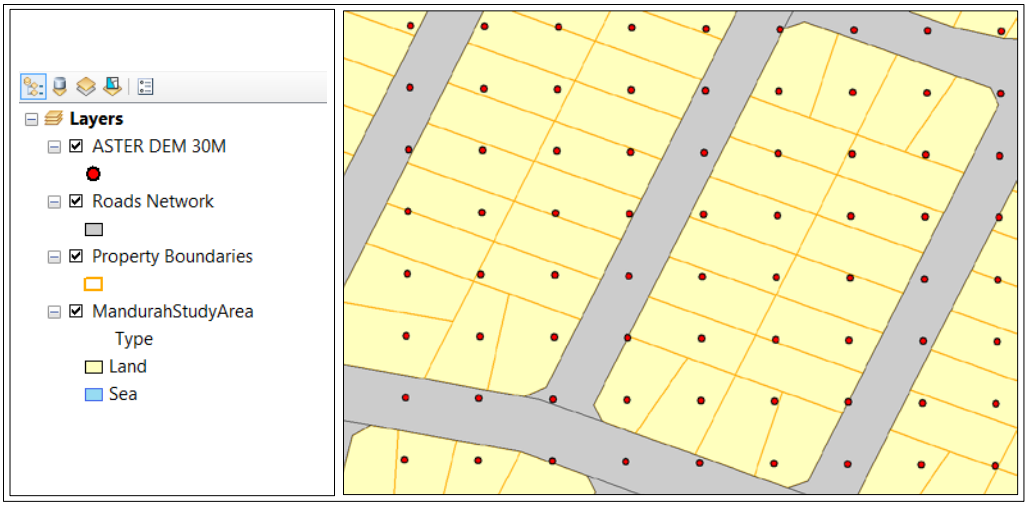

Figure 5.3 An example of spatial distribution using 30 m resolution DEM heights (red dots) covering the land parcels bound by property boundaries (orange lines).

5.3.2.1 Property-based flood modelling based on inundated areas

This technique can be applied to all DEM resolutions (i.e. 1 m, 30 m, and 90 m DEMs), although the higher the resolution the better spatial representation of the inundated area.

This technique is based on three layers: (i) flooded areas, (ii) non-flooded areas (cf. chapter 4.7.1), and (iii) cadastral boundary data. The three layers are overlapped (cf. Figure 5.1). The selection is based on the spatial location function of ArcGIS and is used to choose the parcels that are (i) completely located within flooded areas, (ii) partly flooded, and (iii) not flooded. All parcels located completely inside the inundation area are flagged as fully flooded parcels, while the parcels located on the boundary of the flooded areas are flagged as partially flooded parcels.

5.3.2.2 Property-based flood modelling based on average heights

Apart from identifying parcels that are fully, partly or not flooded, this technique is also very useful when determining the flood condition for parcels that are partially flooded, i.e. located along the boundary of flooded and non-flooded areas (cf. Figures 5.1 and 5.4). As shown in Figures (5.2 and 5.3), the identification of partially flooded parcels requires high-resolution DEM data, such as the 1 m resolution LiDAR DEM data. This technique is applied in several steps:

1. The area of interest is extracted from the DEM data.
2. The elevation data within the selected study area is converted to point features using ArcGIS conversion tool *Raster to Point*. The tool then converts the raster dataset to point features by positioning a point at the centre of the raster cell.
3. The resulting point features store the height value (Z-value) for each point.
4. The next step extracts all DEM heights that fall inside the cadastral boundaries for a selected property (cf. Figure 5.5). This can be done in ArcGIS by using the *select by location* function. This function allows the selection of features from the target layer (DEM heights) based on the relative location to the source layer (e.g. flood boundary).

5. The spatial query method is set to the option “completely within,” which determines the spatial relationship between the target layer and the source layer. This feature will select all the DEM points that fall completely within the boundary of the source layer, including points that touch the boundary of the source layer.

Figure 5.4 An example for parcels that are partially flooded, e.g. on the boundary (red line) between flooded and non-flooded areas.

The average height of each property is calculated by selecting the DEM heights, located within the boundary of each parcel, using the ArcGIS function mentioned above (cf. Figure 5.5). Within ArcGIS, the average height for the selected DEMs is obtained using the *summary statistics* feature on the attribute table, which calculates a summary of statistics for the selected field in the attribute table.

In this instance, the height field was selected resulting in an output table containing the following statistical parameters: sum, mean, maximum, minimum, standard deviation, and count. As this study is interested only in this average height, the mean value is the only statistical result used in the analysis stage. Figure (5.6) shows a sample output for the DEM heights within a selected property, where the mean value represents the average height of the parcel of land.

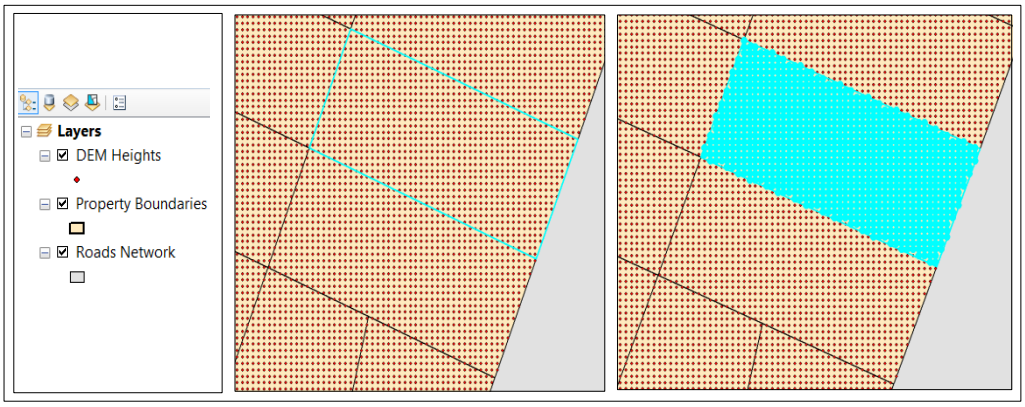

Figure 5.5 Example of the selection of DEM heights within a parcel of land delineated by its cadastral boundary (indicated in blue).

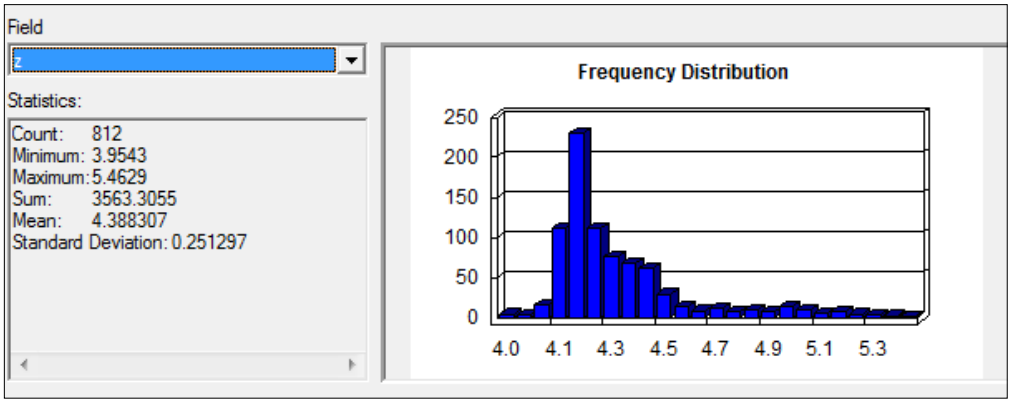

Figure 5.6 Example of the statistical results for selected DEM heights (e.g. Z field). Unit in metres.

The mean height of a property can provide an indication of whether a property is flooded or not. The flood condition can then be assigned by comparing the average height of a property with the height of sea level in the relevant sea level rise scenario. If the average height of the selected parcel is higher than the height of the flooding scenario, the flood condition is flagged as not flooded, and if the average height is less than or equal to the height of the flooding scenario, the parcel is flagged as flooded.

This information can be used to classify a property in terms of general flood risk. However, the average height cannot provide more detailed information, such as a partial flooding of a property. A parcel that is flagged as not flooded or fully flooded, based on the average height, can still be partially flooded (cf. chapter 5.3.2.3). As part of the analysis, the total area for the flooded and not flooded parcels is computed using the *calculate area* tool (cf. Figure 5.1). The next step is to create a map to visualise the flooded areas based on a selected sea level rise scenario (cf. Figure 5.1). The final output is a map showing the classification of properties according to flood risk. These classifications are based on average elevation and supported by information, such as the count, the percentage, and the total area of parcels in each category. This information can be derived from the attribute table by selecting the required flood risk records and obtaining the summary of statistical information for the desired field.

5.3.2.3 Identifying partially flooded parcels

In the previous section 5.3.2.2, the average height is taken as a general indicator as to whether a parcel of land is flooded or not. However, as we have seen, this approach cannot be used to identify partially flooded parcels. Even though a parcel is only partially flooded (cf. Figure 5.9), the average height may indicate that either the parcel is fully flooded or not flooded at all. Therefore, a percentage value must be assigned to a parcel, which will indicate the level of flooding based on the actual area flooded, and the steps are outlined below. Firstly, the sea level rise is allocated using the *contour list* tool in ArcGIS 3D analyst. The obtained layer is a line feature layer, outlining the flood boundaries for the selected sea level rise scenario (cf. Figure 5.7).

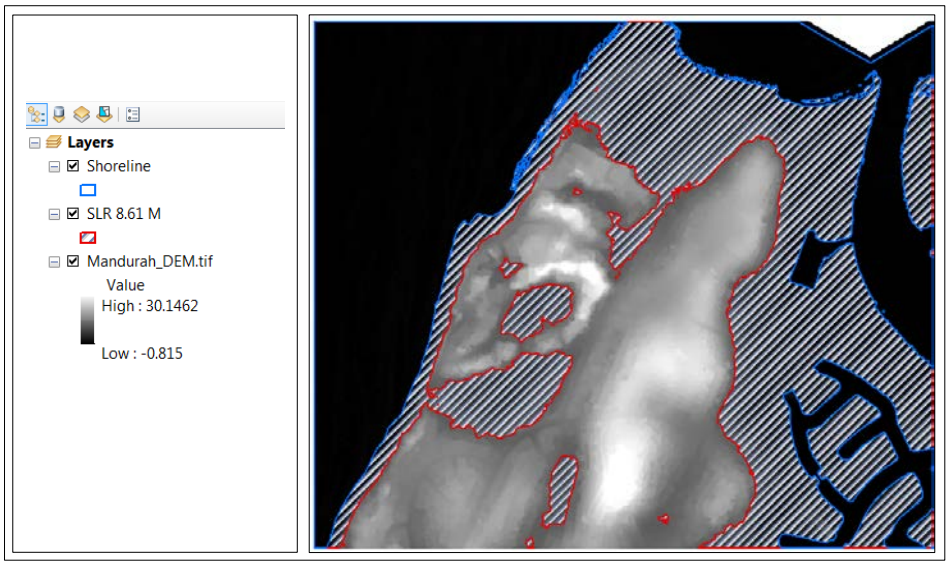

Figure 5.7 Line feature (red line) representing the maximum extent of flooding (i.e. new shoreline after sea level rise, or intersection of new sea level with the terrain).

The line feature represents the intersection of the new sea level with the terrain and is used to select DEM heights located on properties in the flooded area (cf. Figure 5.8). The flooded DEM points are then extracted and combined in a new layer.

Figure 5.8 Example of the extraction of flooded DEM points shown in orange. The flooded DEM points in each property, located in the sea level rise scenario boundaries, have been extracted.

Using the DEM points and flooded DEM point layers, the *select by location* tool is used to select the DEM heights located within a certain parcel boundary (cf. Figure 5.9). Using the spatial query (within the spatial relationship between the target layer and the source layers) will allow selection of all the features that fall within the geometry of the source features. It is important to note the selected features and the source features can have shared boundaries.

Next, the number of whole DEM points, located within or on the parcel boundary, is recorded, and the same procedure is applied for flooded DEM points. Based on this information, the percentage of flooding can be calculated by dividing the number of flooded DEM points by the total number of DEM points within the chosen parcel. All percentage values are stored into a flooded property record for subsequent analysis.

It is worthwhile mentioning here that the percentage of flooded areas can only be derived for the high-resolution LiDAR DEM data (e.g. 1 m resolution). Lower-resolution DEM data (e.g. 30 m or 90 m resolution) is not suited to provide this information on a property-by-property level. Interpolation techniques can be used to produce 1 m contours from a low-resolution 30 m DEM, and then the interpolation could estimate the new raster cell values based on limited number of points available and based on the spatial autocorrelation or the spatial dependence between the heights. However, the resulting 1 m DEM would not be as accurate as the high-resolution DEM. As an example, Figure (5.10) shows the differences between flood boundaries obtained by 1 m LiDAR DEM and the interpolated 1 m from low-resolution 30 m DEM.

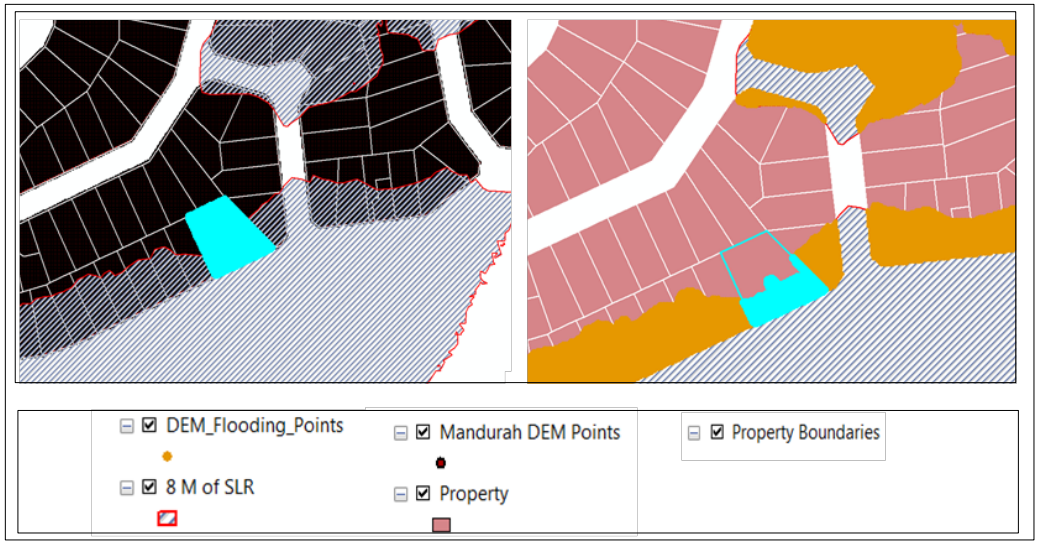

Figure 5.9 Example of the selection process for partially flooded properties (blue area).

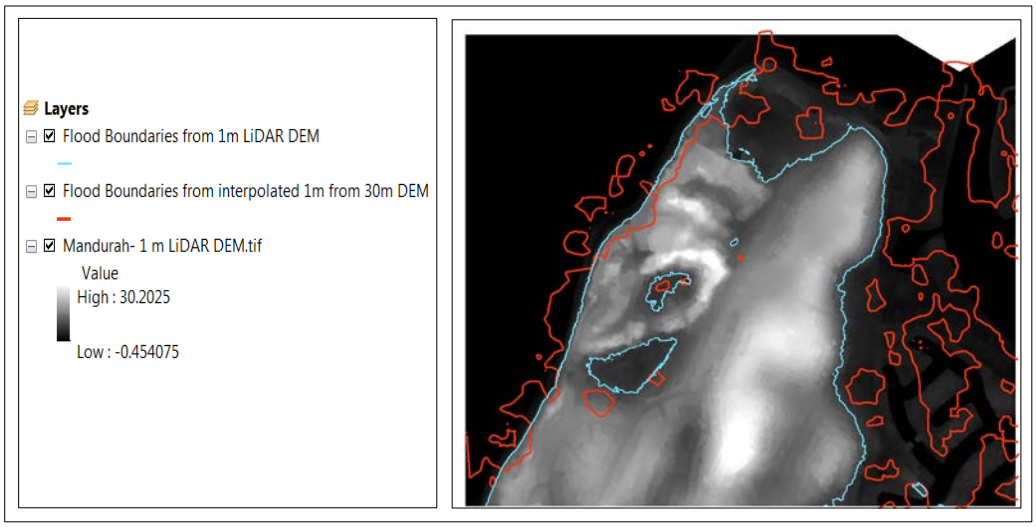

Figure 5.10 Example of the flood boundaries produced by 1 m DEM (shown in light blue) and interpolated 1 m DEM from 30 m DEM (shown in red).

5.3.2.4 Property-based flood classification

Using high-resolution data, such as LiDAR DEM data, the user can apply a more sophisticated analysis and obtain more information about the flood condition. The percentage of flooding can also be estimated for each property, calculated as the ratio between the inundated area and the total property area.

The properties are classified into five categories, based on the calculated percentage of flooding:

1. From 0.00 % to 0.01 %.
2. From 0.01 % to 30.00 %.
3. From 30.01% to 60.00 %.
4. From 60.01 % to 90.00 %.
5. From 90.01 % to 100 %.

Based on the percentage of flooding, the flood category is assigned to each property (i.e. not flooded, partially flooded or fully flooded). The flooding category is set to “Not Flooded” when the percentage of flooding is zero, and the flooding category is set to “Fully Flooded” when the percentage of flooding is more than 90%. In this study, properties flooded by more than 90% are considered fully flooded because these properties are severely affected (cf. Table 5.1).

The “Partially Flooded” category has been assigned to properties where the percentage of flooding ranges from 0.01% to 90% (cf. Table 6.1). The equal interval method is used to classify the partially flooded properties into three equal size categories.

The Australian Bureau of Meteorology uses the following terms to describe flood level, classifying a flood into three different levels (Australian Bureau of Meteorology 2015):

1. Minor flooding: “Causes inconvenience. Low-lying areas next to watercourses are inundated. Minor roads may be closed and low-level bridges submerged. In urban areas inundation may affect some backyards and buildings below the floor level as well as bicycle and pedestrian paths. In rural areas removal of stock and equipment may be required”.
2. Moderate flooding: “In addition to the above, the area of inundation is more substantial. Main traffic routes may be affected. Some buildings may be affected above the floor level. Evacuation of flood-affected areas may be required. In rural areas removal of stock is required”.
3. Major flooding: “In addition to the above, extensive rural areas and/or urban areas are inundated. Many buildings may be affected above the floor level. Properties and towns are likely to be isolated and major rail and traffic routes closed. Evacuation of flood-affected areas may be required. Utility services may be impacted”.

In this study, the above mentioned terms are used to describe the flood level in each property, along with two additional terms: (1) a flood level of “None” (representing zero percentage of flooding), and (2) a flood level of “severe” (representing more than 90% of the percentage of flooding) (cf. Table 5.11).

Table 5.1 Flood classification guide used in this study.

Flood Percentage	Flood Category	Flood Level
0.00-0.01	Not Flooded	None
0.01-30.00	Partially Flooded	Minor
30.01-60.00	Partially Flooded	Moderate
60.01-90.00	Partially Flooded	Major
90.01-100.00	Fully Flooded	Severe

As mentioned previously, the purpose of this study is to provide detailed flood information, which can be gathered using high-resolution data; it is not to develop a classification for flooding condition. Therefore, the percentage of flooding, flooding category, and flood level presented in this research can be amended and updated depending upon the user's need.

5.4 Results for property-based flood modelling

In order to apply and test the methodology developed in the previous chapter, this chapter outlines the potential risks of residential coastal flooding, modelled on a property-by-property level, in the selected study locations of Mandurah and Rockingham.

After the percentage of flooding is calculated, and based on this flood percentage, all properties are assigned a flood category - fully, partially or non-flooded. The percentage of flooding is also used to classify the property's flood level as either none, minor, moderate, major or severe (cf. Table 5.1). Results for all flooding scenarios are based on the 1 m resolution LiDAR DEM data.

All five sea level rise scenarios (presented in chapter 3) are applied to the Mandurah study area. Due to the nature of low-lying topography at the Rockingham study area, only three flooding scenarios are considered. These flooding scenarios are based on a 2.06 m; 5.98 m, and 8.61 m sea level rise. For the remaining two sea level rise scenarios of 10.12 m and 18.73 m, the Rockingham study area will be fully submerged; therefore, in these two remaining scenarios, there is no need to provide detailed information for each property.

The Mandurah study area stretches about 3.00 km along the South West coast of Western Australia and covers a total area of 8.36 km^2. For the property-by-property based flood modelling, a total of 1,999 residential properties were considered, covering an area of 1.966 km^2 and with an average property size of 983 m^2.

The Rockingham study area extends 2.91 km along the South West coast of Western Australia and covers a total area of 1.61 km^2. This area contains 857 residential properties covering an area of 0.950 km^2 and with an average property size of 1,109 m^2.

5.4.1 Sea level rise of 2.06 m in Mandurah

The first scenario analyses property-based flood modelling in Mandurah based on a sea level rise of 2.06 m. This sea level rise scenario is based on the projected sea level by 2100 when taking into account average wave height and the contribution of storm surges (cf. chapter 3.6.5).

Figure (5.11) shows the flooded (partially and fully) and not flooded properties in the Mandurah study area, and is based on the location of the properties being either partially or fully within the flooded areas. As opposed to Figure (5.11), Figure (5.12) shows the percentage of flooding also allowing for the identification of partially flooded parcels. It can be seen in Figure (5.12) that the impact is only minor with the most affected area being at the eastern side of the study area. This is due to the relatively low elevation (e.g. below 2.06 m) of the properties along the marina.

This is also confirmed in Figure (4.3) (cf. chapter 4), which shows the height range of the affected properties ranging from below one metre to almost 6 metres, with an average property height of 2.46 metres. In addition, some properties (situated relatively close to the shoreline) in the north-east and north are also affected. All remaining properties within the study area are not flooded.

The relatively minor impact is further confirmed by the statistical values listed in Table (5.2), which show that only 282 properties with a total area of 287,402 m^2 (or 14.6% of the total area) are inundated at a sea level rise of 2.06 m. The majority of properties (1,717) are not inundated in this flooding scenario. These properties have a total area of 1,678,602 m^2 representing 85.4 % of the area of all properties. Therefore, in this scenario, most of the properties can be considered safe from flooding (cf. Table 5.2).

The percentage of flooding for each property was calculated as the ratio of the inundated area compared to the total property area. The properties are categorised according to their percentage of flooding as given in Table (5.1) (cf. chapter 5.3.2.4). When we analyse the percentage of flooding (cf. Figure 5.12), it reveals again the relatively minor impact of sea level rise in this scenario.

Most of the properties, which are shown as flooded in Figure (5.11), are actually only partly flooded (most of them, less than 30%). Only 44 properties can be considered fully flooded (cf. Table 5.3). The fully flooded properties are all located in the east between the marina and the ocean (cf. Figure 5.12). Here is where property-based flood modelling shows a significant benefit over other less detailed methods. Only with the use of high-resolution data is it possible to model the level of flooding (e.g. partially flooded).

Table (5.3) provides an overview of the percentage of flooding for all properties. It can be seen that 1,717 properties (representing 85.4 % of the total area) can be considered not flooded, with the percentage of flooding ranging from 0.00 to less than 0.01 per cent. Only 44 properties (representing 2.2 % of the total area) are fully inundated in this flooding scenario. The results also show that 236 properties are considered partially flooded (e.g. located at the boundary between not flooded and flooded). Most of the partially flooded properties (207) fall into a percentage range between 0.01 and 30% flooded.

Table 5.2 Property-based flood modelling for the Mandurah study area, assuming a sea level rise of 2.06 m. Results show all properties affected by flooding, irrespective of their level of flooding (i.e. includes partially flooded properties). Area 1 is the total area of the properties and Area 2 is the actual flooded area.

Parcel condition	No of Parcels	Area 1 (m²)	Area 1 (%)	Area 2 (m²)
Flooded	282	287,402	14.6	89,806
Not flooded	1,717	1,678,602	85.4	0
Total	1,999	1,966,004	100	89,806

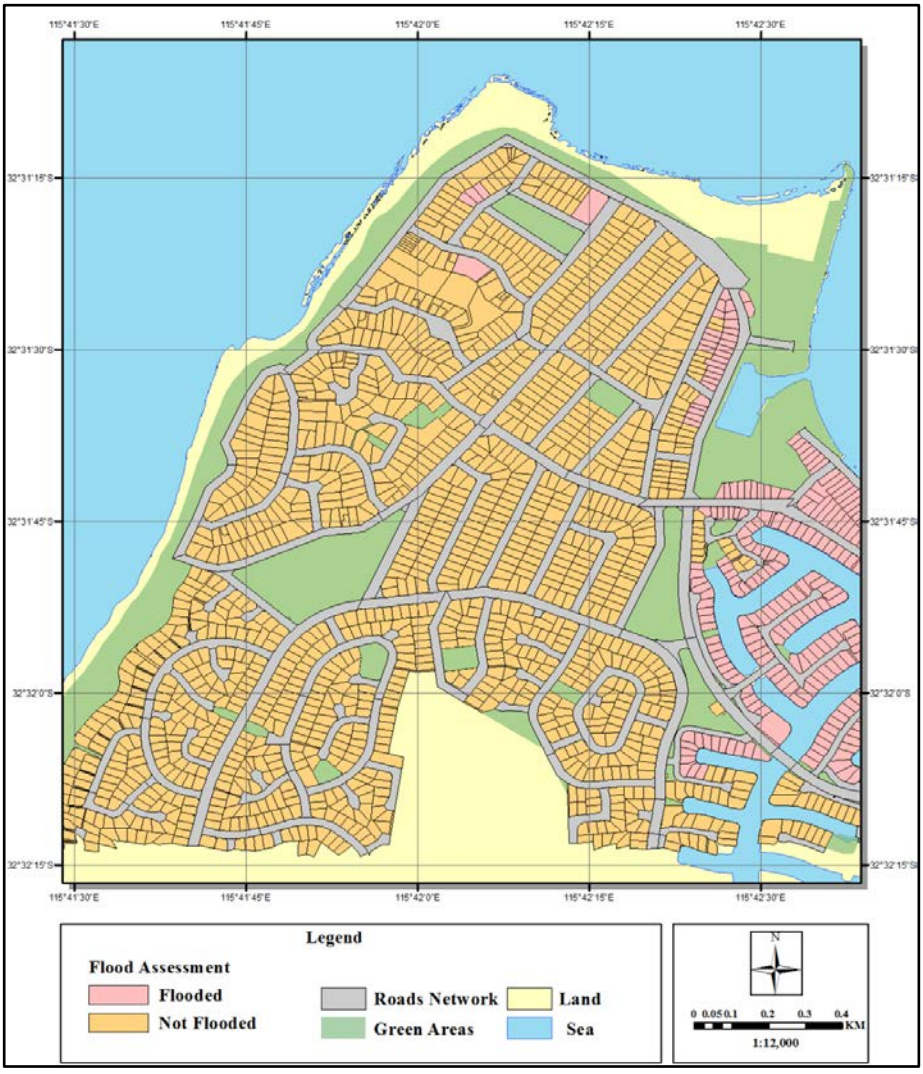

Figure 5.11 Property-based flood modelling for the Mandurah study area assuming a sea level rise of 2.06 m. Flooded areas are shown irrespective of their level of flooding.

Table 5.3 Property-based percentage of flooding for the Mandurah study area, assuming a sea level rise of 2.06 m. Area 1 is the total area of the properties and Area 2 is the actual flooded area.

Flood Percentage	No of Parcels	Area 1 (m²)	Area 1 (%)	Area 2 (m²)	Flood Category	Flood Level
0.00-0.01	1719	1,679,813.39	85.99	5.43	Not Flooded	None
0.01-30.00	207	205,605.31	10.36	29,516.68	Partially Flooded	Minor
30.01-60.00	16	33,522.70	0.80	14,714.70	Partially Flooded	Moderate
60.01-90.00	13	8,433.21	0.65	7,190.06	Partially Flooded	Major
90.01-100.00	44	38,629.70	2.20	38,384.30	Fully Flooded	Severe
Total	1,999	1,966,004.31	100.00	89,811.17		

Figure 5.12 Property-based percentage of flooding for the Mandurah study area, assuming a sea level rise of 2.06 m.

5.4.2 Sea level rise of 2.06 m in Rockingham

The same sea level rise scenario of 2.06 m (cf. chapter 5.4.1.1) is now applied to the Rockingham study area. The numerical results are summarised in Tables (5.4 and 5.5), while the property-based flood modelling is illustrated in Figures (5.13 and 5.14). The results show that this sea level rise scenario has only a minor impact on the Rockingham study area. Almost all residential properties are located outside of flooded areas. Figure (5.13) illustrates that there is only minimal impact in the south-east of the study area. This means that almost all properties are located at an elevation higher than 2.06 m.

Table (5.4) shows that 849 out of the 857 properties (representing an area of 941,438 m^2) are not inundated, which is 99.1% of the total parcel area. Only a very small number of the properties are inundated in this scenario. Only 8 properties are flooded partially and fully representing an area of 8,398 m^2, which is 0.9% of the total area. A small number of flooded properties are surrounded by not flooded properties, indicating a trough of lower elevations surrounded by higher elevations. Interestingly, in this scenario, none of the properties are considered fully flooded (e.g. none are flooded more than 60%, cf. Table 5.5).

A map showing the property-based percentage of flooding (cf. Figure 5.14) confirms previous results and shows that most of the properties (847 properties) are considered not flooded. It can be seen in Table (5.5) that there are no properties with a percentage of flooding larger than 60%. Furthermore, only 10 properties are considered partially flooded, representing less than 1% of the total area, and all of these properties are in the south-east and south.

Table 5.4 Property-based flood modelling for the Rockingham study area, assuming a sea level rise of 2.06 m. Results show all properties affected by flooding, irrespective of their level of flooding (i.e. includes partially flooded properties). Area 1 is the total area of the properties and Area 2 is the actual flooded area.

Parcel condition	No of Parcels	Area 1 (m²)	Area 1 (%)	Area 2 (m²)
Flooded	8	8,398	0.9	1,343
Not flooded	849	941,438	99.1	0
Total	857	949,836	100	1,343

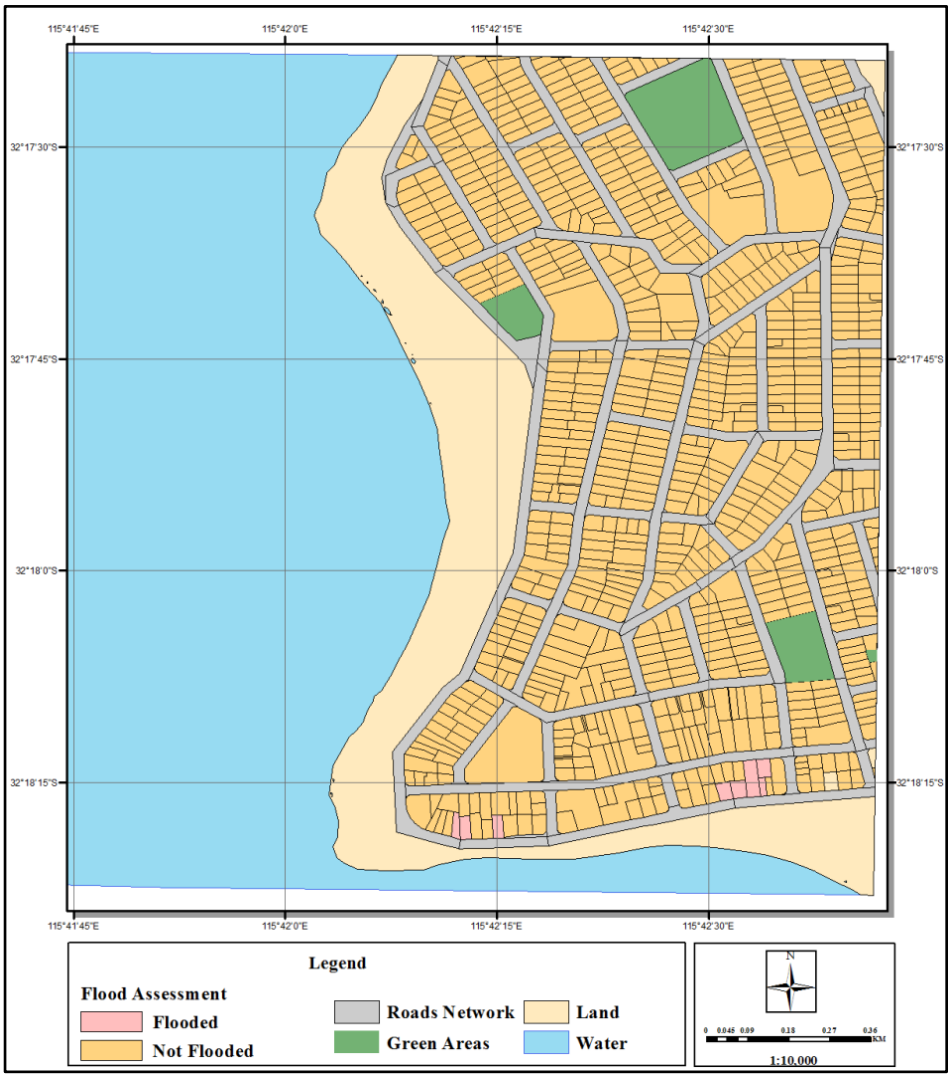

Figure 5.13 Property-based flood modelling for the Rockingham study area, assuming a sea level rise of 2.06 m. Flooded areas are shown irrespective of their level of flooding.

Table 5.5 Property-based percentage of flooding for the Rockingham study area, assuming a sea level rise of 2.06 m. Area 1 is the total area of the properties and Area 2 is the actual flooded area.

Flood percentage	No of Parcels	Area 1 (m²)	Area 1 (%)	Area 2 (m²)	Flood Category	Flood Level
0.00-0.01	847	939,560.74	98.92	1.37	Not Flooded	None
0.01-30.00	9	9,263.42	0.98	851.45	Partially Flooded	Minor
30.01-60.00	1	1,012.00	0.11	493.20	Partially Flooded	Moderate
60.01-90.00	0	0.00	0.00	0.00	Partially Flooded	Major
90.01-100.00	0	0.00	0.00	0.00	Fully Flooded	Severe
Total	857	949,836.16	100.00	1,346.02		

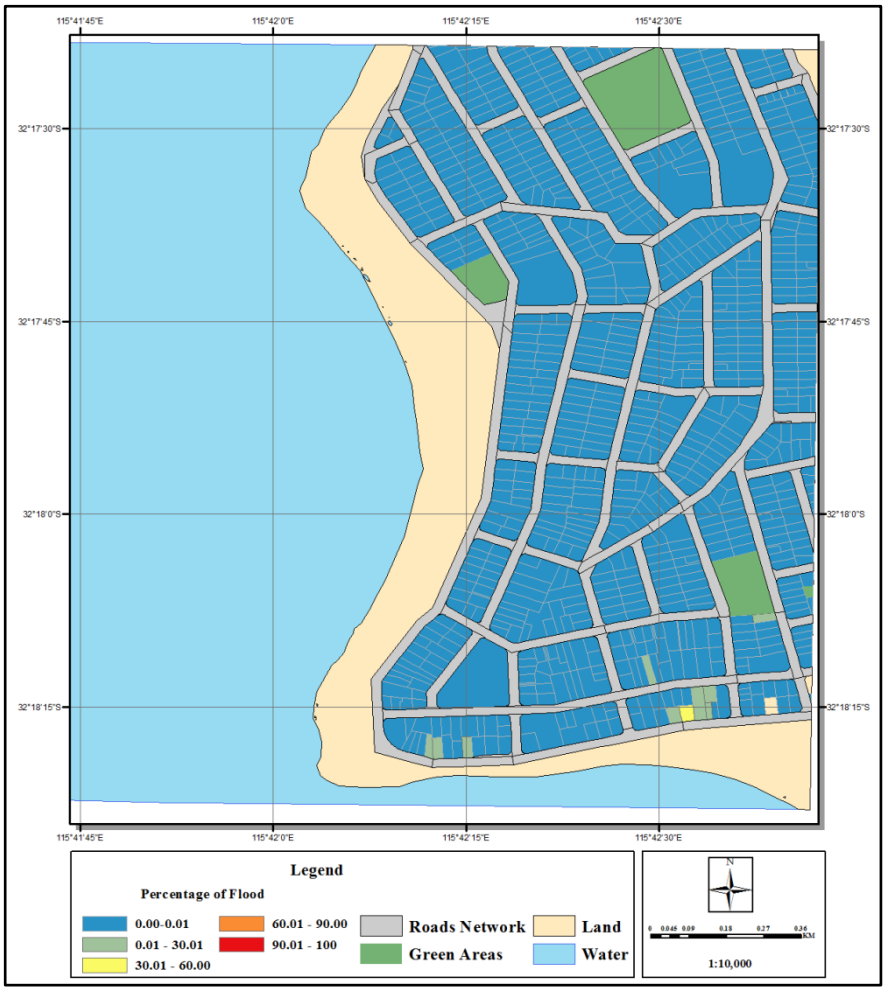

Figure 5.14 Property-based percentage of flooding for the Rockingham study area assuming a sea level rise of 2.06 m.

5.4.3 Sea level rise of 5.98 m in Mandurah

The second flooding scenario adopted in this study corresponds to a sea level rise of 5.98 m, which is the result of the estimated sea level, by the year 2100, including additional short-term effects such as maximum tide, wave, storm surge heights, and seasonal effects (cf. chapter 3.6.5). For the Mandurah study area, there is an increased impact due to flooding, as is documented in Tables (5.6 and 5.7) and Figures (5.15 and 5.16). The impact has mostly increased on properties in the eastern, northern and north-western part of the study area. Only in the south-western part are properties close to the shoreline still unaffected (cf. Figure 5.15), and, as a result, there are more properties identified as flooded when compared to the previous scenario. Interestingly, there are a number of flooded properties, located centrally within the study area, which are surrounded entirely by higher elevated properties that are not flooded. These properties have been excluded from further analysis, as because of the surrounding higher elevations, they would not be flooded.

The numerical results are summarised in Tables (5.6 and 5.7), which show that 22.8% of the total parcels are now indicated as flooded (occupying a total area of 447,595 m^2). However, based on a sea level rise of 5.98 m, 1520 properties are still indicated as not flooded. These properties cover a total area of 1,518,409 m^2, which represents 77.2% of the total area of all parcels within the study area (cf. Table 5.6 and Figure 5.15). Based on the flooding percentages (cf. Figure 5.16), major impacts are located in the eastern and northern parts of the study area, where the majority of fully flooded properties (e.g. flooded by more than 90%) are located. The impact of flooding in the western part of the study area is mostly negligible, as most of the properties are not inundated. However, a few properties located on the top of the western part are either partially or fully affected, with flood levels ranging from minor to severe (cf. Figure 5.16). This is also confirmed by the values in Table (5.7), showing that approximately 76.2% (i.e. 1523 properties) of the total property area is not flooded, compared to 18.2% (i.e. 364 properties) of the properties, which are fully flooded. Moreover, 112 properties with a total area of 154,475 m^2 (or 5.6%) are partially flooded when sea level rises to 5.98 m (cf. Table 5.7 and Figure 5.16).

Table 5.6 Property-based flood modelling for the Mandurah study area, assuming a sea level rise of 5.98 m. Results show all properties affected by flooding irrespective of their level of flooding (i.e. includes partially flooded properties). Area 1 is the total area of the properties and Area 2 is the actual flooded area.

Parcel condition	No of Parcels	Area 1 (m²)	Area 1 (%)	Area 2 (m²)
Flooded	479	447,595	22.8	364,655
Not flooded	1,520	1,518,409	77.2	0
Total	1,999	1,966,004	100	364,655

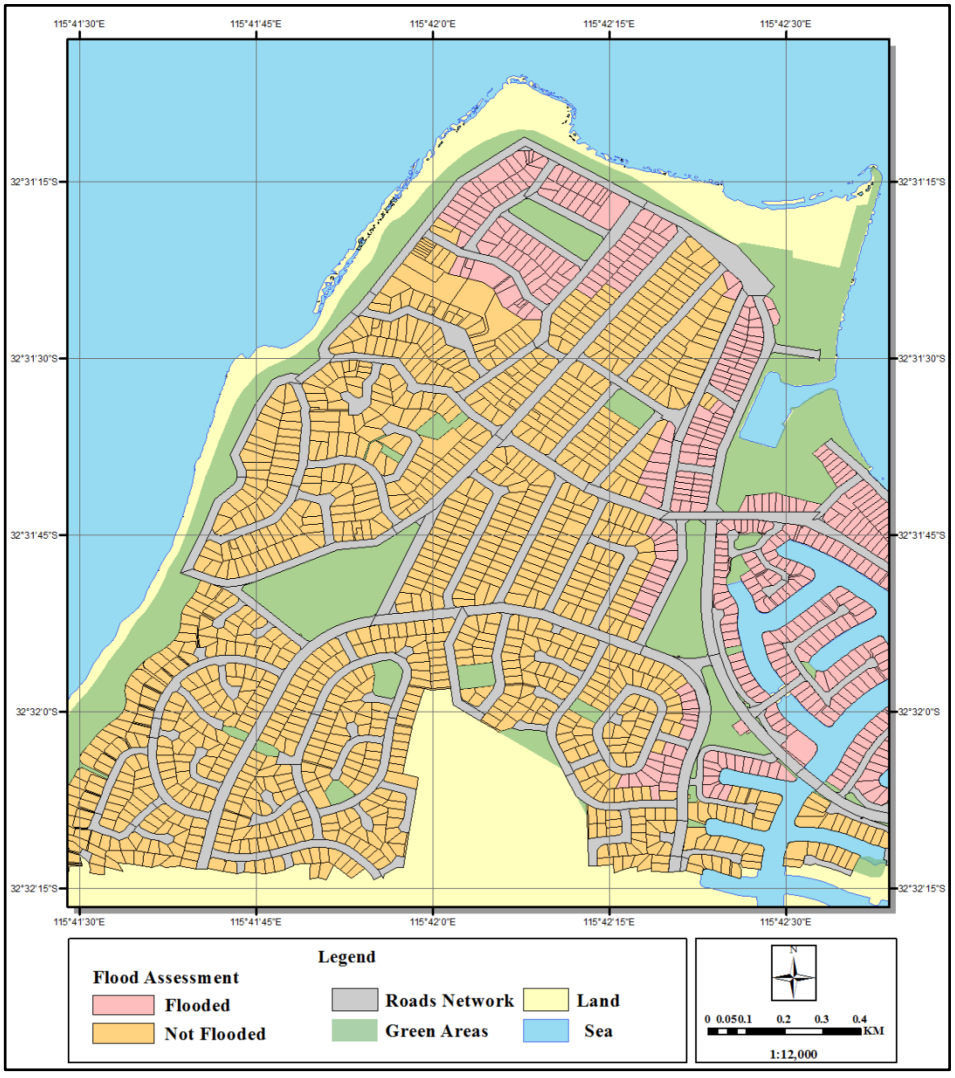

Figure 5.15 Property-based flood modelling for the Mandurah study area, assuming a sea level rise of 5.98 m. Flooded areas are shown irrespective of their level of flooding.

Table 5.7 Property-based percentage of flooding for the Mandurah study area, assuming a sea level rise of 5.98 m. Area 1 is the total area of the properties and Area 2 is the actual flooded area.

Flood percentage	No of Parcels	Area 1 (m²)	Area 1 (%)	Area 2 (m²)	Flood Category	Flood Level
0.00-0.01	1523	1,520,897.20	76.19	18.56	Not Flooded	None
0.01-30.00	40	40,112.11	2.00	3,471.35	Partially Flooded	Minor
30.01-60.00	30	53,661.74	1.50	20,046.02	Partially Flooded	Moderate
60.01-90.00	42	60,701.55	2.10	44,716.27	Partially Flooded	Major
90.01-100.00	364	290,631.71	18.21	289,142.05	Fully Flooded	Severe
Total	1,999	1,966,004.31	100.00	357,394.25		

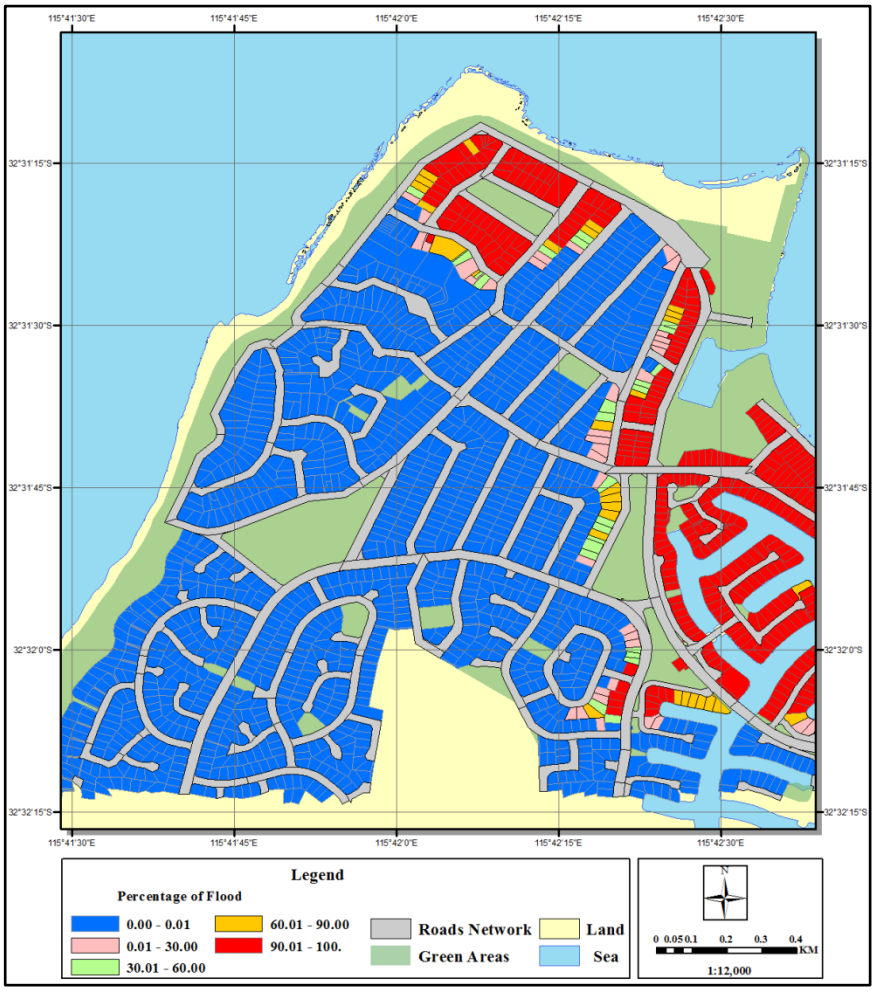

Figure 5.16 Property-based percentage of flooding for the Rockingham study area assuming a sea level rise of 5.98 m.

5.4.4 Sea level rise of 5.98 m in Rockingham

Modelling the effect of coastal flooding in Rockingham at a sea level rise of 5.98 m shows a major impact, indicating that the elevation within the study area is mostly below the sea level rise value of 5.98 m. Figures (4.19 and 4.20) confirm this (cf. chapter 4.8.2); and show a maximum height of approximately 7 metres within the study area.

In this scenario, the study area is almost fully submerged with only few properties unaffected. These are mostly located in the middle of the study area (cf. Figure 5.17 and Table 5.8). Interestingly, the terrain at the Rockingham study site is considered as a plateau, elevated by a few metres. Therefore, there is minimal impact at a 2 m sea level rise, but if sea level rises by only another few metres, there is major impact.

Table (5.8) shows that just over 95% of properties (located within the study area) are impacted by flooding (including some partially flooded properties). This corresponds to 815 properties with a total area of 903,732 m^2. The results also show only 42 properties are not flooded, covering an area of 46,104 m^2 (cf. Table 5.8).

Flooding percentages for the study area indicate more than half (487 parcels or 56.4%) of the properties are fully flooded, therefore severe impacting the study area (cf. Table 5.9 and Figure 5.18). The severe impact happens mostly in the southern part of the study area, where almost all properties are fully inundated. There is also some major impact in the north-east of the study area. The remaining parts are somewhat less impacted, although with significant spatial variations (cf. Figure 5.18).

In addition, 128 properties (or 14.4% of total properties) in the study area are classified as majorly impacted (where the percentage of flooding ranges from 60.01 to 90 per cent). Table (5.9) shows that only 42 properties (4.8%) of 857 are not flooded when sea level rises to 5.98 m. Most of these are located in the inner part of the study area, near to the western side.

Table 5.8 Property-based flood modelling for the Rockingham study area, assuming a sea level rise of 5.98 m. Results show all properties affected by flooding irrespective of their level of flooding (i.e. includes partially flooded properties). Area 1 is the total area of the properties and Area 2 is the actual flooded area.

Parcel condition	No of Parcels	Area 1 (m²)	Area 1 (%)	Area 2 (m²)
Flooded	815	903,732	95.1	700,958
Not flooded	42	46,104	4.9	0
Total	857	949,836	100	700,958

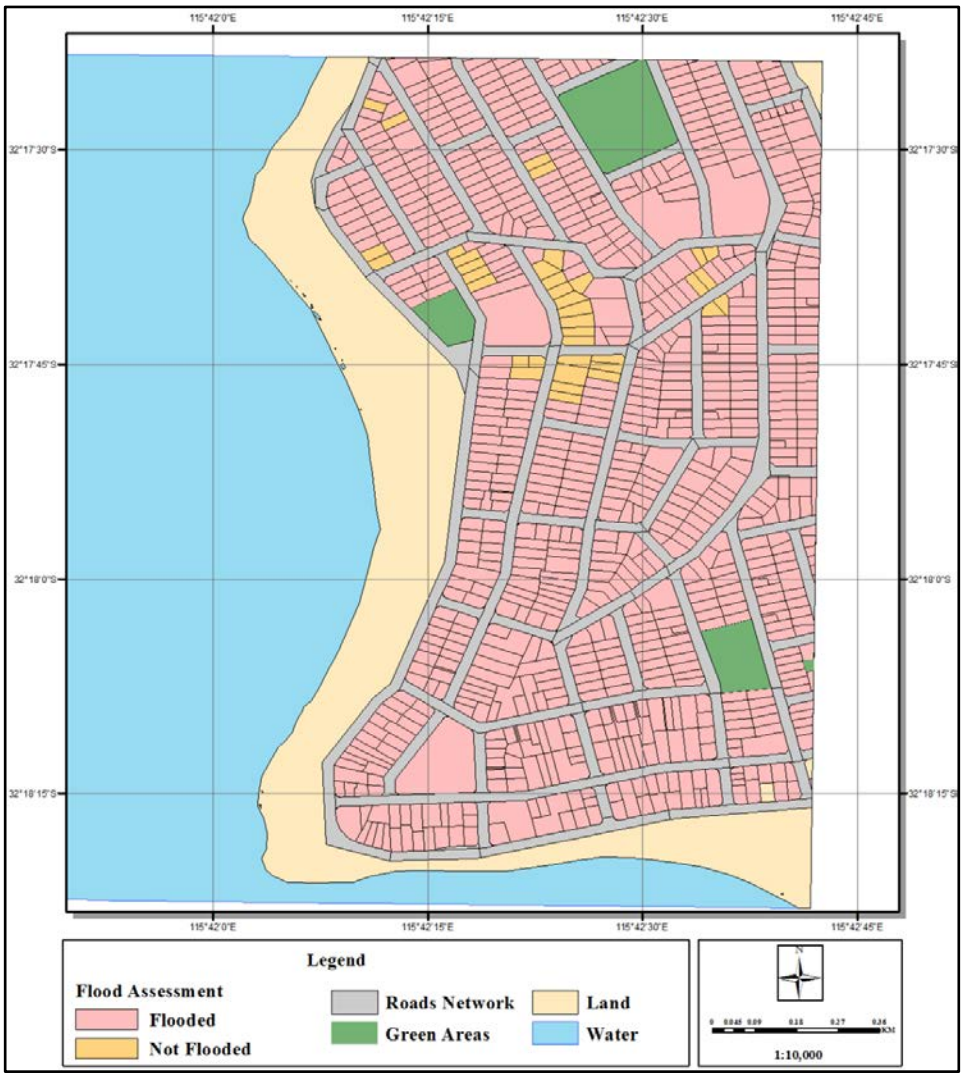

Figure 5.17 Property-based flood modelling for the Rockingham study area assuming a sea level rise of 5.98 m. Flooded areas are shown irrespective of their level of flooding.

Table 5.9 Property-based percentage of flooding for the Rockingham study area, assuming a sea level rise of 5.98 m. Area 1 is the total area of the properties and Area 2 is the actual flooded area.

Flood percentage	No of Parcels	Area 1 (m^2)	Area 1 (%)	Area 2 (m^2)	Flood Category	Flood Level
0.00-0.01	42	46,103.96	4.85	48.82	Not Flooded	None
0.01-30.00	115	132,641.64	13.96	13,058.60	Partially Flooded	Minor
30.01-60.00	85	97,480.93	10.26	44,851.50	Partially Flooded	Moderate
60.01-90.00	128	137,567.32	14.48	108,549.99	Partially Flooded	Major
90.01-100.00	487	536,042.30	56.44	534,498.06	Fully Flooded	Severe
Total	857	949,836.16	100.00	701,006.98		

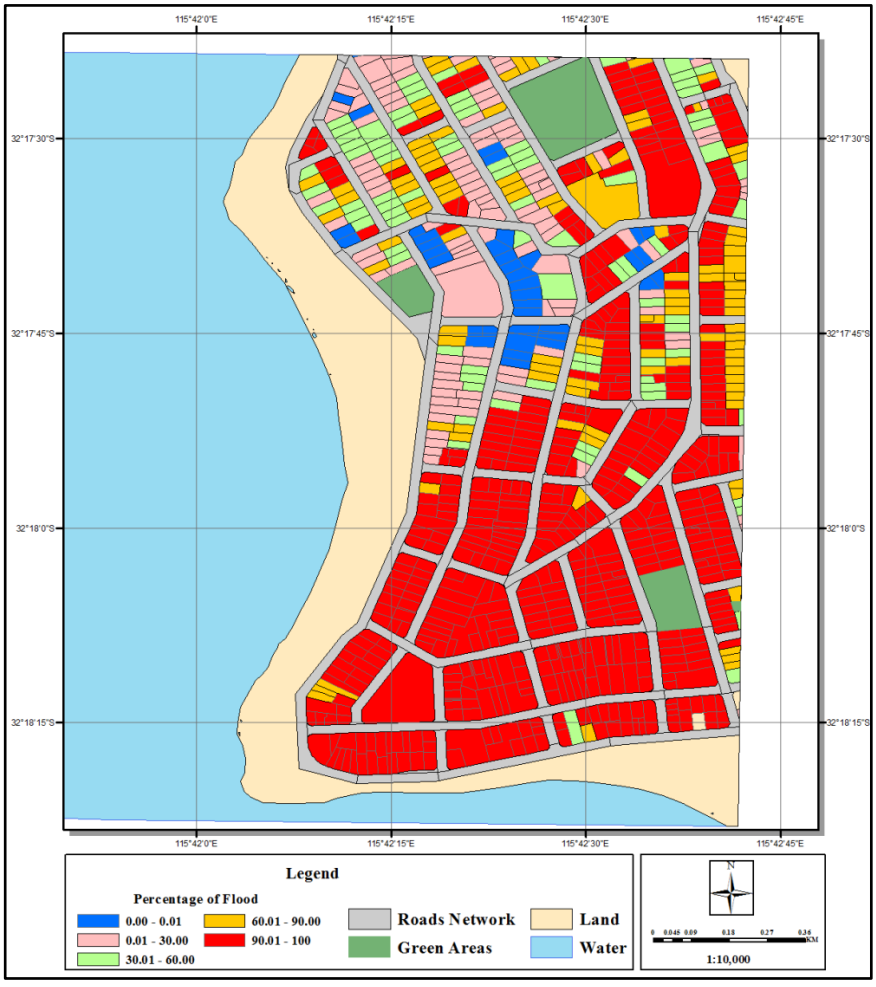

Figure 5.18 Property-based percentage of flooding for the Rockingham study area, assuming a sea level rise of 5.98 m.

5.4.5 Sea level rise of 8.61 m in Mandurah

In the third scenario, property-based flood modelling considers a sea level rise of 8.61 m (cf. chapter 3.6.5). This value represents the contribution of the fully melted Greenland ice sheet, the projected sea level rise by 2100, average wave and storm surge heights. The results for this scenario are summarised in Tables (5.10 and 5.11) and Figures (5.19 and 5.20), which show a slightly increased impact on properties compared to the previous flooding scenario (cf. chapter 5.4.3).

The number of properties affected by flooding in this scenario increases by 121 and raising the total number of affected properties to 600 (cf. Tables 5.6 and 5.10). Here we see a large number of properties impacted by flooding located in the northern and eastern part of the study area (cf. Figure 5.19). The impact on properties located in the western and southern parts of the study area is still minimal, with the majority of properties not impacted at all by a sea level rise of 8.61 m (cf. Figure 5.19). The numerical results in Table (5.10) show that almost 28.5% of the total properties within the study area are either partially or fully inundated when sea level rises to 8.61 m. This corresponds to a total area of 561,168 m^2. However, 71.5% of the properties in the study area are not impacted at all by flooding, which corresponds to a greater area of 1,404,836 m^2 (cf. Table 5.10 and Figure 5.19).

Classifying all properties according to their respective flooding percentage (cf. Figure 5.20) shows that most of the properties along the eastern and northern sides of the study area are fully inundated (i.e. flooded by more than 90%). As a result, the flood level for each of these properties is classified as severe. However, the analysis also confirms that large areas in the south and centre of the study area are not inundated, while properties on the western side are only partially flooded. Only a small number of properties are classified as fully flooded (cf. Figure 5.20). The numerical results provided in Table (5.11) confirm the majority of the properties are classified as not flooded, i.e. not affected by flooding. The results indicate that approximately 22% of the properties are fully flooded (occupying an area of 351,823 m^2), and approximately 8% of properties are partially flooded, with percentages ranging from 0.01 to 90% (cf. Table 5. 11 and Figure 5.20).

Table 5.10 Property-based flood modelling for the Mandurah study area, assuming a sea level rise of 8.61 m. Results show all properties affected by flooding irrespective of their level of flooding (i.e. includes partially flooded properties). Area 1 is the total area of the properties and Area 2 is the actual flooded area.

Parcel condition	No of Parcels	Area 1 (m²)	Area 1 (%)	Area 2 (m²)
Flooded	600	561,168	28.5	441,735
Not flooded	1,399	1,404,836	71.5	0
Total	1,999	1,966,004	100	441,735

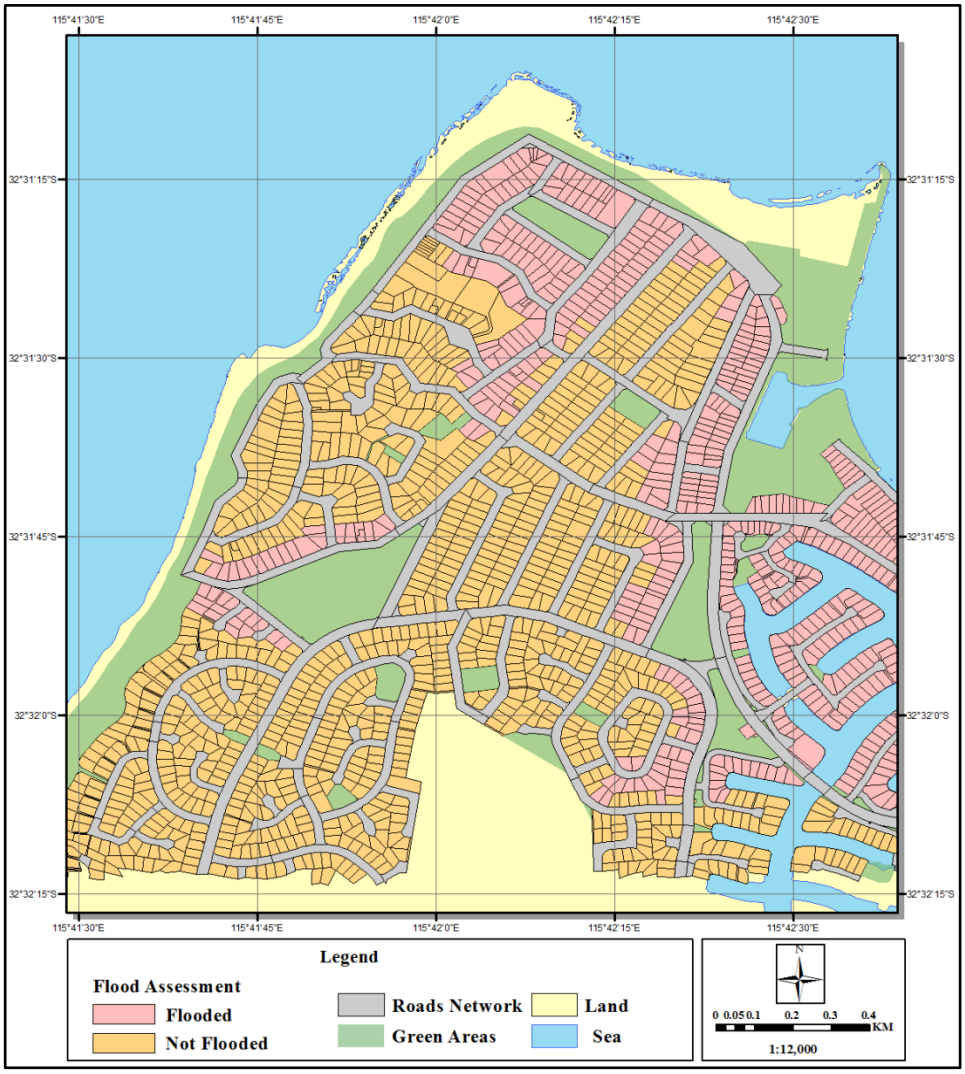

Figure 5.19 Property-based flood modelling for the Mandurah study area, assuming a sea level rise of 8.61 m. Flooded areas are shown irrespective of their level of flooding.

Table 5.11 Property-based percentage of flooding for the Mandurah study area, assuming a sea level rise of 8.61 m. Area 1 is the total area of the properties and Area 2 is the actual flooded area.

Flood percentage	No of Parcels	Area 1 (m²)	Area 1 (%)	Area 2 (m²)	Flood Category	Flood Level
0.00-0.01	1399	1,404,836.20	69.98	43.04	Not Flooded	None
0.01-30.00	68	69,410.60	3.40	4,250.04	Partially Flooded	Minor
30.01-60.00	21	50,428.15	1.05	19,021.40	Partially Flooded	Moderate
60.01-90.00	73	89,506.24	3.65	68,325.00	Partially Flooded	Major
90.01-100.00	438	351,823.13	21.91	350,138.57	Fully Flooded	Severe
Total	1,999	1,966,004.31	100.00	441,778.05		

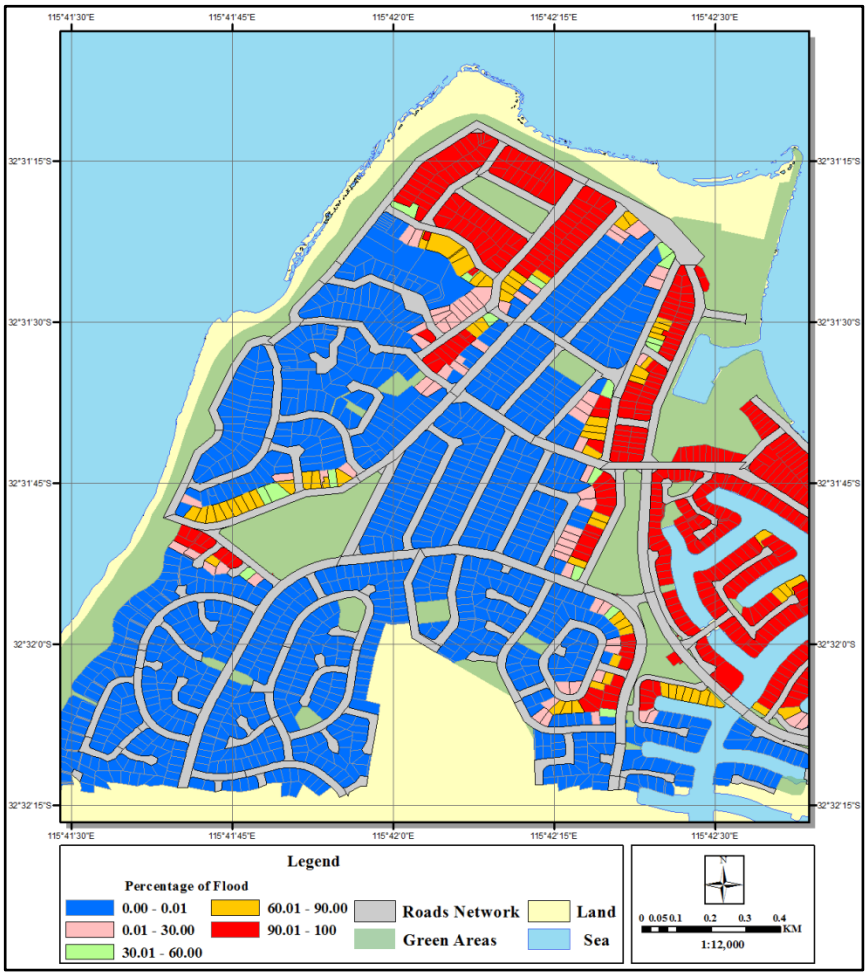

Figure 5.20 Property-based percentage of flooding for the Mandurah study area assuming a sea level rise of 8.61 m.

5.4.6 Sea level rise of 8.61 m in Rockingham

For the Rockingham study area, the flood analysis reveals that a full melt of the Greenland ice sheet will have severe consequences. In this scenario, effectively all properties are affected by flooding, shifting the current coastline by about 800 m towards the east (cf. Figure 5.21). Numerical results provided in Table (5.12) show all but two properties are affected by flooding (occupying an area of 948,036 m^2), which means 99.8%. The two properties not flooded in this scenario are located in the southern part of the study area (cf. Table 5.12 and Figure 5.21).

Analysis of the flooding percentages confirms the severe impact classification of this scenario on the Rockingham study area (cf. Table 5.13 and Figure 5.22). Only a few properties in the east, north, and west of the study area are partially flooded (cf. Figure 5.22). Table (5.13) also shows the majority of properties are identified as fully flooded (percentage of flooding is over 90% and, therefore, classified as severely impacted). Only three properties are classified as not flooded. The numerical results also show that 108 properties are classified as partially flooded, with 66 of these classified as majorly impacted (i.e. percentage of flooding is between 60.01 to 90%).

Table 5.12 Property-based flood modelling for the Rockingham study area, assuming a sea level rise of 8.61 m. Results show all properties affected by flooding irrespective of their level of flooding (i.e. includes partially flooded properties). Area 1 is the total area of the properties and Area 2 is the actual flooded area.

Parcel condition	No of Parcels	Area 1 (m²)	Area 1 (%)	Area 2 (m²)
Flooded	855	948,036	99.8	897,003
Not flooded	2	1,800	0.2	0
Total	857	949,836	100	897,003

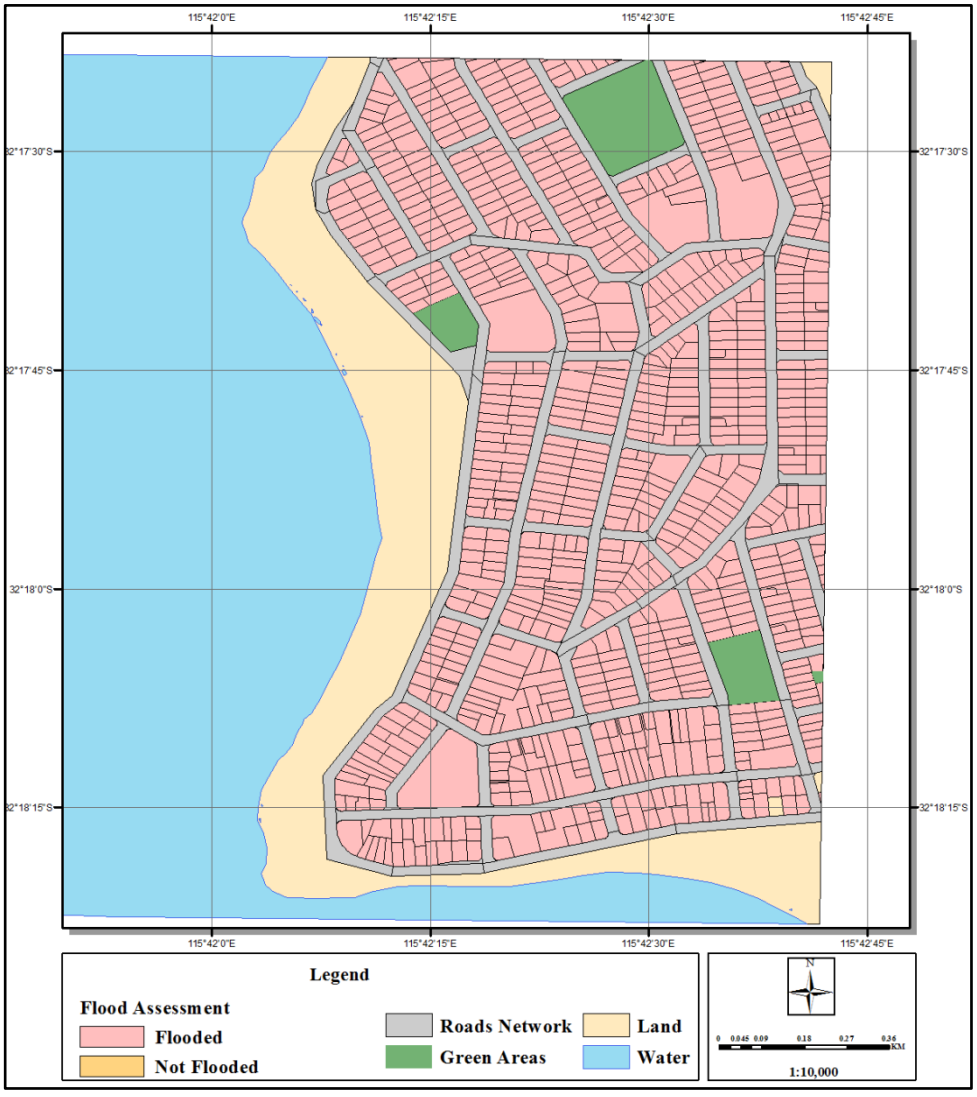

Figure 5.21 Property-based flood modelling for the Rockingham study area assuming a sea level rise of 8.61 m. Flooded areas are shown irrespective of their level of flooding.

Table 5.13 Property-based percentage of flooding for the Rockingham study area, assuming a sea level rise of 8.61 m. Area 1 is the total area of the properties and Area 2 is the actual flooded area.

Flood percentage	No of Parcels	Area 1 (m²)	Area1 (%)	Area 2 (m²)	Flood Category	Flood Level
0.00-0.01	2	1,800.12	0.19	4.83	Not Flooded	None
0.01-30.00	21	22,636.04	2.38	3,351.84	Partially Flooded	Minor
30.01-60.00	21	27,897.71	2.94	12,733.20	Partially Flooded	Moderate
60.01-90.00	66	81,182.85	8.55	65,603.70	Partially Flooded	Major
90.01-100.00	747	816,319.44	85.94	815,314.46	Fully Flooded	Severe
Total	857.00	949,836.16	100.00	897,008.02		

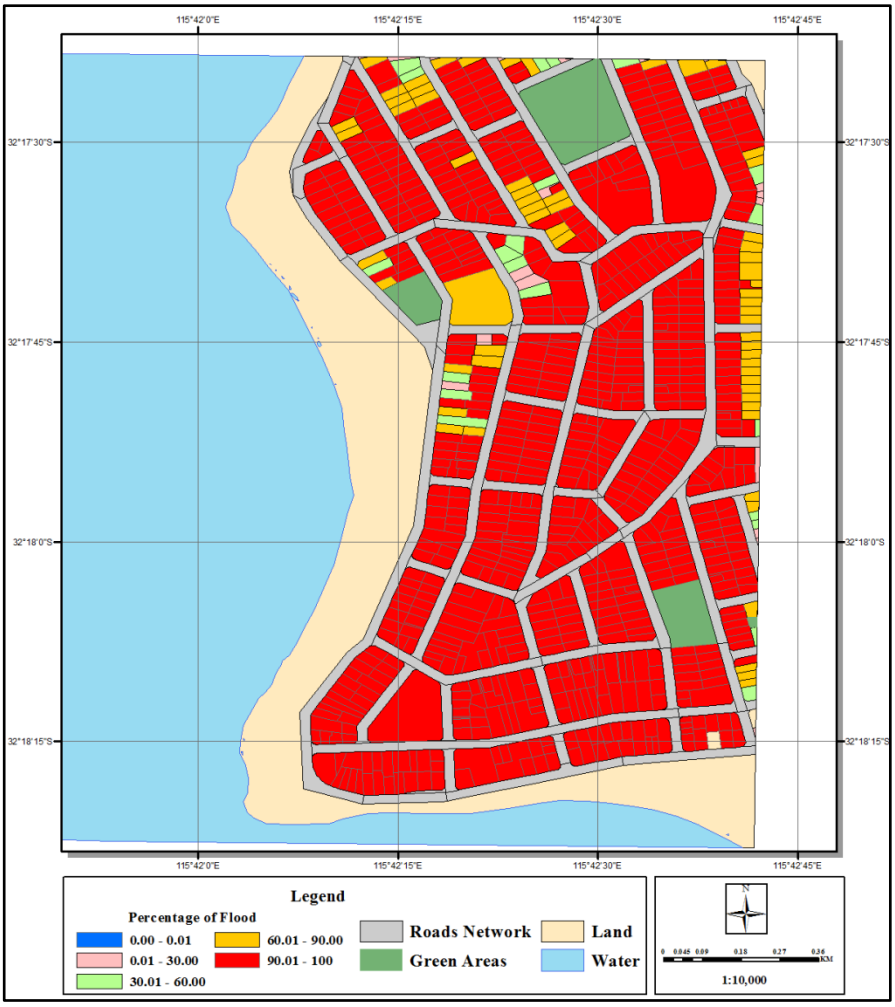

Figure 5.22 Property-based percentage of flooding for the Rockingham study area, assuming a sea level rise of 8.61 m.

5.4.7 Sea level rise of 10.12 m in Mandurah

In this section, we show the impact of coastal flooding on residential areas located near to the shoreline due to the melting of the West Antarctic ice sheet. The sea level rise value for this flooding scenario is obtained by the contribution of the West Antarctic ice sheet and the predicted sea level rise by 2100. For this scenario, the sea level is expected to reach 10.12 m (cf. chapter 3.6.5). This scenario, and the next, is modelled for the Mandurah study area only. This is because the Rockingham study area was already almost fully flooded in the previous scenario. Figure (5.23) shows that almost all properties in the east and north of the study area are highly affected by flooding in this scenario, and some of the properties in the west are also affected by flooding. Many properties within the centre, and south-east parts of the study area are still not affected by flooding (cf. Figure 5.23).

The numerical results obtained for this scenario show that now approximately 36.1% of the properties within the study area are affected by flooding (i.e. 747 properties). This corresponds to an area of about 709,938 m^2. However, a large number of properties within the study area are still not affected (i.e. 1,525 properties). This is approximately 63.9% of all properties, occupying an area of 1,256,065 m^2 (cf. Table 5.14 and Figure 5.23).

Analysis of the flooding percentages for all properties in the Mandurah study area indicates the impact of flooding as severe for most properties along the east and north parts of the study area. Figure (5.24) confirms the impact of flooding in the centre and south-eastern parts of the study area is negligible compared to the other areas. Table (5.15) shows that 1,252 properties are not flooded, representing an area of 1,256,065 m^2. Whereas, 530 properties are identified as fully flooded, corresponding to an area of 437,957 m^2. Another 117 properties are identified as partially inundated, with a small percentage of flooding ranging from 0.01 to 30%, and 100 properties are classified as partially flooded with a higher percentage of flooding, ranging from 30.01 to 90% (cf. Table 5. 15 and Figure 5.24).

Table 5.14 Property-based flood modelling for the Mandurah study area, assuming a sea level rise of 10.12 m. Results show all properties affected by flooding irrespective of their level of flooding (i.e. includes partially flooded properties). Area 1 is the total area of the properties and Area 2 is the actual flooded area.

Parcel condition	No of Parcels	Area 1 (m²)	Area 1 (%)	Area 2 (m²)
Flooded	747	709,938	36.1	530,570
Not flooded	1,252	1,256,066	63.9	0
Total	1,999	1,966,004	100	530,570

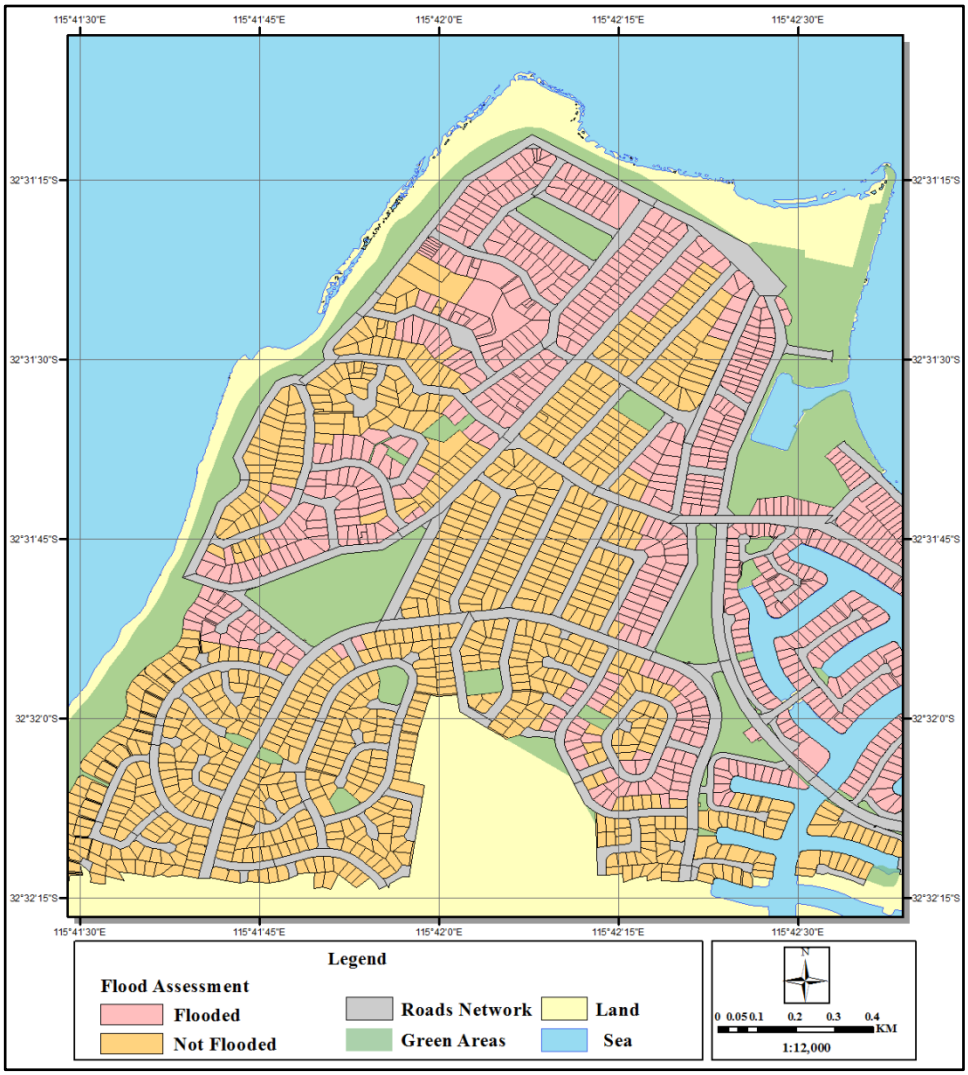

Figure 5.23 Property-based flood modelling for the Mandurah study area, assuming a sea level rise of 10.12 m. Flooded areas are shown irrespective of their level of flooding.

Table 5.15 Property-based percentage of flooding for the Mandurah study area assuming a sea level rise of 10.12 m. Area 1 is the total area of the properties and Area 2 is the actual flooded area.

Flood percentage	No of Parcels	Area 1 (m^2)	Area 1 (%)	Area 2 (m^2)	Flooding Category	Flood Level
0.00-0.01	1252	1,256,065.85	62.63	37.58	Not Flooded	None
0.01-30.00	117	126,555.24	5.85	12,160.97	Partially Flooded	Minor
30.01-60.00	37	67,822.40	1.85	26,264.80	Partially Flooded	Moderate
60.01-90.00	63	77,603.33	3.15	57,446.70	Partially Flooded	Major
90.01-100.00	530	437,957.48	26.51	434,697.27	Fully Flooded	Severe
Total	1,999	1,966,004.31	100.00	530,607.32		

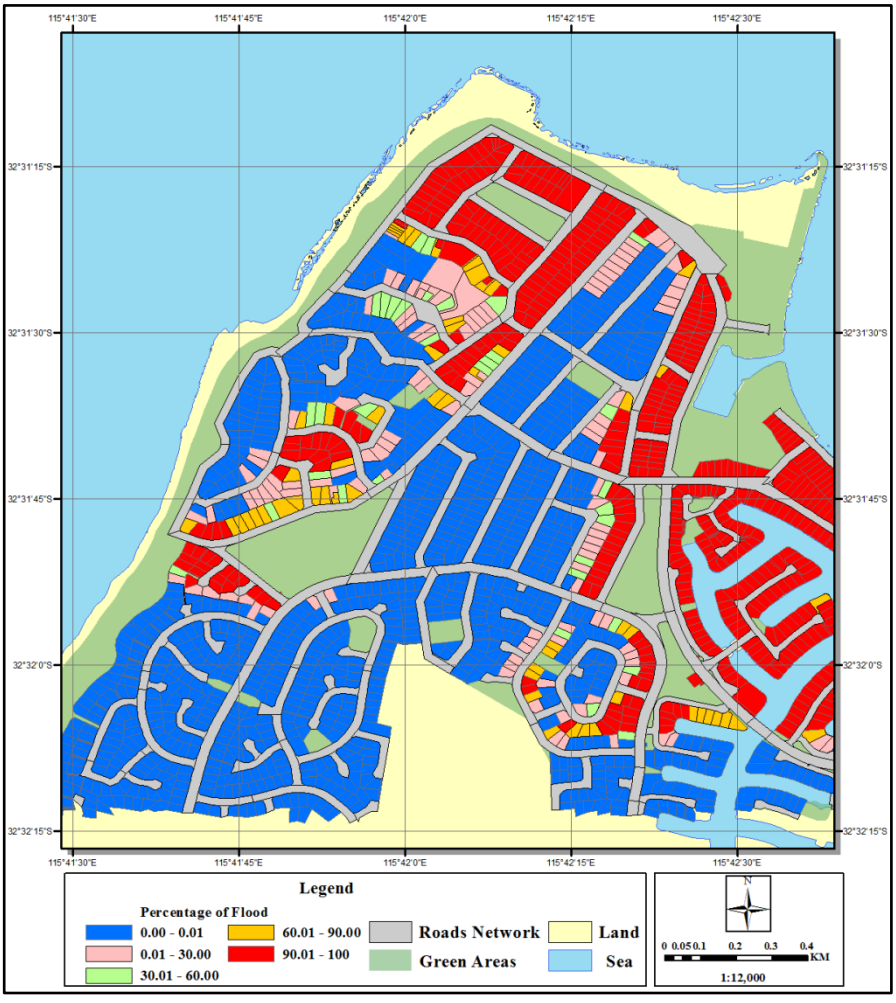

Figure 5.24 Property-based percentage of flooding for the Mandurah study area, assuming a sea level rise of 10.12 m.

5.4.8 Sea level rise of 18.73 m in Mandurah

The worst-case scenario adopted in this study is when the sea level rises to 18.73 m (cf. chapter 3.6.5). For this flooding scenario, the combined contribution of the ice sheets from Greenland and West Antarctic are considered, as well as the projected sea level rise by 2100, the maximum wave, and storm surge heights. Again, only the Mandurah study area has been considered for this scenario.

Due to the extremely high sea level change, in this flooding scenario, a large number of the properties are inundated. From visual inspection of Figure (5.25), it can be seen almost all properties within the study area are affected by flooding. Only a few properties, in the southern and central parts, are not affected by a sea level rise of 18.73 m. This is confirmed by the numerical results, which show that 1,391 of all properties are inundated (representing 66.5% of the total area). However, 608 of all properties are still not affected by flooding, representing an area of 658,543 m^2 (33.5%) (cf. Table 5. 16 and Figure 5.25).

Analysis of flooding percentages (cf. Figure 5.26) also shows severe flood levels in the eastern and northern parts of the study area. Apart from only a few properties in the western part, severe flood levels are indicated. The southern part of the study area is, however, still unaffected by flooding.

Due to the substantial increase in sea level, the numerical results also show a significant increase in properties that are fully flooded. 1,224 properties (61.2%) with total area of 1,092,344 m^2 are now fully flooded. On the other hand, the number of non-flooded properties has decreased to almost half the number in the previous scenario; the number has decreased from 1,252 to 608 properties. The number of partially flooded properties has decreased slightly when compared to the previous flooding scenario. Now 167 properties are classified as partially flooded (cf. Tables (5.15 and 5. 17) and Figures (5.24 and 5.26).

Table 5.16 Property-based flood modelling for the Mandurah study area, assuming a sea level rise of 18.73 m. Results show all properties affected by flooding irrespective of their level of flooding (i.e. includes partially flooded properties). Area 1 is the total area of the properties and Area 2 is the actual flooded area.

Parcel condition	No of Parcels	Area 1 (m²)	Area 1 (%)	Area 2 (m²)
Flooded	1391	1,307,461	66.5	1,188,599
Not flooded	608	658,543	33.5	0
Total	1,999	1,966,004	100	1,188,599

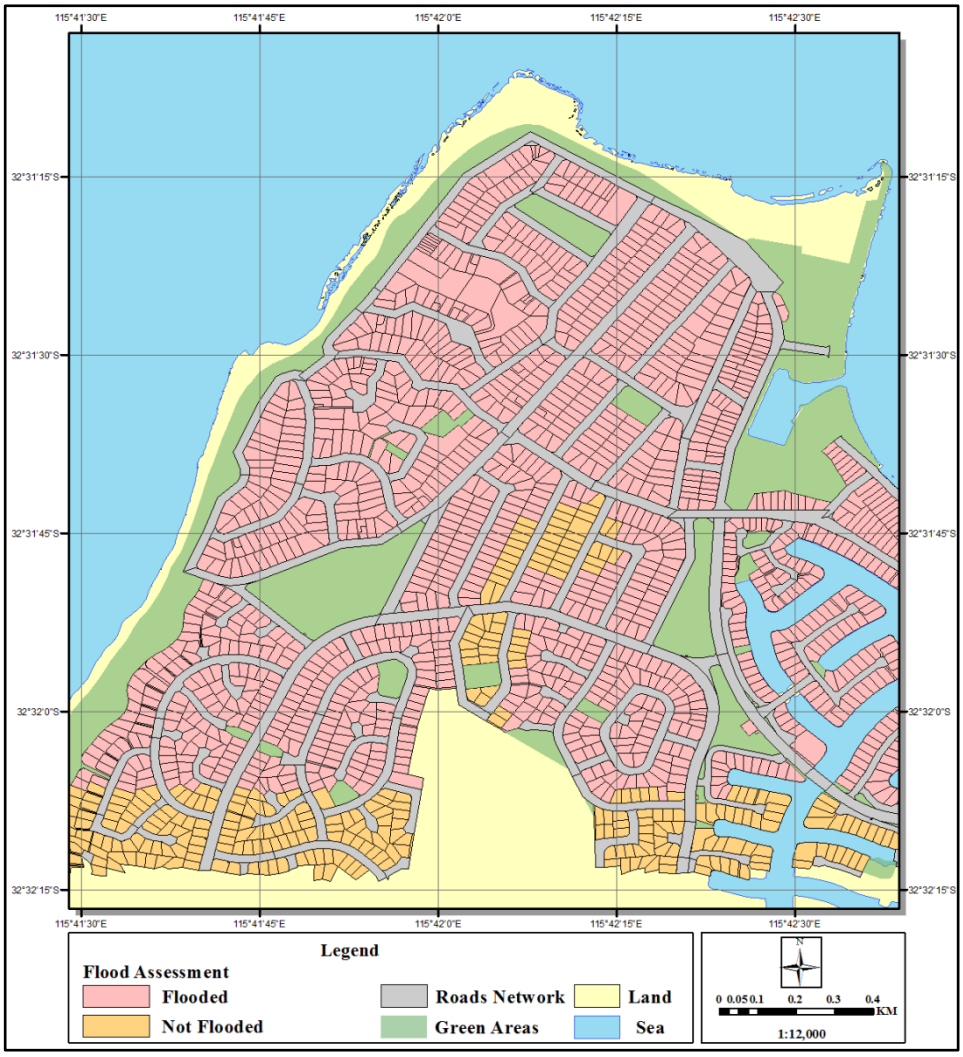

Figure 5.25 Property-based flood modelling for the Mandurah study area, assuming a sea level rise of 18.73 m. Flooded areas are shown irrespective of their level of flooding.

Table 5.17 Property-based percentage of flooding for the Mandurah study area, assuming a sea level rise of 18.73 m. Area 1 is the total area of the properties and Area 2 is the actual flooded area.

Flood percentage	No of Parcels	Area 1 (m²)	Area 1 %	Area 2 (m²)	Flood Category	Flood Level
0.00-0.01	608	658,543.08	30.42	9.83	Not Flooded	None
0.01-30.00	63	66,729.58	3.15	7,126.24	Partially Flooded	Minor
30.01-60.00	34	60,354.58	1.70	23,015.83	Partially Flooded	Moderate
60.01-90.00	70	88,032.87	3.50	67,958.70	Partially Flooded	Major
90.01-100.00	1224	1,092,344.19	61.23	1,090,498.62	Fully Flooded	Severe
Total	1,999	1,966,004.31	100.00	1,188,609.22		

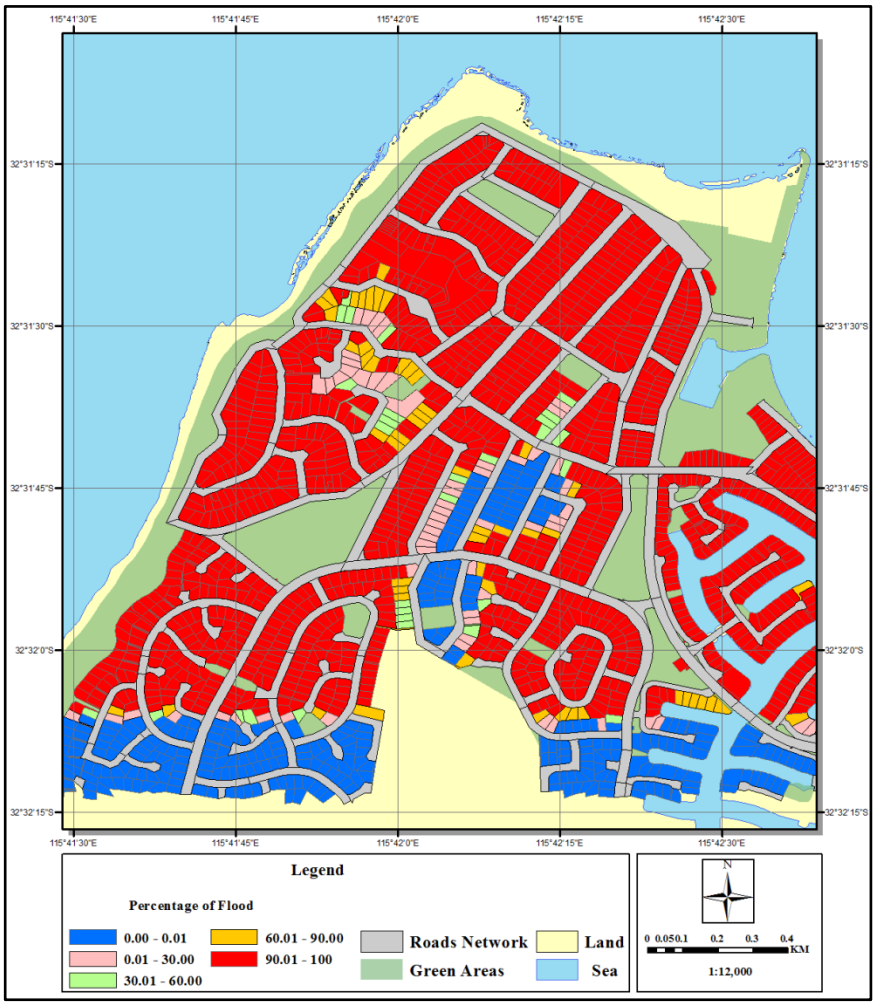

Figure 5.26 Property-based percentage of flooding for the Mandurah study area assuming a sea level rise of 18.73 m.

5.5 Development and implementation of a property-based flood vulnerability index

This step of the research deals with the development and implementation of a property-based flood vulnerability index. In this study, the vulnerability index is obtained using criteria based on the results obtained throughout the previous steps.

The vulnerability index can further be developed based on a number of parameters determined by the user. In this research, the flood vulnerability index is developed based on five parameters. The parameters have been chosen based on (i) the nature of the study, (ii) the suitability of the parameters to the study, and (iii) the availability of data required. The selected parameters are commonly used in studies surrounding vulnerability of coastal areas due to sea level rise (e.g. Schanze et al. 2006; Chakma 2014; Nethengwe 2007). Each parameter has been given a weight value. The weight value reflects the relative importance of that parameter to the vulnerability index.

The properties are classified into five categories based on the vulnerability index. This section describes the development and implementation of a property-based flood vulnerability index. The methodology is explained and applied to sea level rise, and associated flood scenarios, described in chapter 5.4. For the sake of brevity, the result for only one sea level rise scenario (as an example) is shown, for both the Mandurah and Rockingham study area. The scenario considers a sea level rise of 5.98 m, which can be considered a likely sea level rise within the next few centuries. For completeness, the results for the remaining sea level rise scenarios (cf. chapter 3.6.5) are shown in Appendix B.

5.5.1 Introduction

At present, more than 50% of the world's population is living in residential areas or in major cities (Meuser 2010). It is projected that many of the world's largest cities will be vulnerable to the effects of climate change and associated sea level rise. Millions of the world's population may be, Consequently millions, exposed to frequent flood and storm events (Aerts et al. 2009).

The predictions show that large residential areas will further be concentrated around or close to coastal zones, especially in developing countries (Kreimer, Arnold, and Carlin 2007). In this case, the incidence of flooding will increase, due to both an increased river run-off and blockages caused by sea level rise. As a consequence, the number of people exposed to flooding, and related natural disasters, will increase (Aerts et al. 2013; Nicholls 2004; Smith and Ward 1998).

Due to the high concentration of the world's population close to the coastline, the risk of flooding will be much increased (Small and Nicholls 2003). It is expected that the amount of people affected by flood events will rise by 6- and 14- times in a typical year, when the global sea level rises by half a metre and one metre, respectively (Nicholls 2004). This means extreme sea level events, which currently occur approximately once per century, may happen once per decade.

With this in mind, the vulnerability studies, due to sea level rise on a property-by-property level, become very important. Localised information provides local governments with the necessary information to mitigate the risk of coastal flooding in the most likely affected areas, and will minimise the socio-economic impact on coastal areas.

5.5.2 Developing a property-based flood vulnerability index

Many parameters can be considered when deriving and studying the flood vulnerability of coastal areas due to sea level rise. Some of the commonly considered parameters are:

- Elevation and depth of the inundation area (Schanze et al. 2006; Chakma 2014).
- Distance to the water bodies (Chakma 2014).
- Physical components (topography, slope, and aspects) (Nethengwe 2007; Chakma 2014).
- Geology (Chakma 2014).

In addition, socio-economic, hydro-geological, and politico-administrative elements are often considered in coastal vulnerability studies (Balica, Wright, and Meulen 2012). Currently, there are few studies, which look into the development of a flood vulnerability index using high-resolution data in combination with a property-by-property view. This study provides a methodology to develop suitable parameters for a flood vulnerability index, when modelling on a property-by-property level.

All parameters used in this study are related and/or focus on the specific property's geographic location and the potential flood risk level (cf. chapter 5.4). Furthermore, all parameters selected in this study can be easily combined and modelled in ArcGIS. As an example, in this study, five parameters are considered when modelling and assessing the vulnerability of each property due to flooding (cf. Figure 5.27). These property specific parameters are:

1. Flood assessment of the property.
2. Percentage of flooding for each property.
3. Straight-line distance between the property and the closest shoreline.
4. Water level above the property.
5. Slope of the distance between the property and the shoreline.

These parameters are commonly used in studies of the vulnerability of coastal areas due to sea level rise (e.g. Schanze et al. 2006; Chakma 2014; Nethengwe 2007).

Each parameter is given a weight value, reflecting the relative important of that parameter to the flood vulnerability index. In this study, the weights (out of a total of 100) have been selected as (cf. Table 5.18):

- Flood assessment: 20.
- Distance to shoreline: 25.
- Percentage of flooding: 30.
- Water above property: 15.
- Slope: 10.

Each of the above parameters is described in more detail in chapter 5.5.3 below. In addition to the weighting, each parameter is ranked according to risk factors, ranging from 1 to 5, based on the value of the respective parameter. Table (5.18) provides the mapping of each parameter to the five risk factors, categorised as:

- Very low risk: factor 1.
- Low risk: factor 2.
- Moderate risk: factor 3.
- High risk: factor 4.
- Very high risk: factor 5.

The contribution of each parameter is calculated in ArcGIS by a weighted average, i.e. the sum of the multiplied weights of each parameter with the risk factor, and division by the sum of the values of risk factors introduced (i.e. 500). The results (for each property) are then multiplied by 100 (e.g. total of the multiplied weight/500*100). The results of the flood vulnerability index are between 20 and 100 for each property. Based on this, the properties are classified into five equal interval categories based on the value of the flood vulnerability index. These five categories are used to match the five risk categories introduced above, and are given as follows:

- Very low risk: from 20.00 to 36.00.
- Low risk: from 36.01 to 52.00.
- Moderate risk: from 52.01 to 68.00.
- High risk: from 68.01 to 84.00.
- Very high: from 84.01 to 100.

While the selected parameters are common parameters, used to derive information on flood vulnerability (e.g. Schanze et al. 2006; Chakma 2014; Nethengwe 2007), the selected values are somewhat arbitrary (although they aim to reflect relative importance). However, this study does not focus on the development of the most suitable set of parameters and values. The focus is on the development of a methodology using ArcGIS. Based on the methodology, users can select and implement their own parameters of interest and associated values.

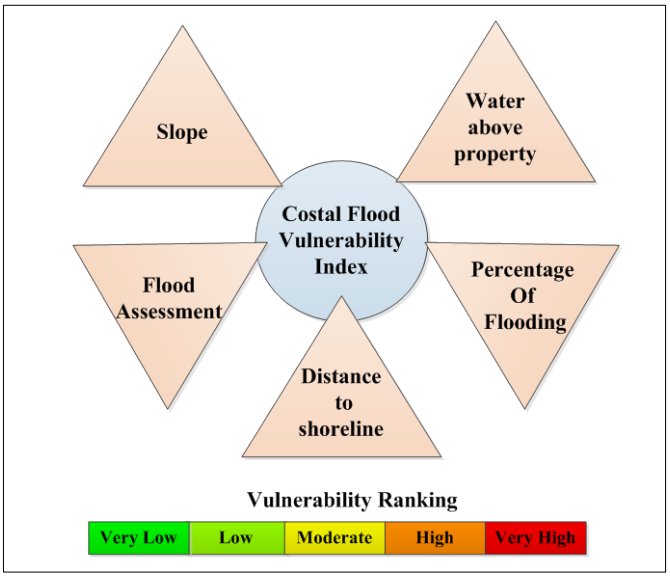

Figure 5.27 Selected parameters modelling a property-based flood vulnerability index.

Table 5.18 Parameters, weighting and risk ranking used for the flood vulnerability index.

Rank	Very low risk	Low	Moderate	High	Very High	Element Weight
Element	1	2	3	4	5	
Flood assessment	Not Flood				Flooded	20
Distance to shoreline (m)	600 - 750	450 - 600	300 - 450	150 - 300	0 - 150	25
Percentage of flooding %	0.00 - 10.00	10.001 - 25.00	25.001 - 45.00	45.001 - 75.00	75.001 - 100.00	30
Average water height above property (m)	00.00 - 1.36	1.36 - 2.72	2.72 - 4.08	4.08 - 5.44	5.44 - 6.80	15
Slope (-)	23.00 - 11.168	11.168 - 7.001	7.001 - 4.158	4.158 - 1.543	1.543 - 0.000	10

5.5.3 Data used for the property-based flood vulnerability index

As described in the previous section, five parameters have been used to assign a vulnerability level for each property. This has been carried out within both the Mandurah and Rockingham study areas. The first parameter considered is the general flood assessment, which provides the information if a property is flooded, irrespective of the level of flooding. This information has been already obtained and documented in chapter 5.4. It is obtained by overlapping the flooded area with the property boundaries. The information on flooding percentages for each property has also been obtained and documented in chapter 5.4.

The second parameter is the shortest distance from the property to the shoreline. The distance has been calculated using the *near analysis* tool in ArcGIS. The tool works by calculating the nearest distance between the two features; the input feature, which is the property's location, and the near feature, which represents the shoreline. In this case, the perpendicular, or nearest, vertex is used to derive the shortest distance between a point and a polyline. In order to perform the analysis, the centre point of each property parcel is derived by using *feature to point* tool in ArcGIS. The tool converts each polygon (property boundary) to a centre point located at the centre of gravity of the polygon, with a unique id assigned to each point. The output shape file, for the distance analysis, is then joined with the property polygon by using the unique id. This helps to transfer the information from the nearest distance shape file to the property shape file, which is used later in the analysis stage.

The third parameter used in the flood vulnerability analysis is the percentage of flooding of each property (cf. chapter 5.3.2.3). This parameter indicates the amount of flooding based on the actual affected (i.e. flooded) area of each property. The information regarding flooding percentages for each property is obtained, presented, and documented in chapter 5.4.

The fourth parameter used in the vulnerability study is the average water level above the property. This parameter represents the amount of the water that will inundate each property and is calculated by subtracting the height of the sea level rise scenario from the average height for the property. The *field calculator* in ArcGIS is used to calculate the water level and assigns it to each property.

The fifth parameter used in the analysis is the slope, representing the variation in elevation compared to the distance, and provides useful information about the nature of the surface. The slope analysis is performed using the DEM using ArcGIS. The slope, in this case, is the ratio of the average property height to the shortest distance to the shoreline (e.g. second parameter).

5.5.4 Results of the flood vulnerability analysis

In order to test the feasibility of the developed flood vulnerability index, analyses have been performed for both the Mandurah and Rockingham study areas. The sea level rise considered is 5.98 m. For the Mandurah study area, the analysis indicates that 63 properties are at very low risk, representing 3.1% of the total properties (cf. Table 5.19 and Figure 5.29). Figure (5.29) shows that these properties are concentrated in the east and southeast corner of the study area. The analysis also indicates the majority of properties (1165 or 58.2%) in Mandurah are at low risk, and they are located mainly in the central, western, and southern parts of the study area.

However, there are 353 properties (17.6%) at moderate risk, 201 properties (10.0%) at high risk of coastal flooding and another 217 properties (10.8%) at a very high risk of flooding. Figure (5.29) reveals the properties with a high and very high risk of flooding are located in the eastern and northern parts of the study area. All properties in Mandurah at moderate risk are concentrated in the west and southwest side of the study area.

For the Rockingham study area, the vulnerability analysis shows that the majority of properties are either at high or very high risk (e.g. 84.0%) of flooding when sea level rises to 5.98 m (cf. Table 5.19 and Figure 5.30). Figure (5.30) shows that the southern part of the study area is more vulnerable than the northern part. Over 42.2% of total properties are at a very high risk of coastal flooding (cf. Table 5.19). Moreover, nearly all of the properties located at the eastern and northern side of the study area are highly affected by coastal flooding, with almost 41.7% of the properties classified as high risk when sea level rises to 5.98 m. Only a few properties (7 or 0.8%) are at very low risk. 41 properties (4.7%) and 89 properties (10.3%) are at a low and moderate risk of flooding respectively. These properties are mostly located in the central western part of the study area (cf. Figure 5.30).

A comparison between both study locations shows that approximately 61.4% of the properties in Mandurah are at a very low risk or low risk of flooding when sea level rises to 5.98 m. For the same sea level rise scenario in Rockingham, only 5.6% of total properties are at a very low risk of flooding. Table (5.19) shows that 217 properties in Mandurah (representing only 10.8 %) are at a very high risk of coastal flooding compared to 362 properties (representing 42.2%) for Rockingham. The percentage of the properties at high risk is much lower for Mandurah (201 or 10.0%) than for Rockingham (358 or 41.7% (cf. Table 5.19 and Figure 5.28).

From both vulnerability analyses, it can be concluded that, at a sea level rise of 5.98 m, properties in Rockingham are much more vulnerable to coastal flooding than properties located in Mandurah. The higher risk for the Rockingham study area is due to low-lying topography, the close distance to the shoreline and the slope parameters (very flat area) (cf. Figure 4.6).

Table 5.19 Flood vulnerability index analyses for both the Mandurah and Rockingham study locations. The sea level rise scenario considered is 5.98 m.

Risk Category	Mandurah		Rockingham	
	No of properties	%	No of properties	%
Very Low 20.00-36.00	63	3.15	7	0.82
Low 36.01-52.00	1165	58.28	41	4.78
Moderate 52.01-68.00	353	17.66	89	10.39
High 68.01-84.00	201	10.06	358	41.77
Very High 84.01-100	217	10.86	362	42.24
Total	1999	100	857	100

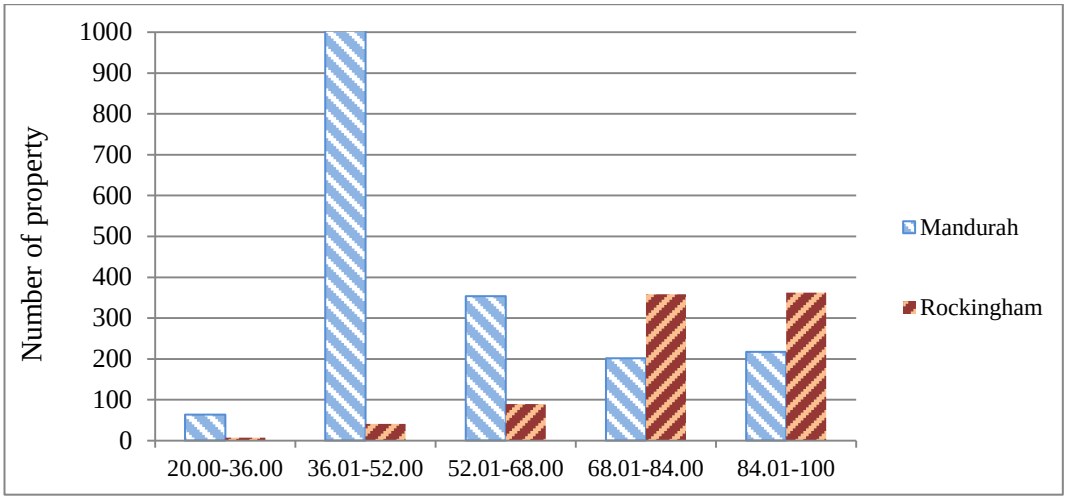

Figure 5.28 Number of properties vs. flood vulnerability index for the Mandurah and Rockingham study locations. The sea level rise scenario considered is 5.98 m.

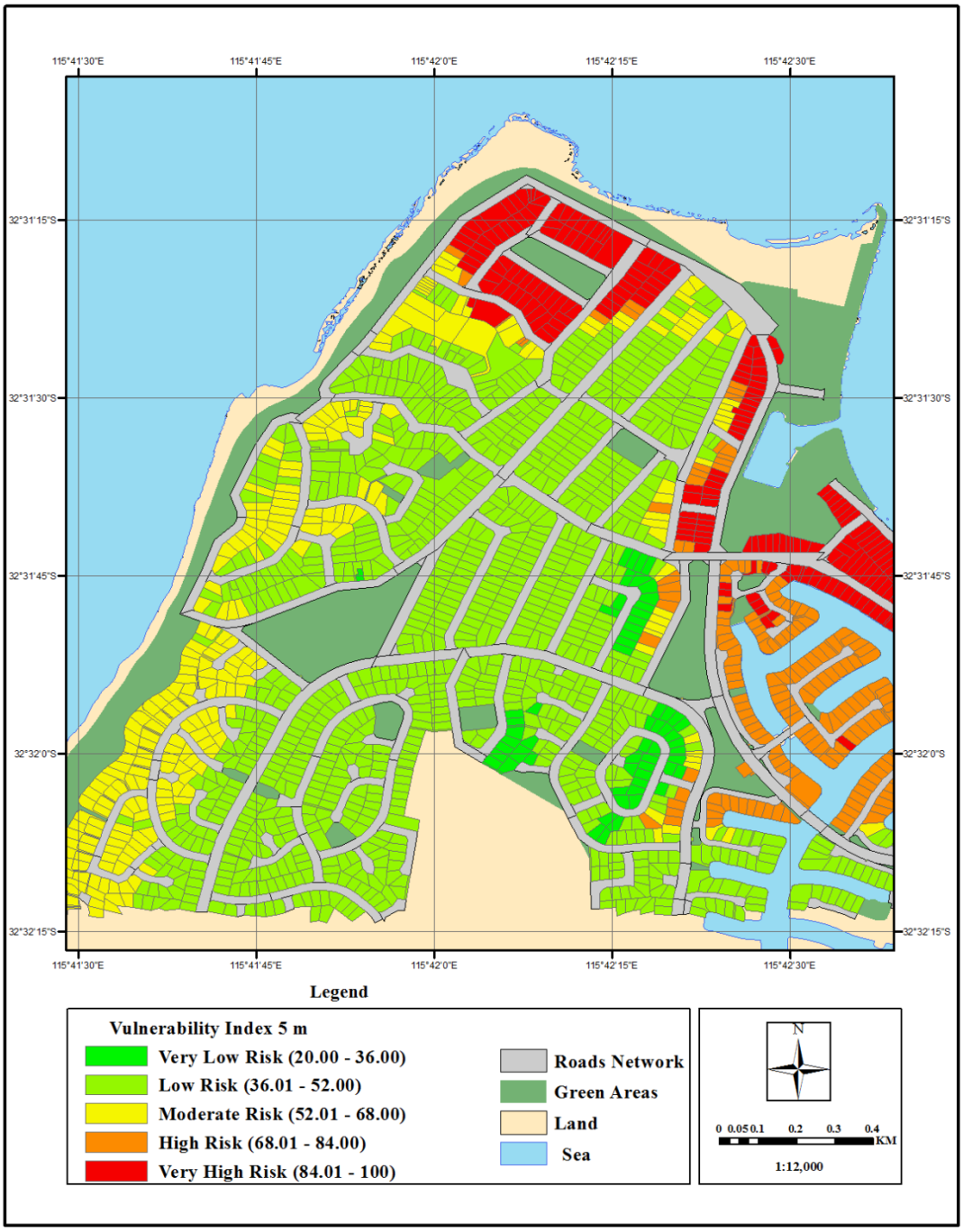

Figure 5.29 Vulnerability analysis for the Mandurah study area. The sea level rise scenario considered is 5.98 m.

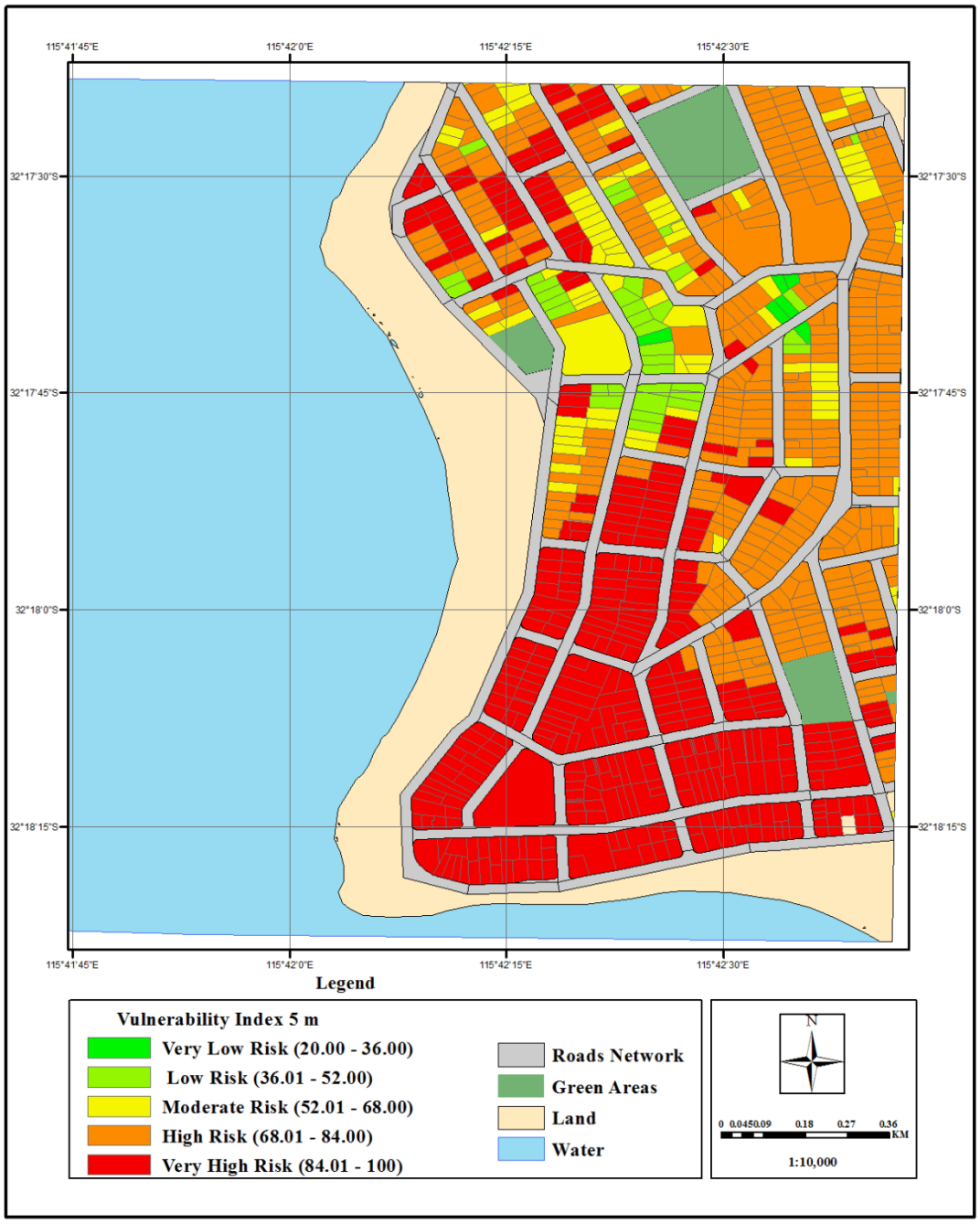

Figure 5.30 Vulnerability analysis for the Rockingham study area. The sea level rise scenario considered is 5.98 m.

5.6 Implementation of a property-based flood GIS

This section describes the main components (required steps) used within this study to implement a prototype for a property-based flood GIS. After this, the section focuses on the design and implementation of user-friendly tools that can conveniently be used by end users. The developed tools will help the end user to avoid manual processing of large data sets and the repetition of rather labour intensive processes.

5.6.1 Main components of a property-based flood GIS

In this section, the main components (steps) required for the development of a property-based flood GIS are outlined. These steps can be implemented as a prototype to model the effect of coastal flooding on a property-by-property level, taking into consideration these requirements can be modified and updated based on user requirements and the application the model will be used for.

Step 1: Sea level rise estimation

The first step that needs to be taken is the projection of future sea level rise. The main aim of this step is to estimate the expected rate of sea level rise, based on historical data and also models, which will project future sea level rise (e.g. by the year 2100). In this study, a number of possible sea level rise scenarios are adopted based on past sea level data (cf. chapter 3).

Step 2: Modelling the spatial extent of flooding

The second step aims to model the spatial extent of flooding for a given area. Through this step the possible flooded and not flooded areas, based on a flooding scenario, are determined for a study area. Identifying the flood-affected area is an essential part of flood modelling, and it will be used here in a property-by-property based flood analysis. High-resolution DEM data is used to model and assess the impact of coastal flooding. High-resolution DEM data, obtained from LiDAR, provides an accurate representation of the terrain and is strongly recommended for use in the flood modelling stage (cf. chapter 4).

Step 3: Property-by-property based flood modelling

The third step will model flooded areas at a high spatial resolution, i.e. on a property-by-property level. The information is obtained by overlapping the extent of flooding (cf. step 2) with property boundaries. This is then used to determine the flood condition for each property. This is carried out by selecting the spatial location function in ArcGIS. The end user can choose from a large array of spatial selection methods, which are available within ArcGIS, to determine the relationship between the two layers. Using high-resolution data, such as LiDAR DEM data, enables the user to apply a more detailed analysis of the space. Only with high-resolution data is it possible to derive a more accurate estimation of the property's flood percentage (cf. chapter 5.3.2.4).

Step 4: Property-based flood vulnerability index

The final step in this study will derive a property-based flood vulnerability index, using criteria and results obtained throughout the previous steps (cf. chapter 5.5). A flood vulnerability index can be developed based on a number of different parameters determined by the user.

5.6.2 ArcGIS ModelBuilder

In this study, ArcGIS ModelBuilder is used to develop two flood-modelling tools (cf. Figure 5.31): a flood information tool and a property-based flood GIS tool. These tools provide the ability to automate manual processing tasks by defining a sequence of steps to be executed in order to solve a given spatial analysis task (e.g. flood modelling). The use of ArcGIS ModelBuilder can help to significantly reduce processing time and assure the quality of outputs (i.e. avoiding manual processing errors (cf. chapters 4.7, 4.8, 5.3, and 5.4). Using ArcGIS ModelBuilder a sequence of processes can be defined, which are executed sequentially (e.g. packaged together). These processes can interact (i.e. outputs from a previous step are used in the next processing step). The overall process is defined through a series of tools, where the variables are the parameters (for each tool) entered by the user (Sterling 2013). Using ArcGIS ModelBuilder allows the user to perform repetitive tasks automatically.

The user also has the ability to save model outputs for future use and/or export outputs as a script to be used on different platforms. Another advantage of using the ArcGIS ModelBuilder tool is the developed tool can be easily shared among users. This is carried out through the python script, or the toolbox within ArcGIS. The ModelBuilder workflow consists of a number of model variables and tool elements. A model variable is the data, or the value, used inside the model, while tool elements are the workflow building boxes used in the model (cf. Figure 5.31).

5.6.3 Flood information tool

Using ArcGIS ModelBuilder, a flood information tool was developed and applied (cf. chapters 4.7 and 4.8) to assess and visualise the flood condition for a user-defined location and flooding scenario. Raster-based data (i.e. a digital elevation model) is used as input data for the flood information tool. The tool examines each raster pixel cell, only if the height of the adopted sea level rise is higher (e.g. flooded) or lower (not flooded) than the DEM height. The result is a new raster image containing the values 0 or 1; a value of 0 indicates the raster cell is not flooded and a value of 1 indicates the raster cell is flooded (cf. Figure 4.14). The resulting raster image is then converted to a vector format, as a polygon feature class, which delineates the flooded and not flooded areas (i.e. for a given area). The *Raster to polygon* tool in ArcGIS is used to convert the raster dataset to polygon features, and the polygon feature within ArcGIS is used to derive the total area for each flood category.

Figures (5.31, 5.32 and 5.33) illustrate the steps followed to create the flood information tool within ArcGIS ModelBuilder. The flowchart provides a diagrammatic representation, which illustrates the sequence of operations to be performed in order to derive the desired flood condition and respective area. The flowchart is considered the first step in designing a property-based flood GIS tool (cf. chapter 5.6.4). The flowchart also plays a vital role in the development process, helping the user to understand the logic behind the flood information tool, as well as in implementation.

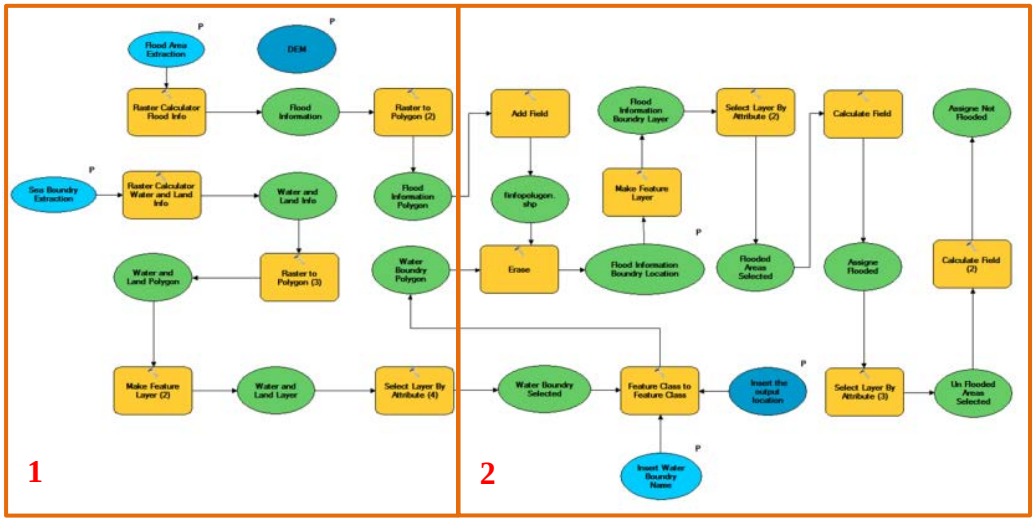

Figure 5.31 Flow chart showing the process implemented in the flood information tool using ArcGIS ModelBuilder. “P” refers to parameter. See Figures 5.32 and 5.33 for zoomed in parts (1 and 2) of this flow chart.

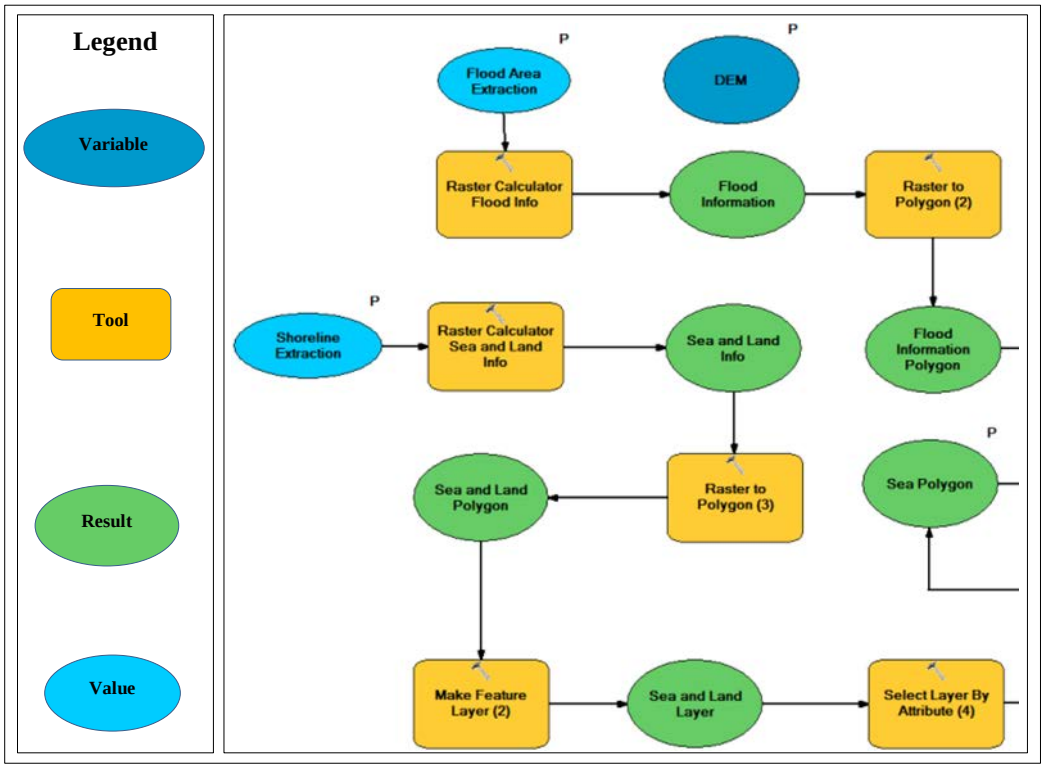

Figure 5.32 Part (1) of the flow chart illustrated in Figure 5.31 showing the process implemented in the flood information tool using ArcGIS ModelBuilder.

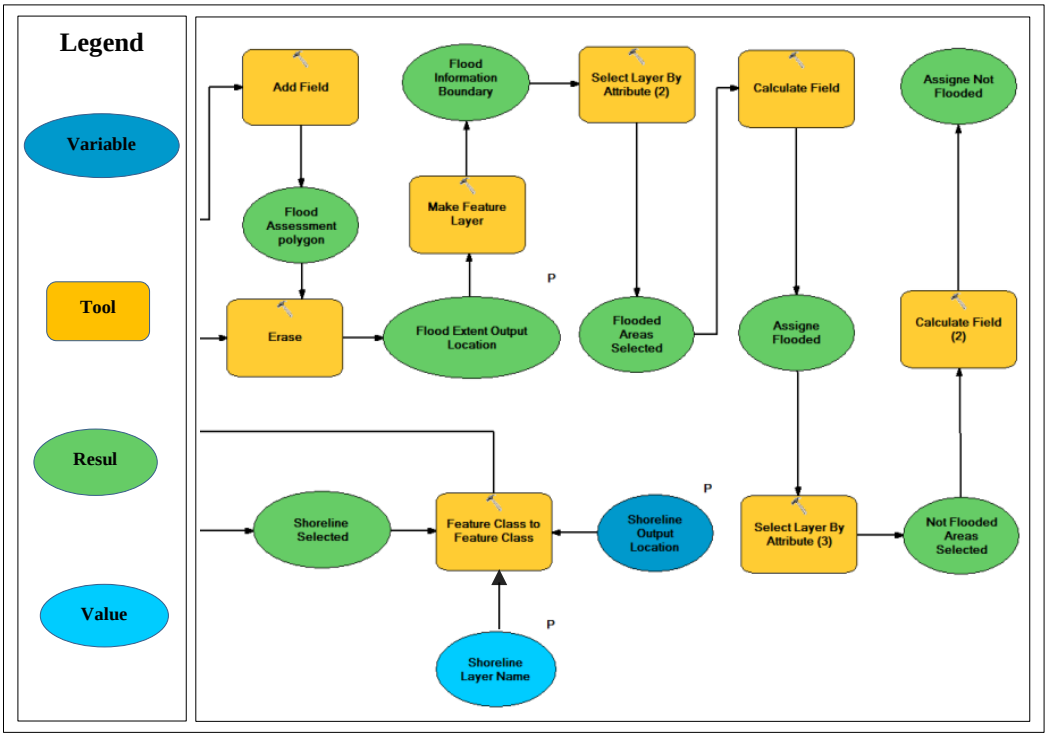

Figure 5.33 Part (2) of the flow chart illustrated in Figure 5.31 showing the process implemented in the flood information tool using ArcGIS ModelBuilder.

The developed flood information tool also contains a dialog tool to specify desired parameters. The dialog tool is an interface where the end user can specify the required processing parameters. Figure (5.34) shows the Graphic User Interface (GUI) of the developed interface, which allows the user to input the following six parameters:

A. Raster based DEM data that will be used in the processing. The user can upload the raster file for the desired study area with the supported raster dataset format in ArcGIS (Tagged Image File Format (*.TIFF), ERDAS IMAGINE (*.IMG), and others).
B. The Map Algebra expression used to specify the sea level height. The output flood raster image is created based on the Map Algebra expression inserted in this field. Here the user can specify the layer, the operator's button and the condition that will be used in the Map Algebra expression.
C. The file name and location for the output file (i.e. where it will be stored).

D. The Map Algebra expression used to specify the shoreline. The obtained shoreline boundary in this tool will be used for further analysis.
E. The file name of the output feature class.
F. The data set location where the output feature class will be stored.

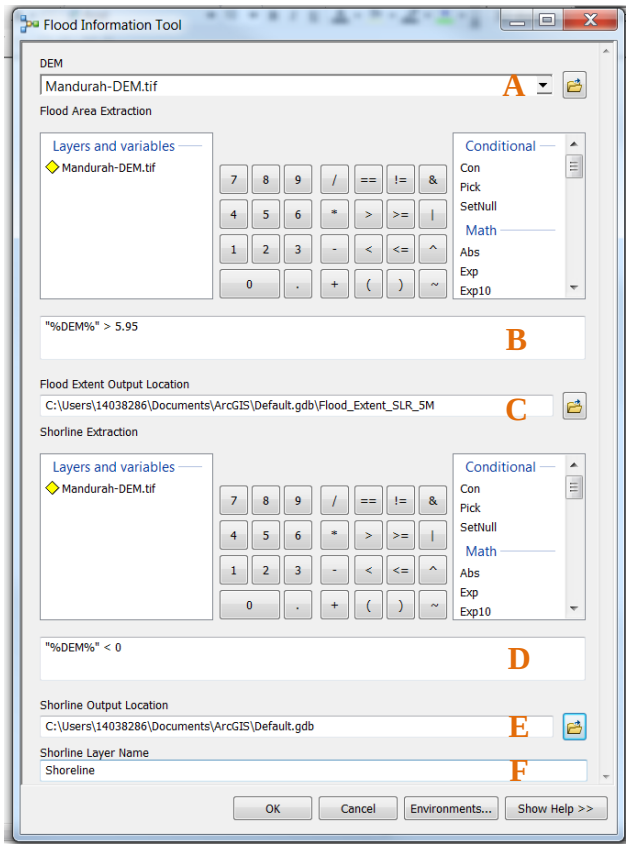

Figure 5.34 Flood information tool GUI.

The input data used by the tool is a raster DEM for the selected study area, and outputs are two vector features. The first output is a polygon feature class, showing the condition of flooding. The polygon classifies the study area as either flooded or not flooded depending on the sea level rise scenario used. The flood condition, along with the respective total area for each flood condition, is documented in the feature class attribute table.

The second output is a polygon feature class, which shows the shoreline. The output feature class can be stored in a file geodatabase, where the stored file can scale up to 1 TB in size. Alternatively, it can be stored in a personal geodatabase, in which case the file size can only reach up to 2 GB. The storage size limitations are set by ArcGIS.

5.6.4 The property-based flood GIS tool

As a main result of this study, a property-based flood GIS tool was developed. This tool is central to the aims of this research, and it is used to examine the flood condition at a property-by-property level. Based on a given sea level rise scenario, the tool examines each individual property to determine if fully flooded, partially flooded or not flooded. For partially flooded properties, the tool estimates the percentage of flooding; this is based on the number of DEM grid cells flooded within an individual property. As part of the flood vulnerability index (cf. chapter 5.5), the slope level (i.e. from each property to the closest shoreline) is also derived.

The ModelBuilder process uses a number of co-dependent ArcGIS tools and variables. Figures (5.35, 5.36, 5.37, 5.38, and 5.39) show the processing steps, which are followed by the property-based flood GIS tool. Lines shown in Figure (5.35) indicate the relationship between ArcGIS tools and their processing sequence. In order to operate the property-based flood GIS tool, the user must supply the following spatial data:

1. Property boundaries as polygon feature class.
2. Coastline boundary as polyline vector data.
3. Raster based DEM data for the given study area.

The property boundaries attribute table must contain height information for each property, which will be used to calculate the percentage of flooding. A unique identification number must also be set for each property in the attribute table.

The property-based flood GIS tool requires the user to input vector based polygon feature classes (from within the study area) containing:

(1) Property boundaries.
(2) The coastline.
(3) The boundary delineating flooded from non-flooded areas (cf. chapter 4).

The raster DEM (for the selected study area) and the attribute table (containing the slope information for each property) must also be inputted.

Main outputs of the developed tool are (1) an attribute table for the average height of each property and (2) a polygon feature class for the flood condition on a property-by-property level. As in the previous tool, the data can be stored in a geodatabase file, where the stored file can scale up to 1 TB in size, or it can be stored in a personal geodatabase, where and the file size can reach up to 2 GB. The storage size limitations are set by ArcGIS.

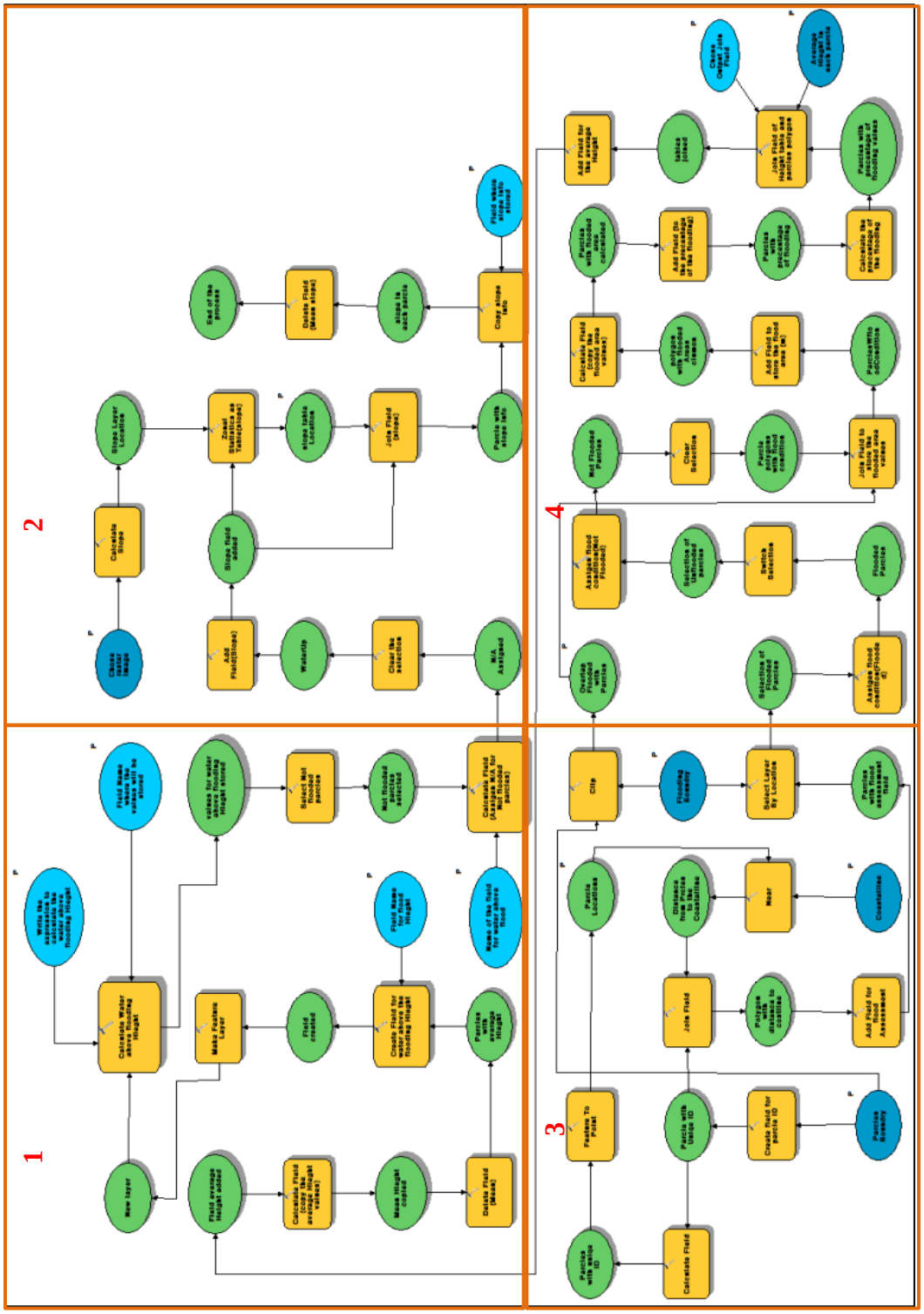

Figure 5.35 ModelBuilder flow chart for the property-based flood GIS tool. See Figures 5.36 to 5.39 for zoomed in parts (1 to 4) of this flow chart.

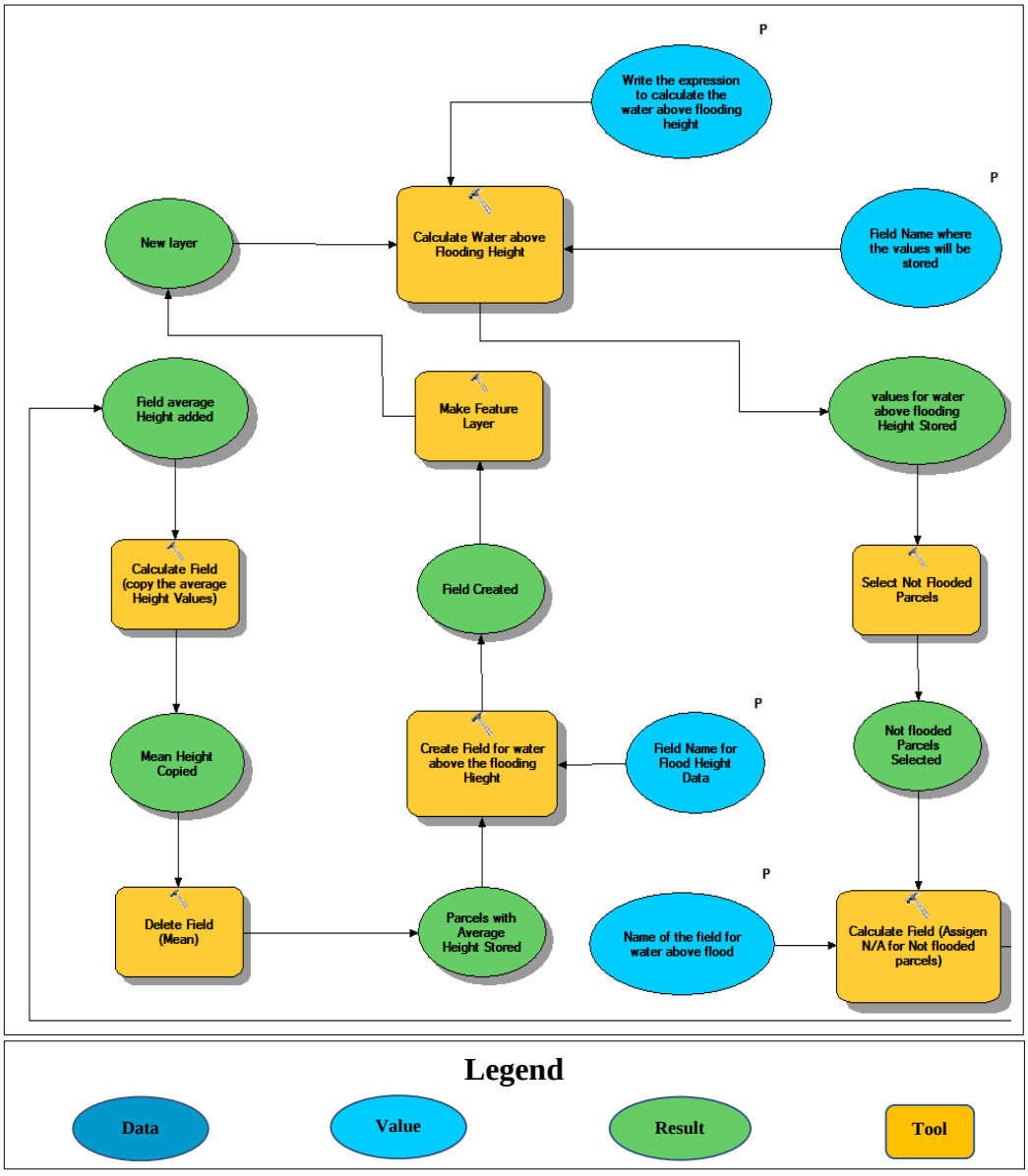

Figure 5.36 Part (1) of the ModelBuilder flow chart illustrated in Figure 5.35 for the property-based flood GIS tool.

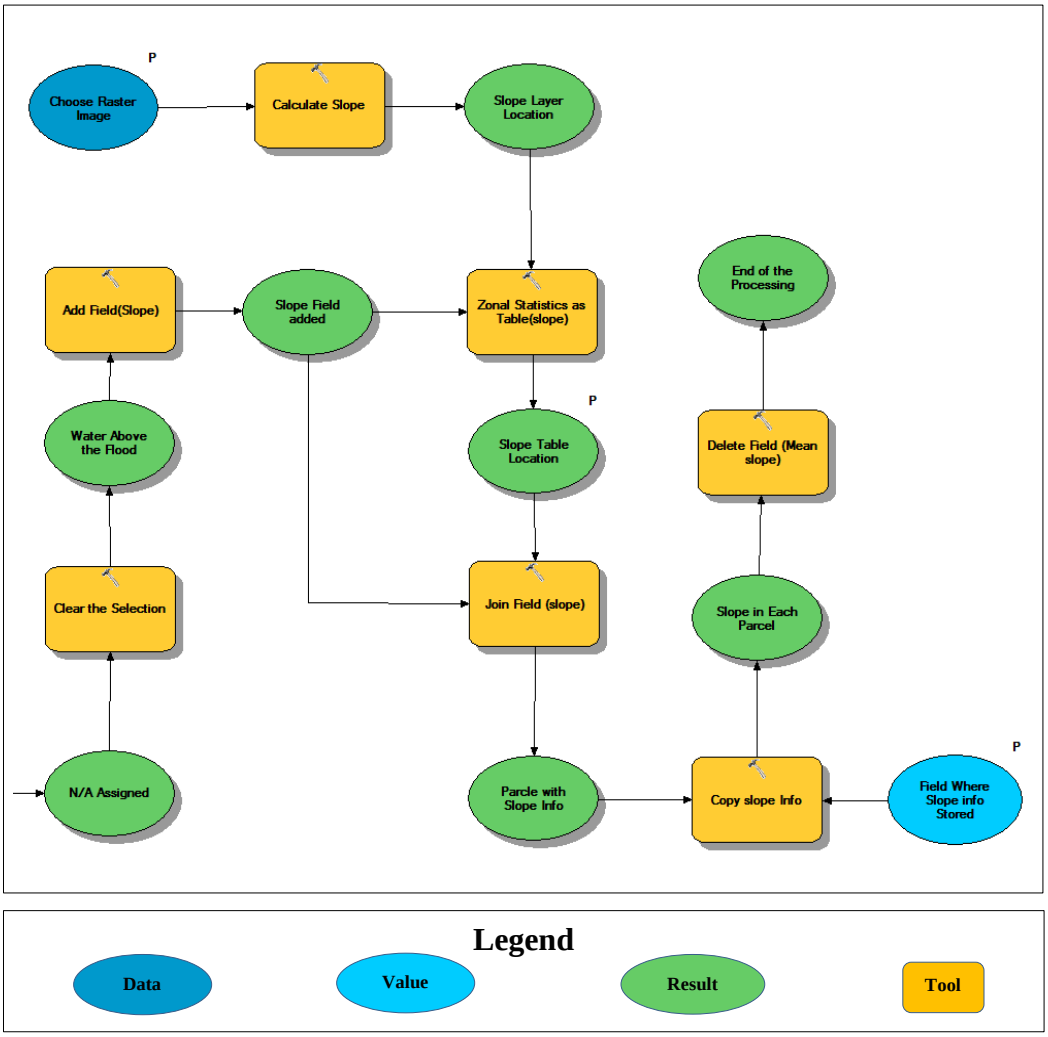

Figure 5.37 Part (2) of the ModelBuilder flow chart illustrated in Figure 5.35 for the property-based flood GIS tool.

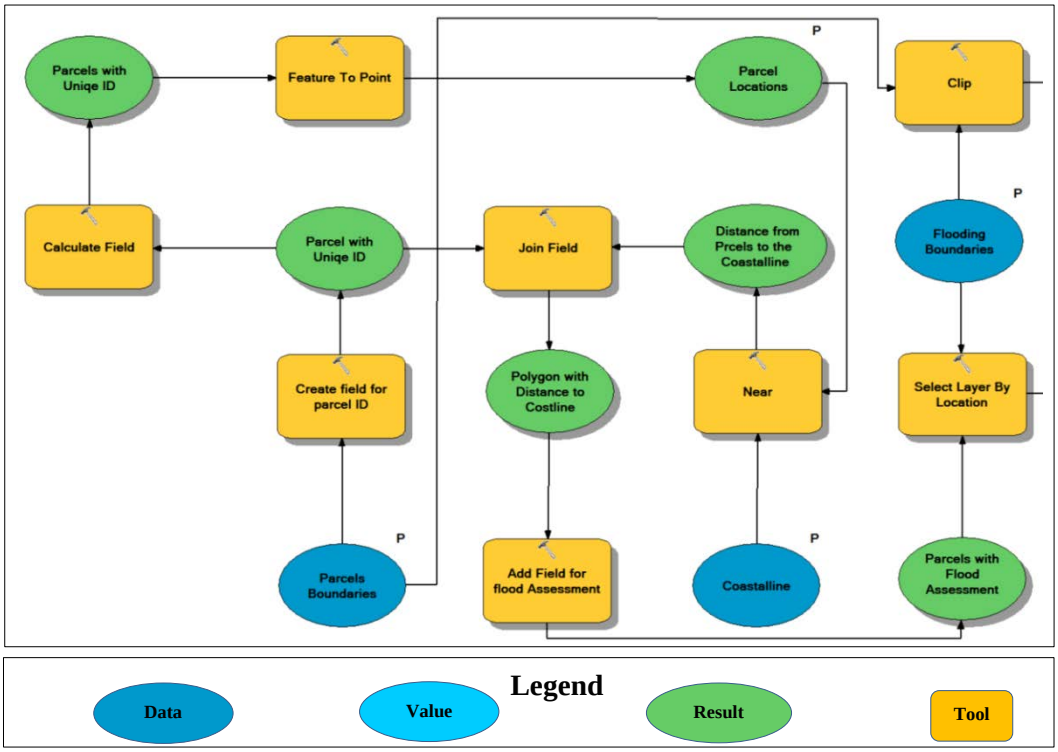

Figure 5.38 Part (3) of the ModelBuilder flow chart illustrated in Figure 5.35 for the property-based flood GIS tool.

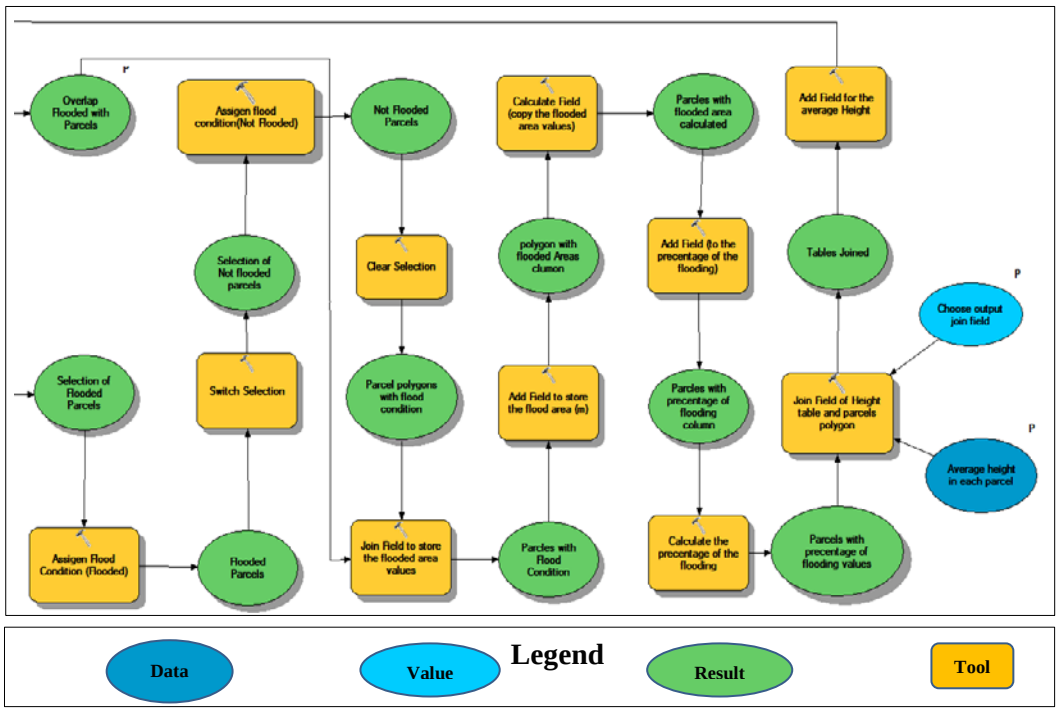

Figure 5.39 Part (4) of the ModelBuilder flow chart illustrated in Figure 5.35 for the property-based flood GIS tool.

Together with the property-based flood GIS tool, a GUI has been designed and implemented to facilitate user selection. The GUI consists of eleven parameters as shown in Figure (5.40). The user can use the GUI to browse for input files, as well as define the location for the output files. The user can also specify the sea level height based on the selected sea level rise scenario. Furthermore, the tool enables the user to upload vector-based data, such as property boundaries, flood information (i.e. flooded and not flooded areas), and the coastline. The raster DEM data can also be uploaded via the GUI (cf. Figures 5.40).

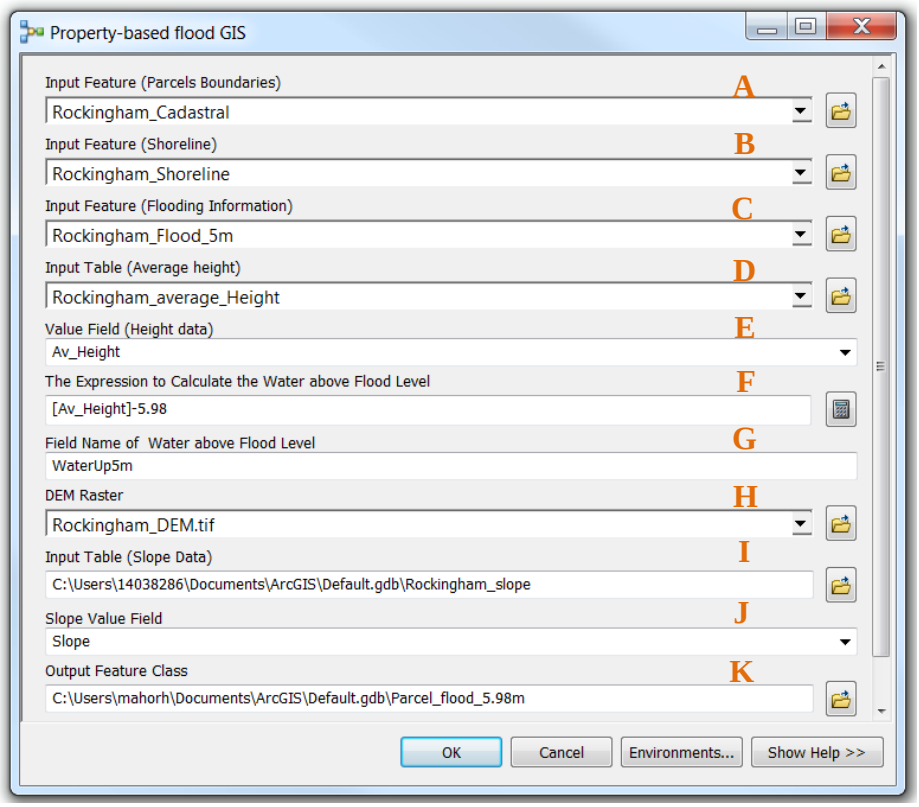

Figure 5.40 Property-based flood GIS tool GUI.

The eleven selections of the GUI (cf. Figure 5.40) are as follows:

A. Input feature: property boundary shapes file (vector data).
B. Input feature: shoreline boundary shape file (vector data).
C. Input feature: flooding information (vector data).
D. Output: Attribute table containing the average height of each property.

E. Field name: where in the attribute table the average height information is stored.
F. Field calculator: here the user can write the expression used to calculate the value (based on the values stored in other columns in the attribute table). In this instance, the field calculator will calculate the total amount of water above the adopted flooding scenario.
G. Field name: where in the attribute table the property's flooding percentage is stored.
H. Input: raster based DEM data to be used in the processing.
I. Input: Slope data attribute table. Here the user can specify the location of the slope data and upload it.
J. Field name: where in the attribute table the slope level information (between the property and the closest shoreline) is stored.
K. Output: File name and location of the output feature class.

5.7 Chapter summary

This chapter described the process used to combine flood information (obtained in chapter 4) with cadastral boundary data. The effects of coastal flooding are modelled on a property-by-property level by applying five sea level rise scenarios to both the Mandurah and Rockingham study locations. In particular, the method of obtaining the percentages of flooding (for each property) has been developed and applied. The identification of any partial flooding (and the corresponding percentage) could only be obtained using high-resolution topography data (e.g. 1 m LiDAR DEM data) combined with cadastral boundary data.

The results obtained by matching properties with flood information (i.e. percentages of flooding) are provided as numerical results and spatial distribution maps, and then discussed. The difference between high-resolution and low-resolution (in terms of the level of detail that can be obtained at a property-by-property level) is also discussed. With respect to the selected study locations, flood analysis confirms the study area of Rockingham is more at risk of flooding than Mandurah. This is due to its low topography and exposed geographic location. Furthermore, the analysis shows that Rockingham will be totally inundated when sea level rises to more than 8 m. The study concludes that flood percentage analysis is essential when identifying the flood level for each individual property located at the transition point between flooded and non-flooded areas.

The research also develops, describes, applies and discusses a methodology for the development of a flood vulnerability index due to coastal flooding. The method is based on five weighted parameters: (1) general flood assessment, (2) the percentage of flooding for each property, (3) straight-line distance between the property and the closest shoreline, (4) average water level above the property, and (5) the slope between the property and the closest shoreline. The weights for each parameter are selected in terms of their relative importance, though may be selected differently based on the choice of the user.

Flood vulnerability index results are documented for both the Mandurah and Rockingham study locations based on a sea level rise scenario of 5.98 m. The results confirm the previously identified outcome: properties in Rockingham are more vulnerable to coastal flooding than in Mandurah.

The chapter concludes with information regarding the development and implementation of a flood information tool and a property-based flood GIS tool. Both tools were used for this study and have been developed using ArcGIS ModelBuilder. Benefits of using the ModelBuilder in ArcGIS are provided, and include the advantages of automated processing. Finally, a description of the developed ModelBuilder tools, including detailed flow charts and GUIs, is provided.

The next chapter is the final chapter in this thesis. It will summarise the thesis stages, along with the main findings of the research, the main contributions of this research and recommendations for future research.

CHAPTER 6

CONCLUSIONS

6.1 Introduction

In the previous chapter, coastal flooding is modelled at a property-by-property level, which is based on two study locations and a flood vulnerability index developed in the previous stage. A brief description of the ModelBuilder tools developed, including the flowchart and the interface of each tool, is provided.

This chapter highlights the important findings of this research. Firstly, a brief summary of all stages (i.e. stage 1-4) is provided. This is followed by a description of the major outcomes and conclusions, including information on how the objectives are addressed by the achieved outcomes. Finally, the contribution of this study to the field of research is outlined, and recommendations for future research direction are provided.

6.2 Summary of the project stages

In this section, brief summaries for each of the four research stages are provided. As illustrated in Figure (1.1) (cf. chapter 1), the research was divided into the following four main stages:

(1) Modelling future sea level rise.
(2) High-resolution flood modelling.
(3) Combination of flood information with property data.
(4) Development and implementation of a property-based flood GIS.

Stage 1: Modelling future sea level rise

The main aim of the first stage (cf. chapter 3) was to provide reasonable estimates of expected sea level rise, by the year 2100, along the south-west coast of Western Australia. In order to gain insight into sea level variations present in the study areas, this part of the research looks at the causes of sea level rise.

It also models and quantifies past sea level variations and studies the correlation between various sea level records.

The sea level rise estimates form the basis for five possible flooding scenarios are then used to examine the effect of coastal flooding within the chosen study area (i.e. stage 2; cf. chapter 4).

This stage of the research commenced by reviewing the common causes of sea level rise, such as ocean processes, land hydrology, interaction between glaciers, ice caps, and ice sheets, global oceans, and atmospheric phenomena, as well as the methods and data used (cf. chapters 3.2 and 3.3). General information on the impact of sea level rise on coastal areas around the globe has also been presented in chapter 3.4.

In this study, tide gauge observations form one basis for the estimation of future sea level rise. Past monthly and yearly sea level measurements are analysed and used to provide estimates of future (linear) sea level rise. The sea level measurements used have been obtained from the four main tide gauge stations covering the study area, e.g. (1) Fremantle tide gauge station, (2) Geraldton tide gauge station, (3) Bunbury tide gauge station, and (4) Hillarys tide gauge station (cf. chapter 3.6).

Apart from tide gauge measurements, this stage also predicts future sea level rise scenarios based on various short- and long-term influences (cf. chapter 3.5.4). Short-term influences on sea level rise include seasonal variations, high astronomical tides, storm surge heights, and inter-annual and -decadal changes (e.g. Leeuwin Current and ENSO). Long-term effects on sea level include the contribution of melting ice sheets over Greenland and the West Antarctic (cf. chapter 3.6.5). Five sea level rise scenarios for the year 2100 are defined, ranging between a 2.06 m and 18.73 m increase (cf. chapter 3.6.5).

In order to study the relationship between the different tide gauge records within the study area, correlation analyses between the different stations were performed. Particular focus was given to the behaviour of correlation with respect to the distance between the stations (cf. chapter 3.7).

Similarly, correlation analyses were performed between the Fremantle tide gauge records and satellite altimetry measurements within a 600 km radius (cf. chapter 3.8). This identified the relationship between coastal sea level and the wider Indian Ocean.

Stage 2: High-resolution flood modelling

For the second stage of this research, two residential study locations along the southwest coast of WA were chosen in order to analyse the extent of coastal flooding for five flooding scenarios (derived in Stage 1). Mandurah and Rockingham were selected as the two study areas. This was due to their contrasting topography and morphology (cf. chapter 4.4). The extent of flooding for each study location and in each scenario was estimated using LiDAR DEM heights with a rather high spatial resolution of 1 m (cf. chapter 4.8). Using the ArcGIS software, the LiDAR DEM data was comprehensively validated before being applied to high-resolution flood modelling.

Apart from using the high-resolution LiDAR DEM data, comparison analyses were also undertaken using lower resolution DEM data (30 m and 90 m resolution). This was in order to study the impact relationship between the use of low- and high-resolution DEM data for flood modelling. The lower resolution DEM data was obtained from re-sampled LiDAR DEM data and independent DEM data from both ASTER (30 m resolution) and SRTM (90 m resolution) (cf. chapter 4.9).

Stage 3: Combining of flood information with property data

As a main aim of this study, the third stage looked at the combination of flood information (obtained from stage 2) with property data. This allowed flood modelling to take place at a property-by-property level rather than on a more regional level. To achieve this, the flood information obtained in stage 2 (for each of the flood scenarios considered) was overlaid with property information, mostly in the form of cadastral boundaries. The property boundaries were obtained as shape files and analysed in ArcGIS together with high-resolution flood information. In order to estimate the flood condition for each individual property, the flood boundaries (e.g. the boundary between the flooded and non-flooded areas) were overlapped with the property boundaries (cf. chapter 5.3).

The use of high-resolution DEM data allowed various types of information to be derived, concerning the condition of flooding for each individual property. This information included the actual area of flooding, the percentage of flooding, the distance from the property to the shoreline, and the average height and slope level of the property to the nearest shoreline (cf. chapters 5.3 and 5.5).

For each study location and sea level rise scenario, thematic maps were generated in ArcGIS showing the fully flooded, partially flooded, and non-flooded properties. Depending on the percentage of flooding found, the properties were classified into five categories: (1) from 0.00 to 0.01 %, (2) from 0.01 % to 30.00 %, (3) from 30.01% to 60.00 %, (4) from 60.01 % to 90.00 %, and (5) from 90 % to 100 %. A flood status was then assigned to each property as follows: not flooded (category 1); partially flooded (categories 2 to 4); fully flooded (category 5).

Based on the severity of flooding, as determined by the percentage of flooding and flood status above, the properties were further classified into five categories: (1) none, (2) minor, (3) moderate, (4) major, and (5) severe flooding (cf. chapter 5).

This stage of the research also included the development of a vulnerability index (cf. chapter 5) based on five parameters: (1) flooding assessment, (2) percentage of flooding of each property, (3) straight-line distance between the property and the closest shoreline, (4) water level above the property, and (5) slope of the straight line between the property and the shoreline. Each of these parameters has been given a weight value representing its relative importance (cf. chapters 5.5.2 and 5.5.3). The value of each parameter is ranked according to risk factors from 1 to 5. The vulnerability index for each property is then calculated using a weighted average (cf. chapter 5.5.2) where the value ranges between 20 and 100.

Based on the vulnerability index, each property was classified into five categories: (1) very low risk from 20.00 to 36.00, (2) low risk from 36.01 to 52.00, (3) moderate risk from 52.01 to 68.00, (4) high risk from 68.01 to 84.00, and (5) very high risk from 84.01 to 100 (cf. chapter 5.5.4).

Stage 4: The development and implementation of a property-based flood GIS.

The final stage of this research (i.e. stage 4), the development and implementation of a prototype for a property-based flood GIS, is covered at the end of chapter 5. This stage combines the outcomes and findings of all previous stages with a view to develop and implement a prototype for a property-based flood GIS.

Using the ArcGIS ModelBuilder, both a flood information tool and a property-based flood GIS tool were developed (cf. chapter 5.6). The flood information tool was used to provide flood related information based on high-resolution DEM data and a selected sea level rise scenario (cf. stage 2). The property-based flood GIS tool then combined the flood information with cadastral boundaries to provide property-related flood and vulnerability information (cf. stage 3). For each tool, user-friendly interfaces have been developed that allow automated processing.

6.3 Research outcomes

The main objective of this research was to assess the feasibility of utilising GIS technology, together with high-resolution LiDAR-derived DEMs and cadastral data, to develop and deploy a property-based flood-model. This main objective was accomplished by addressing three specific objectives as listed in chapter 1.2.1. The outcomes related to each objective are summarised in this chapter.

Outcomes Related to Objective 1:

The first objective in this research was the examination of effect of coastal flooding, due to near-future sea level rise, on residential areas located close to the shoreline. This objective was met in chapter 3, which reviewed the impact of sea level rise on the coastal zone, man-made structures, coastal topography, and geomorphology. Based on the analysis of past tide gauge measurements, short- and long-term sea level variables for five sea level rise scenarios (by 2100) were derived as follows: (1) 2.06 m, (2) 5.98 m, (3) 8.61 m, (4) 10.12 m, and (5) 18.73 m (cf. chapter 3.5.5). These sea level rise scenarios were selected to represent a range from moderate to extreme sea level rise. Each sea level rise scenario was used to model coastal flooding in the selected study locations of Mandurah and Rockingham.

A correlation analysis between the four tide gauge stations (Geraldton, Hillarys, Fremantle, and Bunbury) showed a very strong correlation, with correlation coefficients ranging between 0.935 and 0.983. Even over the longest distance of 592 km between Geraldton and Bunbury, the rather high correlation coefficient of 0.935 was obtained (cf. chapter 3.6). This demonstrates that coastal sea level is highly coherent along the south-west coast of Western Australia, and the information from one sea level record (e.g. Fremantle) is sufficient to model coastal sea level variations across the study location.

A second correlation analysis was performed between the Fremantle tide gauge record and satellite altimetry observations in a 600 km radius around the tide gauge. This revealed generally weaker correlation of sea level variation between the coastal location and the off-shore location as compared to higher correlations between tide gauge records (cf. chapter 3.7). The results also indicated that the satellite altimetry records were less reliable near to the coast (as shown by lower correlations near the shoreline (cf. chapter 3.7) due to land-contamination of the radar pulses.

Objective 2

The second objective of this research was to measure the impact of different Digital Elevation Model (DEM) resolutions on high-resolution flood modelling. This was addressed via a comparison study between low- and high-resolution DEMs (cf. chapter 4).

The above comparison analysis confirmed modelling of the spatial extent of flooding is highly sensitive to the spatial resolution of the topography data used. Results from both study locations, in Mandurah and Rockingham, showed that high-resolution DEMs are important for accurate flood modelling at a high spatial resolution (e.g. meter level) (cf. chapters 4.8 and 4.9). Furthermore, a comparison of the flood boundaries, obtained from high- and low- resolution DEM data, showed that many details of the topographic features are omitted when low-resolution elevation data is used in the flood modelling analysis.

Using low-resolution DEM data also greatly impacted the accuracy and reliability of the data to represent detailed spatial flood extents. It can therefore be said, there were noticeable differences between the use of high and low DEM resolutions (cf. chapter 4.9).

The overall conclusion of this analysis indicates that highly accurate and reliable spatial flood modelling can only be achieved when using high-resolution DEM data. It has equally been shown that low-resolution DEM data (e.g. 30 m and 90 m resolutions) is inadequate in high-resolution flood modelling and is not recommended for detailed studies of urban areas. This is of particular importance when flood modelling at a property-by-property level. Ultimately, the level of detail required for the flood analysis determines which resolution of elevation is to be used.

Objective 3

The third objective of this research was to develop and implement a feasibility study for a property-based flood GIS, and can be considered as the core objective of this research. This objective was addressed through the development and application of both a flood information tool and a property-based flood GIS tool using ArcGIS ModelBuilder (cf. chapter 5.6). Applying these tools, extensive studies were performed at the two study locations for the five sea level rise scenarios selected.

This objective was further addressed by examining the following three aspects:

1. The possibility of flood modelling on a property-by-property level.
2. The combination of high-resolution DEM data with 2D cadastre data (e.g. boundary lines augmented with height information).
3. The development of a vulnerability index based on information from a property-by-property scale (cf. chapter 5.3).

Outputs of the property-by-property based flood modelling again confirmed that the level of detail obtained is highly dependent on the topography data used. Results indicated that detailed flood modelling, on a property-by-property level, could only be achieved when using high-resolution elevation data (cf. chapter 5.4).

The analyses showed various flood conditions on a property-by-property level were only possible to be derived when using high-resolution DEM data. Information that could successfully be derived for individual properties included the degree of flooding (expressed as percentage or by a flood category, cf. chapter 5.4) and individualised flood vulnerability indices (cf. chapter 5.5).

Overall, the successful development and implementation of a property-based flood GIS has demonstrated the important benefits of using high-resolution DEM data (e.g. from LiDAR) for flood modelling in low-lying urban areas such as Rockingham. Consequently, incorporating high-resolution elevation data is strongly recommended for flood modelling on a property-by-property level, especially when a high level of spatial detail and accuracy is required, such as for urban planning, natural disaster management, and rescue planning.

6.4 Contributions

This study provides several important contributions to the field of research, which are summarised below:

1. Comprehensive information is provided on the development of a property-by-property based flood model using spatial technologies such as GIS and remote sensing data. To the best of the author's knowledge, this study can be considered the first attempt in Australia to examine coastal flooding on a property-by-property level. Consequently, outcomes can be used as a reference guide for future studies in the same field of research.
2. This research can be beneficial when expanding knowledge and increasing public awareness about the likely effects of sea level rise, including coastal flooding and vulnerability in the study areas (in particular) and in Australia (in general). This is important as a large proportion of the world's population, (including the population of Australia) is concentrated within coastal areas.
3. Important information has been provided that can help to mitigate and minimize the impacts of coastal flooding on natural habitat, residential areas close to the coast, and coastal properties and infrastructure.

Outcomes of this study will help with the process of decision making, especially in relation to urban planning. In particular, the model developed in this study will assist policy makers to analyse, quantify, and visualise the impact of coastal flooding on individual properties, rather than at a more regional level. This will help to identify the likely risks to residential areas along the coast of Western Australia and provide individualised vulnerability levels for each property.

4. This research greatly contributes to an understanding of the complexity of flood modelling in residential areas, and it also provides the principles required for the development of a flood model on a property-by-property scale. The research applies state of the art GIS and remote sensing technology to model coastal flooding, and therefore, it will give a new perspective to viewing, exploring, analysing, and mapping coastal flooding at high-resolution. Also, the innovative methodology adopted in this study will add, extend, and improve present methods used to study coastal flooding in residential areas.
5. The innovative ModelBuilder tools developed in this research (i.e. the flood information tool and the property-based flood GIS tool) can be used to obtain accurate and reliable information about coastal flooding. The user-friendly interfaces, which have been developed, may motivate students, researchers, professionals, and others, to use the tools. Most importantly, the developed tools can be used for automated processing, which requires little manual processing. Ultimately, the ArcGIS ModelBuilder tools can be easily shared and adapted to suit the user's individualised needs, making them very versatile.
6. Finally, this research provides valuable information regarding the impact of using low- and high-resolution DEM data in flood modelling studies. Outcomes of this study confirm that high-resolution DEM data (e.g. 1 m resolution LiDAR DEM data) is crucial when performing flood modelling at a property-by-property level.

6.5 Future Research Directions and Recommendations

This study successfully developed and implemented a property-based flood GIS to analyse, quantify, and visualise the impact of the coastal flooding due to sea level rise in residential coastal areas of Western Australia. Based on the experience gained throughout this the study, the author proposes a number of recommendations for future research in this field, and in related fields. These recommendations are outlined below:

1. Given that coastal flooding can have a huge impact on residential areas near to the shoreline, and the risk of coastal flooding will increase in the near-future, the identification, and quantification of human, financial and infrastructure loss is strongly recommended. In order to do so, demographic and socio-economic information about each property should be included in the flood modelling data. The developed property-based flood GIS tool used in this research can be easily adapted to include information such as the household size, total income per household, property type (i.e. freehold, company title, group title or state title, leasehold or retirement village) and current market value.
2. Considering that major coastlines are currently home to big business and industry concentrations, including oil refinery, desalination plants, seaports, factories, warehouses, and other businesses, it is recommended that future studies also focus on the possible impact of coastal flooding to the land-use patterns. Particular attention needs to be given to the impact of coastal flooding on commercial, industrial, and public facilities. Further in depth analyses will provide useful information regarding the impact of future sea level rise and coastal flooding on government and private sectors.
3. This research has demonstrated the benefits of using high-resolution elevation data in flood modelling. It has also shown considerable differences between the public, and freely available, DEM data and the higher resolution LiDAR data, when applied to coastal flood modelling. In this regard, further assessment regarding the accuracy, reliability, and consistency of the elevation data is strongly advised. For example, in-situ height checks could be carried out in selected areas.

4. The use of 3D datasets when flood modelling in more complex urban areas can be very useful in obtaining more detailed information on the flood condition. 3D modelling and visualising can positively contribute to providing more detailed information on the flood risk to properties and infrastructure, especially when high-resolution flood modelling is conducted (i.e. on a property-by-property level). Therefore, it is recommended that future studies make use of the integration of LiDAR data and 3D modelling to study coastal flooding, by generating 3D surface maps of the affected flood areas. In addition, information on infrastructure can be included, which will provide more detailed information about the risk to individual properties and can also enhance current methods in flood visualisation.
5. It is also recommended that future studies consider the inclusion of geomorphological information. While often difficult to assess (e.g. lack of data), the inclusion of information related to coastal erosion will improve the accuracy of flood modelling, and more so, the accuracy of risk modelling (e.g. properties built on sand are more likely to be affected than those properties built on rock).

REFERENCES

AAMHatch. 2010. Mandurah to Jandakot ALS survey, edited by Western Australia Department of Water. Perth. Western Australia Department of Water.

Aerts, J., W. Botzen, M. Bowman, P. Dircke, and P. Ward. 2013. *Climate Adaptation and Flood Risk in Coastal Cities*. Edited by W. Botzen, M. Bowman, P. Dircke and P. Ward. Hoboken: Hoboken : Taylor and Francis.

Aerts, J., D. C. Major, M. J. Bowman, P. Dircke, and P. Ward. 2009. *Coastal Cities, Flood Risk Management and A daptation to Climate Change* University of Amsterdam Press.

AL-Habsi, M. 2012. *Examining the correlation analysis between tide gauge records along the Western Australia coastline.*

Alesch, D. J., A. A. Atkisson, and W. J. Petak. 1984. *Natural Hazard Exposures, Losses and Mitigation Costs in the United States, 1970-2000*: National Emergency Training Center.

Alexander, D. E. 1993. *Natural Disasters*: Springer.

Allen, J. R. L., and K. Pye. 1992. *Saltmarshes: Morphodynamics, Conservation, and Engineering Significance*: Cambridge University Press.

Alley, R. B., P. U. Clark, P. Huybrechts, and I. Joughin. 2005. Ice-Sheet and Sea-Level Changes. *Science* 310 (5747): 456-460.

American Geological Institute. 1984. *Glossary of Geology*. Falls Church, Virginia: American Geological Institute.

Anderson, J., K. Milliken, D. Wallace, A. Rodriguez, and A. Simms. 2010. Coastal Impact Underestimated From Rapid Sea Level Rise. *Eos* 91 (23): 205.

Andrew, K. S. 2002. Introduction. In *Environmental Modelling with GIS and Remote Sensing*, 1-7. CRC Press.

Antonov, J. I., S. Levitus, and T. P. Boyer. 2002. Steric sea level variations during 1957–1994: Importance of salinity. *Journal of Geophysical Research: Oceans (1978–2012)* 107 (C12): SRF 14-1-SRF 14-8.

Ashleigh, B. T., D. C. Jeffrey, M. C. Ryan, and B. Michael. 2013. Flood Modeling Using a Synthesis of Multi-Platform LiDAR Data. *Water* 5 (4): 1533.

Atkinson, K. B. 2001. *Close Range Photogrammetry and Machine Vision*: Whittles.

Australian Bureau of Meteorology. 2014. *Climate statistics for Australian locations*. http://www.bom.gov.au/jsp/ncc/cdio/cvg/av?p_stn_num=009225&p_prim_element_index=8&p_display_type=statGraph&period_of_avg=ALL&normals_years=allYearOfData&staticPage= (accessed 17/11/2014).

--------. 2015. *Flood Warning Services*. http://www.bom.gov.au/water/floods/floodWarningServices.shtml (accessed 25/05/2015).

Australian Bureau of Statistics 2011a. *National Regional Profile: Mandurah (C) (Local Government Area)*. http://www.abs.gov.au/ausstats/abs@.nsf/Products/3218.0~2012-13~Main+Features~Western+Australia?OpenDocument#PARALINK2 (accessed 16/11/2014).

--------. 2011b. *National Regional Profile: Rockingham (C) (Local Government Area)*. http://www.abs.gov.au/AUSSTATS/abs@nrp.nsf/Previousproducts/LGA57490Population/People12007-2011?opendocument&tabname=Summary&prodno=LGA57490&issue=2007-2011&num=&view= (accessed 18/11/2014).

Awange, J. L., and J. B. K. Kiema. 2013. *Environmental Geoinformatics: Monitoring and Management / by Joseph L. Awange, John B. Kyalo Kiema*. Edited by J. B. Kyalo Kiema and SpringerLink. Berlin, Heidelberg: Imprint: Springer.

Balica, S., N. Wright, and F. Meulen. 2012. A flood vulnerability index for coastal cities and its use in assessing climate change impacts. *Journal of the International Society for the Prevention and Mitigation of Natural Hazards* 64 (1): 73-105.

Balica, S., and N. G. Wright. 2009. A network of knowledge on applying an indicator-based methodology for minimizing flood vulnerability. *Hydrological Processes* 23 (20): 2983-2986.

--------. 2010. Reducing the complexity of the flood vulnerability index. *Environmental Hazards* 9 (4): 321-339.

Barnes, M. 1993. *Oceanography and Marine Biology, An Annual Review*: Taylor & Francis.

Bartlett, D., and J. Smith. 2005. *GIS for Costal Zone Management*. London: CRC press.

Bartosova, A., D. Clark, V. Novotny, and K. S. Taylor. 2000. *Using GIS to Evaluate the Effects of Flood Risk on Residential Property Values*. Institute for Urban Environmental Risk management, Marquette University. http://epublications.marquette.edu/econ_fac/131/ (accessed 15/02/2015).

Bas van de, S., L. Joost, and H. Claartje. 2012. Sensitivity of Coastal Flood Risk Assessments to Digital Elevation Models. *Sensitivity of Coastal Flood Risk Assessments to Digital Elevation Models* 4 (3): 568-579.

Betts, H. 2002. Flood Damage Analysis Using GIS at Gold Coast City Council. *Australian Journal of Emergency Management* 17 (1): 33-37.

Bin, O., and J. B. Kruse. 2006. Real Estate Market Response to Coastal Flood Hazards. *Natural Hazards Review* 7 (4): 137-144.

Bin, O., J. B. Kruse, and C. E. Landry. 2008. Flood Hazards, Insurance Rates, and Amenities: Evidence From the Coastal Housing Market. *Journal of Risk & Insurance* 75 (1): 63-82. bth.

Bird. 1993. *Submerging coasts : the effects of a rising sea level on coastal environments / Eric C.F. Bird*.

BOM. 2012. *National Tidal Unit*. http://www.bom.gov.au/oceanography/projects/ntc/ntc.shtml (accessed 11/5/2013).

Boon, J. D., J. M. Brubaker, D. R. Forrest, and N. District. 2010. Chesapeake Bay land subsidence and sea level change. *App. Mar. Sci. and Ocean Eng., Report* (425): 1-73.

Bowen, R. E., M. H. Depledge, C. P. Carlarne, and L. E. Fleming. 2014. *Oceans and Human Health: Implications for Society and Well-Being*: Wiley.

Brachmanis, J. 2002. *A regional review of coastal hazards along the south west coast of Western Australia*. http://www.ga.gov.au/corporate_data/69650/69650_full.pdf (accessed 16/11/2012).

Bray, N. 2011. *Valuer-general's property market movement report: snapshot of the 2011 valuation.* Brisbane

Brivio, P. A. 2002. Integration of remote sensing data and GIS for accurate mapping of flooded areas. *International journal of remote sensing* 23 (3): 429-441.

Bruun, P. 1962. Sea-level rise as a cause of shore erosion *Journal of the waterways and harbors divison, American society of civil engineers* 88: 117-130.

Bryant, E. 2008. *Tsunami : the underrated hazard : Springer-Praxis books in geophysical sciences*.

Bryant, E. 2014. *Tsunami: The Underrated Hazard*: Springer.

Burbidge, D., P. R. Cummins, R. Mleczko, and H. K. Thio. 2008. A Probabilistic Tsunami Hazard Assessment for Western Australia. *Pure and applied geophysics* 165 (11-12): 2059-2088.

Bureau of Meteorology. 2012. *Past Tsunami Events*. http://www.bom.gov.au/tsunami/history/index.shtml (accessed 21/11/2013).

Burton, I., and R. W. Kates. 1964. The Perception of Natural Hazards in Resource Management. *Natural Resources Journal* 3: 412-441.

Cadman, S., L. Pain, and V. Vuckovic. 1994. *Perth Basin, Western Australia*. Vol. 10: Department of Primary Industries and Energy, Bureau of Resources Sciences.

Cantzler, H. 2012. *An overview of range images*. http://homepages.inf.ed.ac.uk/rbf/CVonline/LOCAL_COPIES/CANTZLER2/intensity.html (accessed 15/10/2012).

Cazenave, A., and R. S. Nerem. 2004. Present-day sea level change: Observations and causes. *Reviews of Geophysics* 42 (3): RG3001.

Centre for Research on the Epidemiology of Disasters (CRED). 2010. *Disaster Data: A Balanced Perspective*. Brussels. http://cred.be/sites/default/files/CredCrunch19.pdf (accessed 24/10/2014).

Chakma, S. 2014. Analysis of Urban Development Suitability. In *Dhaka Megacity*, ed. A. Dewan and R. Corner, pp 147-161. Springer Netherlands.

Charteris, A. B., W. J. Syme, and W. J. Walden. 2001. *Urban Flood Modelling and Mapping 2D or Not 2D 6th Conference on Hydraulics in Civil Engineering: The State of Hydraulics; Proceedings*.

Chen, J., A. A. Hill, and L. D. Urbano. 2009. A GIS-based model for urban flood inundation. *Journal of Hydrology* 373 (1-2): 184-192.

Cheney, R., B. Douglas, D. Sandwell, J. Marsh, T. Martin, and J. McCarthy. 1984. Applications of satellite altimetry to oceanography and geophysics. *An International Journal for the Study of the Earth Beneath the Sea* 7 (1): 17-32.

Church, J. A., P. L. Woodworth, T. Aarup, and W. S. Wilson. 2007. *Understanding Sea-level Rise and Variability*: Wiley-Blackwell.

Church, J. A., P. L. Woodworth, T. Aarup, and W. S. Wilson. 2010. *Understanding Sea-level Rise and Variability*: Wiley.

Chuvieco, E. 2008. *Earth Observation of Global Change: The Role of Satellite Remote Sensing in Monitoring the Global Environment*: Springer.

Claussen, E., Vicki Arroyo Cochran, Debra P Davis, and Pew Center on Global Climate Change. 2001. *Climate change: science, strategies, & solutions*. Boston Brill.

Colby, J. D., K. A. Mulcahy, and Y. Wang. 2000. Modeling flooding extent from Hurricane Floyd in the coastal plains of North Carolina. *Environmental Hazards* 2 (4): 157-168.

Committee on the National Requirements for Precision Geodetic Infrastructure, Committee on Seismology and Geodynamics, and National Research Council. 2010. *Precise Geodetic Infrastructure:: National Requirements for a Shared Resource*. Washington, DC, USA: National Academies Press.

Connor, R. F., and K. Hiroki. 2005. Development of a method for assessing flood vulnerability. *Water science and technology: a journal of the International Association on Water Pollution Research* 51 (5): 61.

Coveney, S., A. Stewart Fotheringham, M. Charlton, and T. McCarthy. 2010. Dual-scale validation of a medium-resolution coastal DEM with terrestrial LiDAR DSM and GPS. *Computers & Geosciences* 36 (4): 489-499.

Cracknell, A. P., and L. Hayes. 2007. *Interduction to Remote sensing* Second Edition ed: CRC press.

Crostella, A., and J. Backhouse. 2000. *Geology and Petroleum Exploration of the Central and Southern Perth Basin, Western Australia.* Western Australia, Perth.

Crostella, A. A., J. Backhouse, and Geological Survey of Western Australia. 2000. *Geology and petroleum exploration of the central and southern Perth Basin, Western Australia*: Geological Survey of Western Australia.

Cummins, P. R., L. S. L. Kong, and K. Satake. 2009. *Tsunami Science Four Years after the 2004 Indian Ocean Tsunami Part 2*. Germany: Birkhäuser Basel.

Daniel, V. E., R. J. G. M. Florax, and P. Rietveld. 2009. Flooding risk and housing values: An economic assessment of environmental hazard. *Ecological Economics* 69 (2): 355-365.

Darsan, J., H. Asmath, and A. Jehu. 2013. Flood-risk mapping for storm surge and tsunami at Cocos Bay (Manzanilla), Trinidad. *Journal of Coastal Conservation* 17 (3): 679-689.

Dasgupta, S., B. Laplante, S. Murray, and D. Wheeler. 2011. Exposure of developing countries to sea-level rise and storm surges. *Climatic Change* 106 (4): 567-579.

Dawson, B., and M. Spannagle. 2009. *The complete guide to climate change / Brian Dawson and Matt Spannagle*. London & New York: Routledge.

De Moel, H., J. v. Alphen, and J. C. J. H. Aerts. 2009. Flood maps in Europe - Methods, availability and use. *Natural hazards and earth system sciences* 9 (2): 289-301.

Dionne, J.-C., P. J. H. Richard, and J.-S. Vincent. 1987. *Bird, C.E.F. (1985) : Coastline Changes. A Global Review*. Vol. 41. New York, Toronto: John Wiley.

Dominey-Howes, D., and M. Papathoma. 2007. Validating a tsunami vulnerability assessment model (the PTVA Model) using field data from the 2004 indian ocean tsunami. *Natural Hazards* 40 (1): 113-136.

Donnelly, W. A. 1989. HEDONIC PRICE ANALYSIS OF THE EFFECT OF A FLOODPLAIN ON PROPERTY VALUES1. *JAWRA Journal of the American Water Resources Association* 25 (3): 581-586.

Douglas. 2001. *Sea Level Rise*. 75 vols. San Diego: Academic Press.

Douglas, B. 1997. GLOBAL SEA RISE: A REDETERMINATION. *An International Review Journal Covering the Entire Field of Geosciences and Related Areas* 18 (2): 279-292.

Douglas, B. C. 1991. Global sea level rise. *Journal of geophysical research* 96 (C4): 6981-6992.

Douglas, B. C. 1995. Global sea level change: Determination and interpretation. *Reviews of Geophysics* Volume 33 (S1): 1425-1432.

Douglas, B. C., M. S. Kearney, and S. P. Leatherman. 2001. *Sea Level Rise History and Consequences*. Vol. 75. New York.

Dowling, T. P. F., H. Alexanderson, and P. Möller. 2013. The new high-resolution LiDAR digital height model (‘Ny Nationell Höjdmodell’) and its application to Swedish Quaternary geomorphology. *GFF* 135 (2): 145-151.

Du, X., H. Guo, X. Fan, J. Zhu, Z. Yan, and Q. Zhan. 2015. Vertical accuracy assessment of freely available digital elevation models over low-lying coastal plains. *International Journal of Digital Earth*: 1-20.

Duggal, S. K. 2004. *Surveying*: Tata McGraw-Hill.

Durand, F., D. Shankar, F. Birol, S. S. Shenoi, and Chandra. 2008. Estimating boundary currents from satellite altimetry: A case study for the east coast of India. *Journal of Oceanography* 64 (6): 831-845. ProQuest Central; ProQuest SciTech Collection.

Ebert, A., N. Kerle, and A. Stein. 2009. Urban social vulnerability assessment with physical proxies and spatial metrics derived from air- and spaceborne imagery and GIS data. *Journal of the International Society for the Prevention and Mitigation of Natural Hazards* 48 (2): 275-294.

Eliot, M. 2012. Sea level variability influencing coastal flooding in the Swan River region, Western Australia. *Continental Shelf Research* 33 (0): 14-28.

Emery, K. O. 1980. Relative Sea Levels from Tide-Gauge Records. *Proceedings of the National Academy of Sciences of the United States of America* 77 (12): 6968-6972.

Encyclopedia of Coastal Science. 2006. Springer.

ESRI. 2012. *Semivariogram and covariance functions*. http://help.arcgis.com/en/arcgisdesktop/10.0/help/index.html#//003100000036000000 (accessed 22/11/2013).

Farmer, G. T., and J. Cook. 2013. *Climate Change Science: A Modern Synthesis: Volume 1 - The Physical Climate*: Springer.

Feagin, R. A. 2005. Coastal erosion, global sea-level rise, and the loss of sand dune plant habitats. *Frontiers in ecology and the environment* 3 (7): 359-364.

Feagin, R. A., D. J. Sherman, and W. E. Grant. 2005. Coastal erosion, global sea-level rise, and the loss of sand dune plant habitats. *Frontiers in Ecology and the Environment* 3 (7): 359-364.

Fenoglio Marc, L., and E. Tel. 2010. Coastal and global sea level change. *Journal of Geodynamics* 49 (3-4): 151-160.

Fiorani, L. 2008. *LinkLaser applications in environmental monitoring*. Edited by F. Colao. New York: Nova Science Publishers.

French, J. R. 2003. Airborne LiDAR in support of geomorphological and hydraulic modelling. *Earth Surface Processes and Landforms* 28 (3): 321-335.

Fu, L.-L., and A. Cazenave. 2000. *Satellite altimetry and earth sciences a handbook of techniques and applications / Lee-Lueng Fu, Anny Cazenave*. Edited by A. Cazenave. 69 vols. San Diego, Calif; London: Academic Press.

Fukuzono, T., S. Ikeda, and G. Zhai. 2003. Effect of flooding on megalopolitan land prices : a case study of the 2000 Tokai flood in Japan. *Journal of natural disaster science* 25: 23-36. /z-wcorg/.

Gallopín, G. C. 2006. Linkages between vulnerability, resilience, and adaptive capacity. *Global Environmental Change* 16 (3): 293-303.

Gambolati, G., P. Teatini, and M. Gonella. 2002. GIS simulations of the inundation risk in the coastal lowlands of the Northern Adriatic Sea. *Mathematical and Computer Modelling* 35 (9-10): 963-972.

García, D., G. Ramillien, A. Lombard, and A. Cazenave. 2007. Steric sea-level variations inferred from combined topex/poseidon altimetry and GRACE gravimetry. *Pure and Applied Geophysics* 164 (4): 721-731.

Gesch, D. B. 2009. Analysis of lidar elevation data for improved identification and delineation of lands vulnerable to sea-level rise. *Journal of Coastal Research* (SPECIAL ISSUE 53): 49-58.

Google. 2010a. Mandurah. In *Google Earth*. Satellite image. California, USA. Google pty ltd.

--------. 2010b. Rockingham. In *Google Earth*. Satellite image. California, USA. Google pty ltd.

Gornitz, V., S. Couch, and E. K. Hartig. 2001. Impacts of sea level rise in the New York City metropolitan area. *Global and Planetary Change* 32 (1): 61-88.

Gornitz, V. M., R. C. Daniels, T. W. White, and K. R. Birdwell. 1994. The development of a coastal risk assessment database; vulnerability to sea-level rise in the U.S. Southeast. *Journal of Coastal Research* Special issue 12: 327-338. ProQuest SciTech Collection.

Green, R. 2010. *Coastal towns in transition : local perceptions of landscape change / Raymond James Green*. New York: Springer.

Greve, R., and H. Blatter. 2009. *Dynamics of Ice Sheets and Glaciers*: Springer.

Guth, P. 2010. *A special joint symposium of ISPRS Technical Commission IV & AutoCarto in conjunction with ASPRS/CaGIS, Geomorphometric comparison of ASTER GDEM and SRTM*.

Haile, A. T., and T. H. M. Rientjes. 2005. Effects of LIDAR DEM resolution in flood modelling : a model sensitivity study for the city of Tegucigalpa, Honduras. *In: ISPRS 2005 : Vol. XXXVI Comm. 3 W19 proceedings of the ISPRS workshop laser scanning 2005, 12-15 September, Enschede ITC, The Netherlands / ed. by M.G. Vosselman and C. Brenner. Enschede : ITC, 2005. 6 p.*

Hallegatte, S., and J. Corfee-morlot. 2011. Understanding climate change impacts, vulnerability and adaptation at city scale: an introduction. *Climatic Change* 104 (1): 1-12. ProQuest Central; ProQuest SciTech Collection.

Heliani, L. S., N. Widjajanti, I. Endrayanto, Danardono, and H. Panuntun. 2013. Preprocessing of Coastal Satellite Altimetry, Tide Gauges, and GNSS Data: Towards the Possibility of Detected Vertical Deformation of South Java Island. *Procedia Environmental Sciences* 17 (0): 308-316.

Hennecke, W. G. 2004a. GIS-based coastal behavoir modeling and simulation of potential land and property loss: Implications of sea-level rise at Collaroy/Narrabeen Beach, Sydney (Australia). *Coastal management* 32 (4): 449-470.

Hennecke, W. G. 2004b. GIS Modelling of Sea-Level Rise Induced Shoreline Changes Inside Coastal Re-Rntrants – Two Examples from Southeastern Australia. *Natural Hazards* 31 (1): 253-276.

Hirt, C., M. S. Filmer, and W. E. Featherstone. 2010. Comparison and validation of the recent freely available ASTER-GDEM ver1, SRTM ver4.1 and GEODATA DEM-9S ver3 digital elevation models over Australia. *Australian Journal of Earth Sciences* 57 (3): 337-347.

Hoozemans, F. M. J., H. A. Pennekamp, and D. H. T. W. D. Rijkswaters. 1993. *Sea Level Rise: A Global Vulnerability Assessment, Vulnerability Assessments for Population, Coastal Wetlands and Rice Production on a Global Scale; Second Revised Edition*: Ministry of Transport, Public Works and Water.

Horritt, M. S., and P. D. Bates. 2001. Effects of spatial resolution on a raster based model of flood flow. *Journal of Hydrology* 253 (1–4): 239-249.

--------. 2002. Evaluation of 1D and 2D numerical models for predicting river flood inundation. *Journal of Hydrology* 268 (1–4): 87-99.

Huang, S., C. Young, M. Feng, K. Heidemann, M. Cushing, D. M. Mushet, and S. Liu. 2011. Demonstration of a conceptual model for using LiDAR to improve the estimation of floodwater mitigation potential of Prairie Pothole Region wetlands. *Journal of Hydrology* 405 (3–4): 417-426.

Hutchinson, M. F., and T. I. Dowling. 1991. A continental hydrological assessment of a new grid-based digital elevation model of Australia. *Hydrological Processes* 5 (1): 45-58.

Ikeda, M. 1995. *Oceanographic Applications of Remote Sensing*: Taylor & Francis.

Imaduddina, A. H., and W. W. H. Subagyo. 2014. Sea Level Rise Flood Zones: Mitigating Floods in Surabaya Coastal Area. *Procedia - Social and Behavioral Sciences* 135 (0): 123-129.

IPCC. 2001. *Cliamte change 2001: The scientific Basis. Contirbution of working group I to the Third Assessment Report of the Intergovernmental Panel on Climate Change*: Cambridge Unviersity Press, UK.

--------. 2013. *Climate Change 2013: The Physical Science Basis*: Cambridge Unviersity Press, UK.

IPCC, F. A. R. 2007. *the Fourth Assessment Report of the Intergovernmental Panel on Climate Change*. Geneva. http://www.ipcc.ch/publications_and_data/ar4/syr/en/contents.html (accessed 15/03/2010).

Ishii, M., M. Kimoto, K. Sakamoto, and S.-I. Iwasaki. 2006. Steric sea level changes estimated from historical ocean subsurface temperature and salinity analyses. *Journal of Oceanography* 62 (2): 155-170.

Janin, H., and S. A. Mandia. 2012. *Rising Sea Levels: An Introduction to Cause and Impact*: McFarland & Company, Publishers.

Japan Space Systems. 2012. ASTER Global Digital Elevation Model (ASTER GDEM). Japan.

Jarvis, A., H.I. Reuter, A. Nelson, and E. Guevara. 2008. Hole-filled SRTM for the globe Version 4. USA. Consortium for Spatial Information,.

Jenson, S. K. 1991. Applications of hydrologic information automatically extracted from digital elevation models. *Hydrological Processes* 5 (1): 31-44.

Jevrejeva, S., J. C. Moore, A. Grinsted, and P. L. Woodworth. 2008. Recent global sea level acceleration started over 200 years ago? *Geophysical Research Letters* 35 (8): L08715.

Jones, A. 2005. *Potential coastal erosion of the swan coastal plain due to sea level riser*. Edited by I. J. T, ., M. M and C. N, *Natural hazards risk in Perth, Western Australia*: Geoscience Australia.

Jongman, B., P. J. Ward, and J. C. J. H. Aerts. 2012. Global exposure to river and coastal flooding: Long term trends and changes. *Global Environmental Change* 22 (4): 823-835.

Joseph, A. 2011. Chapter 5 - Impact of a Tsunami on Coastal and Island Habitats. In *Tsunamis*, 99-101. Boston: Academic Press.

Jude, S., A. P. Jones, J. E. Andrews, and I. J. Bateman. 2006. Visualisation for Participatory Coastal Zone Management: A Case Study of the Norfolk Coast, England. *Journal of Coastal Research* 22 (6): 1527-1538.

Kellens, W., T. Neutens, P. Deckers, J. Reyns, and P. De Maeyer. 2012. Coastal flood risks and seasonal tourism: analysing the effects of tourism dynamics on casualty calculations. *NATURAL HAZARDS*.

Kellens, W., W. Vanneuville, K. Ooms, and P. D. Maeyer. 2009a. *24th International Cartographic Conference (ICC 2009), Cartographic methods for visualizing sea level rise*. Santiago, Chili International Cartographic Conference, 24th, Proceedings.

--------. 2009b. *24th International Cartographic Conference (ICC 2009), Communicating flood risk to the public by cartography*. Santiago, Chili International Cartographic Conference, 24th, Proceedings.

Kellens, W., R. Zaalberg, T. Neutens, W. Vanneuville, and P. De Maeyer. 2011. An analysis of the public perception of flood risk on the Belgian coast. *RISK ANALYSIS*.

Keller, E. A., and R. H. Blodgett. 2008. *Natural Hazards Earth processes as Hazard, and catastrophes*. Edited by S. Edition. London: Pearson education.

Knight, J. M., P. E. R. Dale, J. Spencer, and L. Griffin. 2009. Exploring LiDAR data for mapping the micro-topography and tidal hydro-dynamics of mangrove systems: An example from southeast Queensland, Australia. *Estuarine, Coastal and Shelf Science* 85 (4): 593-600.

Kraus, K. 2007. *Photogrammetry : geometry from images and laser scans*. 2nd [English] ed.. ed. Berlin: Walter De Gruyter.

Kreimer, A., M. Arnold, and A. Carlin. 2007. *Building safer cities: the future of disaster risk*: World Bank.

Kuhn, M., W. E. Featherstone, O. Makarynskyy, and W. Keller. 2010. Deglaciation-Induced Spatially Variable Sea Level Change:A Simple-Model Case Study for the Greenland and Antarctic Ice Sheets. *International Journal of Ocean and Climate Systems* 1 (2).

Kuhn, M., D. Tuladhar, and R. Corner. 2011. Visualising the spatial extent of predicted coastal zone inundation due to sea level rise in south-west Western Australia. *Ocean & Coastal Management* 54 (11): 796-806.

Lai, J.-S., W.-Y. Chang, Y.-C. Chan, S.-C. Kang, and Y.-C. Tan. 2011. Development of a 3D virtual environment for improving public participation: Case study - The Yuansantze Flood Diversion Works Project Advanced Engineering Informatics. *Advanced engineering informatics* 25 (2): 208.

Leatherman, S. P., K. Zhang, and B. C. Douglas. 2000. Sea level rise shown to drive coastal erosion. *Eos, Transactions American Geophysical Union* 81 (6): 55-57.

Linder, W. 2009. *Digital Photogrammetry : A Practical Course / edited by Wilfried Linder*. Edited by SpringerLink. Berlin, Heidelberg: Berlin, Heidelberg: Springer Berlin Heidelberg.

Lionello, P. 2012. *The Climate of the Mediterranean Region: From the past to the future*. Burlington: Burlington: Elsevier Science.

Lombard, A., D. Garcia, G. Ramillien, A. Cazenave, R. Biancale, J. M. Lemome, F. Flechtner, R. Schmidt, and M. Ishii. 2007. Estimation of steric sea level variations from combined GRACE and Jason-1 data. *Earth Planet. Sci. Lett.* 254 (1-2): 194-202.

Mandlburger, G., C. Hauer, B. Höfle, H. Habersack, and N. Pfeifer. 2009. Optimisation of LiDAR derived terrain models for river flow modelling. *Hydrology and Earth System Sciences* 13 (8): 1453-1466.

Marfai, M. A., and L. King. 2008. Potential vulnerability implications of coastal inundation due to sea level rise for the coastal zone of Semarang city, Indonesia. *Environmental Geology* 54 (6): 1235-1245.

Martínez, M. L. 2008. *Coastal Dunes: Ecology and Conservation/ edited by M. Luisa Martínez, Norbert P. Psuty*. Edited by N. P. Psuty and SpringerLink. Berlin, Heidelberg: Berlin, Heidelberg: Springer Berlin Heidelberg.

McGlone, J. C., E. M. Mikhail, J. S. Bethel, A. S. f. Photogrammetry, R. Sensing, and R. Mullen. 2004. *Manual of Photogrammetry*: American Society for Photogrammetry and Remote Sensing.

McGuire, C. J. 2013. *Adapting to Sea Level Rise in the Coastal Zone: Law and Policy Considerations*: Taylor & Francis.

Menoni, S., and C. Margottini. 2011. *Inside Risk: A Strategy for Sustainable Risk Mitigation*. Milan: Springer.

Mertz, O., K. Halsnæs, J. E. Olesen, and K. Rasmussen. 2009. Adaptation to climate change in developing countries. *Environmental management* 43 (5): 743-752.

Merwade, V. 2008. Uncertainty in Flood Inundation Mapping: Current Issues and Future Directions. *Journal of hydrologic engineering* 13 (7): 608.

Meuser, H. 2010. *Contaminated Urban Soils*: Springer.

Mikhail, E. M., J. C. McGlone, and J. S. Bethel. 2001. *Introduction to modern photogrammetry / Edward M. Mikhail and James S. Bethel and J. Chris McGlone*. Edited by J. C. McGlone and J. S. Bethel. New York: New York: Wiley.

Miller, K. A., and D. N. Yates. 2006. *Climate Change and Water Resources: A Primer for Municipal Water Providers*: American Water Works Association.

Milliman, J., and B. U. Haq. 1996. *Sea-Level Rise and Coastal Subsidence: Causes, Consequences, and Strategies*: Springer.

Mitra, A. 2013. *Sensitivity of Mangrove Ecosystem to Changing Climate*: Springer (India) Private Limited.

Mitrovica, J. X., N. Gomez, and P. U. Clark. 2009. The sea-level fingerprint of West Antarctic collapse. *Science* 323 (5915): 753.

Mörner, N. A. 1976. Eustacy and geoid changes. *Journal of Geology* (84): 123-151.

Nakada, M., and H. Inoue. 2005. Rates and causes of recent global sea-level rise inferred from long tide gauge data records. *Quaternary Science Reviews* 24 (10–11): 1217-1222.

National Oceanic and Atmospheric Administration (NOAA). 2014. *Storm Surge Overview*. http://www.nhc.noaa.gov/surge/ (accessed 11/2/2014).

Nationalkomitee der Bundesrepublik Deutschland für das Internationale Hydrologische Programm der UNESCO und das Operationelle Hydrologische Programm der WMO. 1993. *Sea level changes and their consequences for hydrology and water management: international workshop : 19-23 April 1993, Noordwijkerhout, Netherlands*: Bundesanstalt für Gewässerkunde.

Nerem, R. S. 1995. Global Mean Sea Level Variations from TOPEX/POSEIDON Altimeter Data. *Science* 268 (5211): 708-10.

Nethengwe, N. N. 2007. Integrating Participatory GIS and Political Ecology to Study Flood Vulnerability in the Limpopo Province of South Africa, West Virginia University.

Nicholls, R. J. 1999. Regional issues raised by sea-level rise and their policy implications. *Climate research* 11 (1): 5-18.

--------. 2002. Analysis of global impacts of sea-level rise: A case study of flooding. *Physics and chemistry of the earth* 27 (32-34): 1455-1466.

Nicholls, R. J. 2004. Coastal flooding and wetland loss in the 21st century: changes under the SRES climate and socio-economic scenarios. *Global Environmental Change* 14 (1): 69-86.

Orcutt, J. 2012. *Earth System Monitoring: Selected Entries from the Encyclopedia of Sustainability Science and Technology*: Springer.

Organization of American States. 1990. *Disaster, planning and development: managing natural hazards to reduce loss*: The Department.

Papathoma, M. 2003. Tsunami vulnerability assessment and its implications for coastal hazard analysis and disaster management planning, Gulf of Corinth, Greece. *Natural hazards and earth system sciences* 3 (6): 733-747.

Pethick, J. 2001. Coastal management and sea-level rise. *CATENA* 42 (2-4): 307-322.

Pilkey, O. H. 2009. *The rising sea / Orrin H. Pilkey and Rob Young*. Edited by R. Young and I. ebrary. Washington, DC: Washington, DC: Island Press/Shearwater Books.

Poore, R. Z., S. Richard, J. Williams, and C. Tracey. 2011. *Sea Level and Climate: U.S. Geological Survey Fact Sheet*. http://pubs.usgs.gov/fs/fs2-00/ (accessed 05/07/2013).

Poulter, B. 2008. Raster modelling of coastal flooding from sea-level rise. *International journal of geographical information science* 22 (2): 167-182.

Poulter, B., and P. N. Halpin. 2008. Raster modelling of coastal flooding from sea-level rise. *International Journal of Geographical Information Science* 22 (2): 167-182.

Prakasa Rao, B. S., K. S. R. Murty, and E. Amminedu. 2005. *Geoscience and Remote Sensing Symposium, 2005. IGARSS '05. Proceedings. 2005 IEEE International, 25-29 July 2005: Estimation of flood vulnerability index for delta areas through RS and GIS*.

Pugh, D. 2004. *Changing Sea Levels Effects of Tides, Weather and Climate*. New YORK: Cambridge University Press.

Pugh, D., and P. Woodworth. 2014. *Sea-Level Science: Understanding Tides, Surges, Tsunamis and Mean Sea-Level Changes*: Cambridge University Press.

Purvis, M. J., P. D. Bates, and C. M. Hayes. 2008. A probabilistic methodology to estimate future coastal flood risk due to sea level rise. *Coastal Engineering* 55 (12): 1062-1073.

Rambaldi, A. N., C. S. Fletcher, K. Collins, and R. R. J. McAllister. 2013. Housing Shadow Prices in an Inundation-prone Suburb. *Urban Studies* 50 (9): 1889-1905.

Rignot, E., and R. H. Thomas. 2002. Mass Balance of Polar Ice Sheets. *Science* 297 (5586): 1502-1506.

Rowley, R., J. C. Kostelnick, D. Braaten, X. Li, and J. Meisel. 2007. Risk of Rising Sea Level to Population and Land Area. *Eos* 88 (9): 105.

Sanborn. 2010. *VIRGINIA BASE MAPPING PROGRAM*. http://www.vita.virginia.gov (accessed 18/03/2010).

Sanders, B. F. 2007. Evaluation of on-line DEMs for flood inundation modeling. *Advances in water resources* 30 (8): 1831-1843.

Sarwar, G. M., and M. H. Khan. 2007. Sea Level Rise: A Threat to the Coast of Bangladesh. *Internationales Asienforum* 38 (3-4): 375-397.

Scales, P. C. V. D. C. T., D. E. L. Studies, N. R. Council, and E. R. Commission on Geosciences. 1998. *Decade-to-Century-Scale Climate Variability and Change:: A Science Strategy*: National Academies Press.

Schanze, J., E. Zeman, J. Marsalek, and J. Maršálek. 2006. *Flood Risk Management: Hazards, Vulnerability and Mitigation Measures*: Springer.

Schuckman, K. 2009. *Lesson 5: Fundamentals of Light Detection and Ranging.*

Schumann, G., P. Matgen, M. E. J. Cutler, A. Black, L. Hoffmann, and L. Pfister. 2008. Comparison of remotely sensed water stages from LiDAR, topographic contours and SRTM. *ISPRS Journal of Photogrammetry and Remote Sensing* 63 (3): 283-296.

Schwarz, R. 2012. *Development of an Illumination Simulation Software for the Moon's Surface*: Books on Demand.

Seeber, G. 2003. *Satellite geodesy / Günter Seeber*. Edited by I. Ebrary. 2nd completely rev. and extended ed. Berlin: Walter de Gruyter.

Shatnawi, F., and J. L. Goodall. 2010. Comparison of Flood Top Width Predictions Using Surveyed and LiDAR-Derived Channel Geometries. *Journal of Hydrologic Engineering* 15 (2): 97-106.

Shetye, S. 2005. Tsunamis. *Resonance* 10 (2): 8-19.

Shum, C. K., J. C. Ries, and B. D. Tapley. 1995. The accuracy and applications of satellite altimetry. *Geophysical Journal International* 121 (2): 321-336.

Singh, J. 2009. *Tsunamis: Threats And Management*: I.K. International Publishing House Pvt. Limited.

Small, C., and R. J. Nicholls. 2003. A Global Analysis of Human Settlement in Coastal Zones. *Journal of Coastal Research* 19 (3): 584-599.

Smith, H. 2010. *Perth, Western Australia & the Outback*: Hunter Publishing, Incorporated.

Smith, K. 1992. *Environmental hazards : assessing risk and reducing disaster / Keith Smith*. London & New York: Routledge.

Smith, K., and D. N. Petley. 2004. *Environmental Hazards Assessing risk and reducing disaster*. Fifth edition ed. London: Taylor & Francis.

Smith, K., and R. Ward. 1998. *Floods: physical processes and human impacts* John Wiley & Sons, Ltd.

Snoussi, M., T. Ouchani, A. Khouakhi, and I. Niang-Diop. 2009. Impacts of sea-level rise on the Moroccan coastal zone: Quantifying coastal erosion and flooding in the Tangier Bay. *Geomorphology* 107 (1-2): 32-40.

Sole, A., L. Giosa, L. Nole, V. Medina, and A. Bateman. 2008. Flood risk modelling with LiDAR technology. *Flood Recovery, Innovation and Response* 118: 27-36.

Solomon, S., D. Qin, M. Manning, M. Marquis, K. Averyt, M. M. B. Tignor, J. Henry LeRoy Miller, and Z. Chen. 2007. *Climate Change 2007 : the physical science basis : contribution of Working Group I to the Fourth Assessment Report of the Intergovernmental Panel on Climate Change* United Kingdom and New York, NY, USA: Cambridge University Press.

Stanchev, H., A. Palazov, and M. Stancheva. 2009. 3D GIS Model for Flood Risk Assessment of Varna Bay Due to Extreme Sea Level Rise. *Journal of Coastal Research* (SI 56): 1597-1601.

Sterling, C. 2013. *Creating Custom Tools in ArcGIS – Model Builder*. http://giscollective.org/tutorials/gis-techniques/creating-custom-tools-in-arcgis-model-builder/ (accessed 05/12/2013).

Syme, W. J. 2008. Flooding in Urban Areas - 2D Modelling Approaches for Buildings and Fences 9th National Conference on Hydraulics in Water Engineering: Hydraulics 2008.

Tamisiea, M. E., C. W. Hughes, S. D. P. Williams, and R. M. Bingley. 2014. Sea level: measuring the bounding surfaces of the ocean. *Philosophical transactions. Series A, Mathematical, physical, and engineering sciences* 372 (2025).

The Permanent Service for Mean Sea Level (PSMSL). 1999. *Intergovernmental Oceanographic Commission Reports of Meetings of Experts and Equivalent Bodies*. Toulouse, France. http://www.psmsl.org/train_and_info/training/gloss/gb/gb7/ge6rep.text (accessed 20/01/2014).

--------. 2013. *The permanent service for mean sea level: Further information* http://www.psmsl.org/data/obtaining/psmsl.hel (accessed 6/11/2013).

Thorpe, S. A. 2007. *An Introduction to Ocean Turbulence*: Cambridge University Press.

Thumerer, T., A. P. Jones, and D. Brown. 2000. A GIS based coastal management system for climate change associated flood risk assessment on the east coast of England. *International Journal of Geographical Information Science* 14 (3): 265-281.

Tobin, G. A., and B. E. Montz. 1997. *Natural Hazards: Explanation and Integration*: Guilford Press.

Tregoning, P., and C. Rizos. 2008. *Dynamic Planet: Monitoring and Understanding a Dynamic Planet with Geodetic and Oceanographic Tools*: Springer.

Tsubaki, R., and I. Fujita. 2010. Unstructured grid generation using LiDAR data for urban flood inundation modelling. *Hydrological Processes* 24 (11): 1404-1420.

Turner, A. B., J. D. Colby, R. M. Csontos, and M. Batten. 2013. Flood Modeling Using a Synthesis of Multi-Platform LiDAR Data. *Water* 5 (4): 1533-1560.

UNDRO. 1982. Shelter After Disaster Guidelines for Assistance. In *United Nations Disaster Relief Coordinator*. New York. United Nations.

United Nations Centre for Regional Development. 1996. *United Nations Centre for Regional Development Newsletter*: United Nations Centre for Regional Development.

Urbanski, J. A. 2001. The impact of sea-level rise along the Polish Baltic coast. *Journal of Coastal Conservation* 7 (2): 155-162.

Valiron, F. 2001. *Descriptive Physical Oceanography*: Taylor & Francis.

Varekamp, J. C., and E. Thomas. 1998. Climate change and the rise and fall of sea level over the millennium. *Eos, Transactions American Geophysical Union* 79 (6): 69-75.

Vaze, J., J. Teng, and G. Spencer. 2010. Impact of DEM accuracy and resolution on topographic indices. *Environmental Modelling and Software* 25 (10): 1086-1098.

Viehhauser, M., K. Larsson, and J. Stålnacke. 2006. Impacts of future climate change and sea level rise in the Stockholm region: Part II - GIS analysis of future flooding risks at regional and municipal scales.

Vignudelli, S., A. G. Kostianoy, P. Cipollini, and J. Benveniste. 2011. *Coastal Altimetry*: Springer.

Vigo, M. I., J. M. Sánchez-Reales, M. Trottini, and B. F. Chao. 2011. Mediterranean Sea level variations: Analysis of the satellite altimetric data, 1992–2008. *Journal of Geodynamics* 52 (3–4): 271-278.

Ward, P. J., M. A. Marfai., F. Yulianto., D. R. Hizbaron., and J. C. J. H. Aerts. 2010. Coastal inundation and damage exposure estimation: a case study for Jakarta. *Natural Hazards* 56 (3): 1-18.

Warrick, R. A., E. M. Barrow, and T. M. L. Wigley. 1993. *Climate and Sea Level Change: Observations, Projections, and Implications*: New York.

Webster, T. L., D. L. Forbes, S. Dickie, and R. Shreenan. 2004. Using topographic lidar to map flood risk from storm-surge events for Charlottetown, Prince Edward Island, Canada. *Canadian Journal of Remote Sensing* 30 (1): 64-76.

Western Australian Planning Commission. 2003. *COASTAL PLANNING AND MANAGEMENT MANUAL*. Perth. http://www.planning.wa.gov.au/dop_pub_pdf/Foreword.pdf (accessed 04/05/2013).

White, G. F. 1974. Natural hazards research. In *Directions in Geography*, ed. R. J. Chorley, 193– 216. London: Methuen.

Wigley, T. M. L. 1987. Thermal expansion of sea water associated with global warming. *Nature* 330 (6144): 127-131.

Wolock, D. M., and G. J. McCabe. 2000. Differences in topographic characteristics computed from 100- and 1000-m resolution digital elevation model data. *Hydrological Processes* 14 (6): 987-1002.

Wyatt, P. 2003. *GIS in land and property management*. London: Spon press.

Xiaojun, Y. 1997. *Geoscience and Remote Sensing, 1997. IGARSS '97. Remote Sensing - A Scientific Vision for Sustainable Development., 1997 IEEE International, 3-8 Aug 1997: GIS modeling in coastal flooding analysis: a case study in the Yellow River Delta, China*.

Xingong, L. 2009. GIS analysis of global impacts from sea level rise. *Photogrammetric engineering and remote sensing* 75 (7): 807-818.

Yang, X. 1997. *GIS modeling in coastal flooding analysis: A case study in the Yellow River Delta, China*. http://www.scopus.com/inward/record.url?eid=2-s2.0-0030687111&partnerID=40&md5=a0064fd2d60f976971ebd58c462f4a8c (accessed 25/03/ 2011).

Yohe, G., J. Neumann, P. Marshall, and H. Ameden. 1996. The economic cost of greenhouse-induced sea-level rise for developed property in the United States. *Climatic Change* 32 (4): 387-410.

Yohe, G., and R. S. Tol. 2002. Indicators for social and economic coping capacity—moving toward a working definition of adaptive capacity. *Global Environmental Change* 12 (1): 25-40.

Yu, D., and S. N. Lane. 2006. Urban fluvial flood modelling using a two-dimensional diffusion-wave treatment, part 1: mesh resolution effects. *Hydrological Processes* 20 (7): 1541-1565.

Zhang, K., B. C. Douglas, and S. P. Leatherman. 2004. Global warming and coastal erosion. *Climatic change* 64 (1-2): 41.

APPENDIX A

COMPARISON BETWEEN LOW- AND HIGH-RESOLUTION FLOOD MODELLING

This appendix provides a complete list of all results obtained from the comparison between low- and high-resolution flood modelling using different DEM resolutions for the study sites in Mandurah and Rockingham. A complete description of the methodology and parameter used is given in chapter 4.9 for the sea level rise scenario of 5.98 m.

A.1 Sea level rise of 2.06 meters in Mandurah

Table A.1 Flooded and not flooded areas (and percentage to total area) using different DEMs resolutions for the study area in Mandurah for a sea level rise of 2.06 m. Unit in m2. Note the quite different results for the ASTER 30 m DEM data.

	Flooded	Not Flooded	Total
1 m LiDAR	364,192 15.1%	2,049,665 84.9%	2,413,857 100.0%
Resampled 30 m	1,712,548 45.8%	2,025,102 54.2%	37,376,410 100.0%
Resampled 90 m	452,267 18.3%	2,025,480 81.7%	2,477,747 100.0%
ASTER 30 m	18,387 0.6%	2,966,531 99.4%	2,984,917 100.0%
SRTM 90 m	524,741 20.4%	20,495,010 79.6%	2,574,251 100.0%

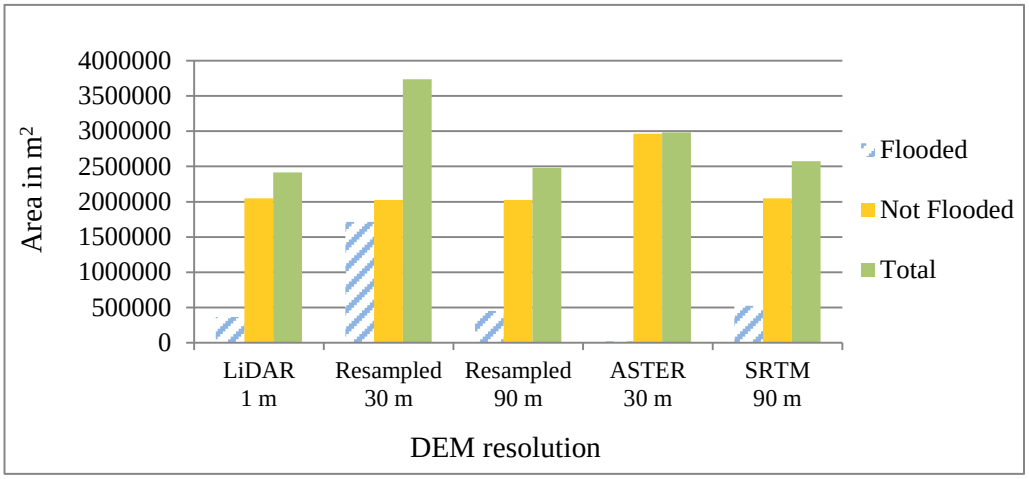

Figure A.1 Flooded and non-flooded areas in Mandurah for a sea level rise of 2.06 m for different DEMs and resolutions.

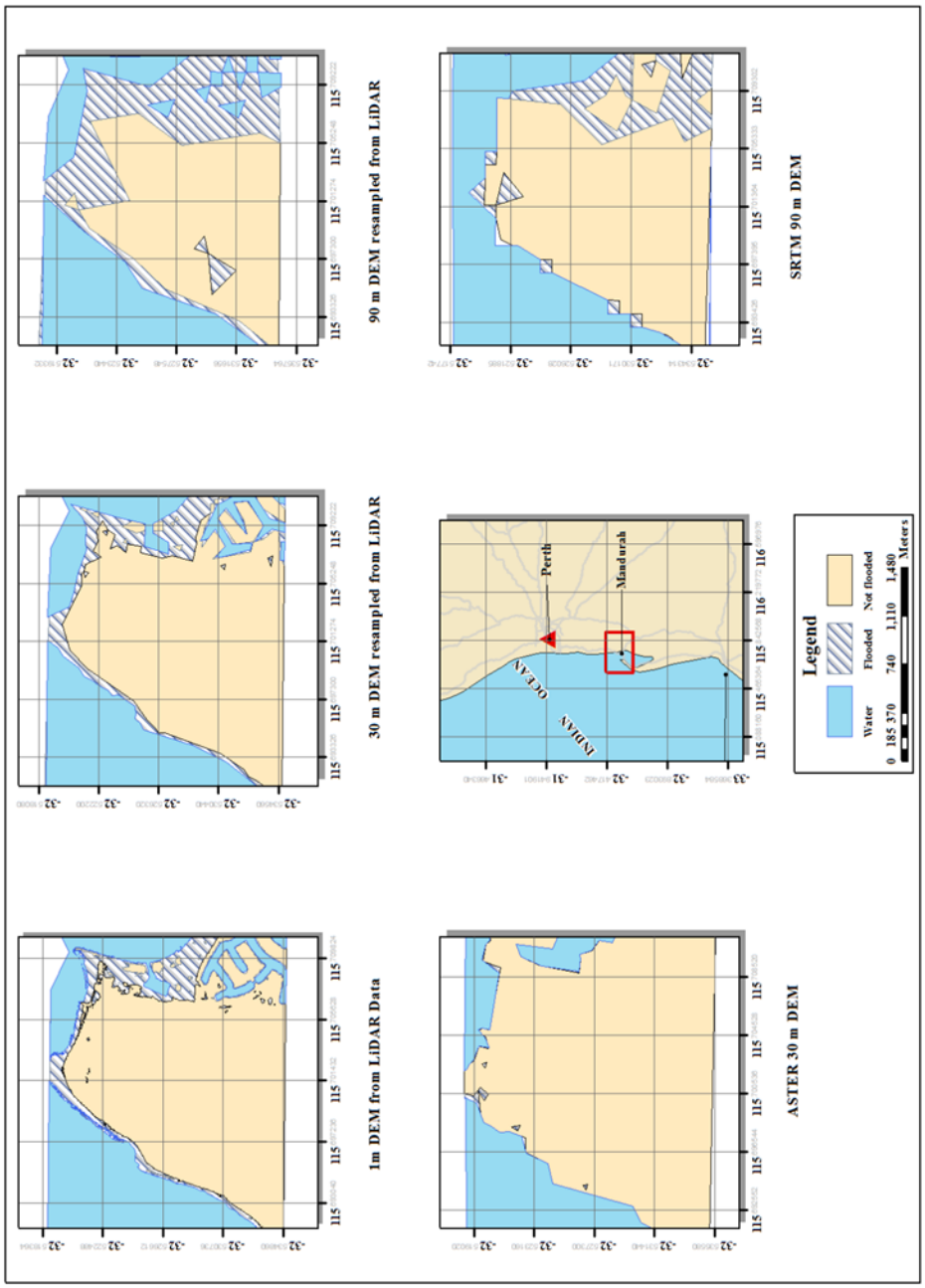

Figure A.2 Flooded areas when sea level rises to 2.06 m in Mandurah by using various DEM resolutions.

A.2 Sea level rise of 2.06 meters in Rockingham

Table A.2 Flooded and not flooded areas (and percentage to total area) using different DEMs resolutions for the study area in Rockingham for a sea level rise of 2.06 m. Unit in m^2. Note the quite different results for the ASTER 30 m DEM data.

	Flooded	Not Flooded	Total
1 m LiDAR	128,144 8.0%	1,482,461 92.0%	1,610,605 100.0%
Resampled 30 m	133,013 8.3%	1,466,006 91.7%	1,599,019 100.0%
Resampled 90 m	137,473 8.4%	1,500,488 91.6%	1,637,961 100.0%
ASTER 30 m	1,174,477 39.7%	1,785,261 60.3%	2,959,737 100.0%
SRTM 90 m	172,135 10.6%	1,453,657 89.4%	1,625,793 100.0%

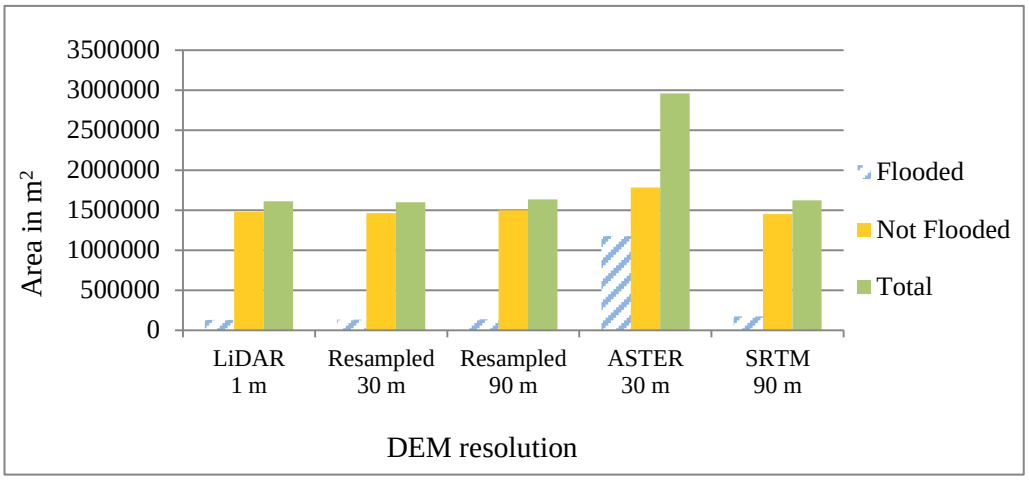

Figure A.3 Flooded and non-flooded areas in Rockingham for a sea level rise of 2.06 m for different DEMs and resolutions.

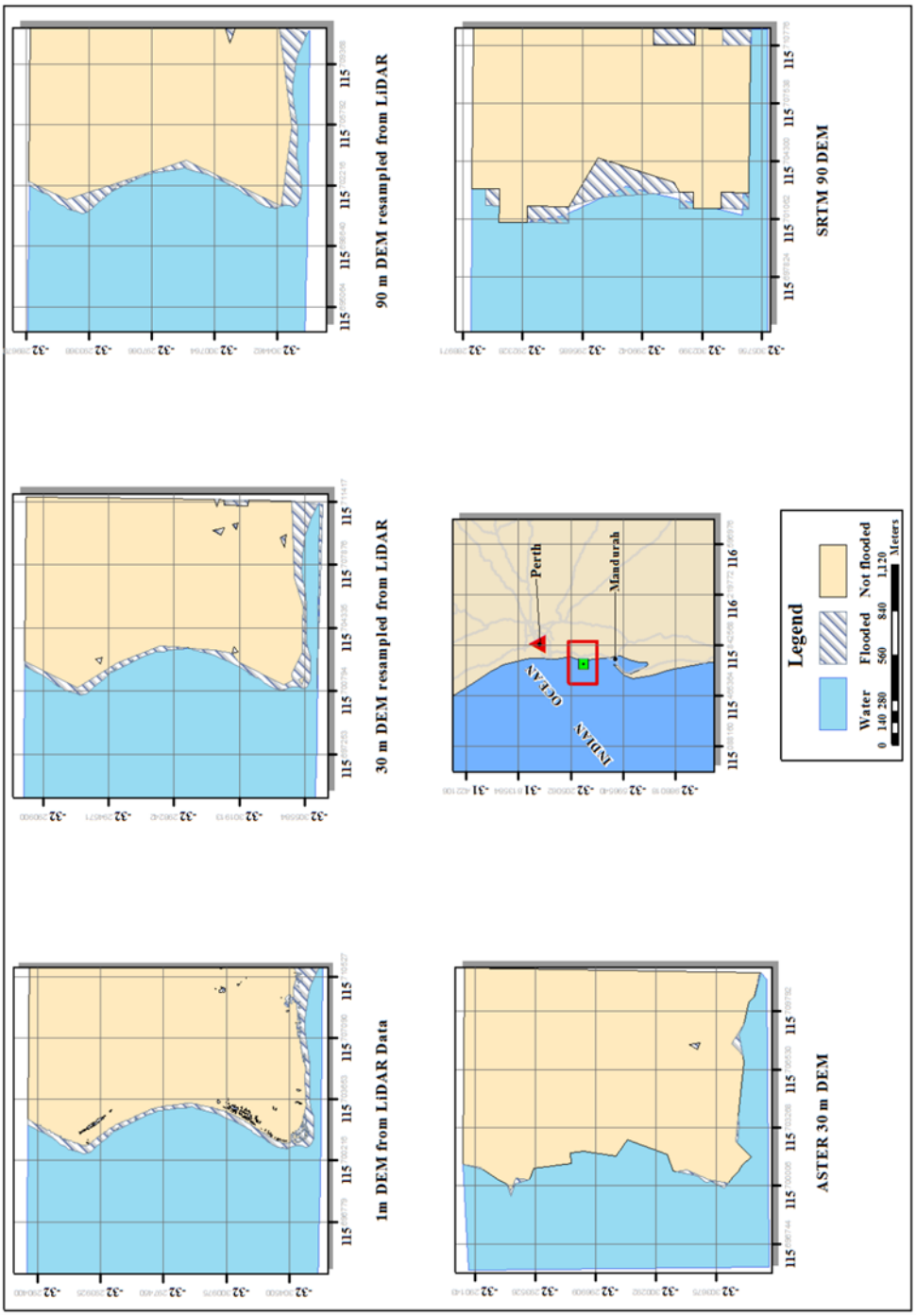

Figure A.4 Flooded areas when sea level rises to 2.06 m in Rockingham by using various DEM resolutions.

A.3 Sea level rise of 8.61 meters in Mandurah

Table A.3 Flooded and not flooded areas (and percentage to total area) using different DEMs resolutions for the study area in Mandurah for a sea level rise of 8.61 m. Unit in m^2. Note the quite different results for the ASTER 30 m DEM data.

	Flooded	Not Flooded	Total
1 m LiDAR	1,175,859 49%	1,238,010 51%	2,413,869 100%
Resampled 30 m	1,163,350 49%	1,227,213 51%	2,390,563 100%
Resampled 90 m	1,112,429 48%	1,221,954 52%	2,334,383 100%
ASTER 30 m	1,341,187 45%	1,638,678 55%	2,979,865 100%
SRTM 90 m	1,224,738 47%	1,363,401 53%	2,588,139 100%

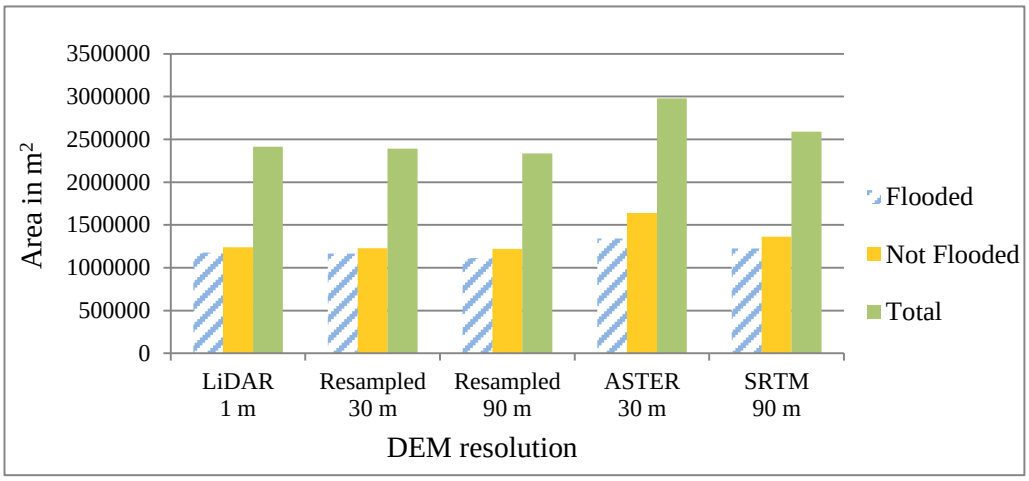

Figure A.5 Flooded and non-flooded areas in Mandurah for a sea level rise of 8.61 m for different DEMs and resolutions.

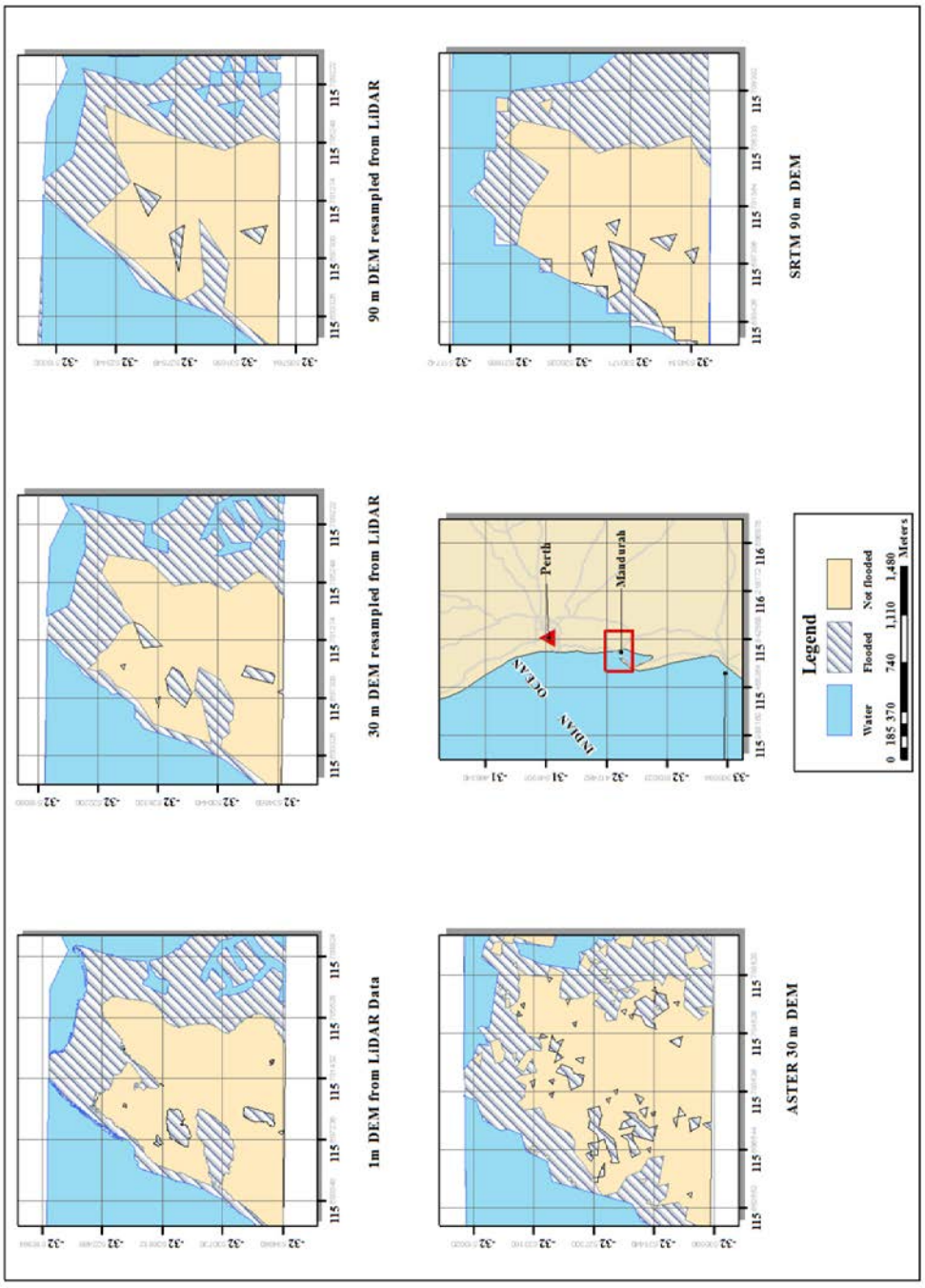

Figure A.6 Flooded areas when sea level rises to 8.61 m in Mandurah by using various DEM resolutions.

A.4 Sea level rise of 8.61 meters in Rockingham

Table A.4 Flooded and not flooded areas (and percentage to total area) using different DEMs resolutions for the study area in Rockingham for a sea level rise of 8.61 m. Unit in m^2. Note the quite different results for the ASTER 30 m DEM data.

	Flooded	Not Flooded	Total
1 m LiDAR	1,588,704 99%	21,764 1%	1,610,468 100%
Resampled 30 m	1,578,419 99%	16,410 1%	1,594,829 100%
Resampled 90 m	1,567,588 99%	16,637 1%	1,584,226 100%
ASTER 30 m	480,905 27%	1,315,927 73%	1,796,832 100%
SRTM 90 m	1,488,551 93%	115,715 7%	1,604,266 100%

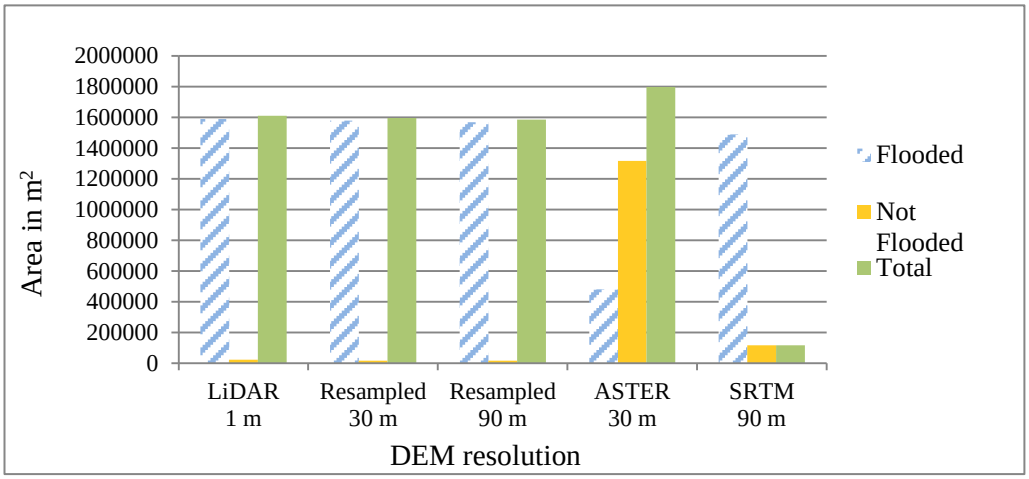

Figure A.7 Flooded and non-flooded areas in Rockingham for a sea level rise of 8.61 m for different DEMs and resolutions.

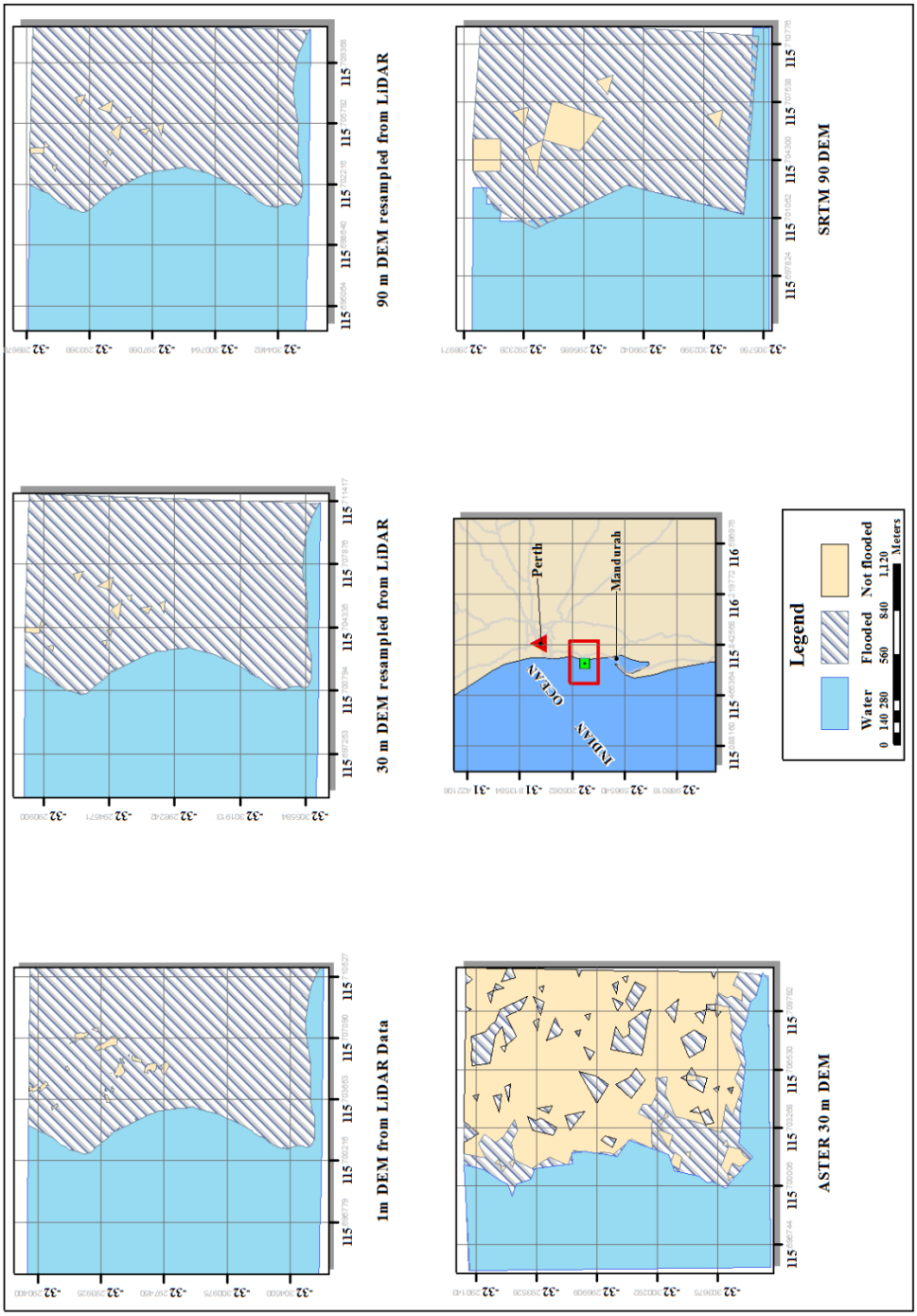

Figure A.8 Flooded areas when sea level rises to 8.61 m in Rockingham by using various DEM resolutions.

A.5 Sea level rise of 10.12 meters in Mandurah

Table A.5 Flooded and not flooded areas (and percentage to total area) using different DEMs resolutions for the study area in Mandurah for a sea level rise of 10.12 m. Unit in m^2. Note the quite different results for the ASTER 30 m DEM data.

	Flooded	Not Flooded	Total
1 m LiDAR	1,345,047 56%	1,068,806 44%	2,413,853 100%
Resampled 30 m	1,329,448 56%	1,062,049 44%	2,391,497 100%
Resampled 90 m	1,292,470 55%	1,041,912 45%	2,334,383 100%
ASTER 30 m	1,760,855 59%	1,216,763 41%	2,977,619 100%
SRTM 90 m	1,474,335 57%	1,114,811 43%	2,589,145 100%

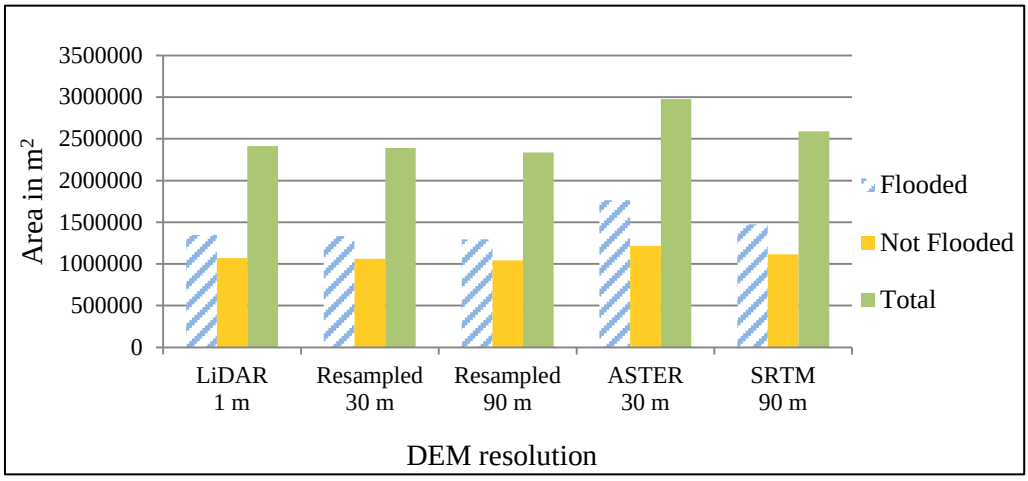

Figure A.9 Flooded and non-flooded areas in Mandurah for a sea level rise of 10.12 m for different DEMs and resolutions.

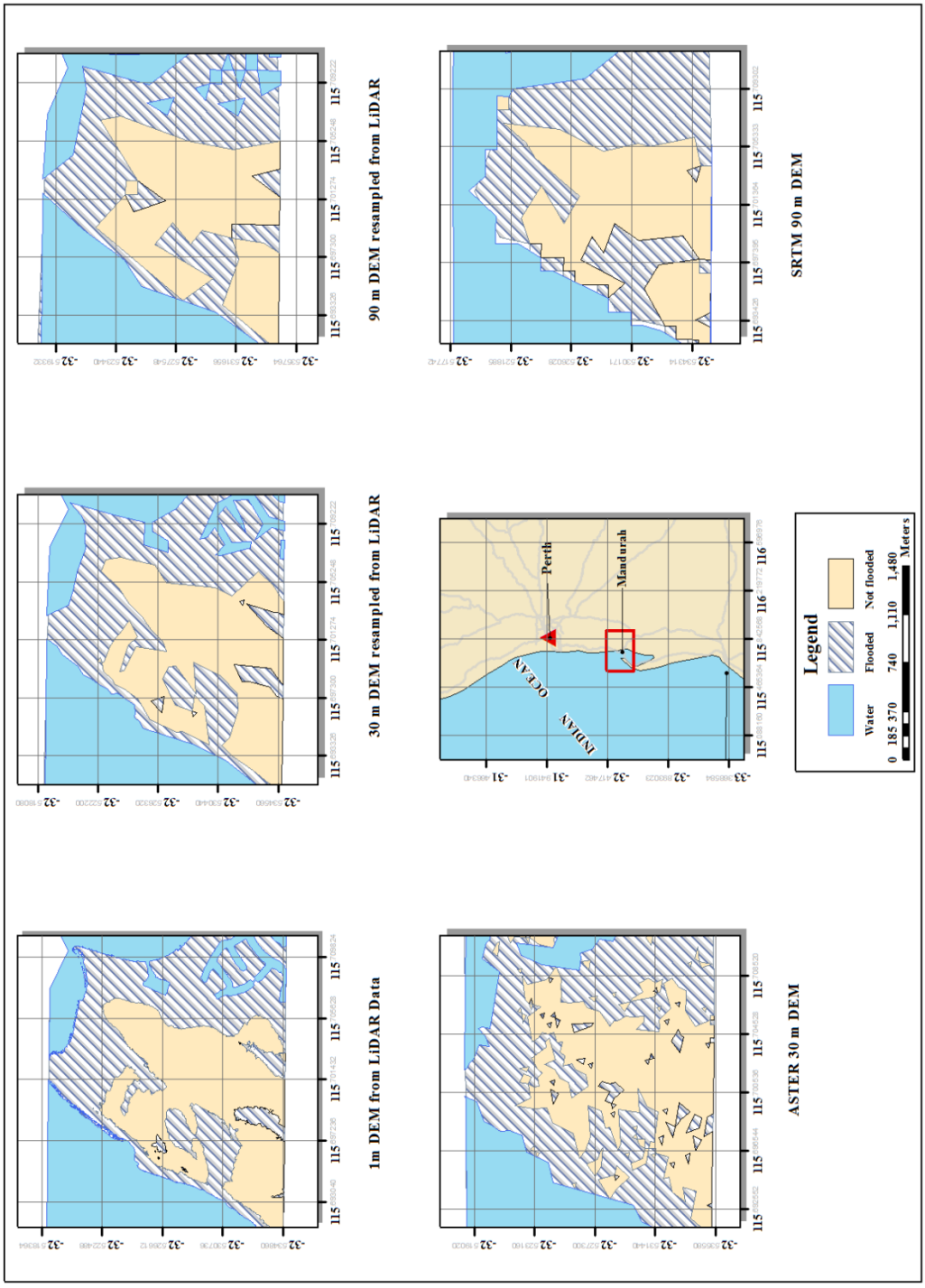

Figure A.10 Flooded areas when sea level rises to 10.12 m in Mandurah by using various DEM resolutions.

A.6 Sea level rise of 10.12 meters in Rockingham

Table A.6 Flooded and not flooded areas (and percentage to total area) using different DEMs resolutions for the study area in Rockingham for a sea level rise of 10.12 m. Unit in m^2. Note the quite different results for the ASTER 30 m DEM data.

	Flooded	Not Flooded	Total
1 m LiDAR	1,606,297 100%	3,738 0%	1,610,035 100%
Resampled 30 m	1,563,886 100%	3,074 0%	1,566,960 100%
Resampled 90 m	1,578,680 100%	5,546 0%	1,584,226 100%
ASTER 30 m	819,648 46%	976,988 54%	1,796,636 100%
SRTM 90 m	1,562,537 100%	5,086 0%	1,567,624 100%

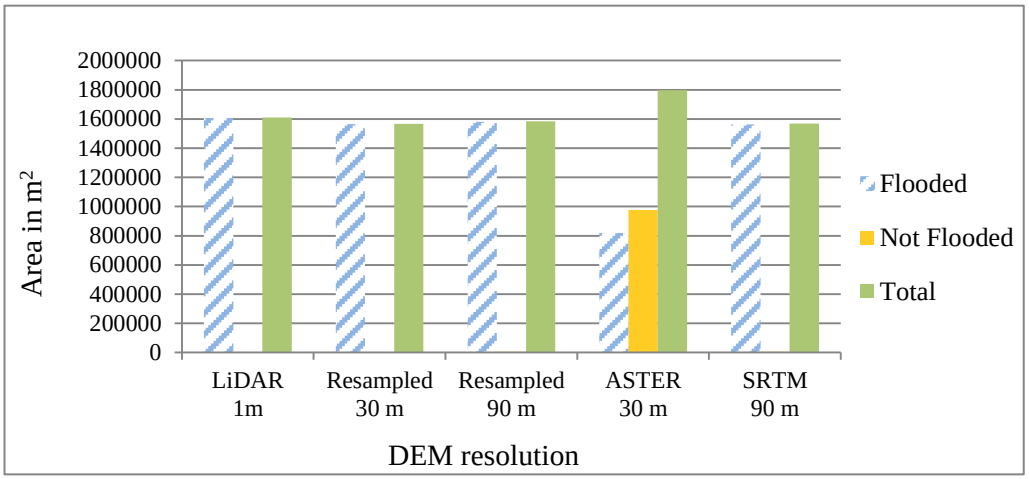

Figure A.11 Flooded and non-flooded areas in Rockingham for a sea level rise of 10.12 m for different DEMs and resolutions.

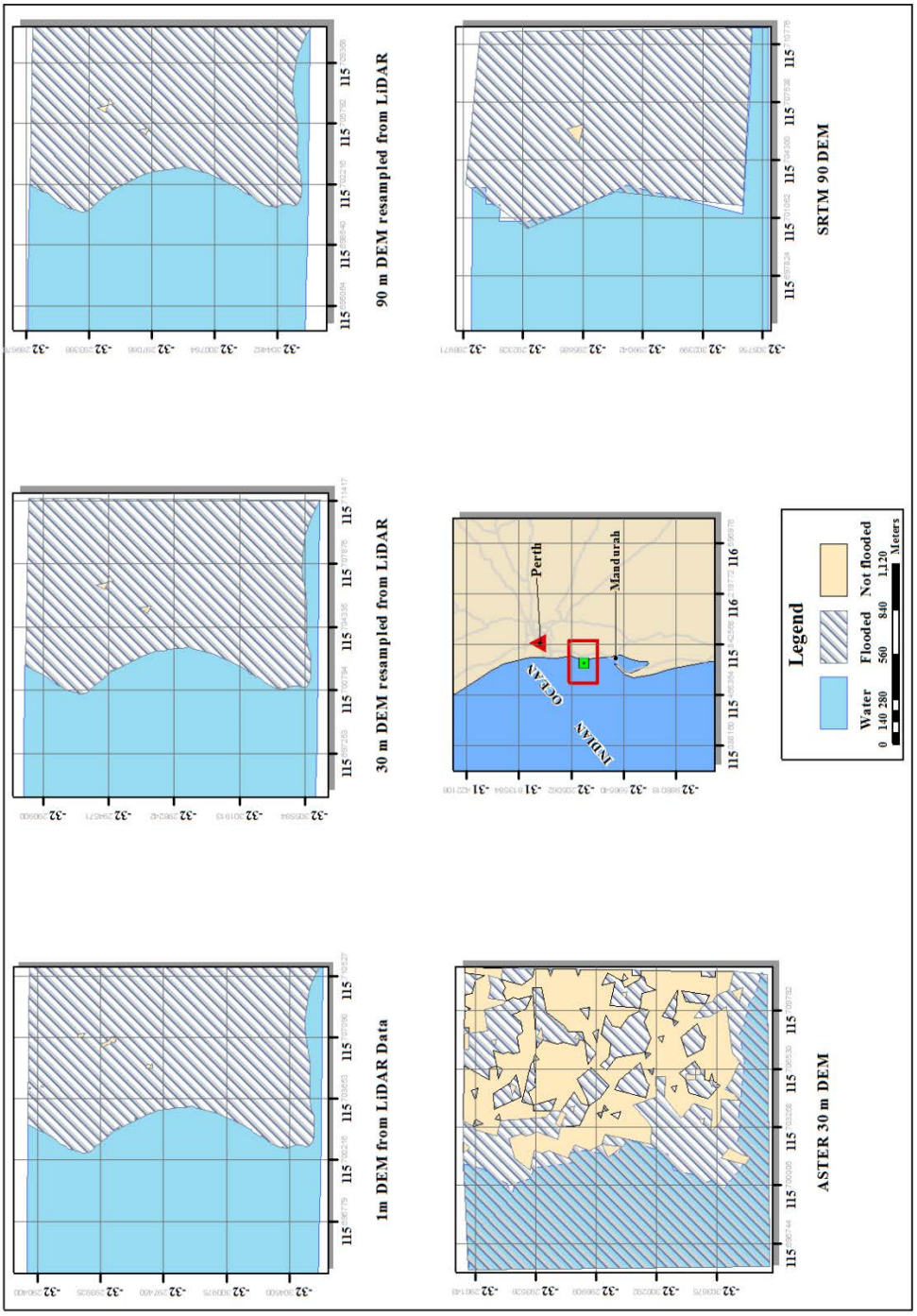

Figure A.12 Flooded areas when sea level rises to 10.12 m in Rockingham by using various DEM resolutions.

A.7 Sea level rise of 18.73 meters in Mandurah

Table A.7 Flooded and not flooded areas (and percentage to total area) using different DEMs resolutions for the study area in Mandurah for a sea level rise of 18.73 m. Unit in m^2. Note the quite different results for the ASTER 30 m DEM data.

	Flooded	Not Flooded	Total
1 m LiDAR	2,246,035 93%	167,095 7%	2,413,130 100%
Resampled 30 m	2,212,176 93%	159,645 7%	2,371,821 100%
Resampled 90 m	2,161,359 94%	128,532 6%	2,289,891 100%
ASTER 30 m	2,778,712 93%	206,594 7%	2,985,306 100%
SRTM 90 m	2,359,500 92%	203,289 8%	2,562,789 100%

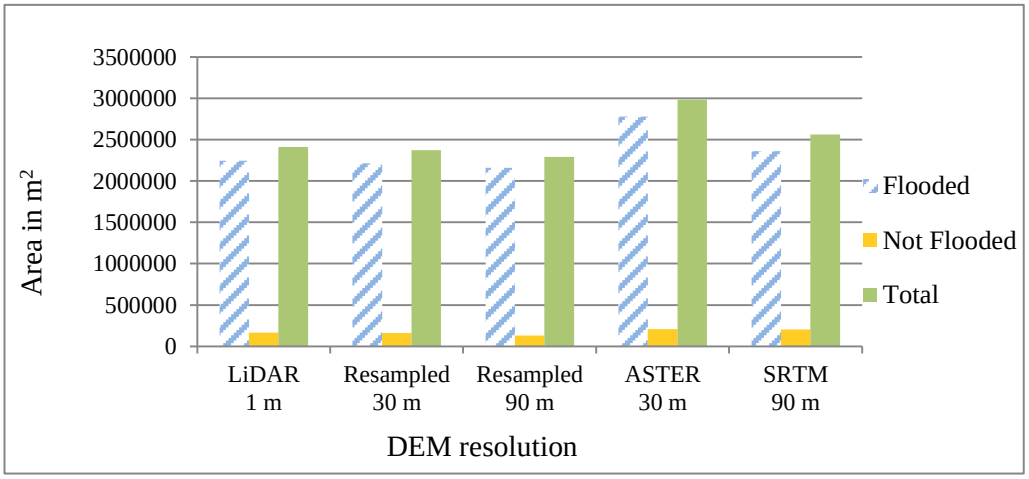

Figure A.13 Flooded and non-flooded areas in Rockingham for a sea level rise of 10.12 m for different DEMs and resolutions.

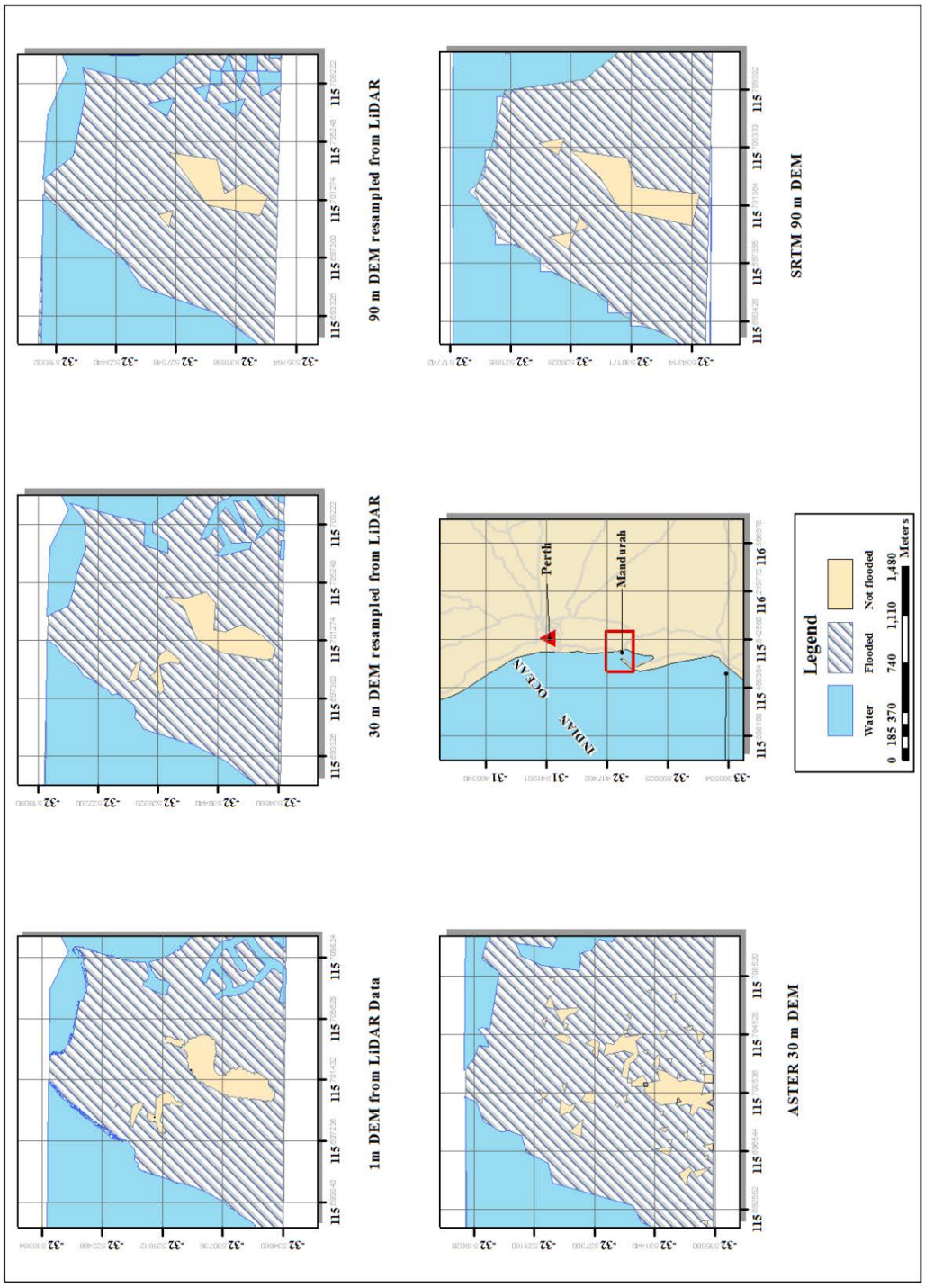

Figure A.14 Flooded areas when sea level rises to18.73 m in Mandurah by using various DEM resolutions.

APPENDIX B

FLOOD VULNERABILITY INDEX ANALYSIS

This appendix provides a complete list of all results obtained from the flood vulnerability analysis for both study sites in Mandurah and Rockingham by using various sea level rise scenario. A complete description of the methodology and parameter used is given in chapter 5.5 for the sea level rise scenario of 5.98 m.

B.1 Flood vulnerability index analysis when Sea level rise to 2.06 meters

Table B.1 Flood vulnerability index analysis for both the Mandurah and Rockingham study locations. The sea level rise scenario considered is 2.06 m.

Risk Category	Mandurah		Rockingham	
	No of the properties	%	No of the properties	%
Very Low 20.00-36.00	704	35.2	508	59.3
Low 36.01-52.00	1116	55.8	319	37.2
Moderate 52.01-68.00	170	8.5	9	1.1
High 68.01-84.00	7	0.4	20	2.3
Very High 84.01-100	2	0.1	1	0.1
total	1999	100	857	100

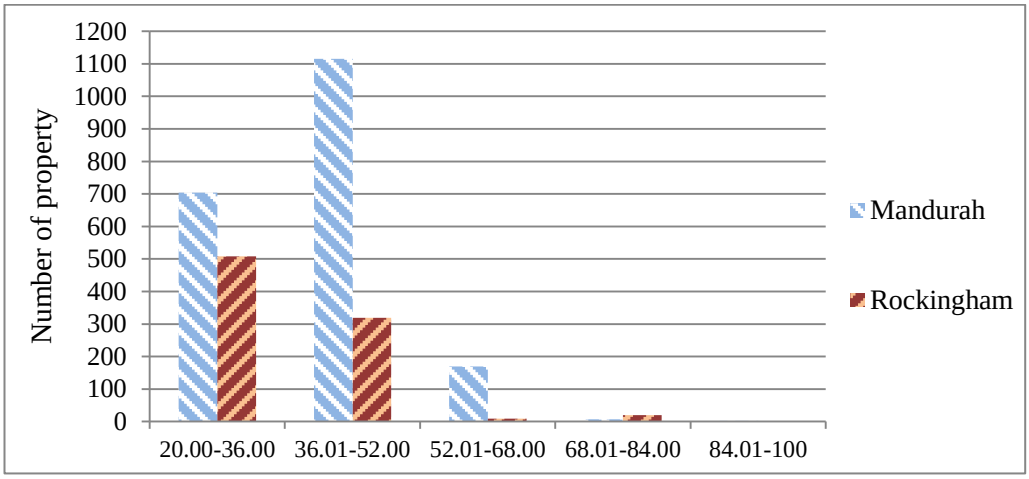

Figure B.1 Number of properties vs. Flood vulnerability index for the Mandurah and Rockingham study locations. The sea level rise scenario considered is 2.06 m.

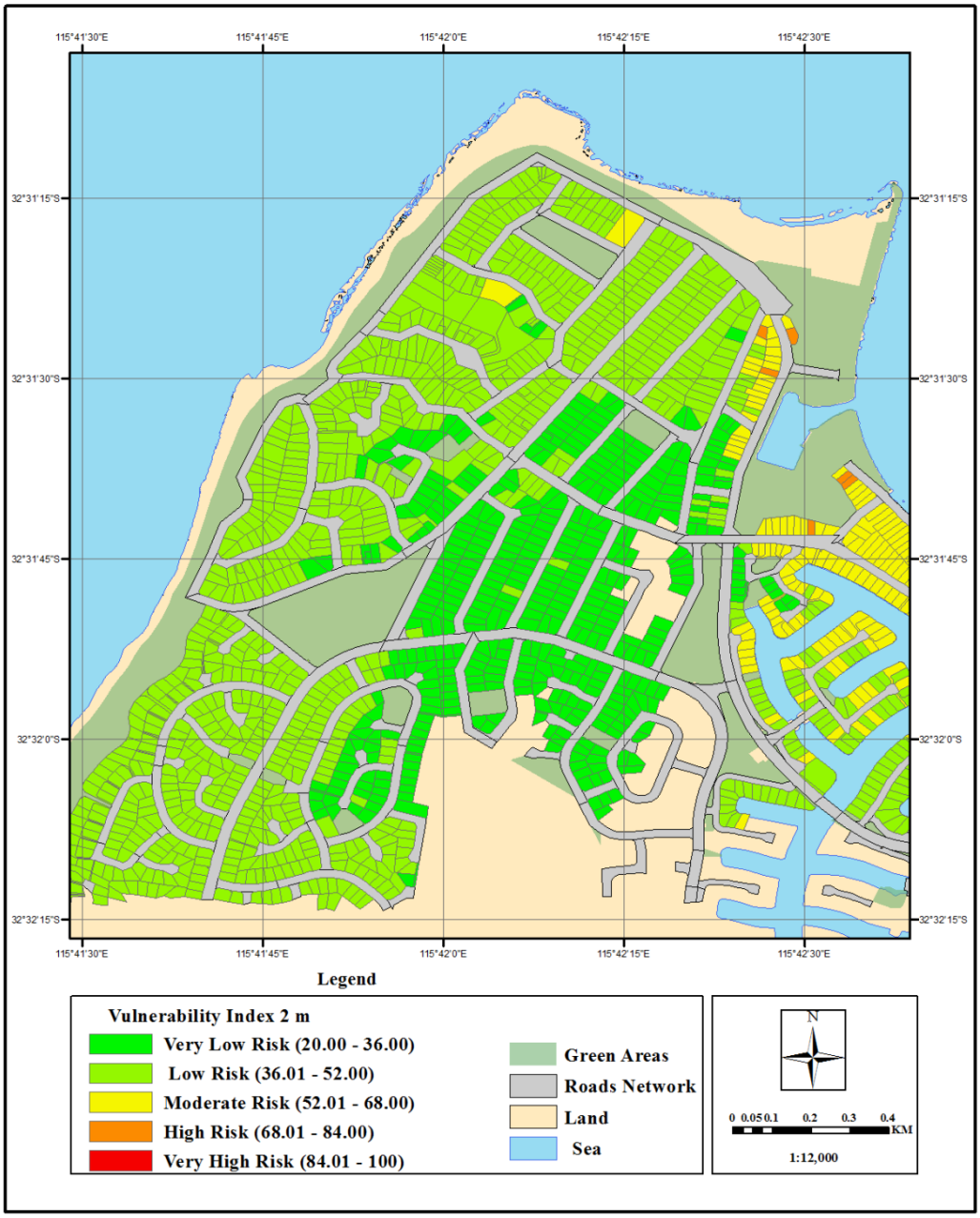

Figure B.2 Flood vulnerability analysis for the Mandurah study area. The sea level rise scenario considered is 2.06 m.

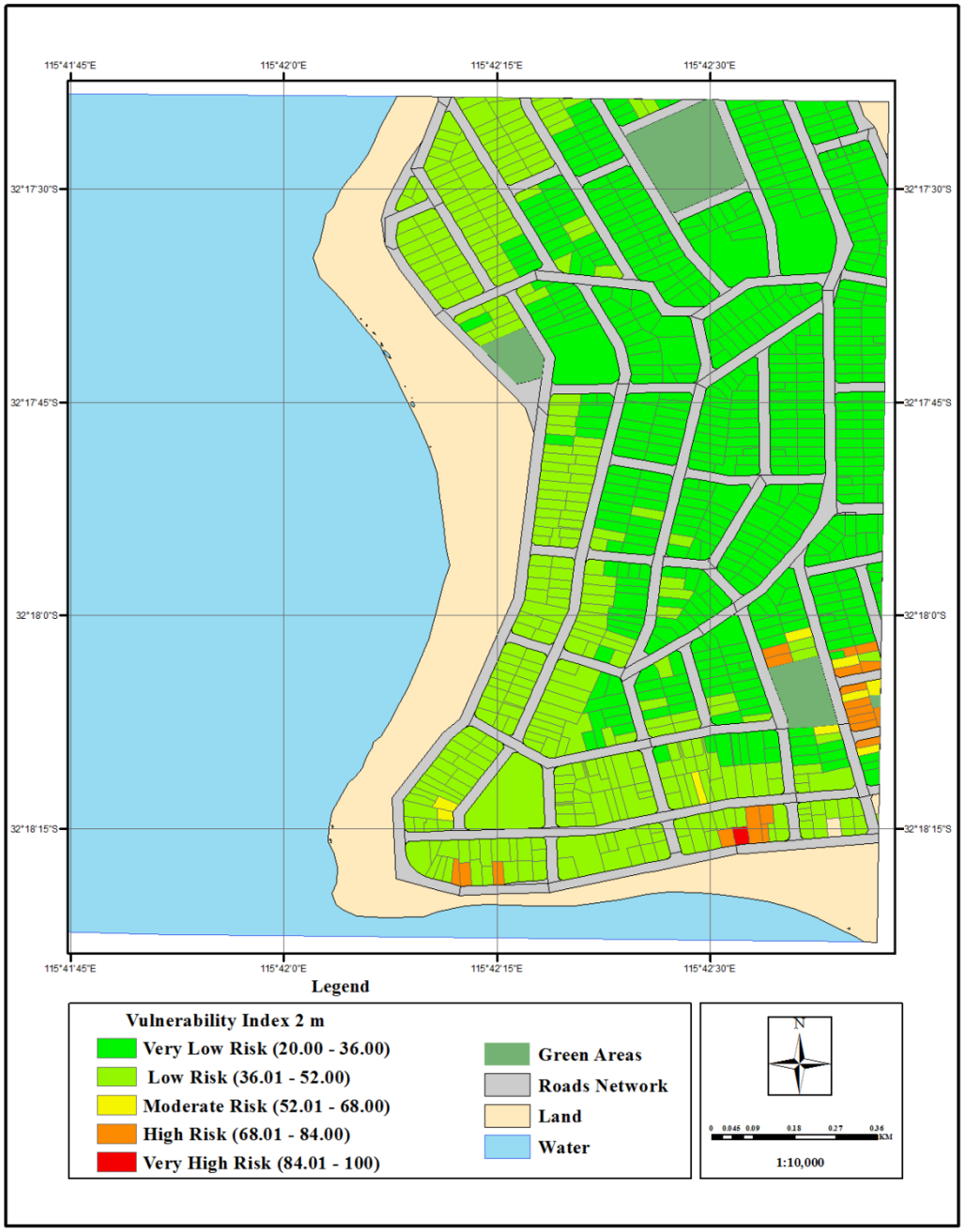

Figure B.3 Flood vulnerability analysis for the Rockingham study area. The sea level rise scenario considered is 2.06 m.

B.2 Flood vulnerability index analysis when Sea level rise to 8.61 meters

Table B.2 Flood vulnerability index analysis for both the Mandurah and Rockingham study locations. The sea level rise scenario considered is 8.61 m.

Risk Category	Mandurah		Rockingham	
	No of the properties	%	No of the properties	%
Very Low 20.00-36.00	582	29.1	2	0.2
Low 36.01-52.00	846	42.3	2	0.2
Moderate 52.01-68.00	46	2.3	15	1.8
High 68.01-84.00	272	13.6	357	41.7
Very High 84.01-100	253	12.7	481	56.1
Total	1999	100	857	100.0

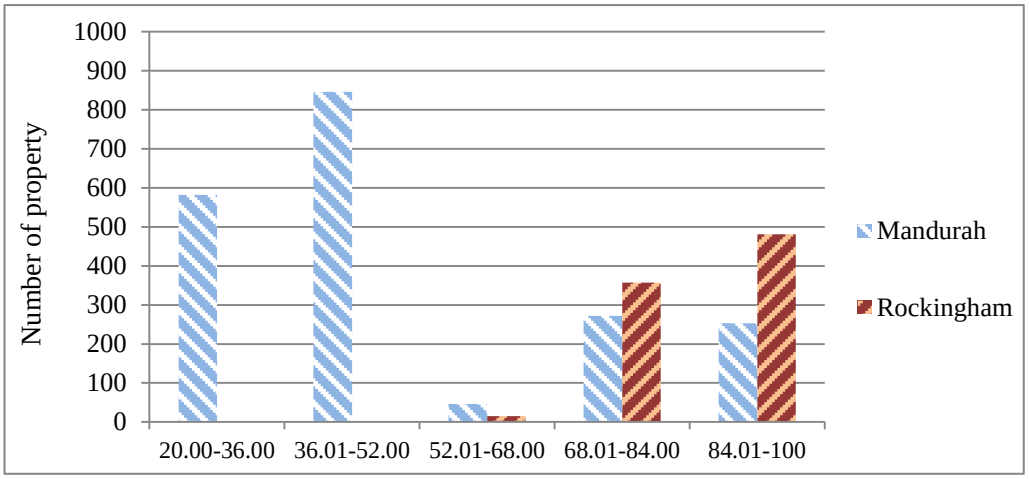

Figure B.4 Number of properties vs. Flood vulnerability index for the Mandurah and Rockingham study locations. The sea level rise scenario considered is 8.61 m.

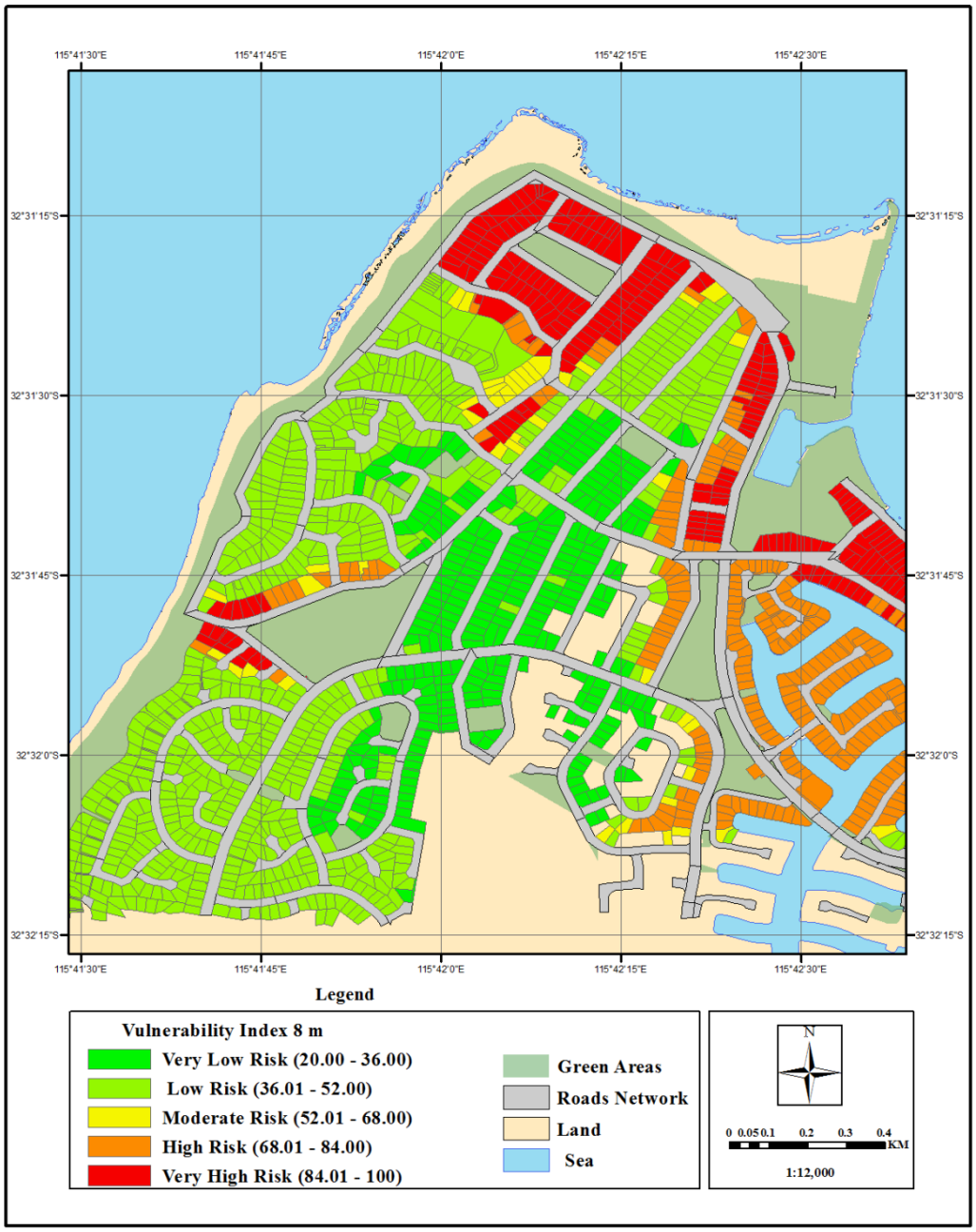

Figure B.5 Flood vulnerability analysis for the Rockingham study area. The sea level rise scenario considered is 8.61 m.

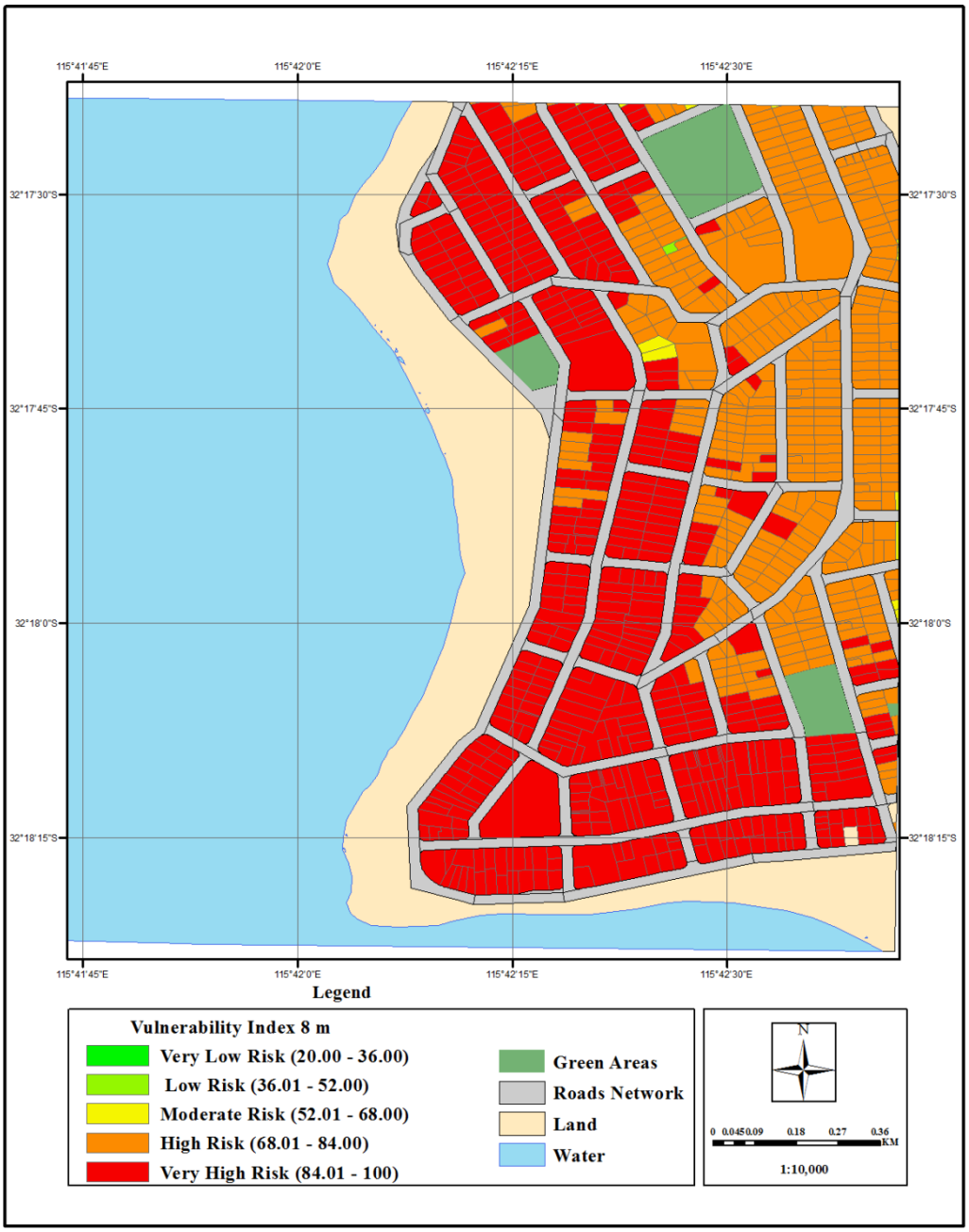

Figure B.6 Flood vulnerability analysis for the Rockingham study area. The sea level rise scenario considered is 8.61 m.

B.3 Flood vulnerability index analysis when Sea level rise to 10.12 meters

Table B.3 Flood vulnerability index analysis for both the Mandurah and Rockingham study locations. The sea level rise scenario considered is 10.12 m.

Risk Category	Mandurah		Rockingham	
	No of the properties	%	No of the properties	%
Very Low 20.00-36.00	233	11.7	2	0.2
Low 36.01-52.00	666	33.3	1	0.1
Moderate 52.01-68.00	348	17.4	15	1.8
High 68.01-84.00	411	20.6	349	40.7
Very High 84.01-100	341	17.1	490	57.2
Total	1999	100.0	857	100.0

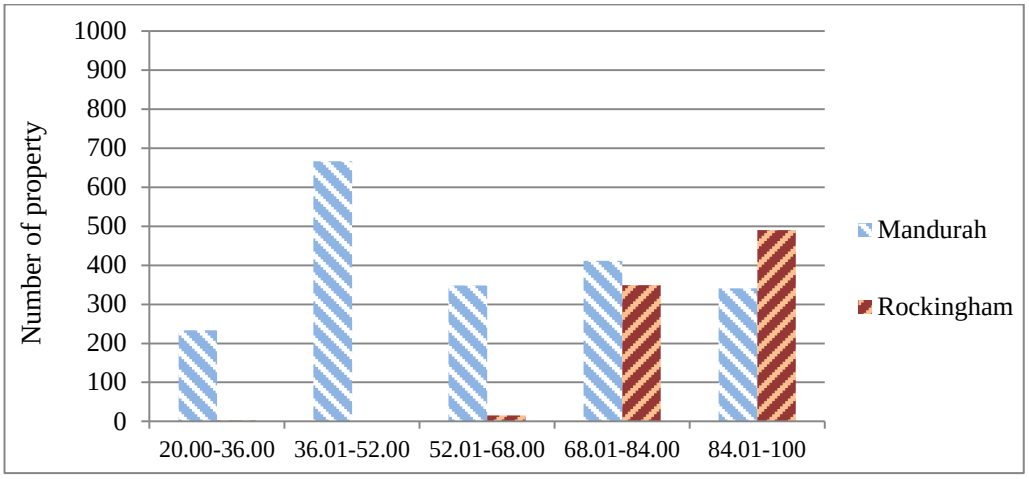

Figure B.7 Number of properties vs. Flood vulnerability index for the Mandurah and Rockingham study locations. The sea level rise scenario considered is 10.12 m.

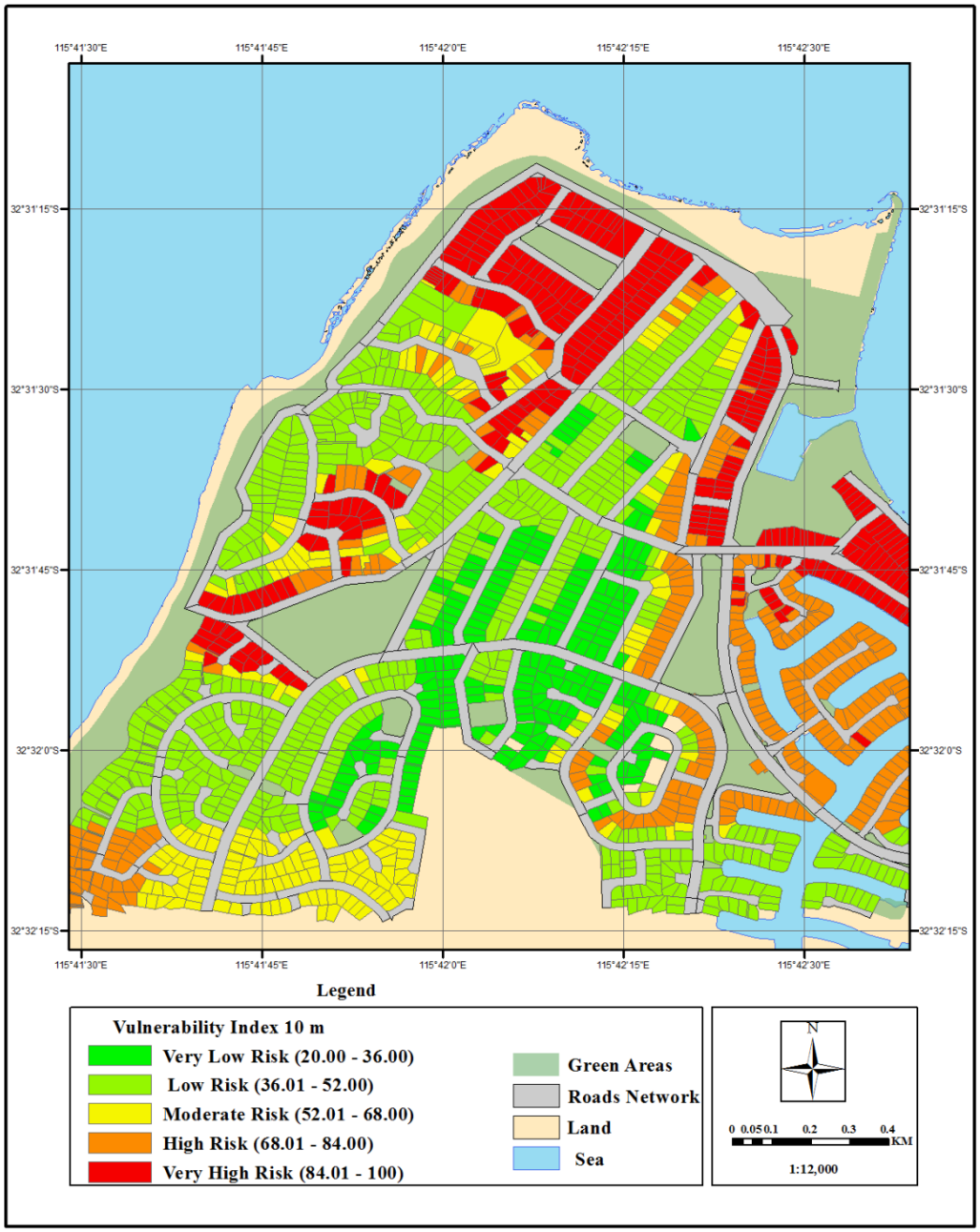

Figure B.8 Flood vulnerability analysis for the Mandurah study area. The sea level rise scenario considered is 10.12 m.

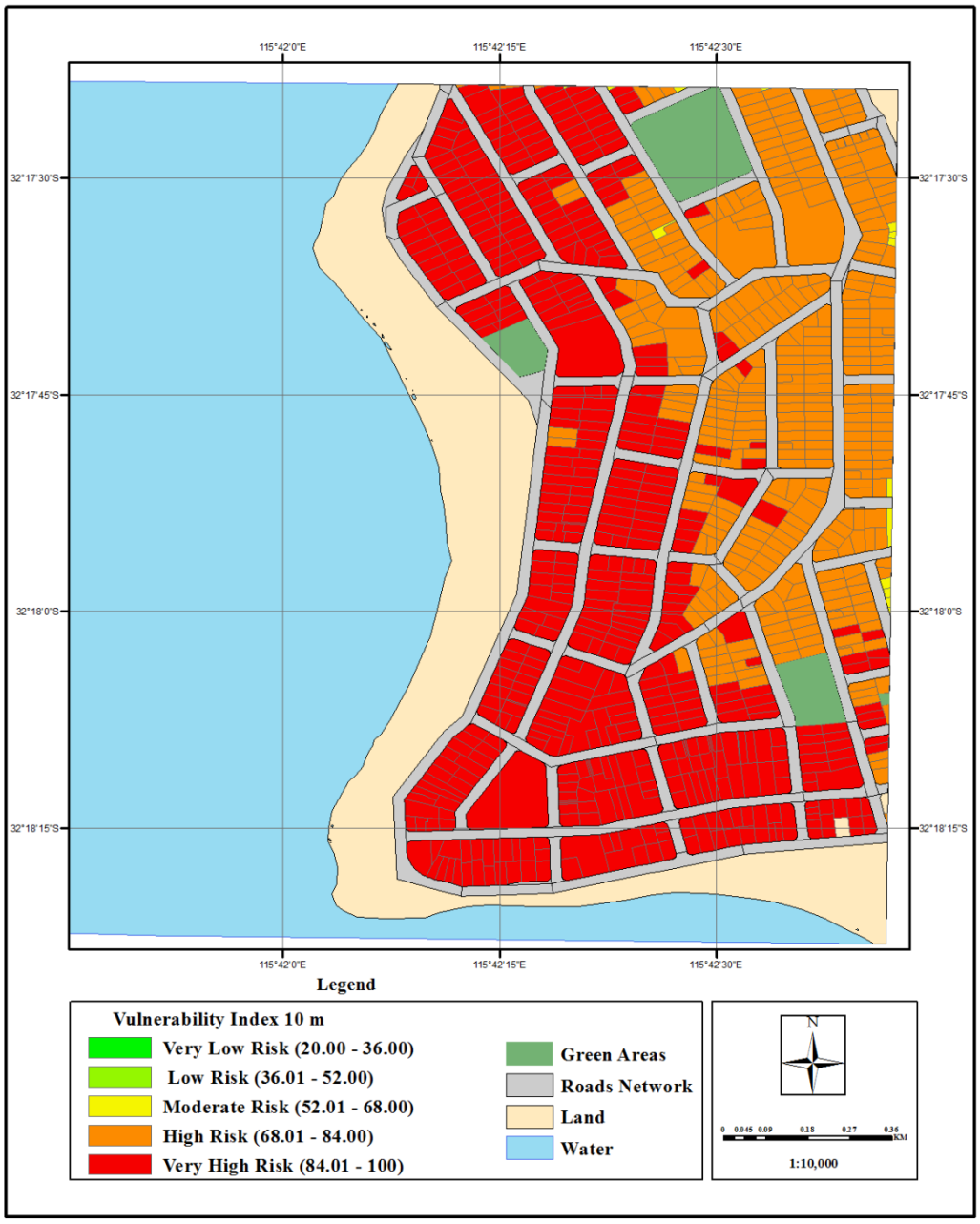

Figure B.9 Flood vulnerability analysis for the Rockingham study area. The sea level rise scenario considered is 10.12 m.

B.4 Flood vulnerability index analysis when Sea level rise of 18.73 meters

Table B.4 Flood vulnerability index analysis for both the Mandurah study location. The sea level rise scenario considered is 18.73 m.

Risk Category	No of the properties	%
Very Low 20.00-36.00	302	15.1
Low 36.01-52.00	322	16.1
Moderate 52.01-68.00	49	2.5
High 68.01-84.00	507	25.4
Very High 84.01-100	819	41.0
Total	1999	100.0

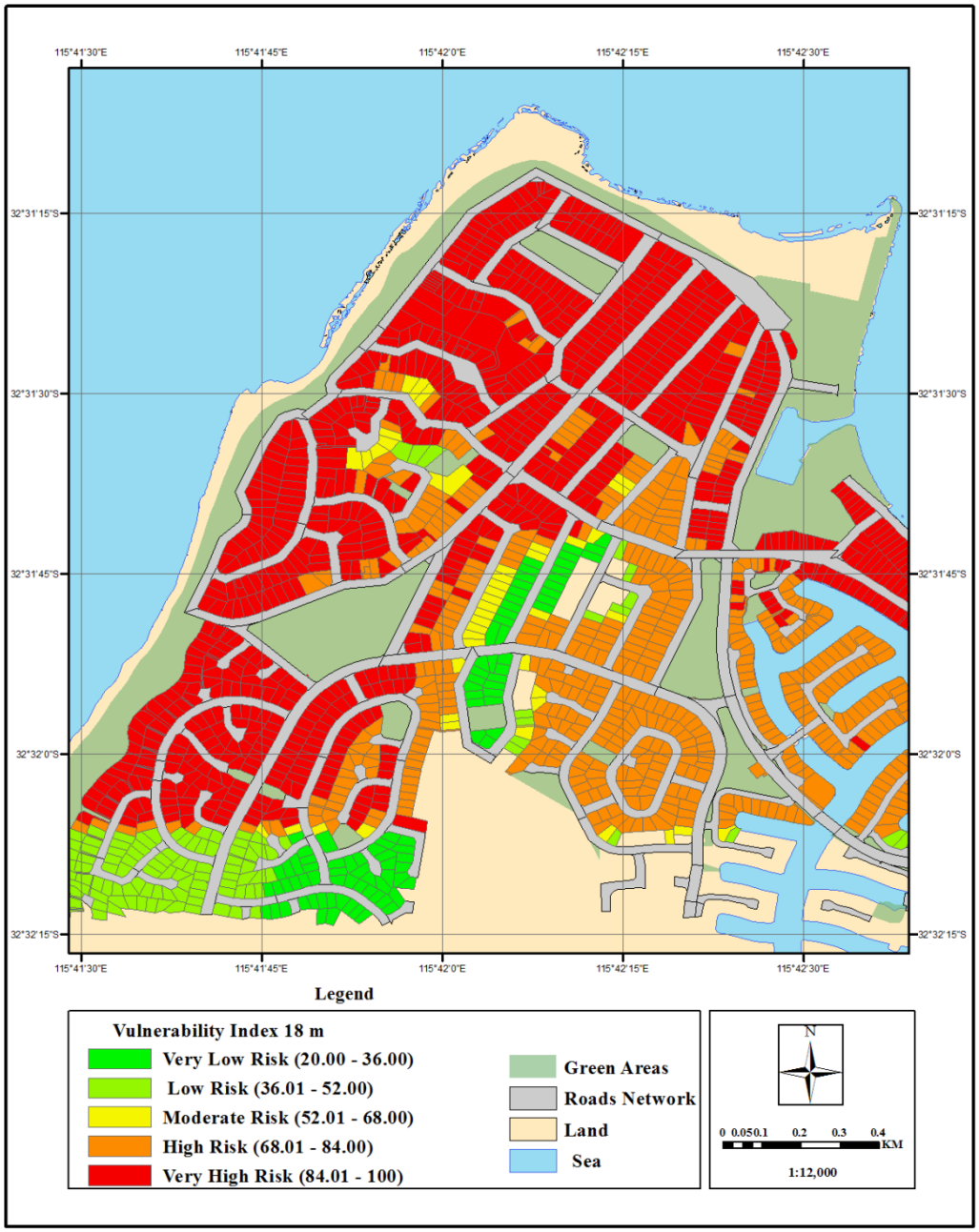

Figure B.10 Flood vulnerability analysis for the Mandurah study area. The sea level rise scenario considered is 18.73 m.